Supplementary Materials for

Directed evolution of nonheme iron enzymes to access abiological radical-relay C(sp^3)−H azidation

Jinyan Rui,[1,*] Qun Zhao,[1,*] Anthony J. Huls,[1,*] Jordi Soler,[2] Jared C. Paris,[3] Zhenhong Chen,[1] Viktor Reshetnikov,[1] Yunfang Yang,[4] Yisong Guo,[3,†] Marc Garcia-Borràs,[2,†] Xiongyi Huang[1,†]

[1]*Department of Chemistry, Johns Hopkins University, Baltimore, MD 21218, USA.*

[2]*Institut de Química Computacional i Catàlisi (IQCC) and Departament de Química, Universitat de Girona, Campus Montilivi, Girona E-17071, Catalonia, Spain*

[3]*Department of Chemistry, Carnegie Mellon University, Pittsburgh, PA 15213, USA*

[4]*College of Chemical Enginering, Zhejiang University of Technology, Hangzhou, Zhejiang 310014, China*

[†]Corresponding author. E-mail: xiongyi@jhu.edu (X.H.); marc.garcia@udg.edu (M.G.B.); ysguo@andrew.cmu.edu (Y.G.)

[*]These authors contributed equally to this work.

Table of Contents

I. Materials and Methods

II. General Procedures

III. Supporting Tables and Schemes

IV. Sequence Information for Final Variants

V. Substrate Synthesis and Characterization

VI. Synthesis and Characterization of Authentic Azidation Products

VII. GC-MS Standard Curves for Azidation Products

VIII. Determination of Enantioselectivity

IX. Preparative Scale Enzymatic Reactions

X. Spectroscopic Studies

XI. Computational Modelling

XII. X-ray Crystallography and the Assignments of Absolute Configuration

XIII. NMR Spectra

I. Materials and Methods

Unless otherwise noted, all chemicals and reagents were obtained from commercial suppliers (Sigma-Aldrich, Alfa Aesar, Acros, AA Blocks, Combi-Blocks) and used without further purification. Silica gel chromatography was carried out using SiliaFlash Irregular Silica Gels F60, 40 - 63 µm, 60 Å. ^{1}H and ^{13}C NMR were recorded on either a Bruker Avance 300, 400 or III HD 400 MHz spectrometer. Chemical shifts (δ) are reported in ppm downfield from tetramethylsilane, using the solvent resonance as the internal standard (^{1}H NMR: δ = 7.26, ^{13}C NMR: δ = 77.4 for $CDCl_3$). Sonication was performed using a Fisherbrand Model 120 Sonic Dismembrator. Chemical reactions were monitored using thin layer chromatography (Merck 60 gel plates) using a UV-lamp for visualization. Gas chromatography-mass spectrometry (GC-MS) analyses were carried out using an Agilent 5977B GC/MSD system and HP-5MS UI column (30.0 m × 0.25 mm) with the following oven temperature setting (helium flow 1 ml/min): Initial: 110 ºC (hold 0 min); Ramp 1: 110-160 ºC (20 ºC/min, hold 0 min); Ramp 2: 160-225 ºC (15 ºC/min, hold 0 min); Ramp 3: 225-270 ºC (30 ºC/min, hold 4 min). Analytical chiral normal-phase HPLC analyses were performed using an Agilent 1260 series instrument with *i*-PrOH and hexanes as the mobile phase. Reverse-phase high-performance liquid chromatography-mass spectrometry (LC-MS) analysis was carried out using Agilent 1260 series instruments and Agilent 1260 LC/MSD iQ series instruments. Semi-preparative HPLC was performed using an Agilent XDB-C18 column (9.4 x 250 mm). Column chromatography was performed on a Biotage Isolera One system using Sfär Silica HC-High Capacity 20 µm columns. Plasmid pET22b(+) was used as a cloning vector, and cloning was performed using Gibson assembly (*1*). Cells were grown using Luria-Bertani (LB) medium or terrific broth (TB) medium (RPI Research). Primer sequences are available upon request. T5 exonuclease, Phusion polymerase, and *Taq* ligase were purchased from New England Biolabs (NEB, Ipswich, MA). Potassium phosphate buffer **(**pH 7.4) was used as a buffering system for whole cells, lysates, and purified proteins, unless otherwise specified.

II. General Procedures

(A) Generation of enzyme variants. All protein variants described in this paper were cloned and expressed using the pET-22b(+) vector or pET-28a(+) vector. The genes encoding non-heme iron proteins used in this work were obtained as a single gBlock (Twist Bioscience), codon-optimized for *E. coli*, and cloned using Gibson assembly into pET-22b(+) between restriction sites *Nde*I and *Xho*I in frame with a *C*-terminal 6xHis-tag or into pET-28a(+) between restriction sites *Nde*I and *BamHI* in frame with an *N*-terminal 6xHis-tag. This plasmid was transformed into *E. cloni*® EXPRESS BL21(DE3) cells (Lucigen).

(B) Enzyme expression. 200 mL TB_{amp} in a 1L flask was inoculated with an overnight culture (2 mL in LB_{amp}) of recombinant *E. cloni*® EXPRESS BL21(DE3) cells containing a pET-22b(+) plasmid encoding the non-heme iron enzyme variant. The culture was shaken at 37 °C and 240 rpm until the OD_{600} was 0.7 (approximately 2 hours). The culture was placed on ice for 20 minutes, and isopropyl *β-D*-1-thiogalactopyranoside (IPTG) was added to final concentrations of 1 mM. The incubator temperature was reduced to 20.5 °C, and the culture was allowed to shake for 24 hours at 180 rpm. Cells were harvested by centrifugation (4 °C, 15 min, 4,000xg) and the cell pellet was resuspended in potassium phosphate buffer (pH 7.4),

(C) Library construction. Site-saturation mutagenesis libraries were generated using a modified QuikChange mutagenesis protocol using Phusion® High-Fidelity DNA Polymerase (New England Biolabs). The PCR products were digested with DpnI, gel purified, and the gaps were repaired using Gibson Mix™ (*1*). Without further purification, 1 μL of the Gibson product was used to transform 50 μL of electrocompetent *Escherichia coli* BL21 *E. cloni* (Lucigen) cells. Random mutagenesis was achieved with error-prone PCR using *Taq* polymerase (New England Biolabs) with a $MnCl_2$ concentration of 300 μM.

(D) Library screening. Single colonies were picked with toothpicks off of LB_{amp} agar plates and grown in deep-well (2 mL) 96-well plates containing LB_{amp} (400 μL) at 37 °C, 240 rpm shaking. After 16 hours, 50 μL aliquots of these overnight cultures were transferred to deep-well 96-well plates containing TB_{amp} (1 mL) using a 12-channel Eppendorf Xplorer® plus electronic pipettor. Glycerol stocks of the libraries were prepared by mixing cells in LB_{amp} (100 μL) with 50% v/v glycerol (100 μL). Glycerol stocks were stored at −80 °C in 96-well microplates. Growth plates were allowed to shake for 3 hours at 37 °C, 240 rpm shaking. The plates were then placed on ice for 30 min. Cultures were induced by adding 10 μL of a solution containing 100 mM isopropyl *β-D*-1-thiogalactopyranoside (IPTG). The incubator temperature was reduced to 20.5 °C, and the induced cultures were allowed to shake for 24 hours (230 rpm). Cells were pelleted (4,500xg, 5 min, 4 °C), resuspended in 400 μL potassium phosphate buffer (pH 7.4), and the plates containing the cell suspensions were transferred to an anaerobic chamber. To deep-well plates of cell suspensions were added sodium azide (10 μL per well, 1.0 M in water), ferrous ammonium sulfate (10 μL per well, 100 mM in water), and the *N*-fluoroamide model substrate (10 μL per well, 400 mM in dimethoxyethane (DME)). The plates were sealed with aluminum sealing tape and shaken at 680 rpm overnight in the chamber. The plates were then removed from the chamber and analyzed via the high-throughput (HTS) screening assay described in section (E). Hits from library screening were confirmed by small-scale biocatalytic reactions, as described in section (H).

(E) High-throughput (HTS) fluorescent detection of azidation product in 96-well plate. The reaction was performed following the procedure in section D. After the reaction, 400 μL of *N,N*- dimethylformamide (DMF) was added to each well and the plate was incubated for 1

hour. The plate was then centrifuged to remove the insolubles. From each well, 5 μL of the supernatant was transferred to a 96-well black fluorescence plate (Caplugs Evergreen) containing 195 μL of 25% aqueous solution of DMF with 77 μM $CuSO_4$, 154 μM BTTAA ligand (Click Chemistry Tools), 5.1 mM ascorbic acid, 25.6 mM KP_i (pH 7.4), and 103 μM of fluorogenic alkyne probe 4-ethynyl-*N*-ethyl-1,8-naphthalimide (*2*). The fluorescence plate was incubated and the formation of the fluorescent triazole product was monitored by a TECAN Spark plate reader outfitted with a plate stacker (excitation wavelength, 357 nm: emission wavelength 462 nm; bandwidth, 20 nm). Validation of hit wells was further investigated by GC-MS. Hits from library screening were confirmed by small-scale biocatalytic reactions, as described in section (H).

(F) Cell lysate preparation. Cell lysates were prepared as follow: *E. coli* cells expressing non-heme iron enzyme variants were pelleted (4,000xg, 5 min, 4 °C), resuspended in potassium phosphate buffer and adjusted to the appropriate OD_{600}. Cells were lysed by sonication (5 minutes, 5 seconds on, 5 seconds off, 40% duty cycle) for two times, aliquotd into 2 mL microcentrifuge tubes, and the cell debris was removed by centrifugation for 10 min (14,000xg, 4 °C). The supernatant was sterile filtered through a 0.45 μm cellulose acetate filter, and the concentration of protein lysate was determined using the described in section (G). Using this protocol, the protein concentrations we typically observed for OD_{600} = 10 lysates are in the 5 - 10 μM range for *sav* HppD and its variants.

(G) Protein concentration determination in cell lysates. The quantity of His-tagged non-heme iron enzymes in cell lysates was determined using the His-tag protein ELISA kit according to the manufacturer's instructions (AKR-130 Cell Biolabs, San Diego, CA). Using this protocol, the protein concentrations we typically observed for OD_{600} = 10 lysates were in the 5 - 10 μM range for wild-type *Sav* HppD and its variants.

(H) Small-scale biotransformations using whole *E. coli* cells. In a typical experiment, ferrous ammonium sulfate (20 μL, 100 mM in water), sodium azide (20 μL, 1 M in water), and *N*-fluoroamide substrate (20 μL, 1.5 M in DME) were added to *E. coli* harboring non-heme iron enzyme variant (400 μL, adjusted to the appropriate OD_{600}) in a 2 mL screw top GC vial in an anaerobic chamber. The vial was capped and shaken at 680 rpm at room temperature for 24 hours. At the end of the reaction, the vial was opened and the reaction was quenched with 6 mL of a hexanes/ethylacetate solution (4:6 v/v) of internal standard 1,2,3-trimethoxybenzene (0.5 mM final concentration). The reaction mixture was transferred to a 15 mL centrifuge tube, vortexed (10 seconds, 3 times), then centrifuged (10,500xg, 5 min) to completely separate the organic and aqueous layers. An aliquot (200 - 300 μL) of the organic layer was used for product quantification via GCMS and enantioselectivity via chiral HPLC or chiral GC. The total turnover numbers (TTNs) reported are calculated with respect to non-heme iron enzymes expressed in *E. coli* and represent the total number of turnovers obtained from the catalyst under the stated reaction conditions.

(I) Protein purification Protein expression was conducted following the protocols detailed in section (B). *E. coli* cells expressing non-heme iron enzyme variants were pelleted (4,000xg, 5 min, 4 °C) and stored at −20 °C for at least 24 hours. The cell pallet was then resuspended in 50 mM KPi buffer containing 100 mM NaCl and 20 mM imidazole (pH 7.5 at 25 °C) (10 mL buffer per gram of cell pellet). Cells were lysed by sonication (5 minutes, 5 seconds on, 5 seconds off, 40% duty cycle) for two times and the cell debris was removed by centrifugation for 10 min (10,300xg, 4 °C). The supernatant was sterile filtered through a 0.45 μm cellulose acetate filter and purified using a 5 mL Ni-NTA column (HisTrap HP, Cytiva) using an ÄKTA

start protein purification system (Cytiva). The proteins were eluted from the column by running a gradient from 20 to 500 mM imidazole over 10 column volumes. Fractions containing purified proteins were detected by SDS-PAGE, pooled and concentrated using Millipore® centrifugal filter. The protein solution was dialyzed first against 1 L of buffer with 10 mM EDTA in 50 mM KPi (pH 7.5 at 25 °C), and then two times against 1 L of 50 mM KPi. Final concentration was measured by absorbance at 280 nm using a NanoDrop spectrophotometer. The theoretical extinction coefficients (M^{-1} cm^{-1}) used for *Sav* HppD and its variants were calculated using ExPASy Bioinformatics Resources Portal, http://www.expasy.org).

III. Supporting Tables, Figures and Schemes

Table S1. Preliminary screening experiments with non-heme iron proteins.[a]

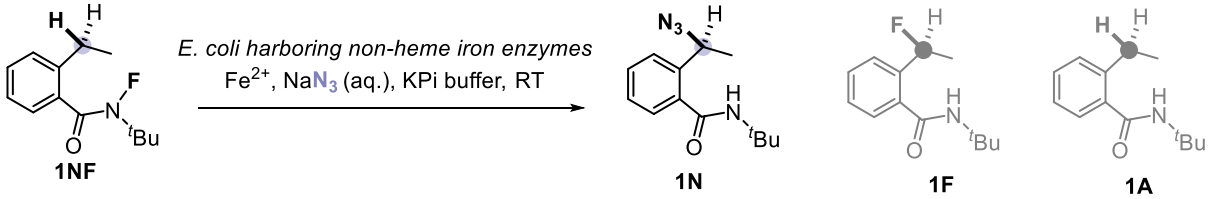

Entry	Enzyme	Organism	Uniprot No.	1N%	e.r.[d]	1F%	1A%
1	**4-hydroxyphenylpyruvate dioxygenase (HppD)[a]**	***Streptomyces avermitilis***	**Q53586**	**33.0 ± 2.0**	**63:37**	**3.7**	**10.0**
2	Proline *cis*-4-hydroxylase (P4H)[b]	*Mesorhizobium japonicum*	Q989T9	0.5	n.d.	0.4	5.0
3	Iron/2-oxoglutarate-dependent halogenase WelO5[b]	*Hapalosiphon welwitschii*	A0A067YX61	0.1	n.d.	0.3	2.5
4	polyoxin hydroxylase PolL[c]	*Streptomyces aureochromogenes*	J7FW05	0.6	n.d.	0.4	8.6
5	Prolyl 4-hydroxylase[c]	*Bacillus anthracis*	A0A4Y1WAP5	n.d.	n.d.	n.d.	n.d.
6	Prolyl 4-hydroxylase[bc]	*Paramecium bursaria Chlorella virus 1*	Q84406	0.2	n.d.	0.7	6.7
7	Iron/2-oxoglutarate-dependent halogenase AsqJ[c]	*Emericella nidulans*	Q5AR53	0.1	n.d.	0.5	5.0
8	Isopenicillin N synthase (IPNS)[b]	*Emericella nidulans*	P05326	4.0 ± 0.1	44:56	1.5	8.0
9	(*S*)-2-hydroxypropylphosphonic acid epoxidase Psf4[b]	*Pseudomonas syringae*	Q9JN69	0.1	n.d.	0.3	3.3
10	KPi buffer without whole-cell catalyst			0.1	n.d.	0.3	0.5
11	*Sav* HppD H187A H270A as the catalyst			0.2	n.d.	0.2	7.5
12	wt *Sav* HppD, no azide addition			n.d.	n.d.	2.2	6.5

[a]1N%,1F%, and 1A% refer to the yield of 1N, 1F, and 1A, respectively. [b]pET-22b(+) was used as the cloning vector. [c]pET-28a(+) was used as the cloning vector. [d]not determined (n.d.)

Procedures: In an anaerobic chamber, ferrous ammonium sulfate (10 μL, 100 mM in water), sodium azide (10 μL, 1 M in water), and *N*-fluoroamide substrate **1NF** (10 μL, 400 mM in DME) were added to *E. coli* harboring non-heme iron enzymes (400 μL, adjusted to OD_{600} = 40) in a 2 mL screw top GC vial. The vial was capped and shaken at 680 rpm at room temperature for 24 hours. At the end of the reaction, the vial was opened and the reaction was quenched with 0.8 mL of a hexanes/ethylacetate solution (4:6 v/v) of internal standard 1,2,3-trimethoxybenzene (0.5 mM final concentration). The reaction mixture was transferred to a 2 mL microcentrifuge tube, vortexed (10 seconds, 3 times), then centrifuged (14,000xg, 5 min) to completely separate the organic and aqueous layers. An aliquot (200 - 300 μL) of the organic layer was used for product quantification via GCMS and enantioselectivity via chiral HPLC or chiral GC.

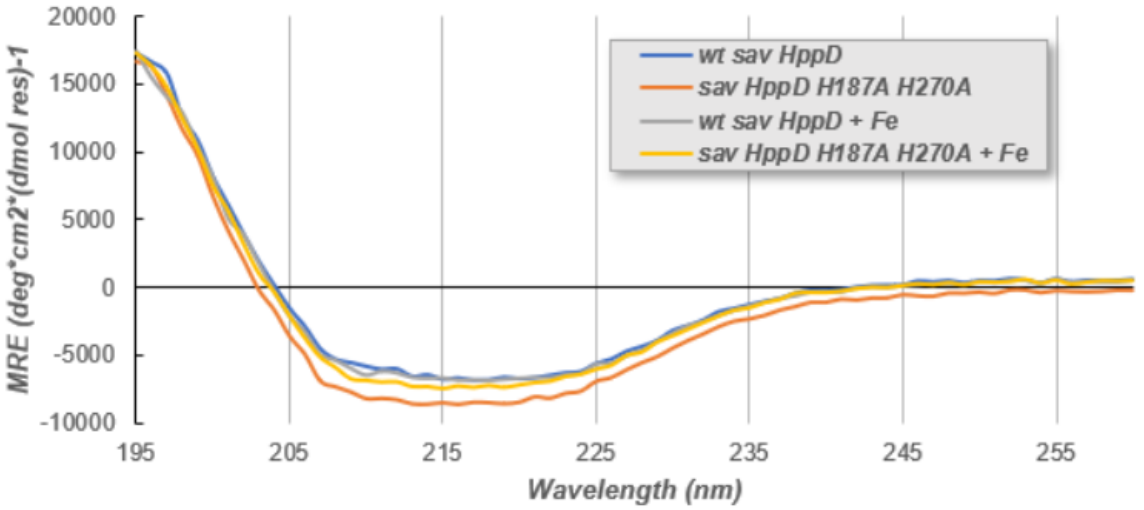

Figure S1. Comparison of the circular dichroism spectra obtained from wt *Sav* HppD and wt *Sav* HppD H187A H270A variant with and without addition of Fe^{2+} salt. Purified protein samples prepared according to general procedure (I) in section 2 were diluted and normalized to 0.2 mg/mL protein. To an aliquot of each sample, a concentrated stock solution of Mohr's salt was added to a final concentration of 10 µM, or water was added to keep a uniform concentration. Spectra were taken between 195 – 260 nm. Molar residue ellipticity (MRE) is reported.

Scheme S1. Determination of coefficient of variation (CV) for the HTS platform.

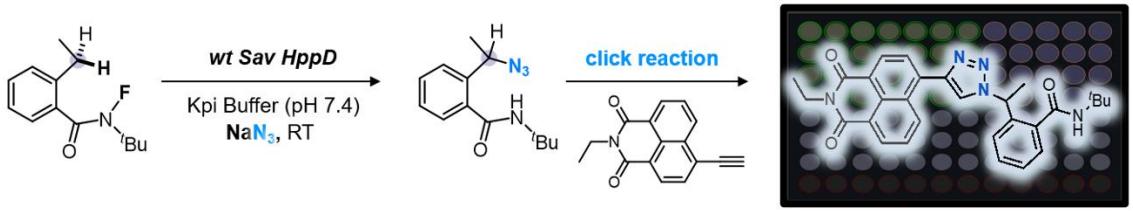

	1	2	3	4	5	6	7	8	9	10	11	12
A	41207	40785.5	44595.75	50439.25	51299.5	47843.25	52707.75	49259.25	23924	49983.5	52163.25	50398.5
B	46630.5	44272.75	44072.25	44542.25	34368.75	52417.5	49840.25	49037.25	52286	52234.5	48372.5	40252.75
C	42424.25	49050	47054.5	48525.75	47222.5	45397.25	44538	42779.75	42135.75	45127.25	47867.5	45206.75
D	44415.25	45526.75	44901	44584.25	44741.25	44970.5	49135.25	46054.75	46582.25	48129.5	45347.5	49271
E	42970.25	46176.5	40598.5	46236.25	45023	46037.25	43791.25	42157	47793	50574	47247.25	48507.75
F	40717.25	41122.25	46519	43427	39159.75	42987.5	44424.25	45050	46642.5	44612	48835	48130.25
G	39735.25	43385.75	38198.75	41582.75	48201.75	40596.75	48484	50614.75	45641	49260	48450	53594.5
H	44991	47474	48722.75	45678	41857.75	41417.5	45464.25	49141.75	46134	44360.25	51275.75	51327.5

Experimental details: A 96-well plate for CV test was prepared according to the procedures described in section D. The protein expression and azidation reaction were performed following the protocols detailed in section D. Each well contained the same biocatalyst (wild-type *Sav* HppD). After the reaction, the azidation products formed in each well were quantified via the protocol described in section E. The CV was determined to be ~9% by dividing the standard deviation by the mean across the whole data set of the 96-well-plate reaction. The 1,8-naphthalimide-based fluorogenic probe was synthesized following the known literature procedure (*2*).

Detection limit

The detection limit of the HTS assay was determined by measuring the fluorescence intensity of samples with varying amount of organic azide product (0 – 260 uM) in a buffer medium containing 15 mM NaN_3. The presence of NaN_3 is to mimic the reaction conditions. Before measurement, samples were treated with 4-ethynyl-*N*-ethyl-1,8-naphthalimide probe and incubated for 1.5 hours following the protocol described in section (E). Reactions containing organic azide were measured in triplicate, and the blank was measured 9 times to determine the standard deviation. Detection limit was calculated from the best-fit equation using the definition of instrument detection limit:

$$S(LOD) = \mu_b + [3.3 \times \sigma_b]$$

Where the signal corresponding to the limit of detection (denoted as S(LOD)) is defined as the signal given from the average signal of the blank measurement, μ_b, plus 3.3 times the standard deviation of the blank, σ_b. With this equation, the detection limit was calculated to be *ca. 4 µM*. There was good linearity between fluorescence intensity and organic azide concentration in the range of 25 – 260 µM of organiz azide.

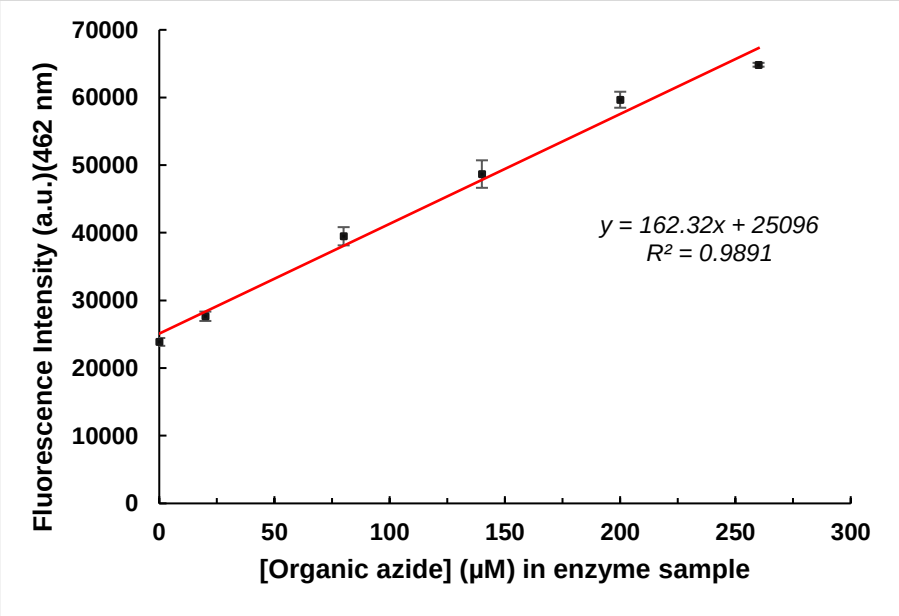

Figure S2. Fluorescence signal of alkyne probe in H_2O/DMF solution (V_{H2O}:V_{DMF} = 7:1, 25 mM KP_i, pH 7.0) in the presence of increasing amount of organic azide.

Table S2. Representative variants of *Sav* HppD identified during the course of evolution.

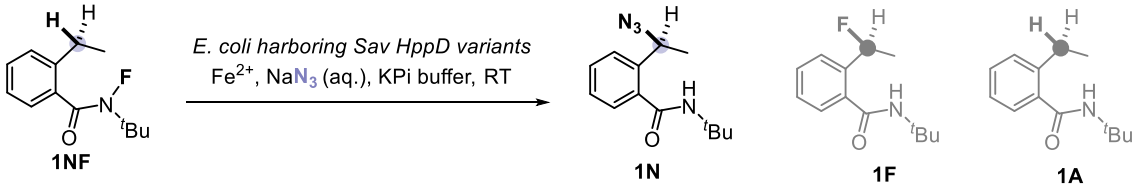

Entry	Acronym	Mutations from wt *Sav* HppD	TTN	e.r.	1N/1F	1N/1A
1	wt *Sav* HppD	None	250 ± 10	63:37	9.0	3.0
2	HppD AQ	V189A N245Q	320 ± 20	76:24	18.8	7.8
3	HppD AQI	V189A N245Q L367I	410 ± 10	79:21	27.6	9.8
4	HppD AQAI	V189A N245Q Q255A L367I	760 ± 20	87:13	35.5	9.3
5	HppD Az1	V189A F216A N245Q Q255A P243A L367I	1340 ± 40	86:14	53.8	15.5
6	HppD ALGFPI	V189A S230L P243G N245F Q255P L367I	430 ± 30	94:6	33.2	13.4
7	HppD Az2	V189A N191A S230L P243G N245F Q255P L367I	490 ± 20	96:4	30.6	19.3

Procedures: In an anaerobic chamber, ferrous ammonium sulfate (10 μL, 100 mM in water), sodium azide (10 μL, 1 M in water), and *N*-fluoroamide substrate **1NF** (10 μL, 400 mM in DME) were added to *E. coli* harboring non-heme iron enzymes (400 μL, adjusted to OD_{600} = 10) in a 2 mL screw top GC vial. The vial was capped and shaken at 680 rpm at room temperature for 24 hours. At the end of the reaction, the vial was opened and the reaction was quenched with 0.8 mL of a hexanes/ethylacetate solution (4:6 v/v) of internal standard 1,2,3-trimethoxybenzene (0.5 mM final concentration). The reaction mixture was transferred to a 2 mL microcentrifuge tube, vortexed (10 seconds, 3 times), then centrifuged (14,000xg, 5 min) to completely separate the organic and aqueous layers. An aliquot (200 - 300 μL) of the organic layer was used for product quantification via GCMS and enantioselectivity via chiral HPLC or chiral GC. Protein concentrations in whole cell solutions were determined using cell lysis and protein concentration measurement protocols described in sections F and G.

Michaelis−Menten Kinetic Analyses

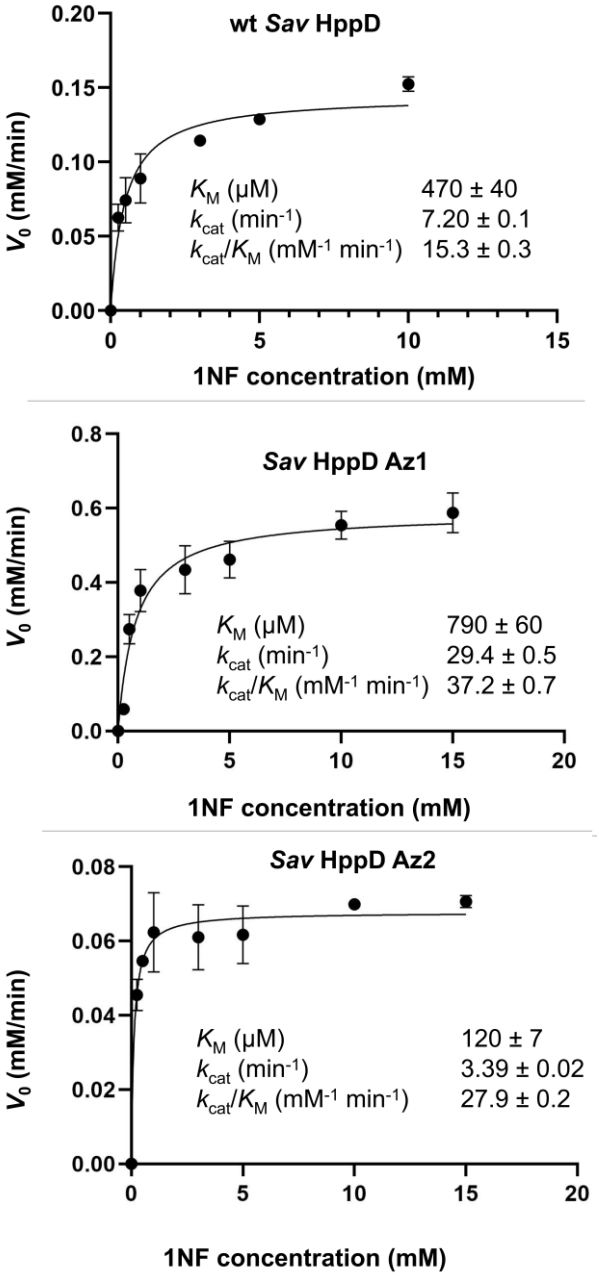

Figure S3. Michaelis-Menton parameters for the C–H azidation catalyzed by wt *Sav* HppD, *Sav* HppD Az1, and *Sav* HppD Az2 variants. **Experimental details**: In an anaerobic chamber, ferrous ammonium sulfate (10 μL, 100 mM in water) and sodium azide (10 μL, 1 M in water) were added to a buffer solution containing purified *Sav* HppD protein variant (20 μM, 2.4 mL) and the solution was shaken at 600 rpm for 5 minutes. A 1,2-dimethoxyethane solution of *N*-fluoroamide substrate **1NF** was added to the solution (final concentration ranging from 0.25 mM to 15 mM in reaction solution). An aliquot of 100 μL of the reaction mixture was removed at 3, 6, 9, 12, and 15 minutes and quenched by vortexing with 300 μL 6:4 EtOAc/hexanes solution containing 0.5 mM (final concentration) internal standard 1,2,3-trimethoxybenzene. After centrifugation at 12,000 rpm for 10 mins, an aliquot (200 μL) of the organic layer was taken for GCMS analysis for product quantification. Experiments were performed in triplicates.

Table S3. Reaction optimization for the biocatalytic azidation reaction

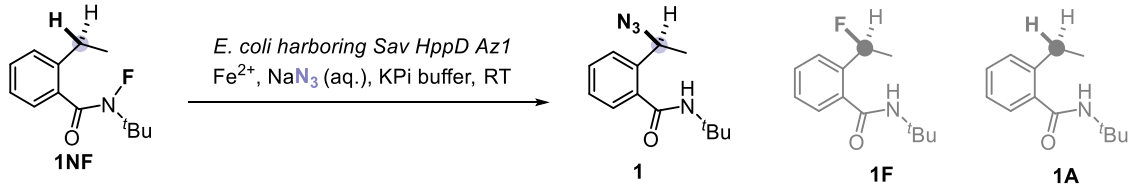

Entry	Variations from initial conditions	TTN	e.r.	1/1F	1/1A
1	None	1340 ± 40	87:13	54.0	15.5
2	NaN_3 (20 µL, 1 M)	1550 ± 40	87:13	52.0	14.0
3	OD_{600} = 10	1940 ± 20	87:13	48.0	16.4
4	**1NF** (10 µL, 800 mM), OD_{600} = 10	2480 ± 30	87:13	52.0	18.0
5	**1NF** (10 µL, 1.5 M), Fe^{2+} (20 uL, 100 mM) NaN_3 (40 µL, 1 M), OD_{600} = 10	3100 ± 60	87:13	47.0	19.5
6[a]	**1NF** (20 µL, 1.5 M), Fe^{2+} (20 uL, 100 mM) NaN_3 (40 µL, 1 M), OD_{600} = 10	4290 ± 50	87:13	55.0	20.0
7	**1NF** (20 µL, 1.5 M), Fe^{2+} (20 uL, 100 mM) NaN_3 (40 µL, 1 M), OD_{600} = 10, **Az2 variant**	260 ± 30	96:4	18.0	7.0
8	**1NF** (10 µL, 400 mM), Fe^{2+} (10 uL, 100 mM) NaN_3 (10 µL, 1 M), OD_{600} = 10, **Az2 variant**	490 ± 20	96:4	30.6	19.3
9	**1NF** (20 µL, 1.5 M), Fe^{2+} (20 uL, 100 mM) NaN_3 (40 µL, 1 M), OD_{600} = 40, **Az2 variant**	1820 ± 50	96:4	34.0	21.0

[a]Extraction was performed with 6 mL of internal standard solution.

Initial conditions: In an anaerobic chamber, ferrous ammonium sulfate (10 µL, 100 mM in water), sodium azide (10 µL, 1 M in water), and *N*-fluoroamide substrate **1NF** (10 µL, 400 mM in DME) were added to *E. coli* harboring *Sav* HppD Az1 (400 µL, adjusted to OD_{600} = 20) in a 2 mL screw top GC vial. The vial was capped and shaken at 680 rpm at room temperature for 24 hours. At the end of the reaction, the vial was opened and the reaction was quenched with 0.8 mL of a hexanes/ethylacetate solution (4:6 v/v) of internal standard 1,2,3-trimethoxybenzene (0.5 mM final concentration). The reaction mixture was transferred to a 2 mL microcentrifuge tube, vortexed (10 seconds, 3 times), then centrifuged (14,000xg, 5 min) to completely separate the organic and aqueous layers. An aliquot (200 - 300 µL) of the organic layer was used for product quantification via GCMS and enantioselectivity via chiral HPLC or chiral GC. Protein concentrations in whole cell solutions were determined using cell lysis and protein concentration measurement protocols described in sections F and G. The conditions in entry 6 (highlighted in blue) were used for substrate scope investigation with Az1 variant, whereas the conditions in entry 9 (highlighted in green) were used for substrate scope investigation with Az2 variant.

Scheme S2. Substrates that are not active for this biocatalytic azidation reaction.

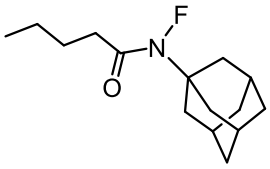
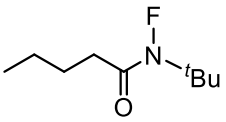
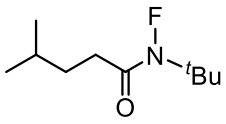
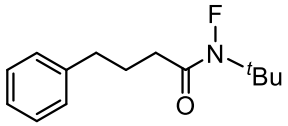
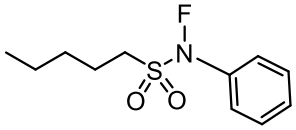
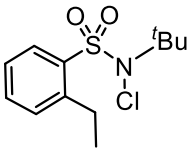
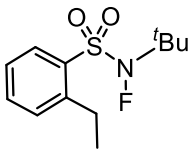
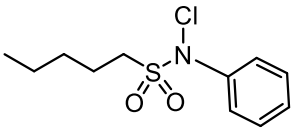
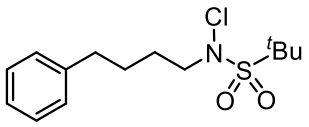
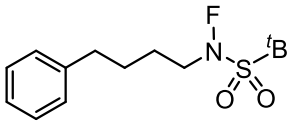

Table S4. Scope of nucleophilic anions for the developed enzymatic radical relay reaction

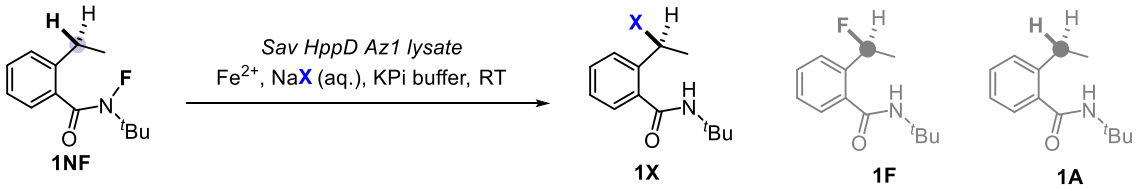

Entry	NaX	1X/internal	e.r.	1F/internal	1A/internal
1	NaF	n.d.	n.d.	0.04	2.5
2	NaBr	n.d.	n.d.	0.04	2.4
3	NaOCN	n.d.	n.d.	0.03	2.1
4	NaSCN	n.d.	n.d.	0.05	2.7
5	$NaNO_2$	n.d.	n.d.	0.03	1.9
6	NaCl	n.d.	n.d.	0.04	2.3
7	NaCN	n.d.	n.d.	0.04	2.4

Procedures: In an anaerobic chamber, ferrous ammonium sulfate (10 μL, 100 mM in water), sodium halide or pseudohalide solution (10 μL, 1 M in water), and *N*-fluoroamide substrate **1NF** (10 μL, 400 mM in DME) were added to a 2 mL vial containing *Sav* HppD Az1 cell lysate (400 μL, obtained from OD_{600} = 20 cell suspension following the general procedure F). The vial was capped and shaken at 680 rpm at room temperature for 24 hours. At the end of the reaction, the vial was opened and the reaction was quenched with 0.8 mL of a hexanes/ethylacetate solution (4:6 v/v) of internal standard 1,2,3-trimethoxybenzene (0.5 mM final concentration). The reaction mixture was transferred to a 2 mL microcentrifuge tube, vortexed (10 seconds, 3 times), then centrifuged (14,000xg, 5 min) to completely separate the organic and aqueous layers. An aliquot (200 - 300 μL) of the organic layer was used for product quantification via GCMS. **1X**/internal refers to the ratio of peak area of **1X** over that of the internal standard as determined by GCMS total ion chromatogram. **1F**/internal and **1A**/internal were defined and calculated accordingly.

Kinetic Isotope Effect

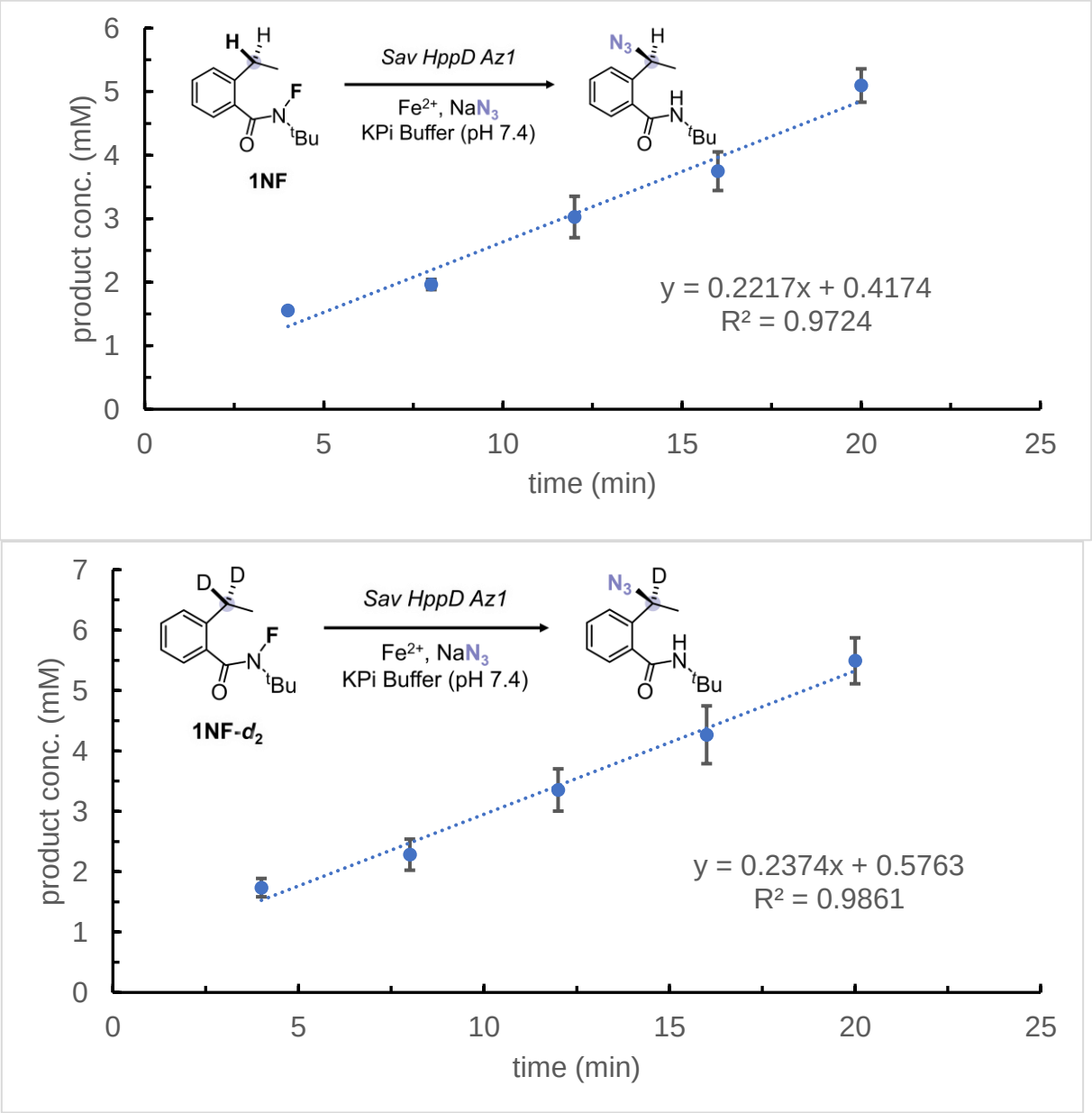

Figure S4. Kinetic isotope effect of C–H azidation catalyzed by *Sav* HppD Az1. Determination of initial rates: Initial rates were measured from independent reactions set up in parallel using purified *Sav* HppD Az1 (protein concentration = 10 µM). Experimental details: In an anaerobic chamber, ferrous ammonium sulfate (10 µL, 100 mM in water) and sodium azide (10 µL, 1 M in water) were added to a buffer solution containing purified *Sav* HppD Az1 (10 µM, 2.4 mL) and the solution was shaken at 600 rpm for 5 minutes. A 1,2-dimethoxyethane solution of *N*-fluoroamide substrate **1NF** was added to the solution (final concentration 10 mM in reaction solution). An aliquot of 100 µL of the reaction mixture was removed at 4, 8, 12, 16, and 20 minutes and quenched by vortexing with 300 µL 6:4 EtOAc/hexanes solution containing 0.5 mM (final concentration) internal standard 1,2,3-trimethoxybenzene. After centrifugation at 12,000 rpm for 10 mins, an aliquot (200 µL) of the organic layer was taken for GCMS analysis for product quantification.

Multivariate analysis of substituent effect

Scheme S3. Multivariate analysis was carried out following the method developed by Fujita and Nishioka using the equation $\log(k_X/k_H) = \rho\sigma + fF + \delta E_s + c$ (3). In this equation, σ is the substituent constant for ordinary polar effect, F is the Swain-Lupton F constant for the consideration of proximal polar effect, and E_s is the substituent constant for steric effect of a substituent, c is the intercept, and ρ, f, and δ are susceptibility constants. **(A)** Multivariate analysis of substituent effect assuming that N−F activation is the rate-determining step. **(B)** Multivariate analysis of substituent effect assuming that 1,5-hydrogen atom transfer is the rate-determining step. For both mechanistic scenarios, low R^2 values were obtained for multivariate analysis. Nonetheless, the negative ρ and f values in both cases suggests the accumulation of partial negative charge in the transition state of the rate-determining step, whereas the positive δ value indicates the steric properties of the substituent could negatively impact the reactivity.

(A)

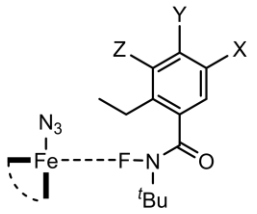

$\log(k_X/k_H) = -0.78\sigma - 0.14F + 0.24E_s + 0.028$
($R^2 = 0.54$)

X	Y	Z	$\log(k_X/k_H)$	σ	F	E_s
H	H	Me	-0.076	-0.17	-0.04	-1.24
H	H	OMe	-0.061	-0.27	0.26	-0.55
H	H	H	0.000	0	0	0
F	H	H	-0.466	0.06	0.43	-0.46
Me	H	H	-0.375	-0.17	-0.04	-1.24
H	F	H	-0.236	0.34	0.43	-0.46

(B)

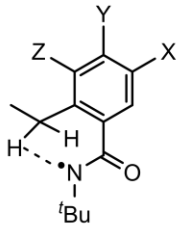

$\log(k_X/k_H) = -0.19\sigma - 0.44F + 0.23E_s + 0.018$
($R^2 = 0.44$)

X	Y	Z	$\log(k_X/k_H)$	σ	F	E_s
H	H	Me	-0.076	-0.07	-0.04	-1.24
H	H	OMe	-0.061	0.12	0.26	-0.55
H	H	H	0.000	0	0	0
F	H	H	-0.466	0.34	0.43	-0.46
Me	H	H	-0.375	-0.07	-0.04	-1.24
H	F	H	-0.236	0.06	0.43	-0.46

Scheme S4. Summary of known catalytic systems for C–N_3 bond formation via metal-catalyzed radical relay mechanisms (*4-7*).

Bao et al. *Nat. Commun.*, **2019**, *10*, 769.

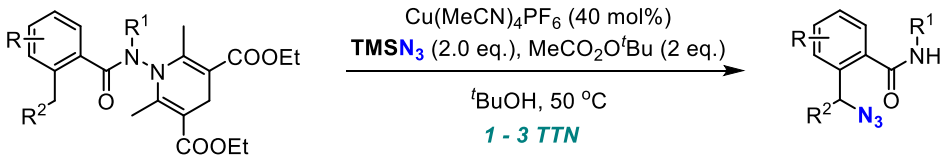

Torres-Ochoa et al. *Chem. Eur. J.*, **2019**, *25*, 9477.

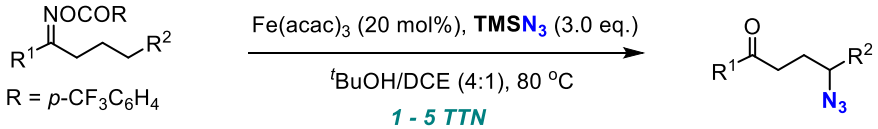

Bian et al. *Org. Biomol. Chem.*, **2020**, *18*, 5354.

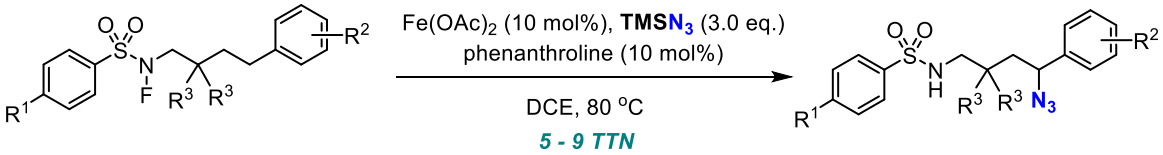

Min et al. *Org. Chem. Front.*, **2021**, *8*, 249

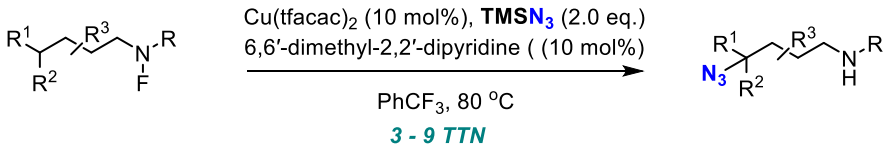

IV. Sequence information for final variants

The DNA sequences encoding 4-hydroxyphenylpyruvate dioxygenase (HppD) from *Streptomyces avermitilis* (Uniprot number Q53586) were codon-optimized for over-expression in *E. coli*, synthesized, and inserted into the NdeI and XhoI restriction sites of expression vector pET-22b(+). The gene sequences of wild-type *Sav* HppD and the final variants *Sav* HppD Az1 and *Sav* HppD Az2 are shown below (mutations highlighted in blue).

wt *Sav* HppD

ATGACGCAGACTACACATCACACGCCCGACACGGCACGTCAGGCAGATCCATTT
CCAGTGAAGGGTATGGATGCTGTTGTGTTCGCTGTAGGTAATGCAAAACAGGCG
GCGCACTATTACAGCACAGCCTTTGGGATGCAGTTGGTGGCCTACAGTGGTCCCG
AAAATGGGAGCCGTGAGACCGCCTCGTATGTCTTGACCAACGGATCAGCGCGTT
TCGTCCTGACAAGCGTTATTAAGCCGGCCACGCCATGGGGACATTTCCTTGCAGA
TCACGTTGCAGAGCACGGAGATGGAGTTGTAGACCTGGCTATTGAAGTCCCCGA
CGCCCGTGCCGCTCACGCCTACGCTATCGAACACGGTGCCCGCTCCGTGGCGGAA
CCGTACGAATTAAAGGACGAGCACGGCACGGTCGTTTTGGCTGCCATCGCCACCT
ACGGCAAAACGCGCCACACACTGGTAGACCGTACGGGCTACGACGGGCCATACT
TGCCGGGGTACGTAGCTGCCGCCCCTATTGTCGAGCCCCCTGCGCACCGCACCTT
CCAAGCTATTGACCACTGTGTAGGTAATGTGGAATTAGGACGCATGAACGAATG
GGTGGGCTTCTATAATAAGGTTATGGGGTTCACCAACATGAAAGAGTTTGTAGGG
GATGACATTGCAACAGAATATTCGGCCCTGATGTCAAAAGTGGTCGCTGATGGG
ACCCTTAAAGTAAAATTTCCCATTAACGAACCCGCTTTAGCAAAGAAGAAATCTC
AAATTGATGAATACTTAGAATTTTACGGAGGAGCGGGAGTCCAACATATCGCTTT
AAACACGGGCGACATCGTGGAGACGGTCCGTACCATGCGTGCAGCTGGGGTACA
ATTCCTGGACACTCCCGATTCATACTATGACACGCTTGGTGAGTGGGTTGGCGAT
ACTCGTGTTCCGGTCGACACTCTTCGTGAGCTGAAAATCTTGGCGGATCGCGACG
AGGATGGATACTTATTACAAATTTTTACTAAACCAGTGCAGGACCGTCCTACCGT
TTTCTTCGAAATTATTGAGCGTCATGGGAGCATGGGGTTTGGTAAGGGGAATTTC
AAGGCCCTTTTTGAGGCAATCGAGCGTGAGCAAGAGAAACGCGGGAATTTA

Sav HppD Az1 (V189A F216A N245Q Q255A P243A L367I)

ATGACGCAGACTACACATCACACGCCCGACACGGCACGTCAGGCAGATCCATTT
CCAGTGAAGGGTATGGATGCTGTTGTGTTCGCTGTAGGTAATGCAAAACAGGCG
GCGCACTATTACAGCACAGCCTTTGGGATGCAGTTGGTGGCCTACAGTGGTCCCG
AAAATGGGAGCCGTGAGACCGCCTCGTATGTCTTGACCAACGGATCAGCGCGTT
TCGTCCTGACAAGCGTTATTAAGCCGGCCACGCCATGGGGACATTTCCTTGCAGA
TCACGTTGCAGAGCACGGAGATGGAGTTGTAGACCTGGCTATTGAAGTCCCCGA
CGCCCGTGCCGCTCACGCCTACGCTATCGAACACGGTGCCCGCTCCGTGGCGGAA
CCGTACGAATTAAAGGACGAGCACGGCACGGTCGTTTTGGCTGCCATCGCCACCT
ACGGCAAAACGCGCCACACACTGGTAGACCGTACGGGCTACGACGGGCCATACT
TGCCGGGGTACGTAGCTGCCGCCCCTATTGTCGAGCCCCCTGCGCACCGCACCTT
CCAAGCTATTGACCACTGT***GCT***GGTAATGTGGAATTAGGACGCATGAACGAATG
GGTGGGCTTCTATAATAAGGTTATGGGGTTCACCAACATGAAAGAG***GCT***GTAGG
GGATGACATTGCAACAGAATATTCGGCCCTGATGTCAAAAGTGGTCGCTGATGG
GACCCTTAAAGTAAAATTT***GCT***ATT***CAG***GAACCCGCTTTAGCAAAGAAGAAATCT
GCTATTGATGAATACTTAGAATTTTACGGAGGAGCGGGAGTCCAACATATCGCTT
TAAACACGGGCGACATCGTGGAGACGGTCCGTACCATGCGTGCAGCTGGGGTAC

AATTCCTGGACACTCCCGATTCATACTATGACACGCTTGGTGAGTGGGTTGGCGA
TACTCGTGTTCCGGTCGACACTCTTCGTGAGCTGAAAATCTTGGCGGATCGCGAC
GAGGATGGATACTTATTACAAATTTTTACTAAACCAGTGCAGGACCGTCCTACCG
TTTTCTTCGAAATTATTGAGCGTCATGGGAGCATGGGGTTTGGTAAGGGGAATTT
CAAGGCC***ATT***TTTGAGGCAATCGAGCGTGAGCAAGAGAAACGCGGGAATTTA

Sav HppD Az2 (V189A N191A S230L P243G N245F Q255P L367I)

ATGACGCAGACTACACATCACACGCCCGACACGGCACGTCAGGCAGATCCATTT
CCAGTGAAGGGTATGGATGCTGTTGTGTTCGCTGTAGGTAATGCAAAACAGGCG
GCGCACTATTACAGCACAGCCTTTGGGATGCAGTTGGTGGCCTACAGTGGTCCCG
AAAATGGGAGCCGTGAGACCGCCTCGTATGTCTTGACCAACGGATCAGCGCGTT
TCGTCCTGACAAGCGTTATTAAGCCGGCCACGCCATGGGGACATTTCCTTGCAGA
TCACGTTGCAGAGCACGGAGATGGAGTTGTAGACCTGGCTATTGAAGTCCCCGA
CGCCCGTGCCGCTCACGCCTACGCTATCGAACACGGTGCCCGCTCCGTGGCGGAA
CCGTACGAATTAAAGGACGAGCACGGCACGGTCGTTTTGGCTGCCATCGCCACCT
ACGGCAAAACGCGCCACACACTGGTAGACCGTACGGGCTACGACGGGCCATACT
TGCCGGGGTACGTAGCTGCCGCCCCTATTGTCGAGCCCCCTGCGCACCGCACCTT
CCAAGCTATTGACCACTGT***GCT***GGT***GCG***GTGGAATTAGGACGCATGAACGAATG
GGTGGGCTTCTATAATAAGGTTATGGGGTTCACCAACATGAAAGAGTTTGTAGGG
GATGACATTGCAACAGAATATTCGGCCCTGATG***CTT***AAAGTGGTCGCTGATGGG
ACCCTTAAAGTAAAATTT***GGT***ATT***TTT***GAACCCGCTTTAGCAAAGAAGAAATCT***C***
CGATTGATGAATACTTAGAATTTTACGGAGGAGCGGGAGTCCAACATATCGCTTT
AAACACGGGCGACATCGTGGAGACGGTCCGTACCATGCGTGCAGCTGGGGTACA
ATTCCTGGACACTCCCGATTCATACTATGACACGCTTGGTGAGTGGGTTGGCGAT
ACTCGTGTTCCGGTCGACACTCTTCGTGAGCTGAAAATCTTGGCGGATCGCGACG
AGGATGGATACTTATTACAAATTTTTACTAAACCAGTGCAGGACCGTCCTACCGT
TTTCTTCGAAATTATTGAGCGTCATGGGAGCATGGGGTTTGGTAAGGGGAATTTC
AAGGCC***ATT***TTTGAGGCAATCGAGCGTGAGCAAGAGAAACGCGGGAATTTA

V. Substrate Synthesis and Characterization

General Procedure for the synthesis of amide precursors

Synthetic procedure A

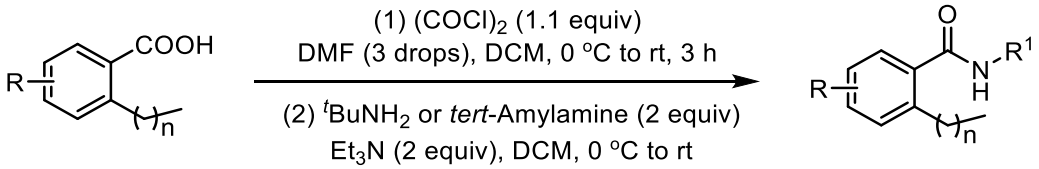

The carboxylic acid starting materials were commercially available or synthesized following a known literature procedure (*8*). To prepare the desired amide, oxalyl chloride (11 mmol, 1.1 equiv) was slowly added at 0 °C to a solution of the acid (10 mmol, 1.0 equiv) and DMF (3 drops) in dry DCM (15 mL). After stirring at room temperature for 3 h, the solvent was removed under vacuum and the residue was dissolved in dry DCM. *t*BuNH$_2$ or *tert*-Amylamine (20 mmol, 2.0 equiv) and Et$_3$N (20 mmol, 2.0 equiv) were added and the reaction was followed by TLC until it completed. Water (100 mL) was added and the resulting mixture was extracted with DCM (3 ´ 150 mL). Removal of the solvent under vacuum and the crude amide was directly used in the next step.

Synthetic procedure B

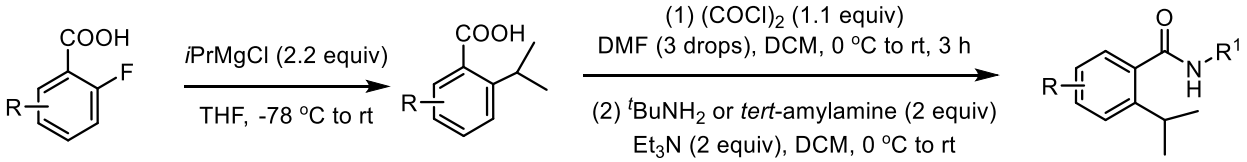

2-fluorobenzoic acid derivative (10 mmol, 1.0 equiv) was dissolved in dry THF and stirred at -78 °C under N$_2$. *i*PrMgCl (22 mmol, 2.2 equiv) was added to the solution at -78 °C. After stirring at room temperature for 48 h, the reaction was quenched with HCl (2.0 M). Then, water (100 mL) was added and the resulting mixture was extracted with DCM (3 ´ 150 mL). Removal of the solvent under vacuum and the crude amide was directly used in the next step. Oxalyl chloride (11 mmol, 1.1 equiv) was slowly added at 0 °C to a solution of the acid (10 mmol, 1.0 equiv) and DMF (3 drops) in dry DCM (15 mL). After stirring at room temperature for 3 h, the solvent was removed under vacuum and the residue was dissolved in dry DCM. *t*BuNH$_2$ or *tert*-Amylamine (20 mmol, 2.0 equiv) and Et$_3$N (20 mmol, 2.0 equiv) were added and the reaction was followed by TLC until it completed. Water (100 mL) was added and the resulting mixture was extracted with DCM (3 ´ 150 mL). Removal of the solvent under vacuum and the crude amide was directly used in the next step.

General Procedure for the synthesis of *N*-fluoro-2-alkylbenzamides

This synthesis protocol was following the known literature procedure (*9*). Namely, amide derivative (10 mmol, 1.0 equiv) was dissolved in dry THF and stirred at 0 °C under N$_2$. *n*BuLi (12 mmol, 1.2 equiv) was added dropwise. The reaction was maintained at 0 °C for 1.5 h. NFSI (1.5 equiv, 0.5 M in THF) was added. The reaction was left overnight in the ice bath and allowed to warm to room temperature. After 16 h, the reaction was quenched with 1 M aqueous HCl. Then, Water (100 mL) was added and the resulting mixture was extracted with DCM (3

´ 150 mL). Removal of the solvent under vacuum and the crude was purified by Biotage flash chromatography to afford *N*-fluoroamides as yellow to red liquid.

***N*-(*tert*-butyl)-2-ethyl-*N*-fluorobenzamide (1NF)**

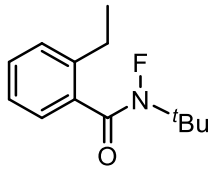

^{1}H NMR (300.1 MHz, $CDCl_3$): δ 7.38-7.18 (m, 4H), 2.74 (q, *J* = 7.6 Hz, 2H), 1.56 (d, *J* = 2.0 Hz, 9H), 1.25 (t, *J* = 7.6 Hz, 3H); **^{13}C NMR (75 MHz, $CDCl_3$):** δ 175.0 (d, *J* = 11.0 Hz), 141.6 (d, *J* = 2.2 Hz), 134.6 (d, *J* = 1.1 Hz), 130.0 (d, *J* = 1.1 Hz), 128.9 (d, *J* = 1.1 Hz), 127.1 (d, *J* = 4.4 Hz), 125.3 (d, *J* = 1.1 Hz), 64.2 (d, *J* = 10.3 Hz), 27.14 (d, *J* = 5.5 Hz), 26.1, 15.6; **^{19}F NMR (282.4 MHz, $CDCl_3$):** δ -62.8 (s). HRMS calcd for C26H36F2KN2O2 (2M + K) 485.2382, found 485.2395. HRMS calcd for $C_{26}H_{36}F_2KN_2O_2$ (2M + K) 485.2382, found 485.2395.

***N*-(*tert*-butyl)-2-ethyl-*N*-fluoro-5-methylbenzamide (2NF)**

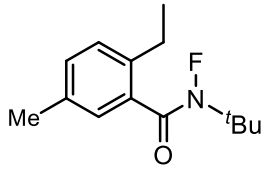

^{1}H NMR (300.1 MHz, $CDCl_3$) δ 7.16-7.15 (m, 2H), 7.12-7.11 (m, 1H), 2.69 (q, *J* = 7.6 Hz, 2H), 2.33 (s, 3H), 1.55 (d, *J* = 2.0 Hz, 9H), 1.22 (t, *J* = 7.6 Hz, 3H); **^{13}C NMR (75 MHz, $CDCl_3$)** δ 175.2 (d, *J* = 11.0 Hz), 138.5 (d, *J* = 2.2 Hz), 134.9 (d, *J* = 1.1 Hz), 134.5 (d, *J* = 1.1 Hz), 130.8 (d, *J* = 1.1 Hz), 128.8 (d, *J* = 1.1 Hz), 127.5 (d, *J* = 4.2 Hz), 64.3 (d, *J* = 10.5 Hz), 27.2 (d, *J* = 6.0 Hz), 25.7, 20.8, 15.7; **^{19}F NMR (282.4 MHz, $CDCl_3$)** δ -62.9 (s). HRMS calcd for $C_{28}H_{40}F_2KN_2O_2$ (2M + K) 513.2695, found 513.2689.

***N*-(*tert*-butyl)-2-ethyl-*N*,5-difluorobenzamide (3NF)**

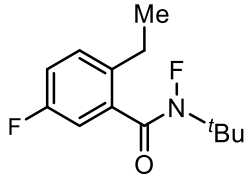

^{1}H NMR (300.1 MHz, $CDCl_3$) δ 7.24-7.19 (m, 1H), 7.09-6.99 (m, 2H), 2.69 (q, *J* = 7.6 Hz, 2H), 1.55 (d, *J* = 2.0 Hz, 9H), 1.22 (t, *J* = 7.6 Hz, 3H); **^{13}C NMR (75 MHz, $CDCl_3$)** δ 173.3 (dd, *J* = 11.0 Hz, 2.2 Hz), 160.3 (dd, *J* = 245.3 Hz, 1.4 Hz), 137.3 (dd, *J* = 3.8 Hz, 2.2 Hz), 135.9 (dd, *J* = 7.0 Hz, 0.8 Hz), 130.5 (dd, *J* = 7.0 Hz, 1.4 Hz), 116.9 (dd, *J* = 21.0 Hz, 1.4 Hz), 114.5 (dd, *J* = 23.1 Hz, 4.4 Hz), 64.5 (d, *J* = 10.3 Hz), 27.1 (d, *J* = 5.5 Hz), 25.4, 15.7; **^{19}F NMR (282.4 MHz, $CDCl_3$)** δ -63.2 (s), -116.9 – -117.0 (m). HRMS calcd for $C_{26}H_{34}F_4KN_2O_2$ (2M + K) 521.2193, found 521.2188.

***N*-(*tert*-butyl)-2-ethyl-*N*,4-difluorobenzamide (4NF)**

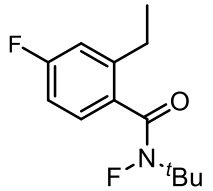

^{1}H NMR (300.1 MHz, $CDCl_3$) δ 7.33-7.26 (m, 1H), 6.98-6.87 (m, 2H), 2.74 (q, *J* = 7.6 Hz, 2H), 1.54 (d, *J* = 2.1 Hz, 9H), 1.24 (t, *J* = 7.6 Hz, 3H); **^{13}C NMR (75 MHz, $CDCl_3$)** δ 174.1 (d, *J* = 10.6 Hz), 163.6 (dd, *J* = 246.2 Hz, 1.4 Hz), 145.1 (dd, *J* = 7.6 Hz, 1.8 Hz), 130.6 (dd, *J* = 3.4 Hz, 0.8 Hz), 129.5 (dd, *J* = 8.1 Hz, 4.2 Hz), 115.7 (dd, *J* = 21.0 Hz, 1.3 Hz), 112.4 (dd, *J* = 21.0 Hz, 1.3 Hz), 64.4 (d, *J* = 10.5 Hz), 27.1 (d, *J* = 5.6 Hz), 26.0 (d, *J* = 1.8 Hz), 15.2; **^{19}F NMR (282.4 MHz, $CDCl_3$)** δ -63.2 (s), -116.9 – -117.0 (m). HRMS calcd for $C_{26}H_{34}F_4KN_2O_2$ (2M + K) 521.2193, found 521.2188.

***N*-(*tert*-butyl)-2-ethyl-*N*-fluoro-3-methylbenzamide (5NF)**

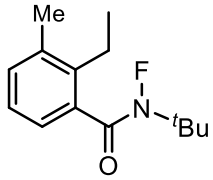

^{1}H NMR (300.1 MHz, $CDCl_3$) δ 7.34-7.14 (m, 3H), 2.73 (q, *J* = 7.6 Hz, 2H), 2.38 (s, 3H), 1.59 (d, *J* = 2.0 Hz, 9H), 1.21 (t, *J* = 7.6 Hz, 3H); **^{13}C NMR (75 MHz, $CDCl_3$)** δ 175.5 (d, *J* = 11.0 Hz), 139.4 (d, *J* = 2.2 Hz), 136.7 (d, *J* = 1.4 Hz), 135.4 (d, *J* = 1.1 Hz), 131.8, 125.3, 124.6 (d, *J* = 5.8 Hz), 64.2 (d, *J* = 10.2 Hz), 27.2 (d, *J* = 4.8 Hz), 23.4, 19.2 (d, *J* = 1.4 Hz), 14.5; **^{19}F NMR (282.4 MHz, $CDCl_3$)** δ -62.0 (s). HRMS calcd for $C_{28}H_{40}F_2KN_2O_2$ (2M + K) 513.2695, found 513.2689.

2-ethyl-*N*-fluoro-*N*-(*tert*-pentyl)benzamide (6NF)

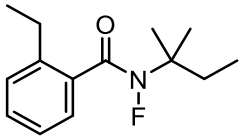

^{1}H NMR (300.1 MHz, $CDCl_3$) δ 7.35-7.21 (m, 4H), 2.74 (q, *J* = 7.6 m, 2H), 1.92 (q, *J* = 7.6 Hz, 2H), 1.53 (d, *J* = 1.9 Hz, 6H), 1.25 (t, *J* = 7.6 Hz, 3H), 1.03 (t, *J* = 7.6 Hz, 3H); **^{13}C NMR (75 MHz, $CDCl_3$)** δ 174.2 (d, *J* = 11.1 Hz), 141.4 (d, *J* = 2.2 Hz), 134.8 (d, *J* = 0.8 Hz), 129.9 (d, *J* = 1.4 Hz), 128.8 (d, *J* = 1.1 Hz), 127.0 (d, *J* = 4.2 Hz), 125.3 (d, *J* = 1.4 Hz), 67.3 (d, *J* = 9.8 Hz), 32.9 (d, *J* = 5.2 Hz), 26.1, 24.9 (d, *J* = 5.5 Hz), 15.6, 8.6; **^{19}F NMR (282.4 MHz, $CDCl_3$)** δ -64.7 (s). HRMS calcd for $C_{28}H_{40}F_2KN_2O_2$ (2M + K) 513.2695, found 513.2689.

***N*-(tert-butyl)-2-ethyl-*N*-fluoro-3-methoxybenzamide (7NF)**

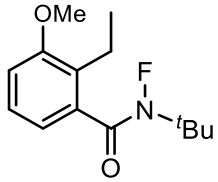

^{1}H NMR (300.1 MHz, $CDCl_3$) δ 7.21-7.12 (m, 1H), 6.90-6.87 (m, 2H), 3.84 (s, 3H), 2.69 (q, *J* = 7.6 Hz, 2H), 2.69 (d, *J* = 2.6 Hz, 9H), 1.21 (t, *J* = 7.6 Hz, 3H); **^{13}C NMR (75 MHz, $CDCl_3$)** δ 174.6 (d, *J* = 11.0 Hz), 157.5, 136.1, 130.1 (d, *J* = 2.2 Hz), 126.4 (d, *J* = 1.2 Hz), 118.7 (d, *J* = 3.8 Hz), 111.5 (d, *J* = 1.5 Hz), 64.3 (d, *J* = 11 Hz), 55.5, 27.2 (d, *J* = 5.4 Hz), 20.7, 14.4; **^{19}F NMR (282.4 MHz, $CDCl_3$)** δ -62.6 (s). HRMS calcd for $C_{28}H_{40}F_2KN_2O_4$ (2M + K) 545.2593, found 545.2602.

***N*-(*tert*-butyl)-*N*-fluoro-2-propylbenzamide (8NF)**

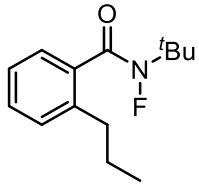

^{1}H NMR (300.1 MHz, $CDCl_3$) δ 7.36-7.30 (m, 2H), 7.25-7.18 (m, 2H), 2.68 (q, *J* = 7.6 Hz, 2H), 1.68-1.60 (m, 2H), 1.55 (d, *J* = 2.0 Hz, 9H), 0.95 (t, *J* = 7.6 Hz, 3H); **^{13}C NMR (75 MHz, $CDCl_3$)** δ 174.9 (d, *J* = 11.1 Hz), 140.1 (d, *J* = 2.2 Hz), 134.9 (d, *J* = 0.8 Hz), 129.8 (d, *J* = 1.4 Hz), 129.6 (d, *J* = 1.1 Hz), 127.2 (d, *J* = 4.4 Hz), 125.3 (d, *J* = 1.4 Hz), 64.2 (d, *J* = 9.6 Hz), 35.1, 27.1 (d, *J* = 5.3 Hz), 24.6, 14.0; **^{19}F NMR (282.4 MHz, $CDCl_3$)** δ -62.8 (s). RMS calcd for $C_{28}H_{40}F_2KN_2O_2$ (2M + K) 513.2695, found 513.2689.

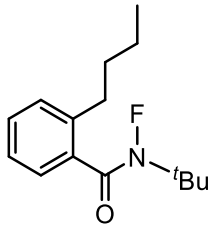

***N*-(*tert*-butyl)-2-butyl-*N*-fluorobenzamide (9NF)**

^{1}H NMR (300.1 MHz, $CDCl_3$) δ 7.34-7.30 (m, 2H), 7.25-7.21 (m, 2H), 2.71 (q, *J* = 7.6 Hz, 2H), 1.85-1.60 (m, 2H), 1.56 (d, *J* = 2.0 Hz, 9H), 1.43-1.31 (m, 2H), 0.95 (t, *J* = 7.6 Hz, 3H); **^{13}C NMR (75 MHz, $CDCl_3$)** δ 174.9 (d, *J* = 11.1 Hz), 140.3 (d, *J* = 2.2 Hz), 134.8 (d, *J* = 0.8 Hz), 129.8 (d, *J* = 1.4 Hz), 129.6 (d, *J* = 1.1 Hz), 127.2 (d, *J* = 4.4 Hz), 125.3 (d, *J* = 1.4 Hz), 64.3 (d, *J* = 9.6 Hz), 33.6, 32.8, 27.1 (d, *J* = 5.3 Hz), 22.7, 13.9; **^{19}F NMR (282.4 MHz, $CDCl_3$)** δ -62.8 (s). HRMS calcd for $C_{30}H_{44}F_2KN_2O_2$ (2M + K) 541.3008, found 541.3002.

2-(but-3-en-1-yl)-*N*-(*tert*-butyl)-*N*-fluorobenzamide (10NF)

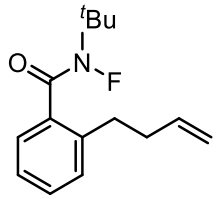

^{1}H NMR (300.1 MHz, $CDCl_3$) δ 7.38-7.24 (m, 4H), 5.93-5.84 (m, 1H), 5.10-4.99 (m, 2H), 2.87-2.82 (m, 2H), 2.44-2.39 (m, 2H), 1.57 (d, *J* = 2.0 Hz, 9H); **^{13}C NMR (75 MHz, $CDCl_3$)** δ 174.8 (d, *J* = 10.8 Hz), 139.3 (d, *J* = 2.2 Hz), 137.8, 134.9, 129.9, 129.7, 127.32 (d, *J* = 4.3 Hz), 125.6, 115.0, 64.2 (d, *J* = 10.2 Hz), 35.5, 32.6, 27.1 (d, *J* = 5.5 Hz); **^{19}F NMR (282.4 MHz, $CDCl_3$)** δ -62.8 (s). HRMS calcd for $C_{30}H_{40}F_2KN_2O_2$ (2M + K) 537.2695, found 537.2689.

***N*-(*tert*-butyl)-*N*-fluoro-2-methylbenzamide** (**11NF**)

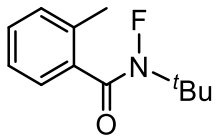

^{1}H NMR (300 MHz, $CDCl_3$) δ 7.36-7.31 (m, 2H), 7.28-7.23 (m, 2H), 2.43 (s, 3H), 1.57 (d, *J* = 2.2 Hz, 9H); **^{13}C NMR (75 MHz, $CDCl_3$)** δ 175.0 (d, *J* = 11.4 Hz), 135.4 (d, *J* = 2.4 Hz), 135.1 (d, *J* = 1.1 Hz), 130.4 (d, *J* = 1.1 Hz), 129.9 (d, *J* = 1.4 Hz), 127.2 (d, *J* = 4.5 Hz), 125.3 (d, *J* = 1.1 Hz), 64.4 (d, *J* = 10.4 Hz), 27.2 (d, *J* = 5.5 Hz), 19.3; **^{19}F NMR (282 MHz, $CDCl_3$)** δ -64.1 (s). HRMS calcd for $C_{24}H_{32}F_2KN_2O_2$ (2M + K) 457.2069, found 457.2076.

4-bromo-*N*-(*tert*-butyl)-*N*-fluoro-2-methylbenzamide (12NF)

^{1}H NMR (300 MHz, $CDCl_3$) δ 7.40-7.36 (m, 2H), 7.28-7.23 (d, *J* = 8.2 Hz, 1H), 2.40 (s, 3H), 1.56 (d, *J* = 2.0 Hz, 9H); **^{13}C NMR (75 MHz, $CDCl_3$)** δ 173.9 (d, *J* = 11.2 Hz), 137.8 (d, *J* = 2.3 Hz), 133.9 (d, *J* = 1.0 Hz), 133.4, 128.8 (d, *J* = 4.5 Hz), 128.6 (d, *J* = 1.0 Hz), 124.1 (d, *J* = 1.1 Hz), 64.6 (d, *J* = 10.1 Hz), 27.1 (d, *J* = 5.2 Hz), 19.2; **^{19}F NMR (282 MHz, $CDCl_3$)** δ -63.9 (s). HRMS calcd for $C_{24}H_{30}Br_2F_2KN_2O_2$ (2M + K) 615.0259, found 615.0266.

***N*-(*tert*-butyl)-*N*-fluoro-5-methoxy-2-methylbenzamide (13NF)**

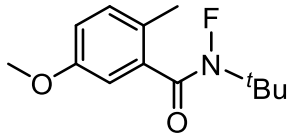

^{1}H NMR (300 MHz, $CDCl_3$) δ 7.14-7.11 (m, 1H), 6.90-6.86 (m, 2H), 3.81 (s, 3H), 2.34 (s, 3H), 1.57 (d, *J* = 2.1 Hz, 9H); **^{13}C NMR (75 MHz, $CDCl_3$)** δ 174.6 (d, *J* = 11.0 Hz), 157.2 (d, *J* = 1.0 Hz), 135.8 (d, *J* = 1.0 Hz), 131.4 (d, *J* = 1.0 Hz), 127.1 (d, *J* = 2.6 Hz), 115.9 (d, *J* = 1.5 Hz), 112.3 (d, *J* = 4.6 Hz), 64.4 (d, *J* = 10.1 Hz), 55.4, 27.2 (d, *J* = 5.4 Hz), 18.3; **^{19}F NMR (282 MHz, $CDCl_3$)** δ -64.5 (s). HRMS calcd for $C_{26}H_{36}F_2KN_2O_4$ (2M + K) 517.2280, found 517.2289.

***N*-(*tert*-butyl)-*N*,5-difluoro-2-methylbenzamide (14NF)**

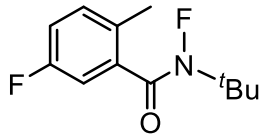

^{1}H NMR (300 MHz, $CDCl_3$) δ 7.28-7.16 (m, 1H), 7.07-6.99 (m, 2H), 2.37 (s, 3H), 1.57 (d, *J* = 2.0 Hz, 9H); **^{13}C NMR (75 MHz, $CDCl_3$)** δ 173.4 (dd, *J* = 11.0 Hz, *J* = 2.4 Hz), 159.4 (dd, *J* = 245.0 Hz, *J* = 1.5 Hz), 136.3 (d, *J* = 7.6 Hz), 131.9 (dd, *J* = 7.6 Hz, *J* = 1.0 Hz), 130.9 (dd, *J* = 3.6 Hz, *J* = 2.5 Hz), 116.7 (dd, *J* = 21.0 Hz, *J* = 1.2 Hz), 114.1 (dd, *J* = 23.2 Hz, *J* = 4.5 Hz), 64.5 (d, *J* = 10.4 Hz), 27.1 (d, *J* = 5.2 Hz), 18.5; **^{19}F NMR (282 MHz, $CDCl_3$)** δ -64.6 (s), -116.9 – -117.0 (m). HRMS calcd for $C_{24}H_{30}F_4KN_2O_2$ (2M + K) 493.1880, found 493.1890.

***N*-(*tert*-butyl)-*N*-fluoro-2-isopropylbenzamide (15NF)**

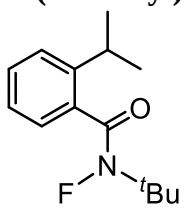

^{1}H NMR (300 MHz, $CDCl_3$) δ 7.44-7.37 (m, 2H), 7.30-7.20 (m, 2H), 3.26-3.12 (m, 1H), 1.59 (d, *J* = 2.0 Hz, 9H), 1.29 (d, *J* = 7.0 Hz, 6H); **^{13}C NMR (75 MHz, $CDCl_3$)** δ 175.1 (d, *J* = 11.4 Hz), 145.9 (d, *J* = 2.5 Hz), 134.4, 129.9 (d, *J* = 1.2 Hz), 126.6 (d, *J* = 4.0 Hz), 125.6 (d, *J* = 1.2 Hz), 125.3 (d, *J* = 1.2 Hz), 64.4 (d, *J* = 10.6 Hz), 30.3, 27.2 (d, *J* = 6.0 Hz), 23.9; **^{19}F NMR (282 MHz, $CDCl_3$)** δ -62.2 (s). HRMS calcd for $C_{28}H_{40}F_2KN_2O_2$ (2M + K) 513.2695, found 513.2689.

***N*-(*tert*-butyl)-*N*,5-difluoro-2-isopropylbenzamide (16NF)**

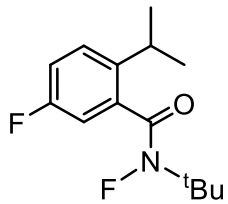

^{1}H NMR (300 MHz, $CDCl_3$) δ 7.33-7.26 (m, 1H), 7.10-7.04 (m, 1H), 6.97-6.93 (m, 1H), 3.18-3.04 (m, 1H), 1.56 (d, *J* = 2.0 Hz, 9H), 1.23 (d, *J* = 7.2 Hz, 6H); **^{13}C NMR (75 MHz, $CDCl_3$)** δ 173.4 (dd, *J* = 11.4 Hz, *J* = 2.4 Hz), 160.2 (dd, *J* = 246.0 Hz, *J* = 1.5 Hz), 141.6 (dd, *J* = 3.4 Hz, *J* = 2.4 Hz), 135.6 (dd, *J* = 6.8 Hz, *J* = 1.2 Hz), 127.4 (dd, *J* = 7.6 Hz, *J* = 1.2 Hz), 116.9 (dd, *J* = 20.8 Hz, *J* = 1.2 Hz), 113.4 (dd, *J* = 23.4 Hz, *J* = 4.5 Hz), 64.6 (d, *J* = 10.1 Hz), 29.9, 27.1 (d, *J* = 5.0 Hz), 24.1; **^{19}F NMR (282 MHz, $CDCl_3$)** δ -62.6 (s), -116.8 – -116.9 (m). HRMS calcd for $C_{28}H_{38}F_4KN_2O_2$ (2M + K) 549.2506, found 549.2514.

***N*-fluoro-2-isopropyl-*N*-(*tert*-pentyl)benzamide (17NF)**

^{1}H NMR (300 MHz, $CDCl_3$) δ 7.41-7.34 (m, 2H), 7.26-7.19 (m, 2H), 3.21-3.12 (m, 1H), 1.96-1.88 (m, 2H), 1.53 (d, *J* = 2.2 Hz, 6H), 1.26 (d, *J* = 6.4 Hz, 6H), 1.29 (t, *J* = 7.5 Hz, 3H); **^{13}C NMR (75 MHz, $CDCl_3$)** δ 174.3 (d, *J* = 11.2 Hz), 145.8 (d, *J* = 2.4 Hz), 134.5, 129.9 (d, *J* = 1.2 Hz), 126.5 (d, *J* = 4.0 Hz), 125.6 (d, *J* = 1.2 Hz), 125.3 (d, *J* = 1.2 Hz), 67.4 (d, *J* = 10.6 Hz), 32.9 (d, *J* = 4.6 Hz), 30.4, 24.9 (d, *J* = 6.0 Hz), 24.0, 8.6; **^{19}F NMR (282 MHz, $CDCl_3$)** δ -64.0 (s). HRMS calcd for $C_{30}H_{44}F_2KN_2O_2$ (2M + K) 541.3008, found 541.3016.

VI. Synthesis and Characterization of Authentic Azidation Products

Racemic standard references of azidation products were prepared *via* an iron-catalyzed C–H azidation reaction reported previously (*5*). Namely, a 40 mL vial with screw cap and PTFE septum was charged with a stir bar, $Fe(OAc)_2$ (17 mg, 0.1 mmol), and 1,10-phenanthroline (18 mg, 0.1 mmol). The vial was evacuated and backfilled with Ar for three times. *N*-fluoroamide substrate (1 mmol) and trimethylsilyl azide ($TMSN_3$) were dissolved in 10 mL dichloroethane and the resulting solution was added to the 40 mL vial containing the catalyst and the ligand. The vial was capped and the reaction mixture was stirred under 80 °C for 24 hours. The crude reaction mixture was purified by semi-prep HPLC with water and acetonitrile as the mobile phases.

2-(1-azidoethyl)-*N*-(*tert*-butyl)benzamide (1N)

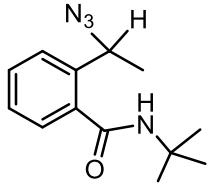

^{1}H NMR (300 MHz, $CDCl_3$) δ 7.53-7.30 (m, 4H), 5.78 (brs, 1H), 5.17 (q, *J* = 6.8 Hz, 1H), 1.60 (d, *J* = 6.8 Hz, 3H), 1.49 (s, 9H); **^{13}C NMR (75 MHz, $CDCl_3$)** δ 168.8, 139.1, 136.8,

130.2, 127.8, 126.8, 126.6, 57.4, 52.1, 28.8, 21.4. HRMS calcd for $C_{26}H_{36}KN_8O_2$ (2M + K) 531.2598, found 531.2593.

2-(1-azidoethyl)-*N*-(*tert*-butyl)-5-methylbenzamide (2N)

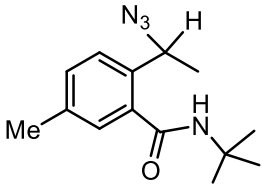

^{1}H NMR (300 MHz, $CDCl_3$) δ 7.39 (d, *J* = 8.2 Hz, 1H), 7.26 (dd, *J* = 8.2 Hz, *J* = 1.8 Hz, 1H), 7.19 (d, *J* = 1.8 Hz, 1H), 5.79 (brs, 1H), 5.10 (q, *J* = 6.8 Hz, 1H), 2.37 (s, 3H), 1.57 (d, *J* = 6.8 Hz, 3H), 1.49 (s, 9H); **^{13}C NMR (75 MHz, $CDCl_3$)** δ 168.8, 139.1, 136.8, 130.2, 127.8, 126.8, 126.6, 57.4, 52.1, 28.8, 21.4. HRMS calcd for $C_{28}H_{40}KN_8O_2$ (2M + K) 559.2911, found 559.2906.

2-(1-azidoethyl)-*N*-(*tert*-butyl)-5-fluorobenzamide (3N)

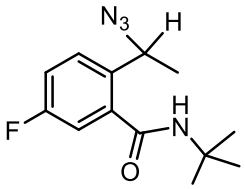

^{1}H NMR (300 MHz, $CDCl_3$) δ 7.51-7.47 (m, 1H), 7.18-7.08 (m, 2H), 5.78 (brs, 1H), 5.10 (q, *J* = 6.4 Hz, 1H), 1.58 (d, *J* = 6.4 Hz, 3H), 1.49 (s, 9H); **^{13}C NMR (75 MHz, $CDCl_3$)** δ 167.3, 161.7 (d, *J* = 247.2 Hz), 138.6 (d, *J* = 6.8 Hz), 134.8 (d, *J* = 4.5 Hz), 128.7 (d, *J* = 8.2 Hz), 117.1 (d, *J* = 21.6 Hz), 114.0 (d, *J* = 23.0 Hz), 56.9, 52.3, 28.7, 21.3; **^{19}F NMR (282.4 MHz, $CDCl_3$)** δ -112.5 – -112.6 (m). HRMS calcd for $C_{26}H_{34}F_2KN_8O_2$ (2M + K) 567.2410, found 567.2404.

2-(1-azidoethyl)-*N*-(*tert*-butyl)-4-fluorobenzamide (4N)

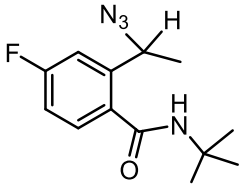

^{1}H NMR (300 MHz, $CDCl_3$) δ 7.41-7.36 (m, 1H), 7.24-7.20 (m, 1H), 7.04-6.98 (m, 1H), 5.74 (brs, 1H), 5.20 (q, *J* = 6.3 Hz, 1H), 1.58 (d, *J* = 6.3 Hz, 3H), 1.49 (s, 9H). **^{13}C NMR (75 MHz, $CDCl_3$)** δ 167.9, 163.6 (d, *J* = 247.5 Hz), 142.5 (d, *J* = 6.8 Hz), 132.8 (d, *J* = 4.4 Hz), 129.0 (d, *J* = 8.7 Hz), 114.7 (d, *J* = 21.5 Hz), 113.9 (d, *J* = 23.0 Hz), 57.0, 52.2, 28.8, 21.4; **^{19}F NMR (282.4 MHz, $CDCl_3$)** δ -108.5 – -108.6 (m). HRMS calcd for $C_{26}H_{34}F_2KN_8O_2$ (2M + K) 567.2410, found 567.2404.

2-(1-azidoethyl)-*N*-(*tert*-butyl)-3-methylbenzamide (5N)

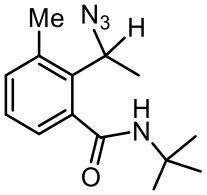

^{1}H NMR (300 MHz, $CDCl_3$) δ 7.28-7.18 (m, 3H), 5.67 (brs, 1H), 5.18 (q, *J* = 6.8 Hz, 1H), 2.48 (s, 2H), 1.65 (d, *J* = 6.8 Hz, 3H), 1.49 (s, 9H); **^{13}C NMR (75 MHz, $CDCl_3$)** δ 170.1, 138.5,

136.9, 135.9, 132.8, 127.5, 125.0, 58.2, 51.9, 28.8, 20.2, 19.8. HRMS calcd for $C_{28}H_{40}KN_8O_2$ (2M + K) 559.2911, found 559.2906.

2-(1-azidoethyl)-*N*-(*tert*-pentyl)benzamide (6N)

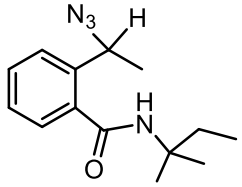

^{1}H NMR (300 MHz, $CDCl_3$) δ 7.44-7.28 (m, 4H), 5.53 (brs, 1H), 1.87 (q, J = 8.4 Hz, 2H), 1.80 (s, 6H), 0.99 (t, J = 8.4 Hz, 3H); **^{13}C NMR (75 MHz, $CDCl_3$)** δ 170.8, 141.9, 137.6, 129.2, 128.7, 127.4, 126.1, 64.3, 54.6, 33.1, 28.6, 26.1, 8.4. HRMS calcd for $C_{28}H_{40}KN_8O_2$ (2M + K) 559.2911, found 559.2906.

2-(1-azidoethyl)-*N*-(*tert*-butyl)-3-methoxybenzamide (7N)

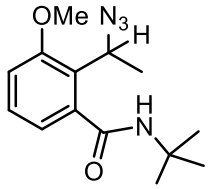

^{1}H NMR (300 MHz, $CDCl_3$) δ 7.30-7.25 (m, 1H), 6.98-6.90 (m, 2H), 5.69 (brs, 1H), 5.07 (q, *J* = 6.8 Hz, 1H), 3.90 (s, 3H), 1.70 (d, *J* = 6.8 Hz, 3H), 1.48 (s, 9H); **^{13}C NMR (75 MHz, $CDCl_3$)** δ 169.0, 158.0, 139.3, 128.9, 126.3, 119.3, 122.3, 55.7, 55.5, 52.0, 28.7, 18.9. HRMS calcd for $C_{28}H_{40}KN_8O_4$ (2M + K) 591.2810, found 591.2819.

2-(1-azidopropyl)-*N*-(*tert*-butyl)benzamide (8N)

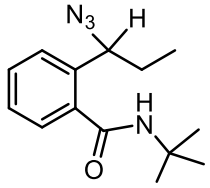

^{1}H NMR (300 MHz, $CDCl_3$) δ 7.48-7.30 (m, 4H), 5.74 (brs, 1H), 4.93 (t, *J* = 7.2 Hz, 1H), 1.94-1.84 (m, 2H), 1.50 (s, 9H), 0.99 (d, *J* = 7.0 Hz, 3H); **^{13}C NMR (75 MHz, $CDCl_3$)** δ 168.8, 137.9, 137.4, 130.1, 127.8, 126.9, 126.8, 63.7, 52.1, 29.1, 28.8, 10.9. HRMS calcd for $C_{28}H_{40}KN_8O_2$ (2M + K) 559.2911, found 559.2906.

2-(1-azidobutyl)-*N*-(*tert*-butyl)benzamide (9N)

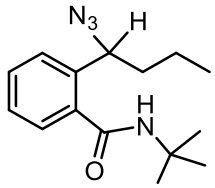

^{1}H NMR (300 MHz, $CDCl_3$) δ 7.48-7.33 (m, 4H), 5.76 (brs, 1H), 5.03-4.98 (m, 1H), 1.87-1.79 (m, 2H), 1.51 (s, 9H), 1.54-1.27 (m, 2H), 0.95 (t, *J* = 7.2 Hz, 3H); **^{13}C NMR (75 MHz, $CDCl_3$)** δ 168.8, 138.1, 137.3, 130.1, 127.8, 126.9, 126.8, 61.9, 52.1, 37.9, 28.8, 19.6, 13.7. HRMS calcd for $C_{30}H_{44}KN_8O_2$ (2M + K) 587.3224, found 587.3219.

2-(1-azidobut-3-en-1-yl)-*N*-(*tert*-butyl)benzamide (10N)

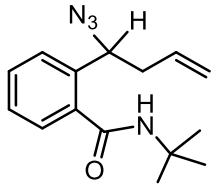

^{1}H NMR (300 MHz, $CDCl_3$) δ 7.52-7.28 (m, 4H), 5.86-5.74 (m, 1H), 5.19-5.10 (m, 3H), 2.65-2.60 (m, 2H), 1.49 (s, 9H); **^{13}C NMR (75 MHz, $CDCl_3$)** δ 168.7, 137.5, 137.1, 133.8, 130.2, 127.9, 127.1, 126.8, 118.3, 61.6, 52.1, 40.3, 28.8. HRMS calcd for $C_{30}H_{40}KN_8O_2$ (2M + K) 583.2911, found 583.2920.

2-(azidomethyl)-*N*-(*tert*-butyl)benzamide (11N)

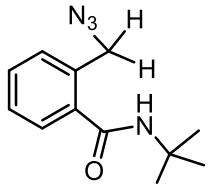

^{1}H NMR (300 MHz, $CDCl_3$) δ 7.51-7.35 (m, 4H), 5.92 (brs, 1H), 4.59 (s, 2H), 1.50 (s, 9H); **^{13}C NMR (75 MHz, $CDCl_3$)** δ 168.3, 137.4, 133.3, 130.2, 130.0, 128.5, 127.5, 52.7, 52.1, 28.8. HRMS calcd for $C_{24}H_{32}KN_8O_2$ (2M + K) 503.2285, found 503.2292.

2-(azidomethyl)-4-bromo-*N*-(*tert*-butyl)benzamide (12N)

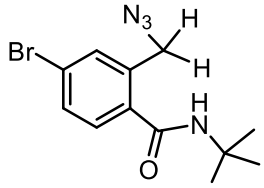

^{1}H NMR (300 MHz, $CDCl_3$) δ 7.57-7.49 (m, 2H), 7.36-7.28 (m, 1H), 5.86 (brs, 1H), 4.58 (s, 2H), 1.49 (s, 9H); **^{13}C NMR (75 MHz, $CDCl_3$)** δ 167.38, 135.99, 135.78, 132.72, 131.41, 128.96, 124.27, 52.73, 52.28, 52.15, 28.76. HRMS calcd for $C_{24}H_{30}Br_2KN_8O_2$ (2M + K) 661.0475, found 661.0483.

2-(azidomethyl)-*N*-(*tert*-butyl)-5-methoxybenzamide (13N)

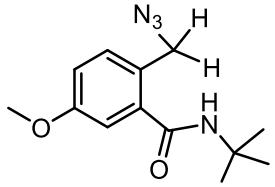

^{1}H NMR (300 MHz, $CDCl_3$) δ 7.70 (d, *J* = 8.6 Hz, 1H), 7.04 (d, *J* = 2.8 Hz, 1H), 6.95 (dd, *J* = 8.6 Hz, *J* = 2.8 Hz, 1H), 5.99 (brs, 1H), 4.49 (s, 2H), 3.86 (s, 3H), 1.49 (s, 9H). **^{13}C NMR (75 MHz, $CDCl_3$)** δ 168.0, 159.6, 139.0, 131.8, 124.9, 115.3, 113.5, 55.5, 52.5, 52.1, 28.8. HRMS calcd for $C_{26}H_{36}KN_8O_4$ (2M + K) 563.2497, found 563.2503.

2-(azidomethyl)-N-(tert-butyl)-5-fluorobenzamide (14N)

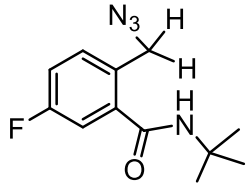

^{1}H NMR (300 MHz, $CDCl_3$) δ 7.38-7.34 (m, 1H), 7.23-7.19 (m, 1H), 7.16-7.10 (m, 1H), 5.93 (brs, 1H), 4.54 (s, 2H), 1.50 (s, 9H).**^{13}C NMR (75 MHz, $CDCl_3$)** δ 166.90 (d, *J* = 2.2 Hz), 162.23 (d, *J* = 249.2 Hz), 139.36 (d, *J* = 6.8 Hz), 132.06 (d, *J* = 8.2 Hz), 129.11 (d, *J* = 3.4 Hz), 116.97 (d, *J* = 21.2 Hz), 114.98 (d, *J* = 22.2 Hz), 52.35, 52.11, 28.73. **^{19}F NMR (282.4 MHz, $CDCl_3$)** δ -113.0 – -113.1 (m). HRMS calcd for $C_{24}H_{30}F_2KN_8O_2$ (2M + K) 539.2097, found 539.2091.

2-(2-azidopropan-2-yl)-*N*-(*tert*-butyl)benzamide (15N)

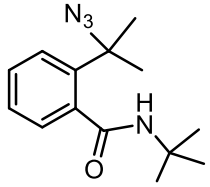

^{1}H NMR (300 MHz, $CDCl_3$) δ 7.43-7.28 (m, 4H), 5.64 (brs, 1H), 1.80 (s, 6H), 1.50 (s, 9H); **^{13}C NMR (75 MHz, $CDCl_3$)** δ 170.8, 141.9, 137.5, 129.2, 128.7, 127.4 126.1, 64.3, 51.8, 28.6, 28.6. HRMS calcd for $C_{28}H_{40}KN_8O_2$ (2M + K) 559.2911, found 559.2920.

2-(2-azidopropan-2-yl)-N-(tert-butyl)-5-fluorobenzamide (16N)

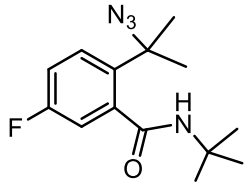

^{1}H NMR (300 MHz, $CDCl_3$) δ 7.41-7.37 (m, 1H), 7.08-7.01 (m, 2H), 5.63 (brs, 1H), 1.78 (s, 6H), 1.49 (s, 9H). **^{13}C NMR (75 MHz, $CDCl_3$)** δ 169.2, 161.3 (d, *J* = 247.2 Hz), 139.3 (d, *J* = 7.8 Hz), 137.7 (d, *J* = 4.6 Hz), 128.2 (d, *J* = 7.8 Hz), 115.9 (d, *J* = 6.4 Hz), 115.6 (d, *J* = 4.6 Hz), 63.9, 51.9, 28.6, 28.6. **^{19}F NMR (282.4 MHz, $CDCl_3$)** δ -114.2 – -114.3 (m). HRMS calcd for $C_{28}H_{38}F_2KN_8O_2$ (2M + K) 595.2723, found 595.2726.

2-(2-azidopropan-2-yl)-*N*-(*tert*-pentyl)benzamide (17N)

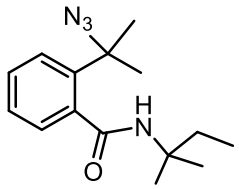

^{1}H NMR (300 MHz, $CDCl_3$) δ 7.44-7.28 (m, 4H), 5.53 (brs, 1H), 1.87 (q, *J* = 8.4 Hz, 2H), 1.80 (s, 6H), 0.99 (t, *J* = 8.4 Hz, 3H). **^{13}C NMR (75 MHz, $CDCl_3$)** δ 170.8, 141.9, 137.6, 129.2, 128.7, 127.4, 126.1, 64.3, 54.6, 33.1, 28.6, 26.1, 8.4. HRMS calcd for $C_{30}H_{44}KN_8O_2$ (2M + K) 587.3224, found 587.3228.

N-(tert-butyl)-2-((4-((((8R,9S,13S,14S)-13-methyl-17-oxo-7,8,9,11,12,13,14,15,16,17-decahydro-6H-cyclopenta[a]phenanthren-3-yl)oxy)methyl)-1H-1,2,3-triazol-1-yl)methyl)benzamide (19)

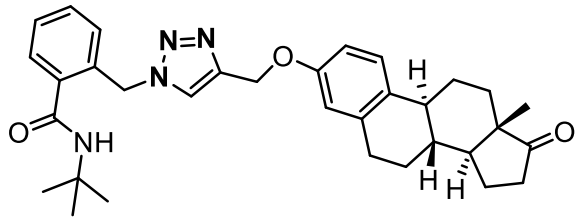

^{1}H NMR (300 MHz, $CDCl_3$) δ 7.92 (s, 1H), 7.45-7.35 (m, 4H), 7.22-7.19 (m, 1H), 6.81-6.73 (m, 2H), 5.97 (brs, 1H), 5.74 (s, 2H), 5.16 (s, 2H), 2.93-2.88 (m, 2H), 2.57-2.33 (m, 2H), 2.19-1.95 (m, 6H), 1.71-1.39 (m, 14H), 0.92 (s, 3H). **^{13}C NMR (75 MHz, $CDCl_3$)** δ 220.9, 168.4, 156.3, 144.2, 137.9, 136.9, 133.1, 133.0, 132.6, 130.7, 128.9, 127.2, 126.4, 124.0, 114.8, 112.4, 62.0, 52.2, 51.3, 50.4, 48.0, 44.0, 38.3, 35.9, 31.6, 29.7, 28.8, 26.5, 25.9, 21.6, 13.9.

VII. GC-MS Standard Curves for Azidation Products

Product formation in enzymatic reactions was quantified by GC-MS based on standard curves. To determine the standard calibration curves, stock solutions of chemically synthesized azidation products were prepared at various concentrations (0.5 – 5.0 mM in 4:6 hexanes/EtOAc) with added internal standard 1,2,3-trimethoxybenzene with a final concentration of 0.5 mM in the stock solutions of azidation products. All data points represent the average of quadruplicate runs. The standard curves plot product concentration in mM (y-axis) against the ratio of product area to internal standard area on GC-MS (x-axis). Mass spectrum of the azide compound was added below the calibration curve.

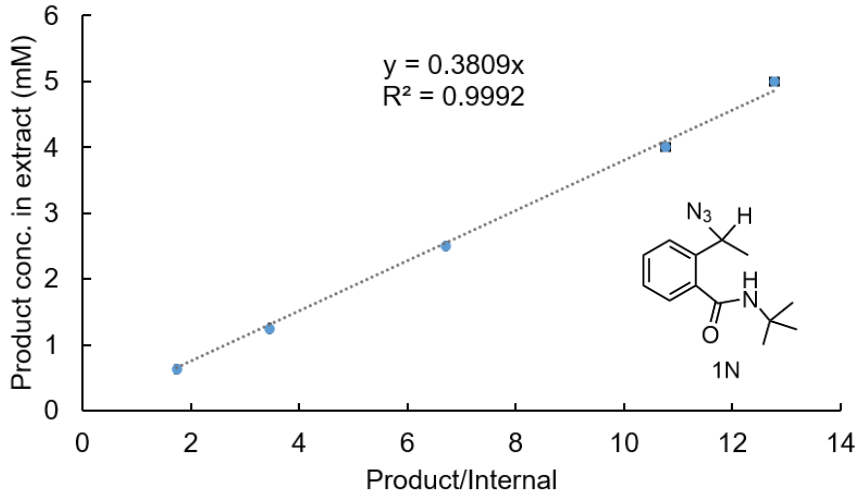

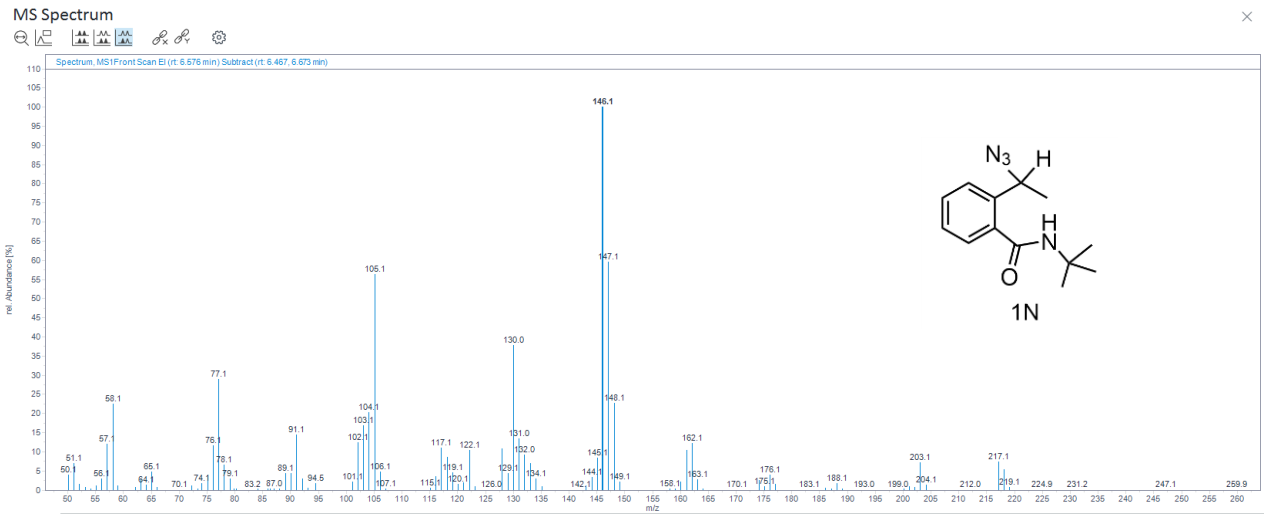

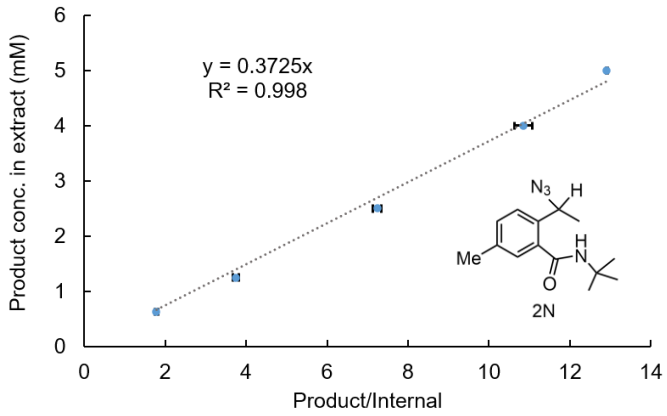
y = 0.3725x
R² = 0.998
Product conc. in extract (mM)
Product/Internal
N3
H
Me
H
N
O
2N

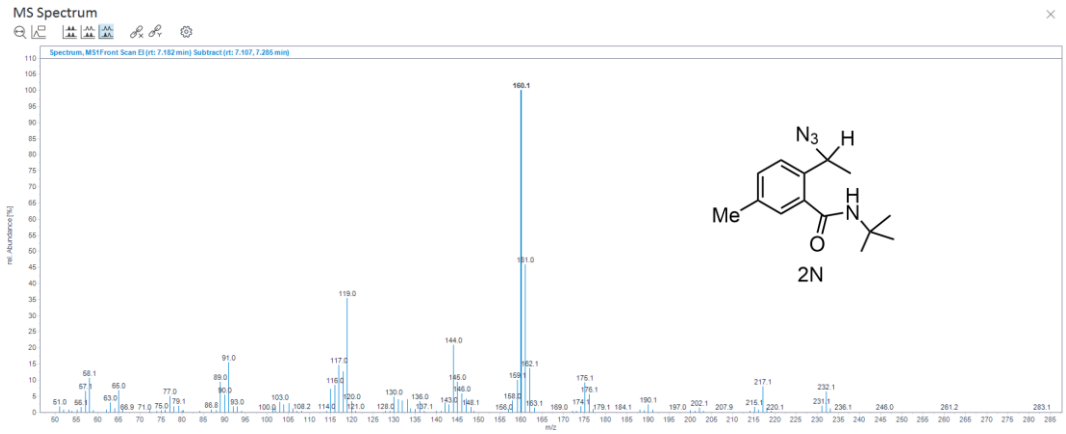
MS Spectrum
Spectrum, MS1Front Scan EI (rt: 7.182 min) Subtract (rt: 7.107, 7.285 min)
rel. Abundance [%]
m/z
N3
H
Me
H
N
O
2N

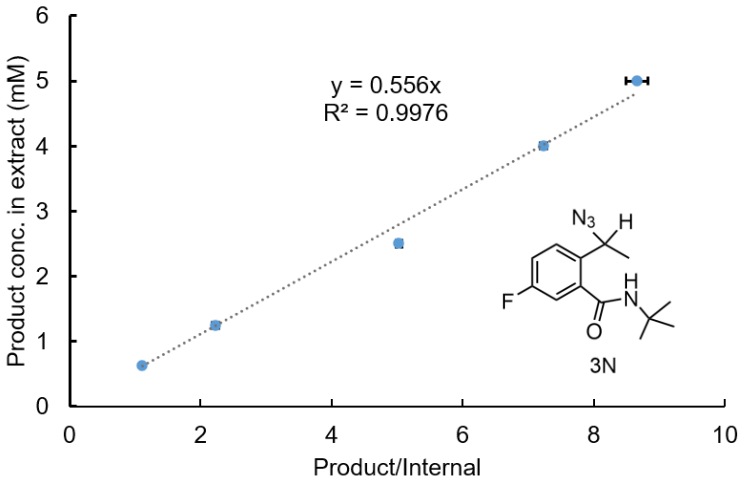
y = 0.556x
R² = 0.9976
Product conc. in extract (mM)
Product/Internal
N3
H
F
H
N
O
3N

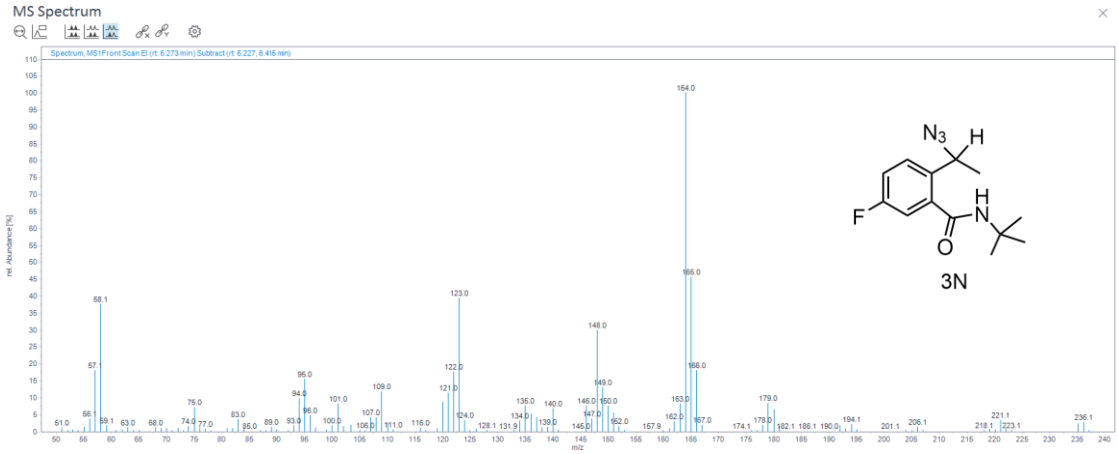
MS Spectrum
Spectrum, MS1Front Scan EI (rt: 6.273 min) Subtract (rt: 6.227, 6.415 min)
rel. Abundance [%]
m/z
N3
H
F
H
N
O
3N

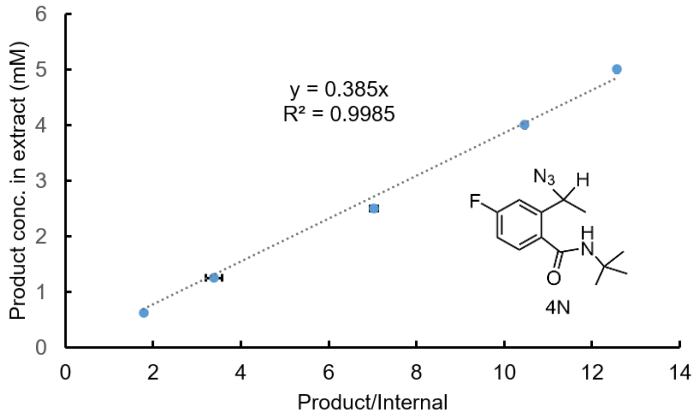
y = 0.385x
R² = 0.9985
Product conc. in extract (mM)
Product/Internal
4N

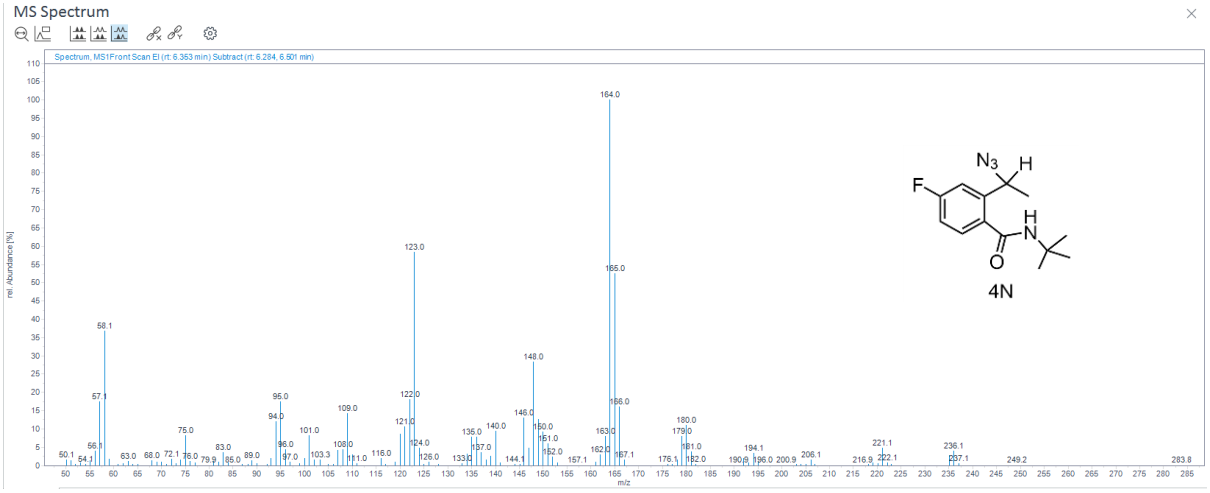
MS Spectrum
4N

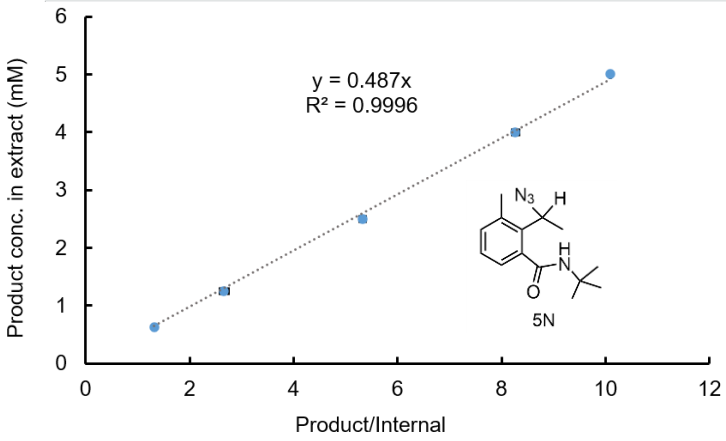
y = 0.487x
R² = 0.9996
Product conc. in extract (mM)
Product/Internal
5N

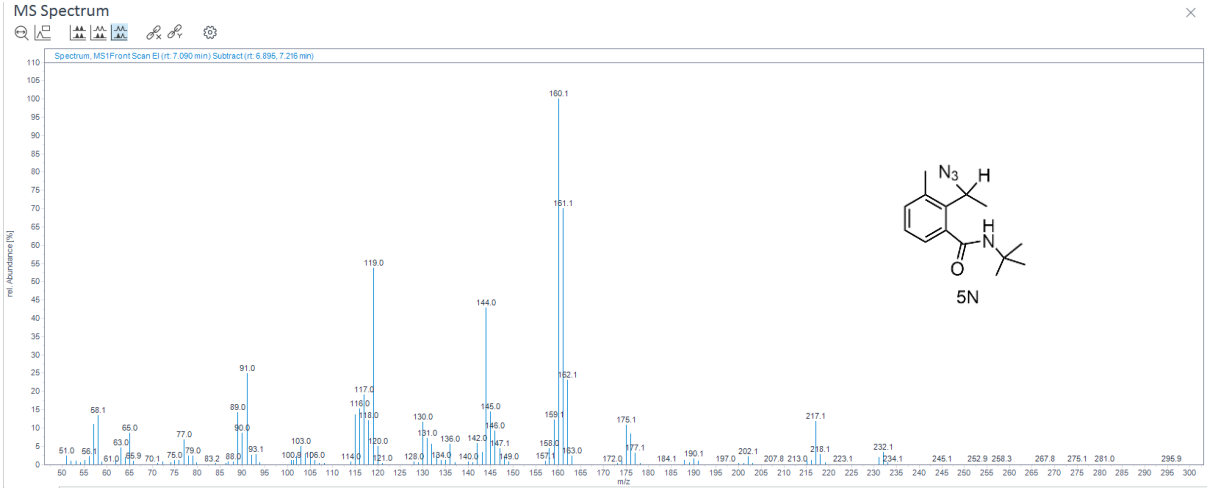
MS Spectrum
5N

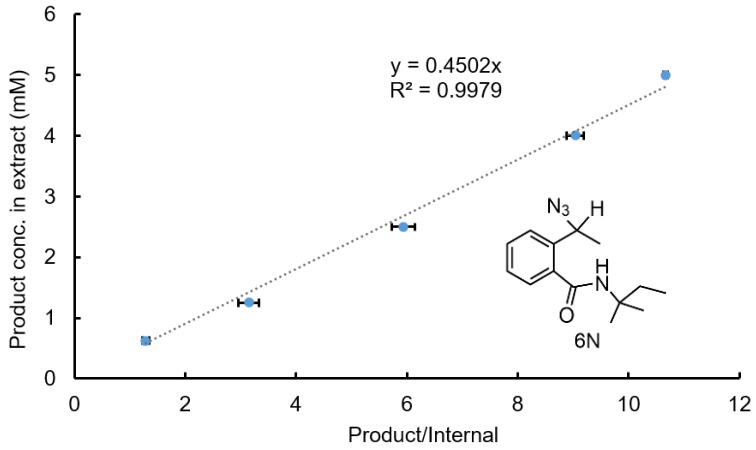
y = 0.4502x
R² = 0.9979
Product conc. in extract (mM)
Product/Internal
6N

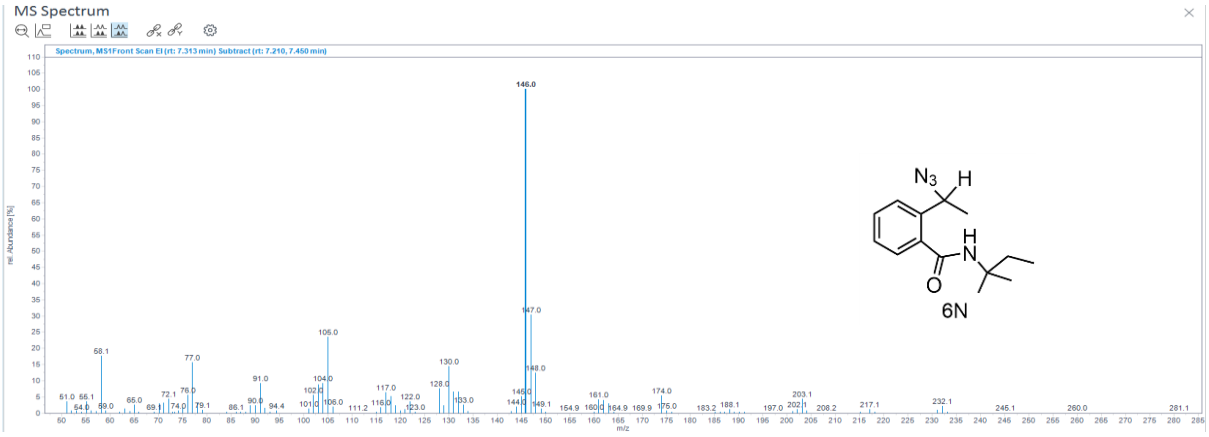
MS Spectrum
Spectrum, MS1Front Scan EI (rt: 7.313 min) Subtract (rt: 7.210, 7.460 min)
6N

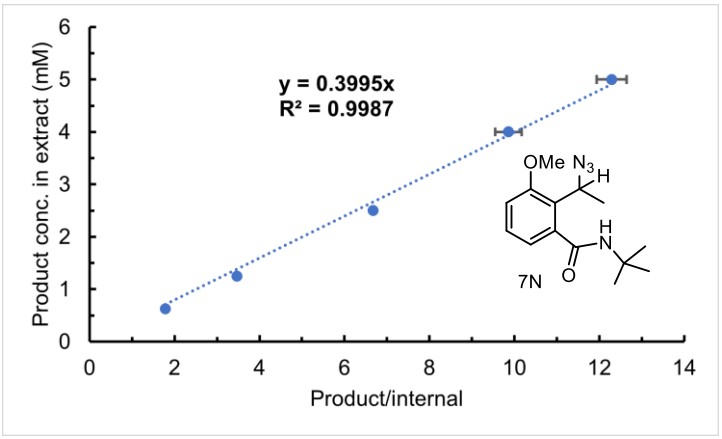
y = 0.3995x
R² = 0.9987
Product conc. in extract (mM)
Product/internal
7N

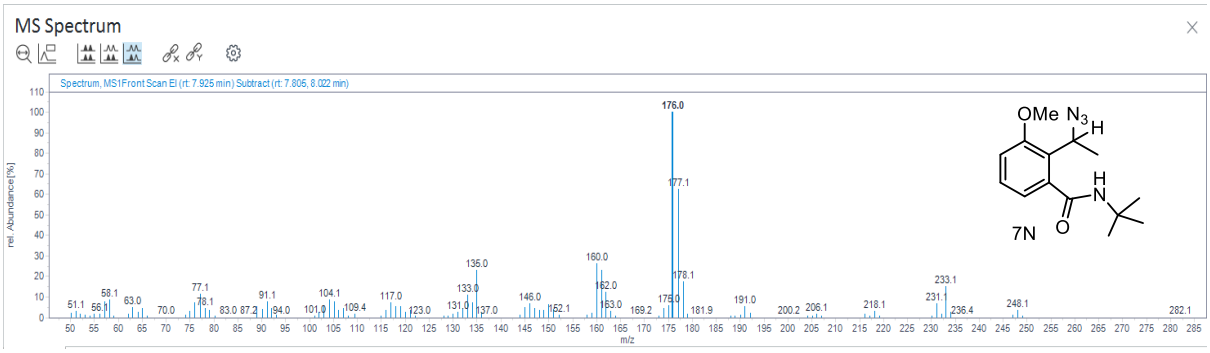
MS Spectrum
Spectrum, MS1Front Scan EI (rt: 7.925 min) Subtract (rt: 7.805, 8.022 min)
7N

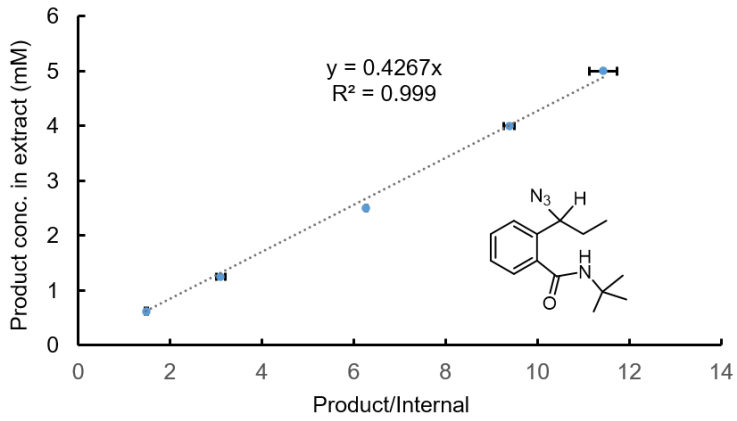
y = 0.4267x
R² = 0.999
Product conc. in extract (mM)
Product/Internal

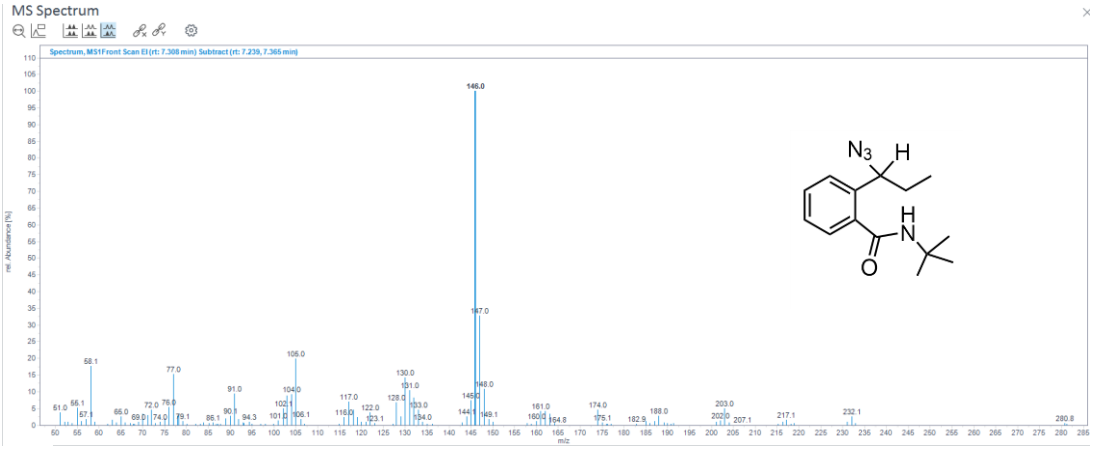
MS Spectrum
Spectrum, MS1Front Scan EI (rt: 7.308 min) Subtract (rt: 7.239, 7.365 min)
rel. Abundance [%]
m/z

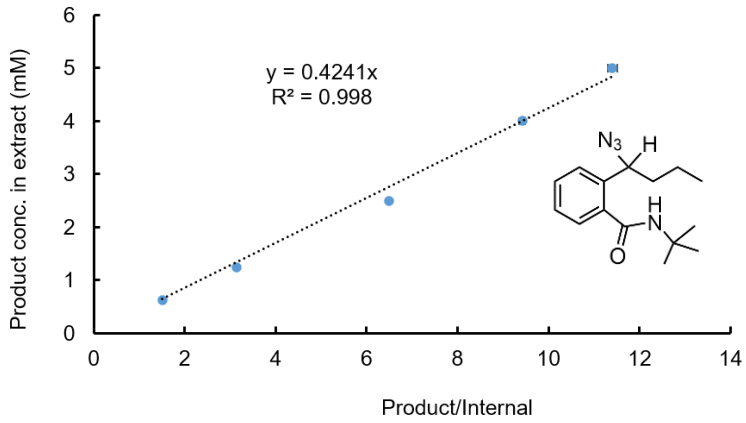
y = 0.4241x
R² = 0.998
Product conc. in extract (mM)
Product/Internal

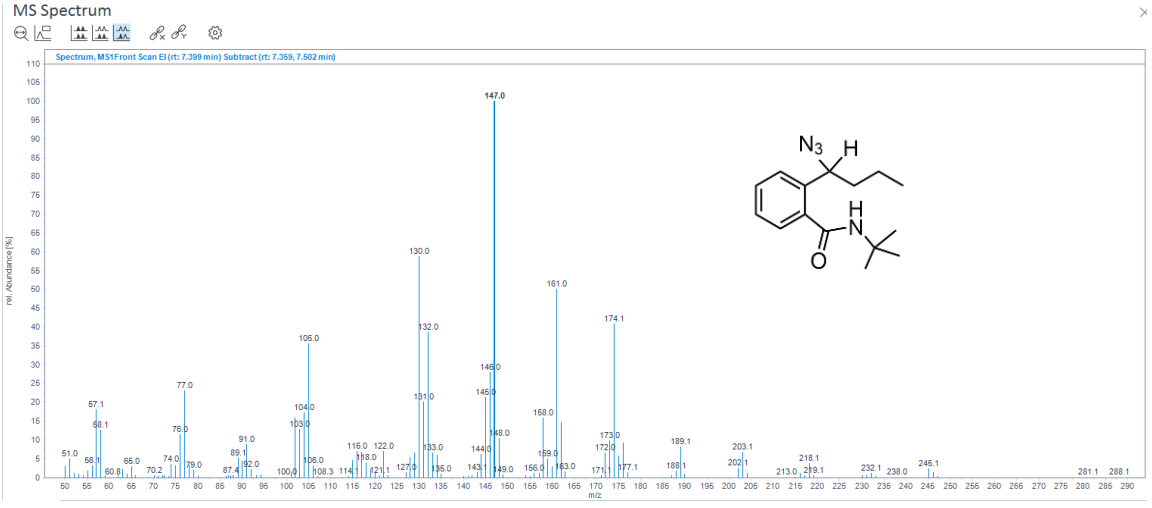
MS Spectrum
Spectrum, MS1Front Scan EI (rt: 7.399 min) Subtract (rt: 7.359, 7.502 min)
rel. Abundance [%]
m/z

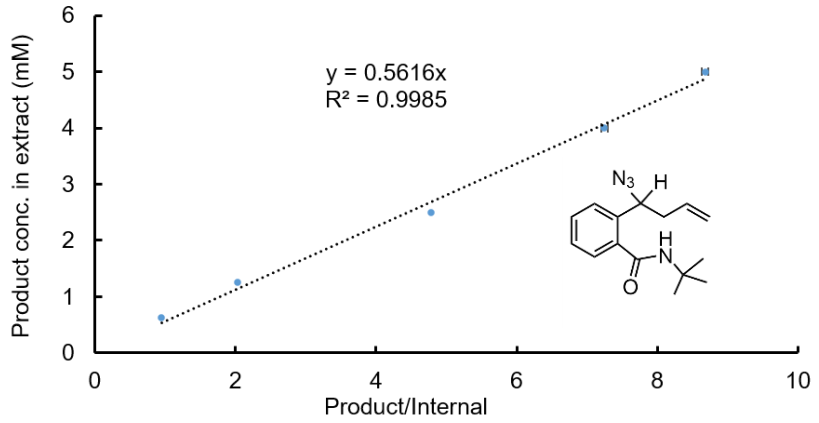
y = 0.5616x
R² = 0.9985
Product conc. in extract (mM)
Product/Internal
0
1
2
3
4
5
6
0
2
4
6
8
10
N3
H
H
N
O

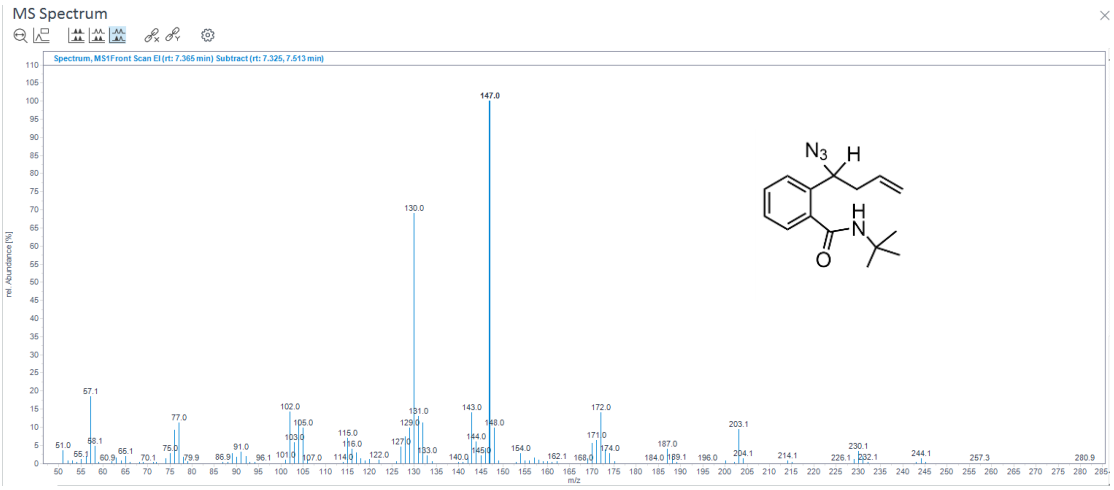
MS Spectrum
Spectrum, MS1Front Scan EI (rt: 7.365 min) Subtract (rt: 7.325, 7.513 min)
rel. Abundance [%]
m/z
147.0
130.0
57.1
N3
H
H
N
O

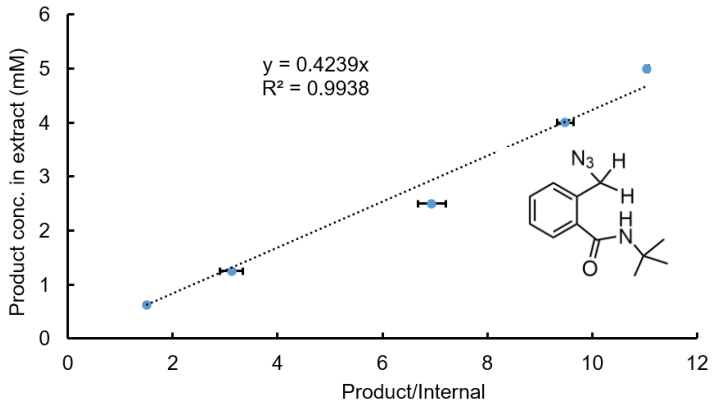
y = 0.4239x
R² = 0.9938
Product conc. in extract (mM)
Product/Internal
0
1
2
3
4
5
6
0
2
4
6
8
10
12
N3
H
H
H
N
O

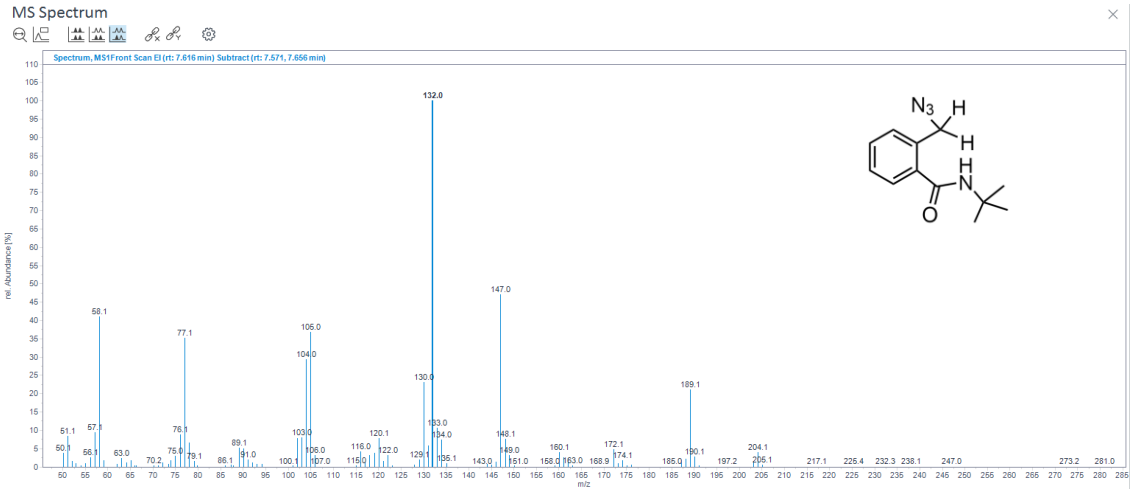
MS Spectrum
Spectrum, MS1Front Scan EI (rt: 7.616 min) Subtract (rt: 7.571, 7.656 min)
rel. Abundance [%]
m/z
132.0
147.0
58.1
N3
H
H
H
N
O

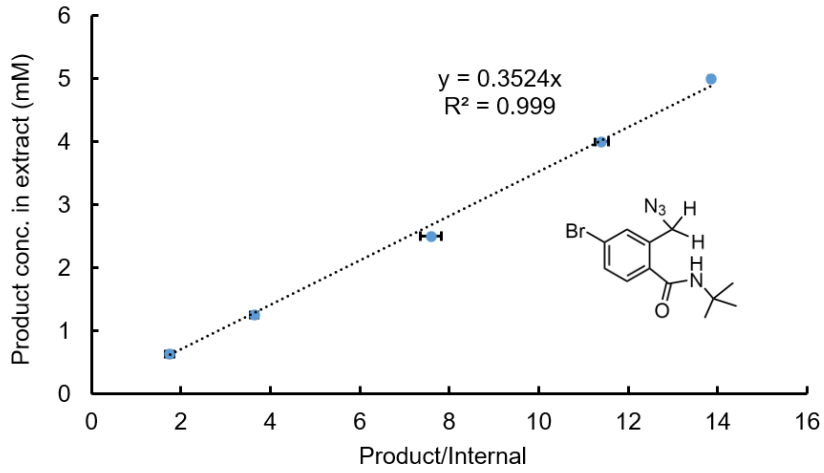
y = 0.3524x
R² = 0.999
Product conc. in extract (mM)
Product/Internal
0
1
2
3
4
5
6
0
2
4
6
8
10
12
14
16
N3
H
Br
O

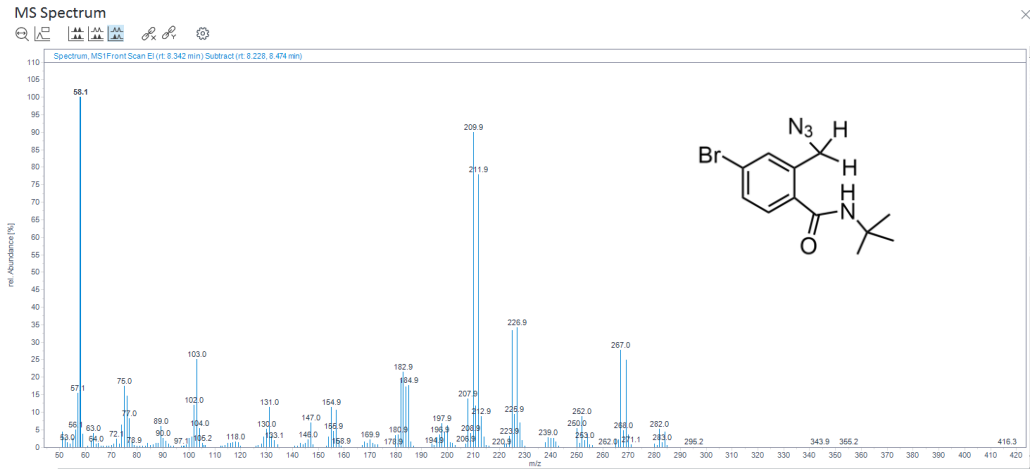
MS Spectrum
Spectrum, MS1Front Scan EI (rt: 8.342 min) Subtract (rt: 8.228, 8.474 min)
rel. Abundance [%]
m/z
58.1
209.9
211.9
226.9
267.0
103.0
182.9
184.9
N3
H
Br
O

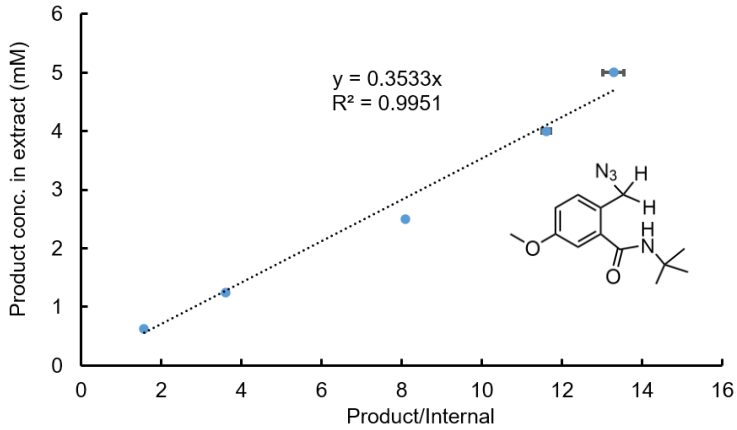
y = 0.3533x
R² = 0.9951
Product conc. in extract (mM)
Product/Internal
0
1
2
3
4
5
6
0
2
4
6
8
10
12
14
16
N3
H
O

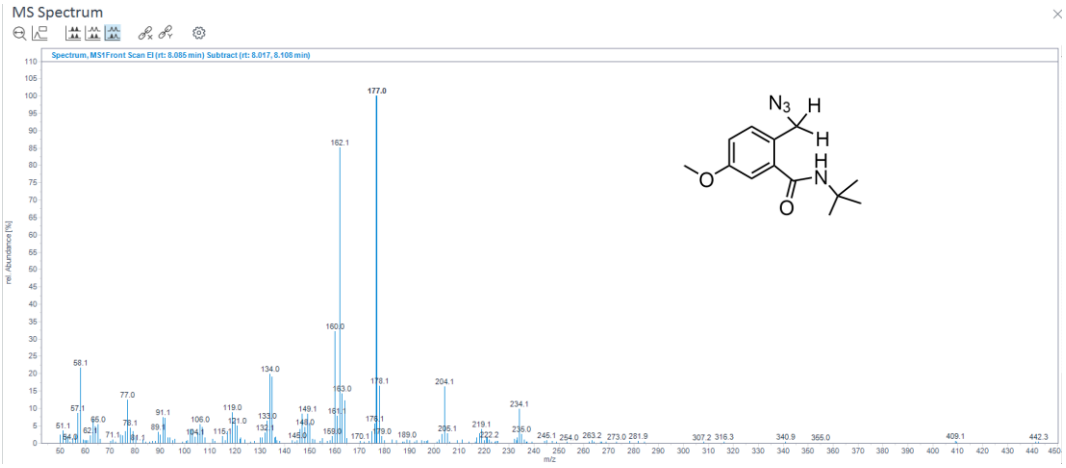
MS Spectrum
Spectrum, MS1Front Scan EI (rt: 8.085 min) Subtract (rt: 8.017, 8.108 min)
rel. Abundance [%]
m/z
N3
H
H
H
N
O
O

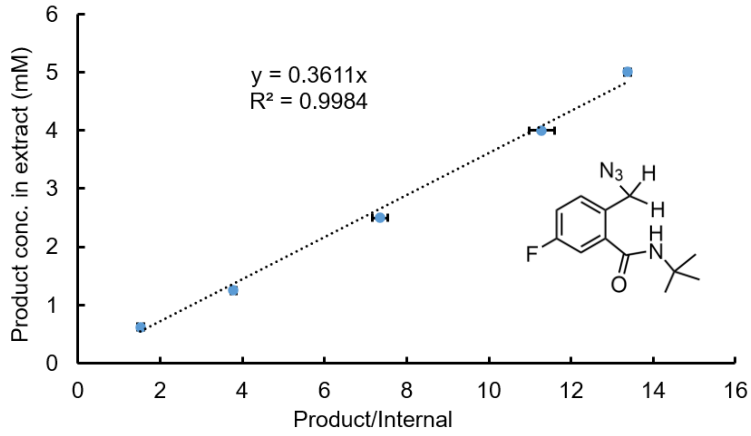
y = 0.3611x
R² = 0.9984
Product conc. in extract (mM)
Product/Internal
N3
H
H
H
N
F
O

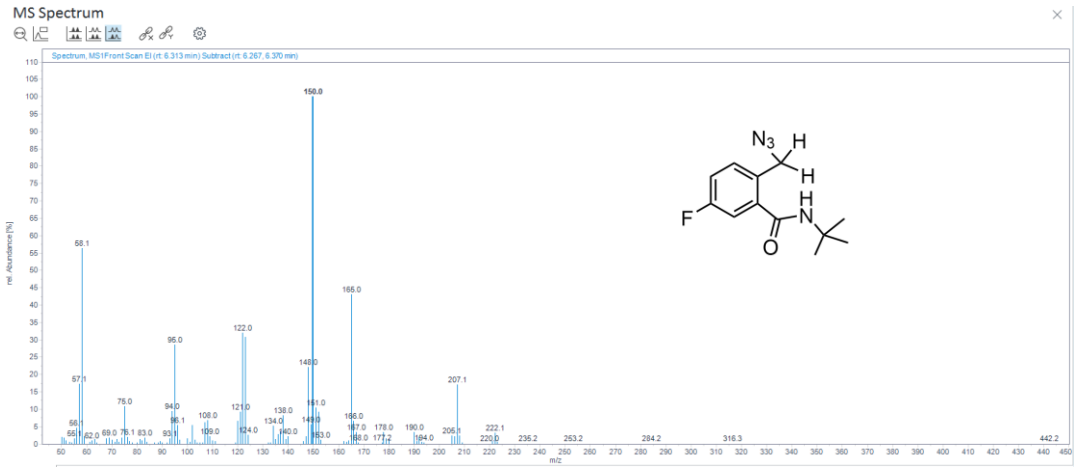
MS Spectrum
Spectrum, MS1Front Scan EI (rt: 6.313 min) Subtract (rt: 6.267, 6.370 min)
rel. Abundance [%]
m/z
N3
H
H
H
N
F
O

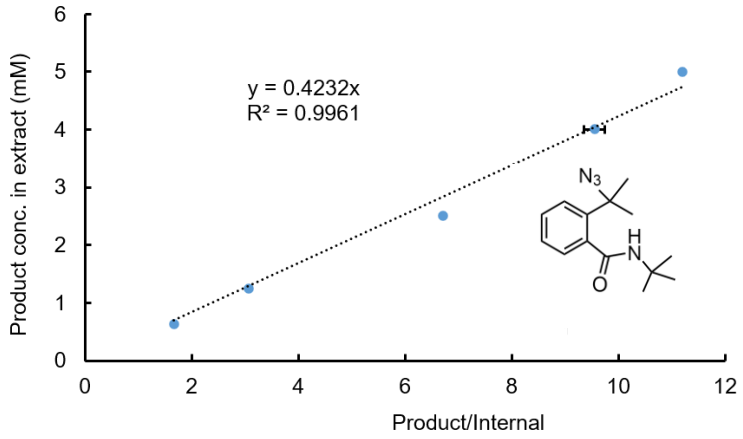
y = 0.4232x
R² = 0.9961
Product conc. in extract (mM)
Product/Internal
N3
H
N
O

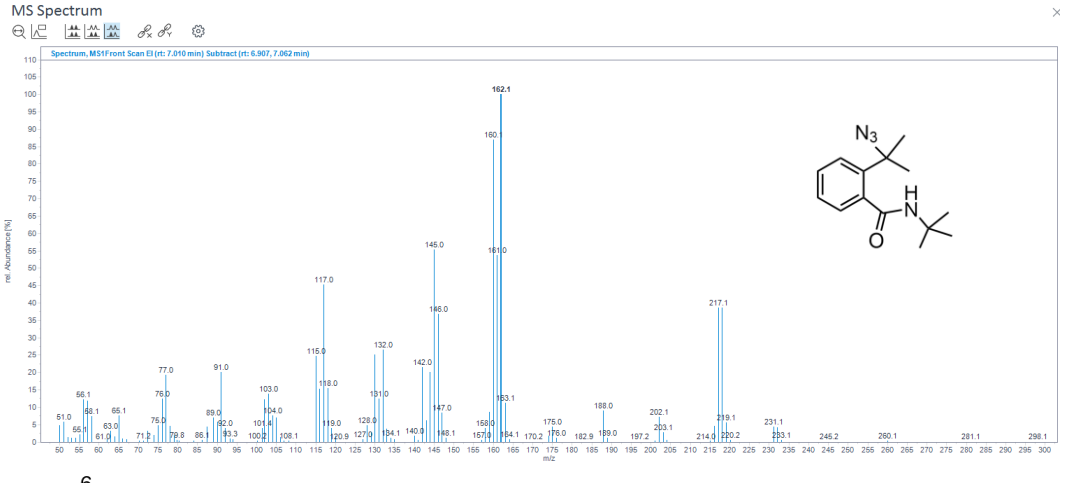
MS Spectrum
Spectrum, MS1Front Scan EI (rt: 7.010 min) Subtract (rt: 6.907, 7.062 min)
rel. Abundance [%]
m/z
N3
H
N
O

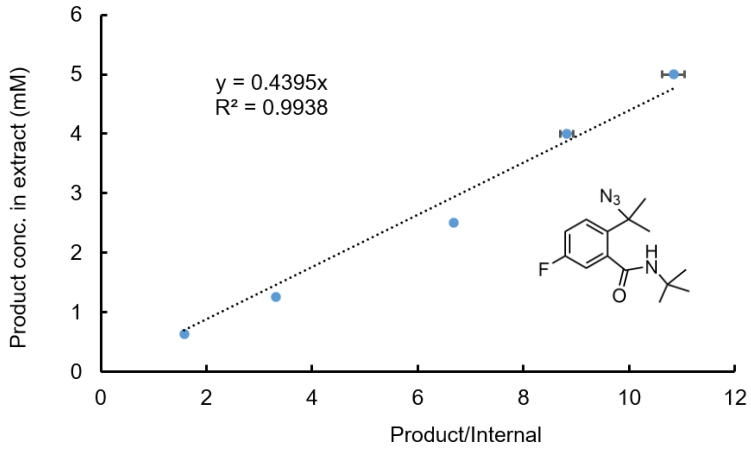
y = 0.4395x
R² = 0.9938
Product conc. in extract (mM)
Product/Internal
N3
F
H
N
O

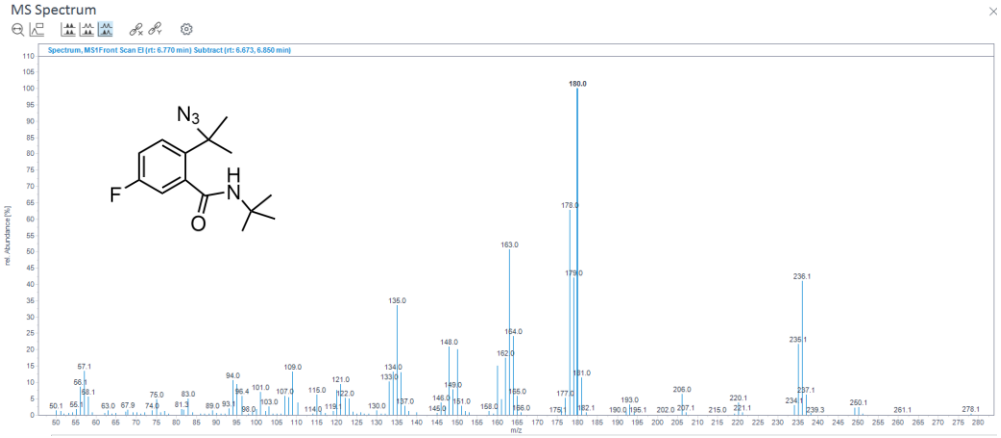
MS Spectrum
Spectrum, MS1Front Scan EI (rt: 6.770 min) Subtract (rt: 6.673, 6.850 min)
rel. Abundance [%]
m/z
N3
F
H
N
O

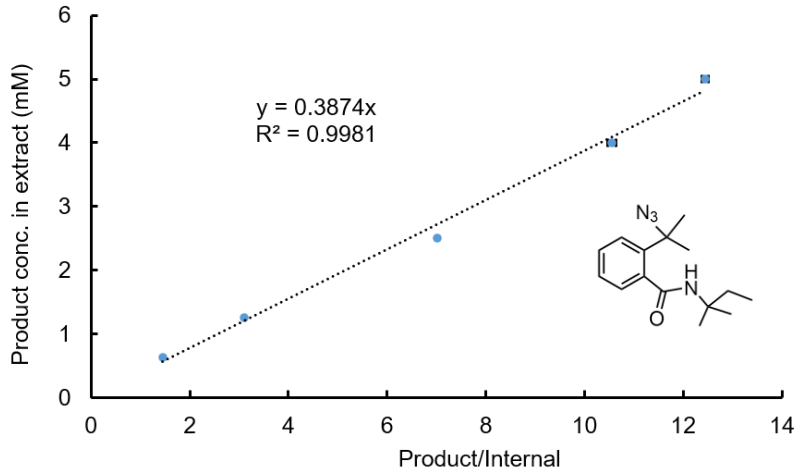
y = 0.3874x
R² = 0.9981
Product conc. in extract (mM)
Product/Internal
N3
H
N
O

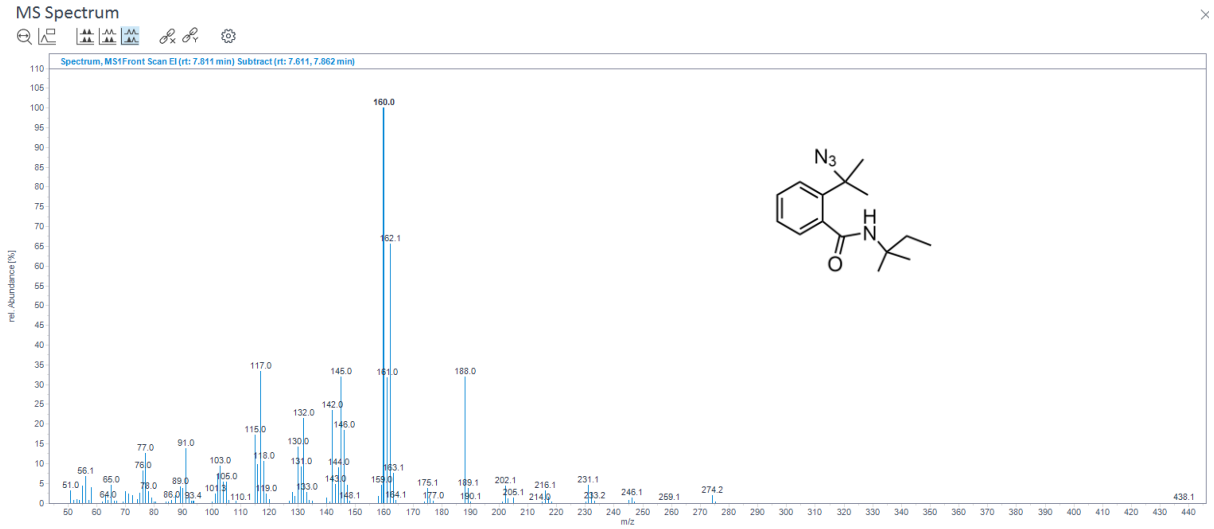
MS Spectrum
Spectrum, MS1Front Scan EI (rt: 7.811 min) Subtract (rt: 7.611, 7.862 min)
rel. Abundance [%]
m/z
160.0
162.1
188.0
117.0
N3
H
N
O

VIII. Determination of Enantioselectivity

All e.r. values of enzymatically synthesized azidation products were determined using normal-phase chiral HPLC. The absolute configuration of enzymatically synthesized azidation product **1N** was determined to be *S via* X-ray crystallography. The absolute configurations of all other azidation products were inferred by analogy, assuming the facial selectivity of the C–N_3 bond forming step remains the same as that of **1N**. Each chiral determination of the enzymatic product was performed along with the chiral HPLC analysis of the corresponding racemic standard to confirm the retention time of both enantiomers.

Conditions: CHIRALPAK® IC (4.6 × 250 mm, 5 mic), 1% ^{i}PrOH/hexanes, 0.5 mL/min.

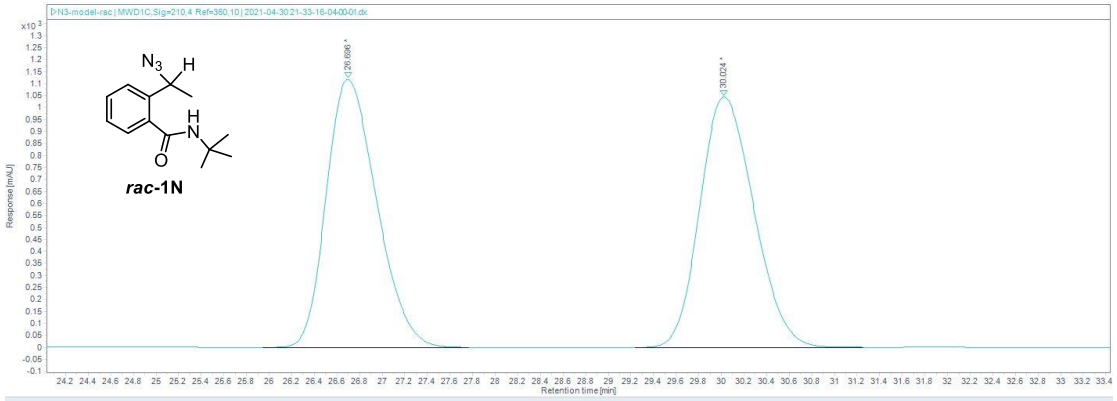

Injection Results

Peaks | Summary

#	Name	Signal description	RT (min)	Area	Area%	Height	Height%	Amount	Concentration	Start time (min)	End time (min)
2		MWD1C,Sig=210,4 Ref=360,10	30.024	34727.424	50.128	1044.637	48.31			29.235	31.256
1		MWD1C,Sig=210,4 Ref=360,10	26.696	34549.505	49.872	1117.608	51.69			25.941	27.768

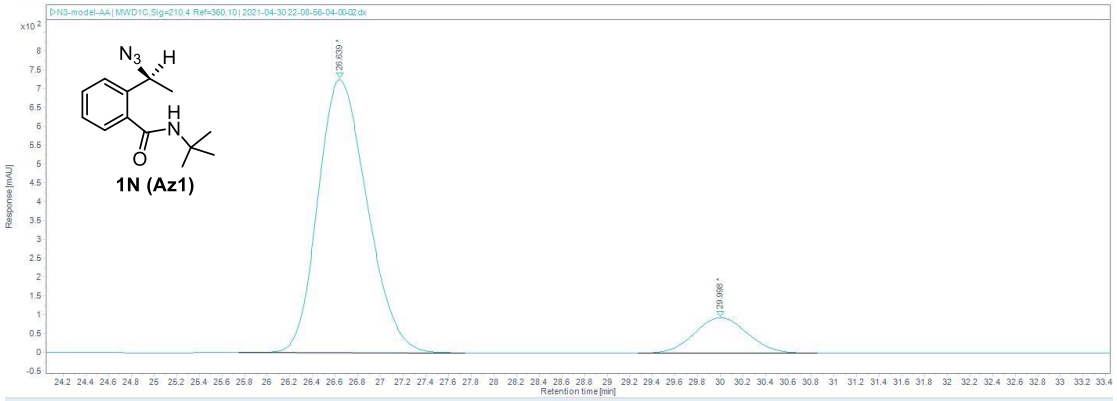

Injection Results

Peaks | Summary

#	Name	Signal description	RT (min)	Area	Area%	Height	Height%	Amount	Concentration	Start time (min)	End time (min)
2		MWD1C,Sig=210,4 Ref=360,10	29.998	3098.602	12.416	94.556	11.55			29.269	30.851
1		MWD1C,Sig=210,4 Ref=360,10	26.639	21858.629	87.584	724.155	88.45			25.745	27.742

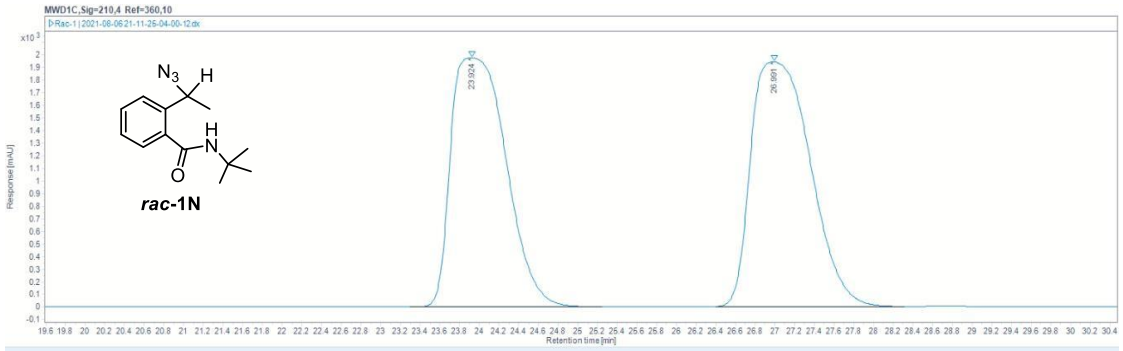

Injection Results

Peaks | Summary

#	Name	Signal description	RT (min)	Area	Area%	Height	Height%	Amount	Concentration	Start time (min)	End time (min)
2		MWD1C,Sig=210,4 Ref=360,10	26.991	81494.473	51.430	1940.417	49.54			26.401	28.313
1		MWD1C,Sig=210,4 Ref=360,10	23.924	76964.092	48.570	1976.720	50.46			23.295	25.245

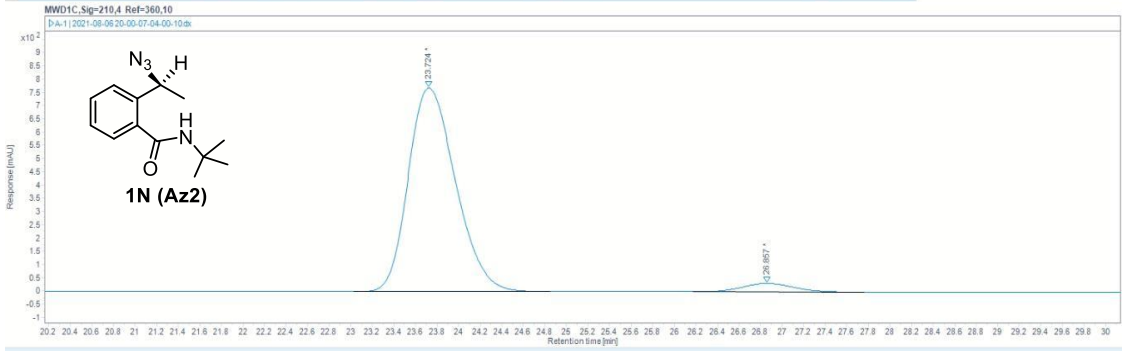

Injection Results

Peaks | Summary

#	Name	Signal description	RT (min)	Area	Area%	Height	Height%	Amount	Concentration	Start time (min)	End time (min)
2		MWD1C,Sig=210,4 Ref=360,10	26.857	1057.972	4.320	31.995	4.00			26.170	27.762
1		MWD1C,Sig=210,4 Ref=360,10	23.724	23429.837	95.680	768.773	96.00			23.027	24.847

Conditions: CHIRALPAK® IC (4.6 × 250 mm, 5 mic), 1% ^{i}PrOH/hexanes, 0.5 mL/min.

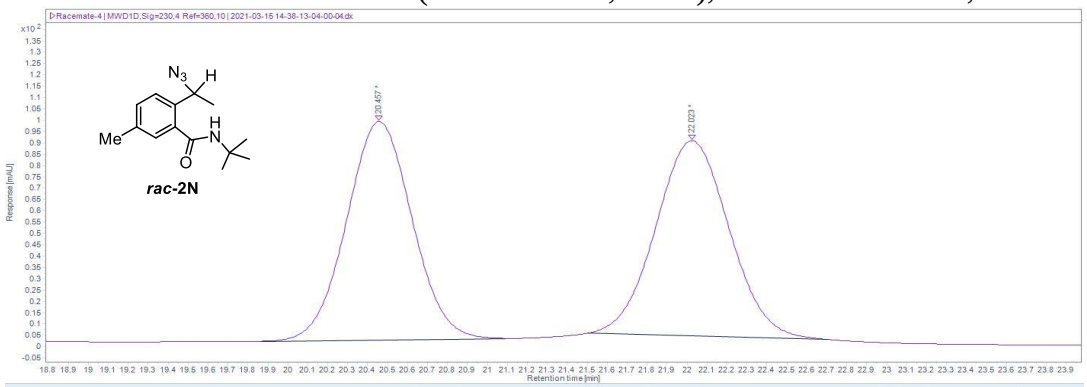

Injection Results

Peaks | Summary

#	Name	Signal description	RT (min)	Area	Area%	Height	Height%	Amount	Concentration	Start time (min)	End time (min)
2		MWD1D,Sig=230,4 Ref=360,10	22.023	2209.769	50.125	86.244	47.21			21.502	22.708
1		MWD1D,Sig=230,4 Ref=360,10	20.457	2198.779	49.875	96.431	52.79			19.864	21.088

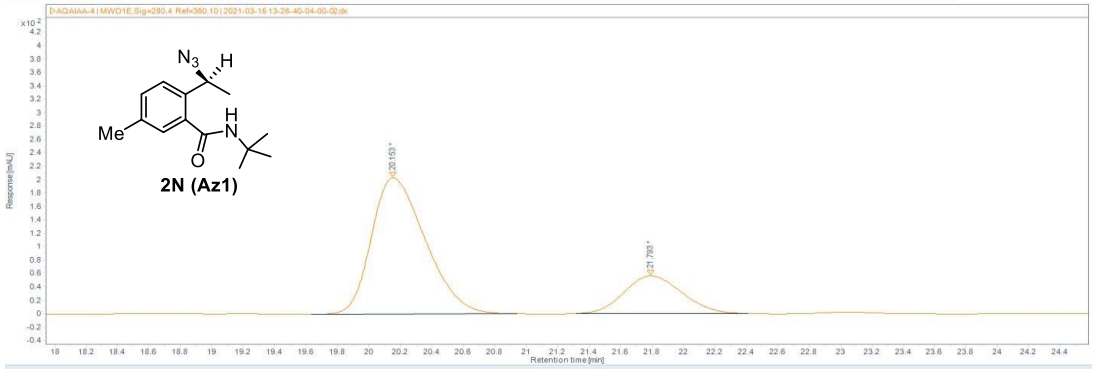

Injection Results

Peaks | Summary

#	Name	Signal description	RT (min)	Area	Area%	Height	Height%	Amount	Concentration	Start time (min)	End time (min)
1		MWD1E,Sig=280,4 Ref=360,10	20.153	4854.363	77.081	203.389	78.34			19.632	20.941
2		MWD1E,Sig=280,4 Ref=360,10	21.793	1443.414	22.919	56.234	21.66			21.317	22.412

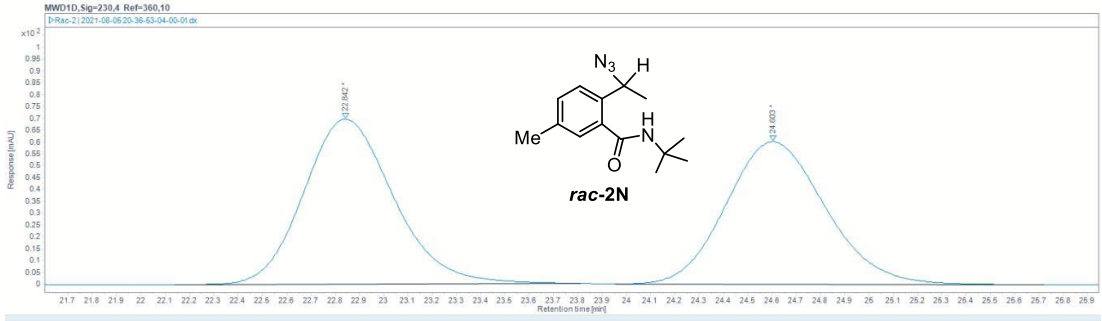

Injection Results

Peaks | Summary

#	Name	Signal description	RT (min)	Area	Area%	Height	Height%	Amount	Concentration	Start time (min)	End time (min)
2		MWD1D,Sig=230,4 Ref=360,10	24.603	1716.320	48.801	60.135	46.32			23.953	25.720
1		MWD1D,Sig=230,4 Ref=360,10	22.842	1800.650	51.199	69.701	53.68			22.138	23.812

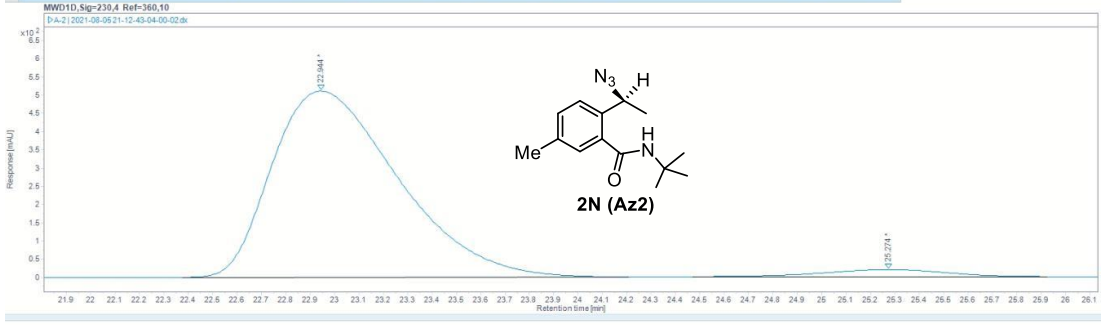

Injection Results

Peaks | Summary

#	Name	Signal description	RT (min)	Area	Area%	Height	Height%	Amount	Concentration	Start time (min)	End time (min)
2		MWD1D,Sig=230,4 Ref=360,10	25.274	668.382	3.512	19.425	3.66			24.471	25.924
1		MWD1D,Sig=230,4 Ref=360,10	22.944	18364.887	96.488	510.591	96.34			22.377	24.207

Conditions: CHIRALPAK® IC (4.6 × 250 mm, 5 mic), 1% ^{i}PrOH/hexanes, 0.5 mL/min.

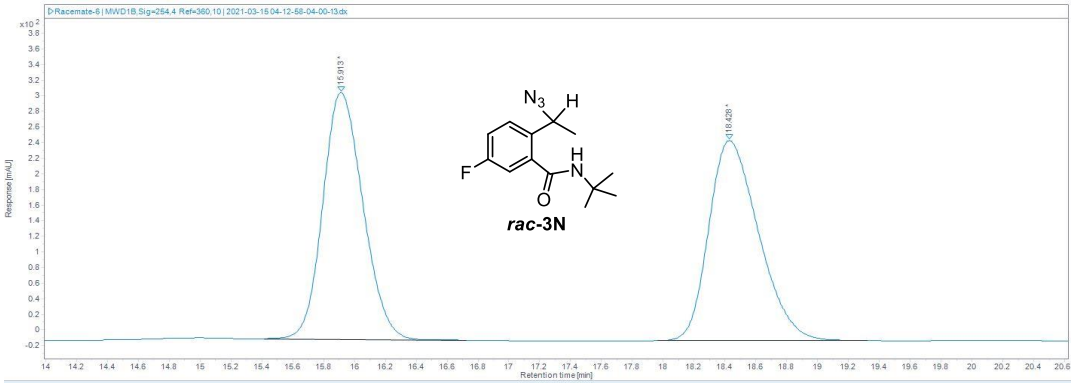

Injection Results

Peaks | Summary

#	Name	Signal description	RT (min)	Area	Area%	Height	Height%	Amount	Concentration	Start time (min)	End time (min)
2		MWD1B,Sig=254,4 Ref=360,10	18.428	5745.806	50.165	256.186	44.75			17.966	19.321
1		MWD1B,Sig=254,4 Ref=360,10	15.913	5707.957	49.835	316.305	55.25			15.417	16.725

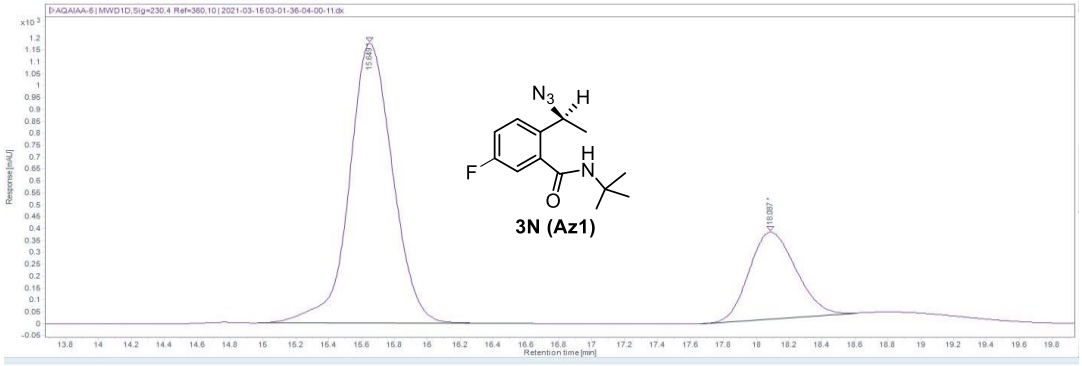

Injection Results

Peaks | Summary

#	Name	Signal description	RT (min)	Area	Area%	Height	Height%	Amount	Concentration	Start time (min)	End time (min)
2		MWD1D,Sig=230,4 Ref=360,10	18.087	7189.204	24.940	364.572	23.66			17.654	18.608
1		MWD1D,Sig=230,4 Ref=360,10	15.649	21636.837	75.060	1176.211	76.34			14.968	16.641

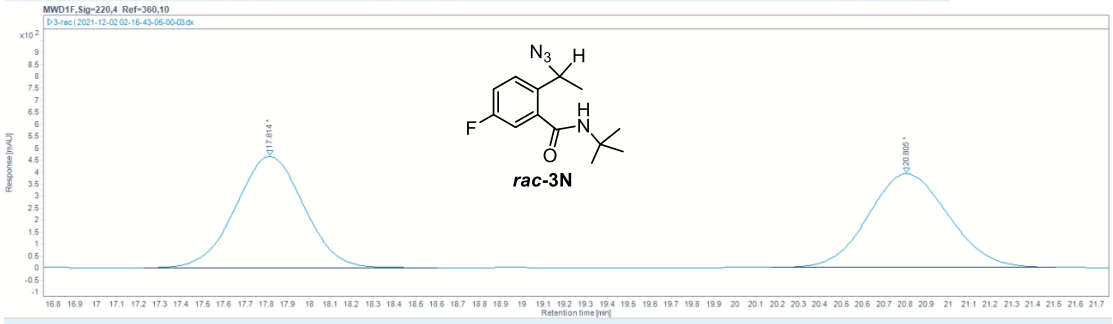

Injection Results

Peaks | Summary

#	Name	Signal description	RT (min)	Area	Area%	Height	Height%	Amount	Concentration	Start time (min)	End time (min)
2		MWD1F,Sig=220,4 Ref=360,10	20.805	10205.254	49.617	390.289	45.64			20.169	21.503
1		MWD1F,Sig=220,4 Ref=360,10	17.814	10362.815	50.383	464.764	54.36			17.223	18.595

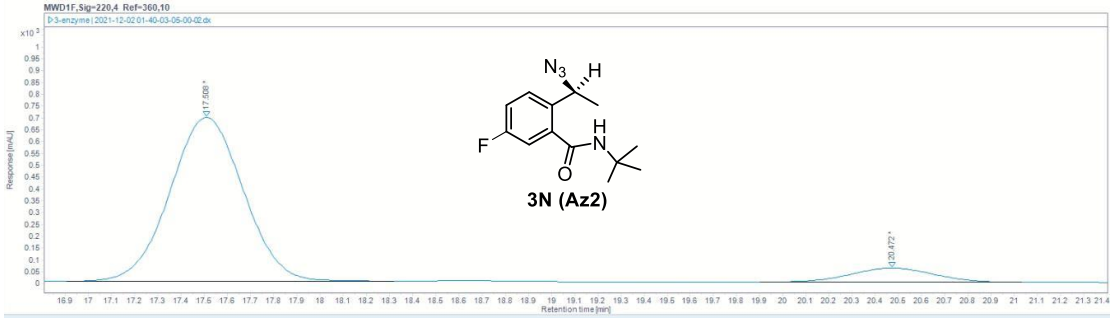

Injection Results

Peaks | Summary

#	Name	Signal description	RT (min)	Area	Area%	Height	Height%	Amount	Concentration	Start time (min)	End time (min)
2		MWD1F,Sig=220,4 Ref=360,10	20.472	1480.626	8.839	59.123	7.87			19.901	21.032
1		MWD1F,Sig=220,4 Ref=360,10	17.508	15270.095	91.161	692.185	92.13			16.907	18.319

Conditions: CHIRALPAK® IC (4.6 × 250 mm, 5 mic), 1% ^{i}PrOH/hexanes, 0.5 mL/min.

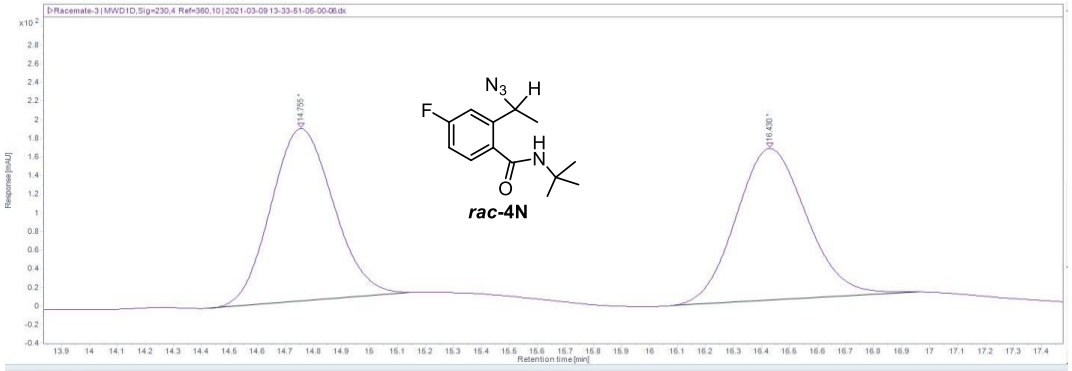

Injection Results

Peaks Summary

#	Name	Signal description	RT (min)	Area	Area%	Height	Height%	Amount	Concentration	Start time (min)	End time (min)
2		MWD1D,Sig=230,4 Ref=360,10	16.430	2854.699	49.865	162.697	46.82			16.076	16.962
1		MWD1D,Sig=230,4 Ref=360,10	14.755	2870.124	50.135	184.820	53.18			14.421	15.141

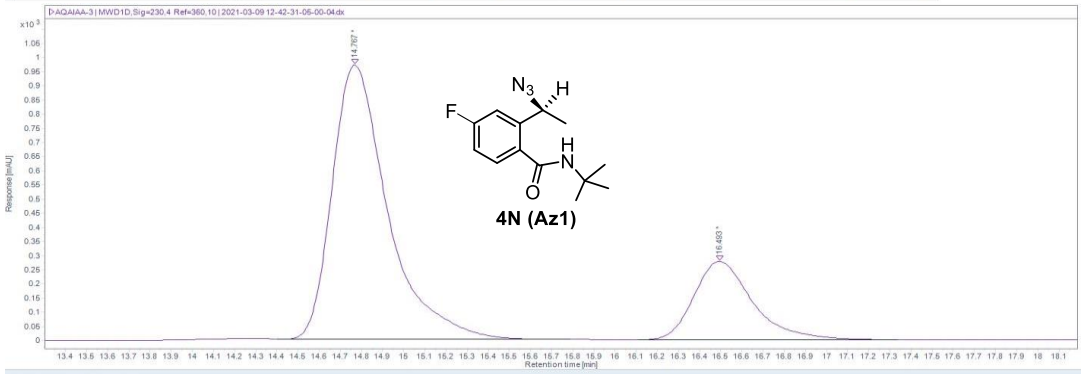

Injection Results

Peaks Summary

#	Name	Signal description	RT (min)	Area	Area%	Height	Height%	Amount	Concentration	Start time (min)	End time (min)
2		MWD1D,Sig=230,4 Ref=360,10	16.493	5373.020	23.345	277.427	22.27			16.109	17.334
1		MWD1D,Sig=230,4 Ref=360,10	14.767	17642.406	76.655	968.362	77.73			14.401	15.785

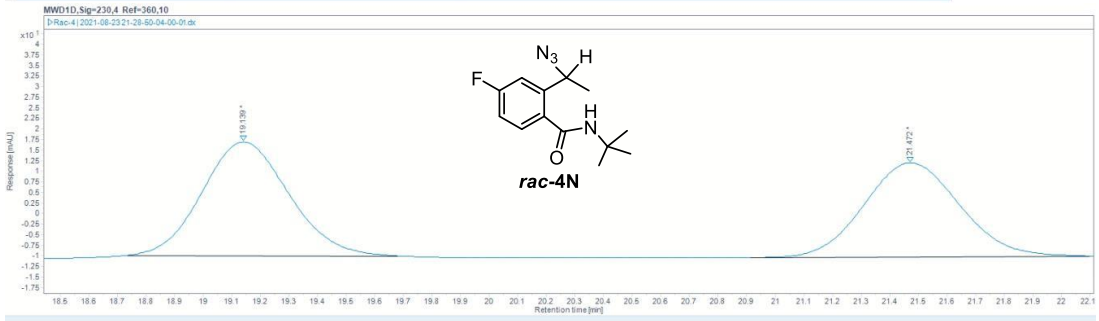

Injection Results

Peaks Summary

#	Name	Signal description	RT (min)	Area	Area%	Height	Height%	Amount	Concentration	Start time (min)	End time (min)
2		MWD1D,Sig=230,4 Ref=360,10	21.472	516.787	47.690	22.223	45.27			20.915	22.099
1		MWD1D,Sig=230,4 Ref=360,10	19.139	566.857	52.310	26.867	54.73			18.734	19.681

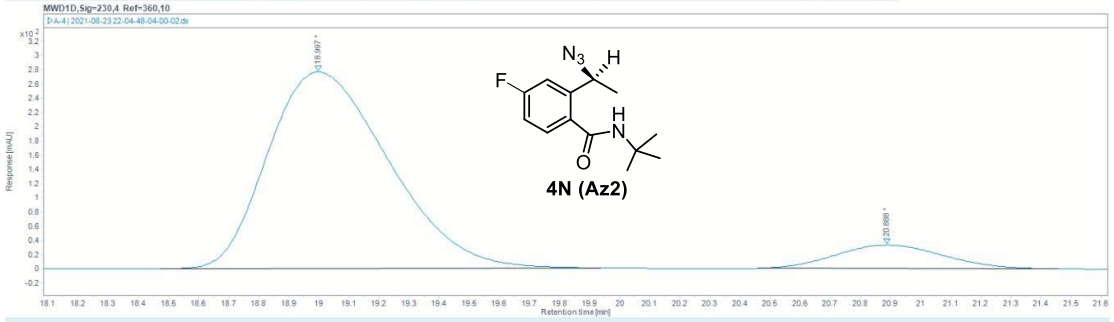

Injection Results

Peaks Summary

#	Name	Signal description	RT (min)	Area	Area%	Height	Height%	Amount	Concentration	Start time (min)	End time (min)
2		MWD1D,Sig=230,4 Ref=360,10	20.888	822.332	9.636	32.978	10.66			20.458	21.458
1		MWD1D,Sig=230,4 Ref=360,10	18.997	7711.197	90.364	276.301	89.34			18.472	19.935

Conditions: CHIRALPAK® IC (4.6 × 250 mm, 5 mic), 2% ^{i}PrOH/hexanes, 0.5 mL/min.

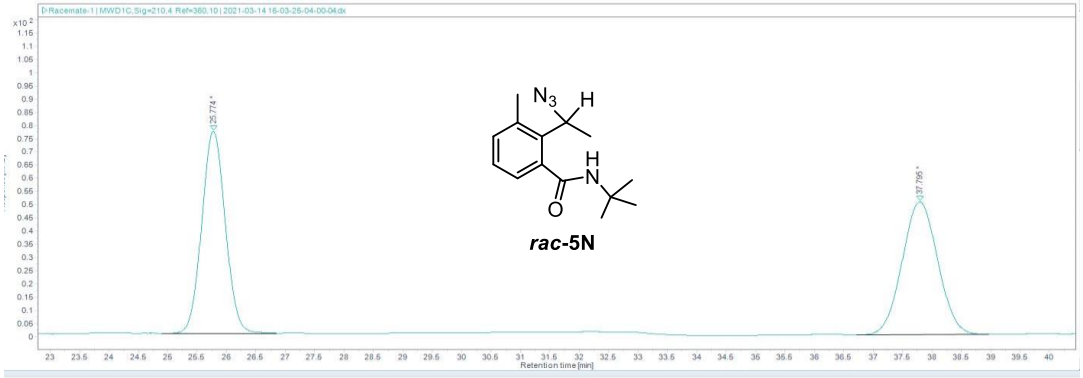

Injection Results

Peaks | Summary

#	Name	Signal description	RT (min)	Area	Area%	Height	Height%	Amount	Concentration	Start time (min)	End time (min)
2		MWD1C,Sig=210,4 Ref=360,10	37.795	2112.633	49.864	50.232	39.62			36.721	38.961
1		MWD1C,Sig=210,4 Ref=360,10	25.774	2124.132	50.136	76.538	60.38			24.899	26.850

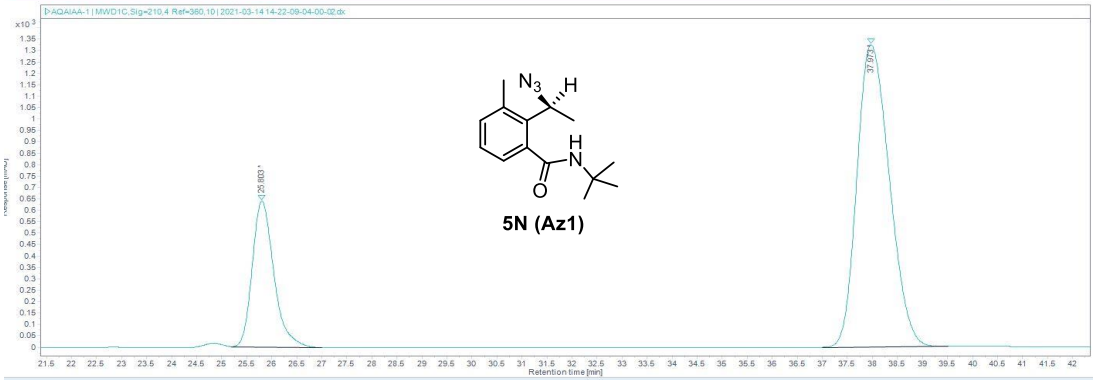

Injection Results

Peaks | Summary

#	Name	Signal description	RT (min)	Area	Area%	Height	Height%	Amount	Concentration	Start time (min)	End time (min)
2		MWD1C,Sig=210,4 Ref=360,10	37.973	59638.788	75.735	1323.199	67.43			36.995	39.512
1		MWD1C,Sig=210,4 Ref=360,10	25.803	19107.816	24.265	639.237	32.57			25.202	26.996

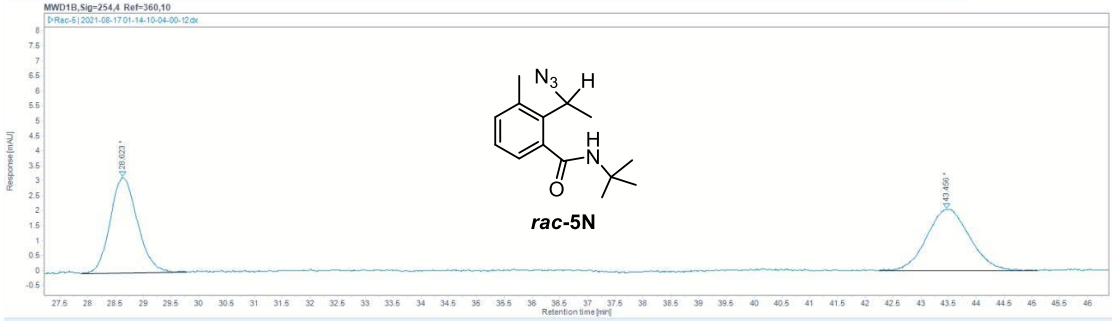

Injection Results

Peaks | Summary

#	Name	Signal description	RT (min)	Area	Area%	Height	Height%	Amount	Concentration	Start time (min)	End time (min)
2		MWD1B,Sig=254,4 Ref=360,10	43.456	109.670	50.386	2.042	39.10			42.242	45.099
1		MWD1B,Sig=254,4 Ref=360,10	28.623	107.992	49.614	3.181	60.90			27.877	29.769

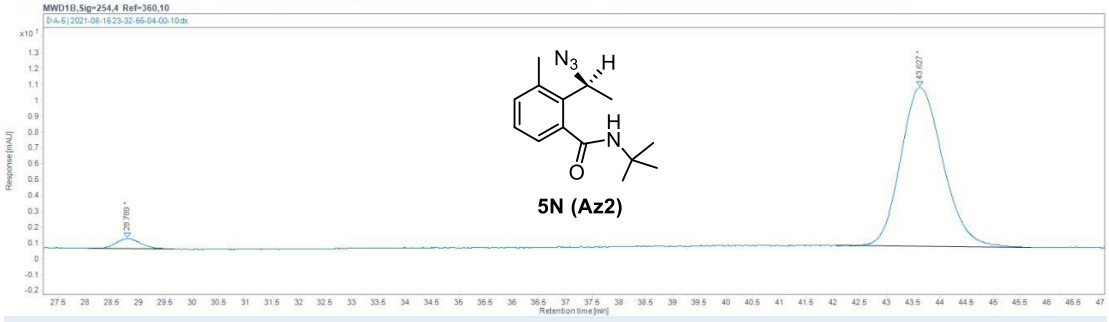

Injection Results

Peaks | Summary

#	Name	Signal description	RT (min)	Area	Area%	Height	Height%	Amount	Concentration	Start time (min)	End time (min)
2		MWD1B,Sig=254,4 Ref=360,10	43.627	554.500	96.449	10.037	93.99			42.049	45.701
1		MWD1B,Sig=254,4 Ref=360,10	28.789	20.418	3.551	0.642	6.01			28.077	29.660

Conditions: CHIRALPAK® IC (4.6 × 250 mm, 5 mic), 1% ^{i}PrOH/hexanes, 0.5 mL/min.

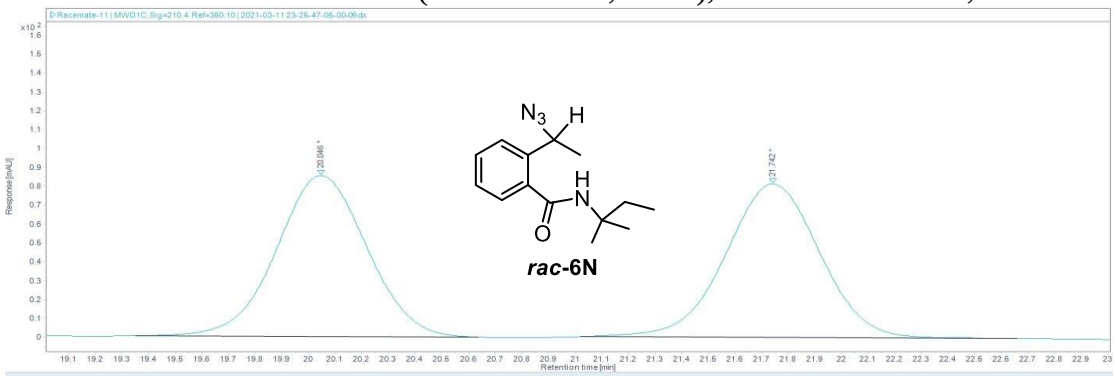

Injection Results

Peaks | Summary

#	Name	Signal description	RT (min)	Area	Area%	Height	Height%	Amount	Concentration	Start time (min)	End time (min)
2		MWD1C,Sig=210,4 Ref=360,10	21.742	2005.207	49.831	81.255	48.81			21.023	22.659
1		MWD1C,Sig=210,4 Ref=360,10	20.046	2018.846	50.169	85.226	51.19			19.350	20.636

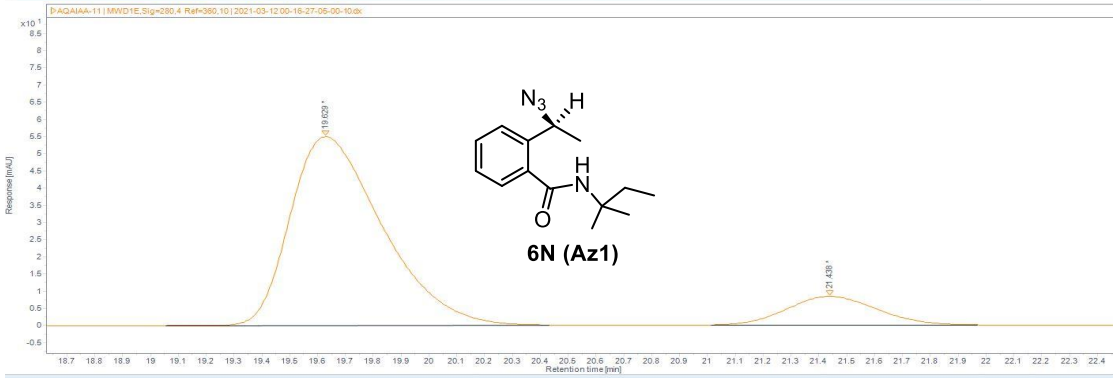

Injection Results

Peaks | Summary

#	Name	Signal description	RT (min)	Area	Area%	Height	Height%	Amount	Concentration	Start time (min)	End time (min)
1		MWD1E,Sig=280,4 Ref=360,10	19.629	1259.565	87.187	54.902	86.90			19.054	20.432
2		MWD1E,Sig=280,4 Ref=360,10	21.438	185.099	12.813	8.278	13.10			21.011	21.970

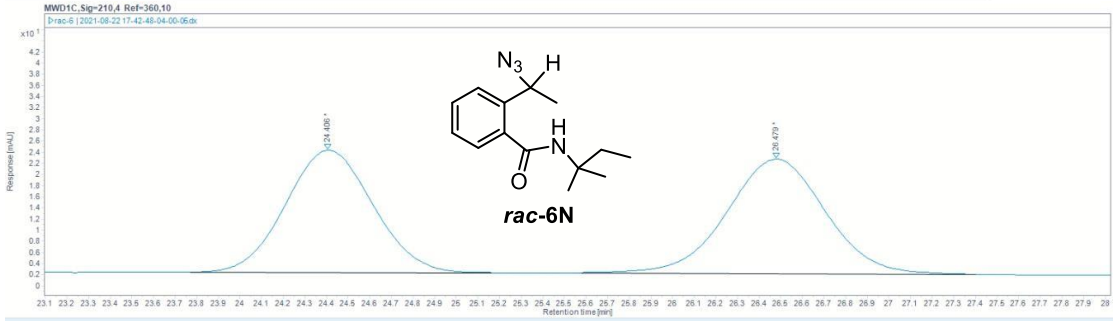

Injection Results

Peaks | Summary

#	Name	Signal description	RT (min)	Area	Area%	Height	Height%	Amount	Concentration	Start time (min)	End time (min)
2		MWD1C,Sig=210,4 Ref=360,10	26.479	648.961	51.315	20.537	48.36			25.577	27.403
1		MWD1C,Sig=210,4 Ref=360,10	24.406	615.701	48.685	21.928	51.64			23.769	25.161

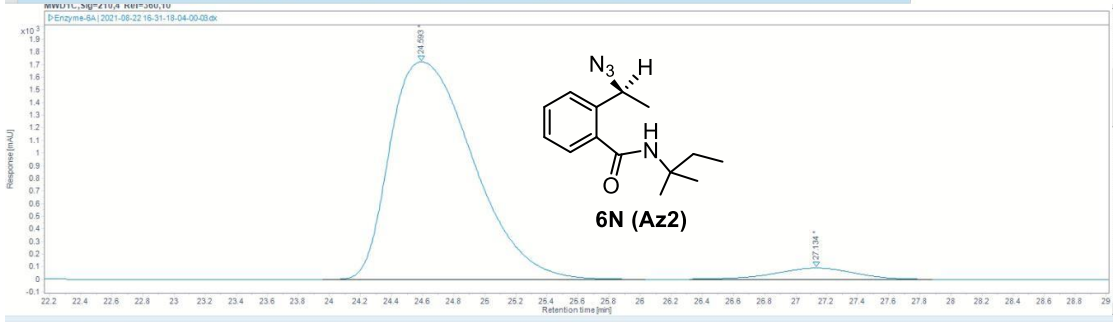

Injection Results

Peaks | Summary

#	Name	Signal description	RT (min)	Area	Area%	Height	Height%	Amount	Concentration	Start time (min)	End time (min)
2		MWD1C,Sig=210,4 Ref=360,10	27.134	3132.631	4.644	88.522	4.88			26.314	27.877
1		MWD1C,Sig=210,4 Ref=360,10	24.593	64317.220	95.356	1723.939	95.12			23.954	26.034

Conditions: CHIRALPAK® IC (4.6 × 250 mm, 5 mic), 2% ^{i}PrOH/hexanes, 0.5 mL/min.

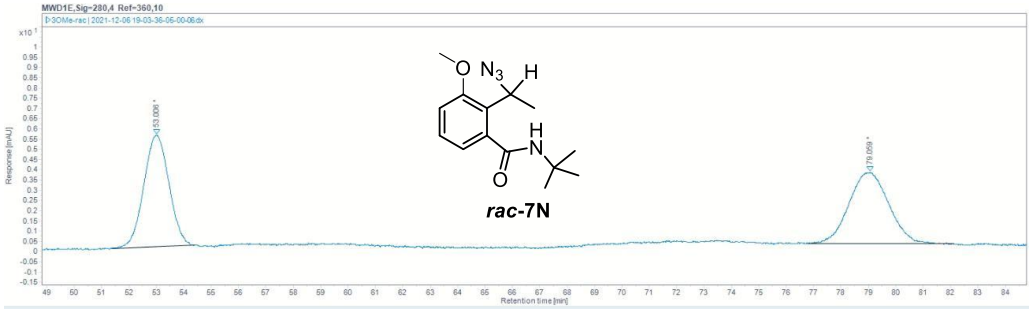

Injection Results

Peaks | Summary

#	Name	Signal description	RT (min)	Area	Area%	Height	Height%	Amount	Concentration	Start time (min)	End time (min)
2		MWD1E,Sig=280,4 Ref=360,10	79.059	349.770	50.211	3.469	38.89			76.777	82.110
1		MWD1E,Sig=280,4 Ref=360,10	53.006	346.836	49.789	5.451	61.11			51.361	54.398

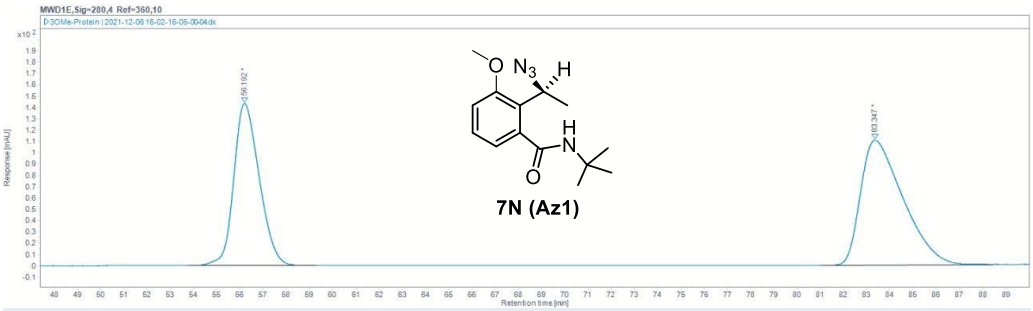

Injection Results

Peaks | Summary

#	Name	Signal description	RT (min)	Area	Area%	Height	Height%	Amount	Concentration	Start time (min)	End time (min)
2		MWD1E,Sig=280,4 Ref=360,10	83.347	13981.586	56.119	110.466	43.54			81.015	88.453
1		MWD1E,Sig=280,4 Ref=360,10	56.192	10932.558	43.881	143.256	56.46			53.773	59.276

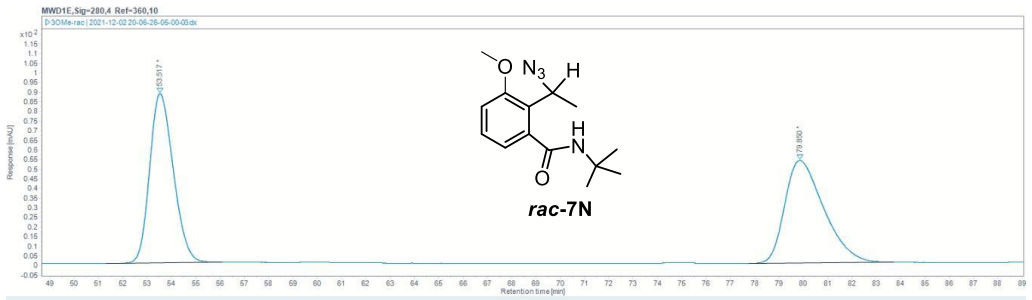

Injection Results

Peaks | Summary

#	Name	Signal description	RT (min)	Area	Area%	Height	Height%	Amount	Concentration	Start time (min)	End time (min)
2		MWD1E,Sig=280,4 Ref=360,10	79.850	5947.915	50.033	53.284	37.73			77.766	83.717
1		MWD1E,Sig=280,4 Ref=360,10	53.517	5940.042	49.967	87.929	62.27			51.317	56.083

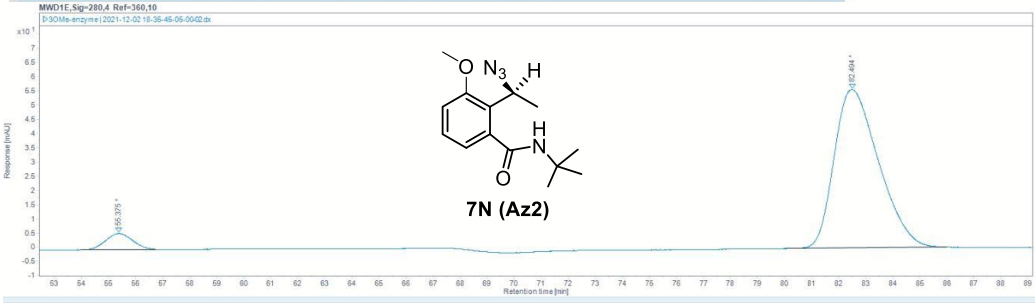

Injection Results

Peaks | Summary

#	Name	Signal description	RT (min)	Area	Area%	Height	Height%	Amount	Concentration	Start time (min)	End time (min)
2		MWD1E,Sig=280,4 Ref=360,10	82.494	6364.623	94.244	55.772	90.82			80.076	85.980
1		MWD1E,Sig=280,4 Ref=360,10	55.375	388.719	5.756	5.635	9.18			54.003	56.755

Conditions: CHIRALPAK® IC (4.6 × 250 mm, 5 mic), 1% ^{i}PrOH/hexanes, 0.5 mL/min.

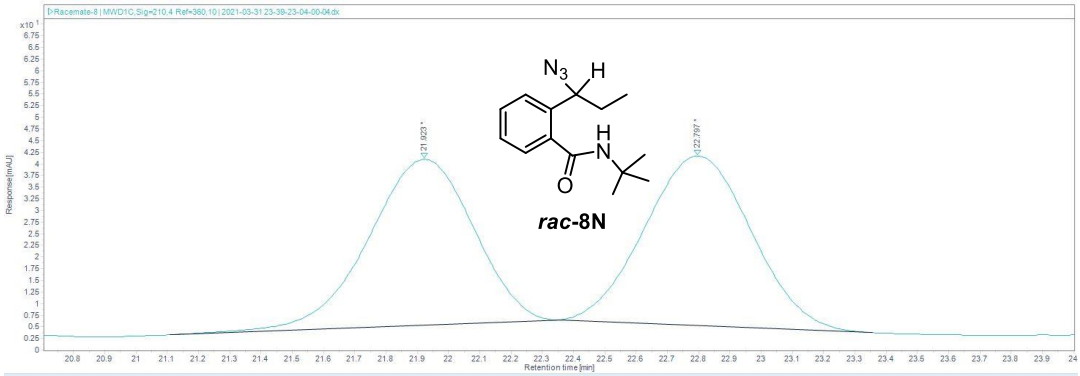

Injection Results

Peaks | Summary

#	Name	Signal description	RT (min)	Area	Area%	Height	Height%	Amount	Concentration	Start time (min)	End time (min)
2		MWD1C,Sig=210,4 Ref=360,10	22.797	863.492	50.960	36.397	50.56			22.360	23.357
1		MWD1C,Sig=210,4 Ref=360,10	21.923	830.955	49.040	35.584	49.44			21.108	22.360

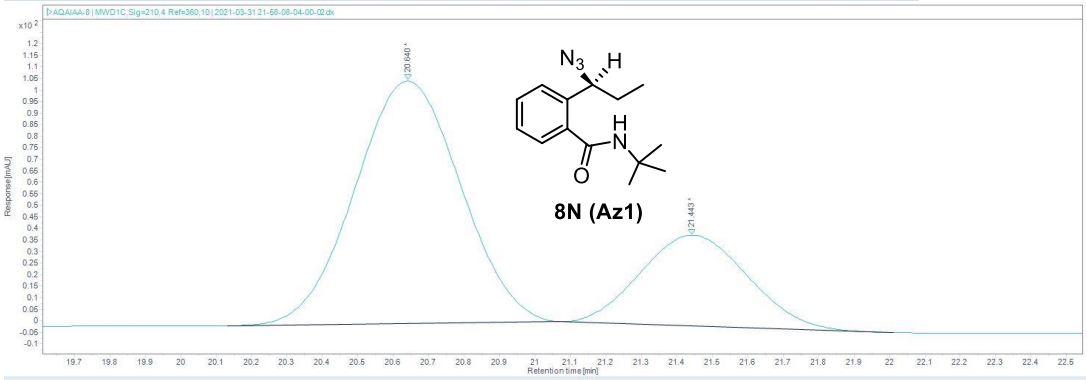

Injection Results

Peaks | Summary

#	Name	Signal description	RT (min)	Area	Area%	Height	Height%	Amount	Concentration	Start time (min)	End time (min)
2		MWD1C,Sig=210,4 Ref=360,10	21.443	827.000	27.501	39.384	27.26			21.066	22.011
1		MWD1C,Sig=210,4 Ref=360,10	20.640	2180.206	72.499	105.112	72.74			20.133	21.066

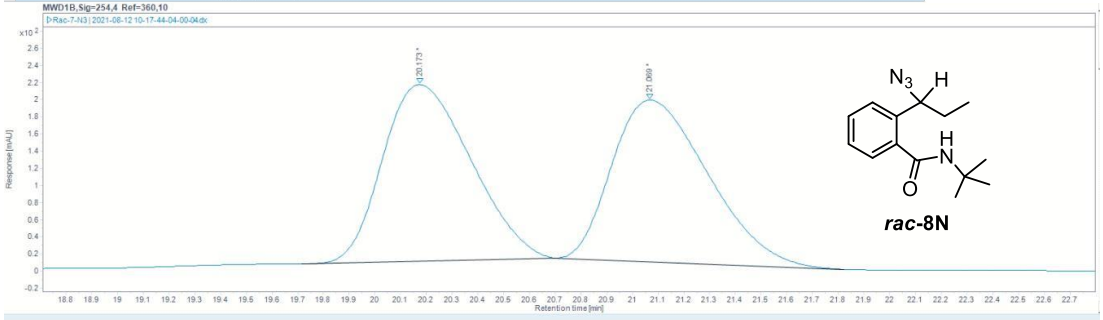

Injection Results

Peaks | Summary

#	Name	Signal description	RT (min)	Area	Area%	Height	Height%	Amount	Concentration	Start time (min)	End time (min)
2		MWD1B,Sig=254,4 Ref=360,10	21.069	4885.870	49.924	188.355	47.78			20.693	21.823
1		MWD1B,Sig=254,4 Ref=360,10	20.173	4900.705	50.076	205.880	52.22			19.717	20.693

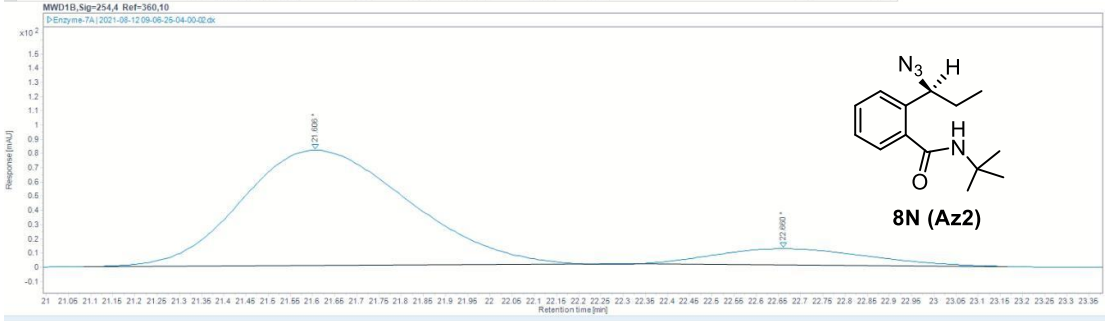

Injection Results

Peaks | Summary

#	Name	Signal description	RT (min)	Area	Area%	Height	Height%	Amount	Concentration	Start time (min)	End time (min)
2		MWD1B,Sig=254,4 Ref=360,10	22.660	276.541	11.517	11.482	12.39			22.324	23.166
1		MWD1B,Sig=254,4 Ref=360,10	21.606	2124.688	88.483	81.193	87.61			21.084	22.324

Conditions: CHIRALPAK® IC (4.6 × 250 mm, 5 mic), 1% ^{i}PrOH/hexanes, 0.10 mL/min.

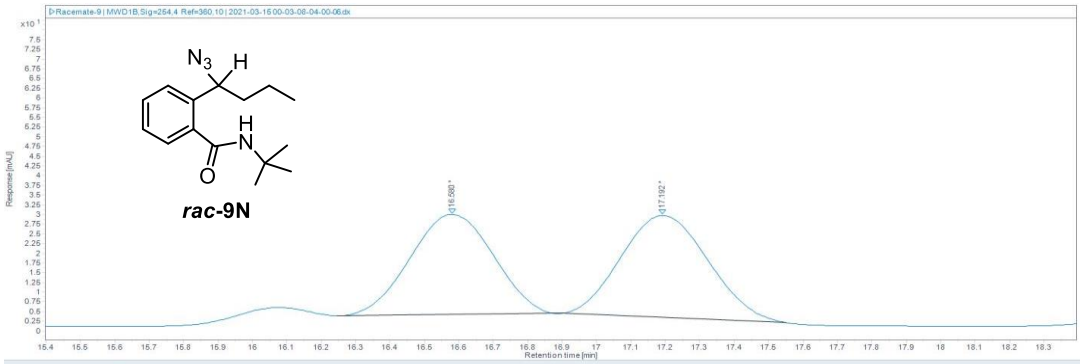

Injection Results

Peaks | Summary

#	Name	Signal description	RT (min)	Area	Area%	Height	Height%	Amount	Concentration	Start time (min)	End time (min)
1		MWD1B,Sig=254,4 Ref=360,10	16.580	433.020	48.309	25.816	49.57			16.244	16.897
2		MWD1B,Sig=254,4 Ref=360,10	17.192	463.332	51.691	26.263	50.43			16.897	17.551

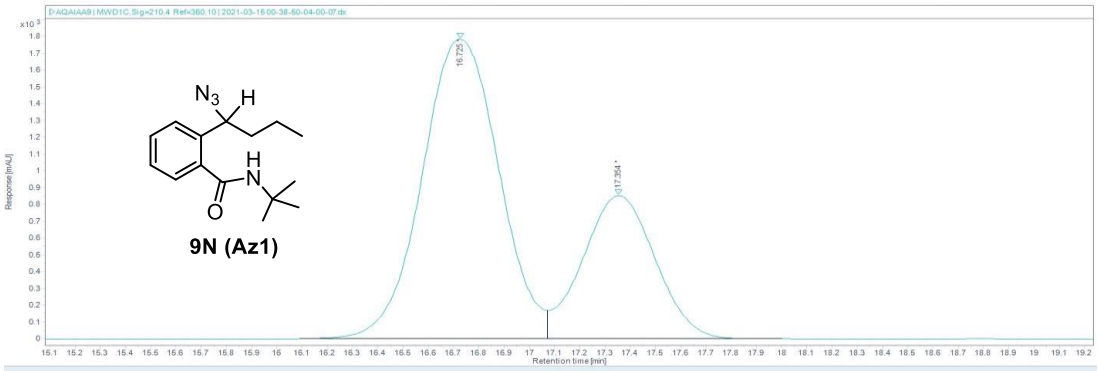

Injection Results

Peaks | Summary

#	Name	Signal description	RT (min)	Area	Area%	Height	Height%	Amount	Concentration	Start time (min)	End time (min)
2		MWD1C,Sig=210,4 Ref=360,10	17.354	16959.275	31.088	851.007	32.32			17.071	18.002
1		MWD1C,Sig=210,4 Ref=360,10	16.725	37592.489	68.912	1782.428	67.68			16.091	17.071

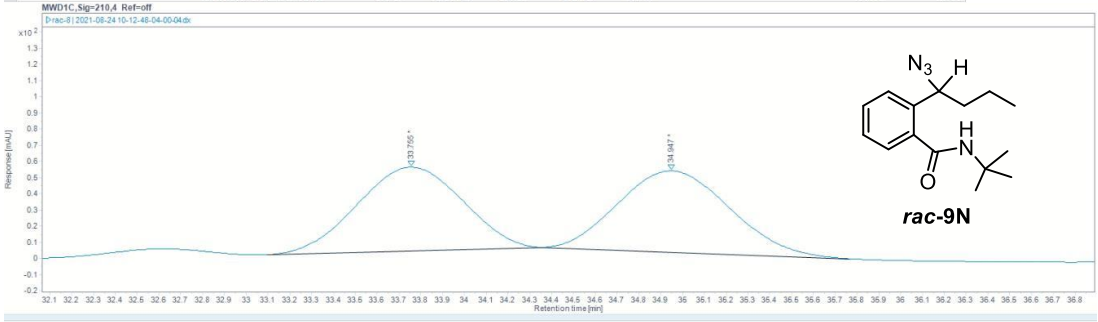

Injection Results

Peaks | Summary

#	Name	Signal description	RT (min)	Area	Area%	Height	Height%	Amount	Concentration	Start time (min)	End time (min)
2		MWD1C,Sig=210,4 Ref=off	34.947	1787.079	50.738	50.268	49.29			34.356	35.768
1		MWD1C,Sig=210,4 Ref=off	33.755	1735.086	49.262	51.722	50.71			33.098	34.356

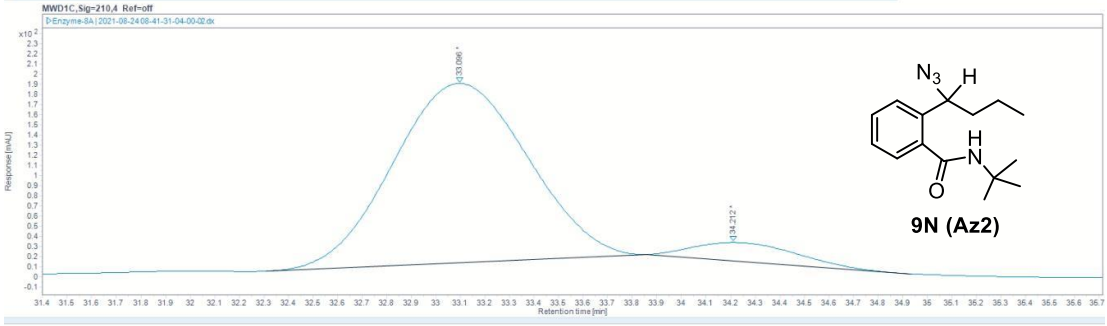

Injection Results

Peaks | Summary

#	Name	Signal description	RT (min)	Area	Area%	Height	Height%	Amount	Concentration	Start time (min)	End time (min)
2		MWD1C,Sig=210,4 Ref=off	34.212	543.528	7.465	18.164	9.31			33.858	34.936
1		MWD1C,Sig=210,4 Ref=off	33.096	6737.461	92.535	177.044	90.69			32.311	33.858

Conditions: CHIRALPAK® IC (4.6 × 250 mm, 5 mic), 1% ^{i}PrOH/hexanes, 0.25 mL/min.

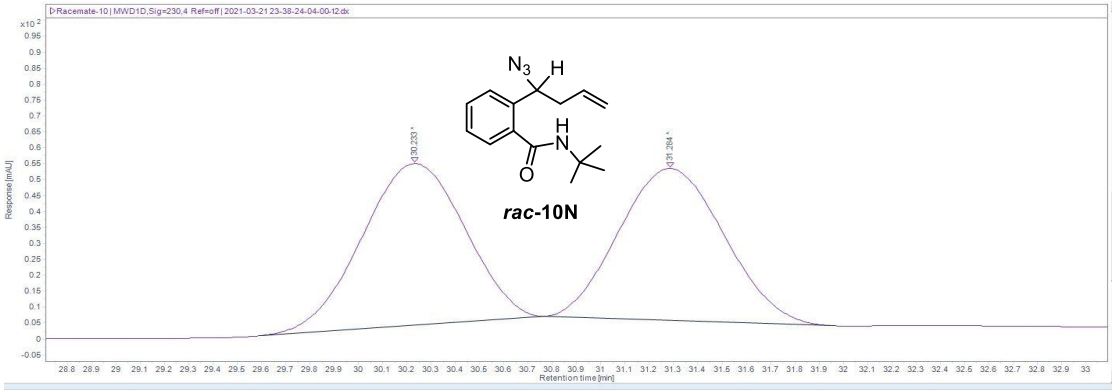

Injection Results

Peaks | Summary

#	Name	Signal description	RT (min)	Area	Area%	Height	Height%	Amount	Concentration	Start time (min)	End time (min)
2		MWD1D,Sig=230,4 Ref=off	31.284	1439.617	49.032	47.657	48.46			30.764	31.968
1		MWD1D,Sig=230,4 Ref=off	30.233	1496.484	50.968	50.687	51.54			29.591	30.764

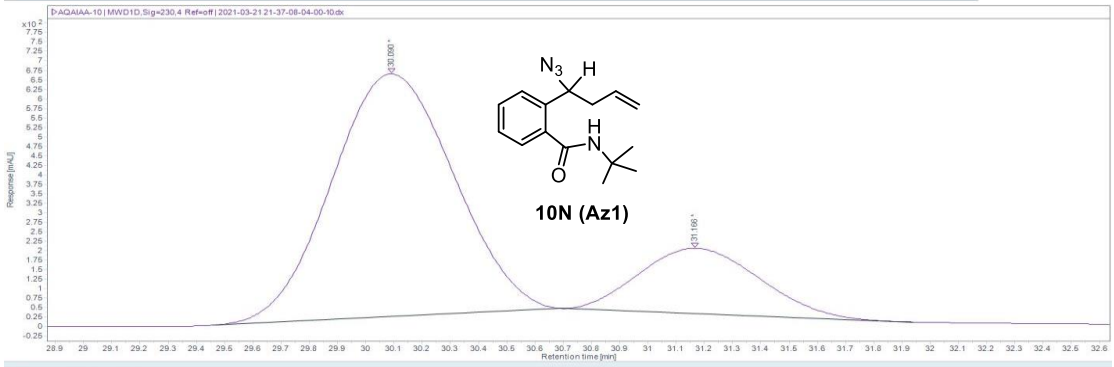

Injection Results

Peaks | Summary

#	Name	Signal description	RT (min)	Area	Area%	Height	Height%	Amount	Concentration	Start time (min)	End time (min)
2		MWD1D,Sig=230,4 Ref=off	31.166	5098.783	20.955	171.801	21.18			30.691	31.942
1		MWD1D,Sig=230,4 Ref=off	30.090	19233.583	79.045	639.413	78.82			29.457	30.691

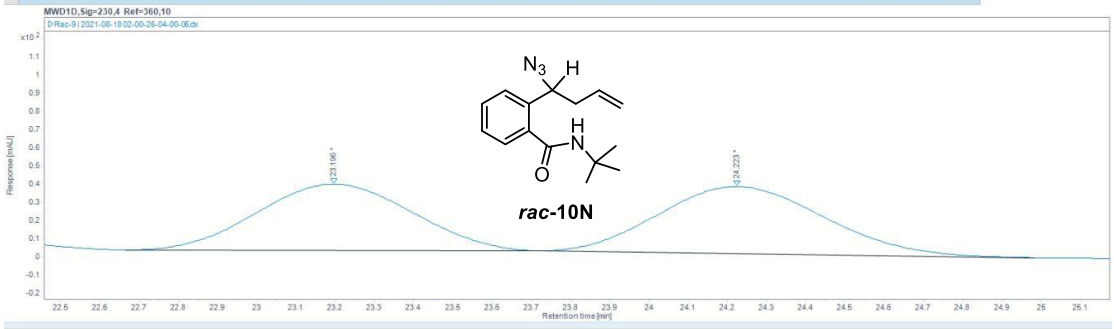

Injection Results

Peaks | Summary

#	Name	Signal description	RT (min)	Area	Area%	Height	Height%	Amount	Concentration	Start time (min)	End time (min)
2		MWD1D,Sig=230,4 Ref=360,10	24.223	1078.182	51.996	36.803	50.30			23.735	24.985
1		MWD1D,Sig=230,4 Ref=360,10	23.196	995.392	48.004	36.366	49.70			22.664	23.735

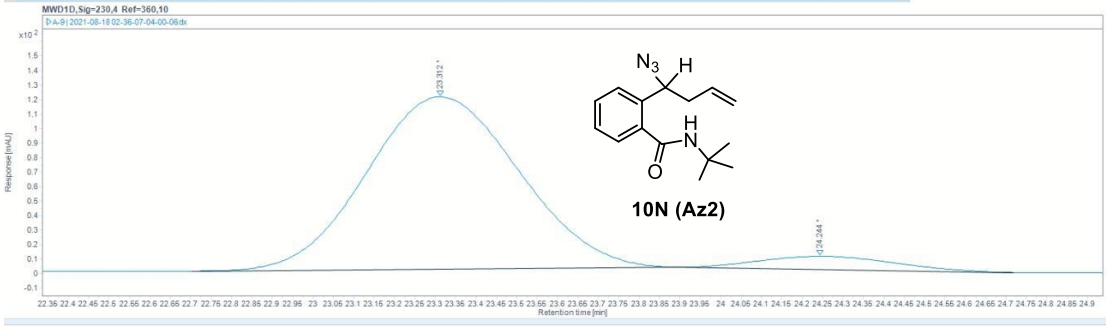

Injection Results

Peaks | Summary

#	Name	Signal description	RT (min)	Area	Area%	Height	Height%	Amount	Concentration	Start time (min)	End time (min)
2		MWD1D,Sig=230,4 Ref=360,10	24.244	209.408	6.354	9.074	7.10			23.890	24.717
1		MWD1D,Sig=230,4 Ref=360,10	23.312	3086.081	93.646	118.705	92.90			22.702	23.890

IX. Preparative Scale Enzymatic Reactions

Preparation of whole-cell suspensions for azidation reactions: Two hundred milliliter TB_{amp} in a one-liter flask was inoculated with an overnight culture (2 mL in LB_{amp}) of recombinant *E. cloni*® EXPRESS BL21(DE3) cells containing a pET22b(+) plasmid encoding the non-heme iron enzyme variant. The culture was shaken at 37 °C and 250 rpm until the OD_{600} was 0.7 (approximately 2 hours). The culture was placed on ice for 30 minutes, and isopropyl *β-D*-1-thiogalactopyranoside (IPTG) was added to final concentrations of 1 mM. The incubator temperature was reduced to 20.5 °C, and the culture was allowed to shake for 24 hours at 180 rpm. Cells were harvested by centrifugation (4 °C, 15 min, 4,000xg) and resuspended in KPi buffer (pH 7.4) and adjusted to OD_{600} = 20. The whole-cell suspension was placed on ice and bubbled with Ar for 15 min.

Biocatalytic synthesis of (2-(1-azidoethyl)-*N*-(*tert*-butyl)benzamide (1N) (0.75 mmol scale reaction): Under anaerobic conditions, to a 40 mL vial were added 15 mL of *Sav* HppD Az1 whole-cell suspension (OD_{600} = 20), ferrous ammonium sulfate (0.5 mL, 100 mM in water), sodium azide (1 mL, 1 M in water), and *N*-fluoroamide substrate **1NF** (0.5 mL, 1.5 M in DME)**.** The vial was capped and shaken at 680 rpm in an anaerobic chamber at room temperature for 48 hours. The reaction mixture was then transferred to a 50-mL Falcon tube and mixed with 30 mL 6:4 EtOAc *via* vortexing (30 s for three times). The organic and aqueous layers were then separated via centrifugation (10,500xg, 5 min). After removal of the organic layers, two additional rounds of extraction were performed. The combined organic extracts were dried over anhydrous Na_2SO_4, concentrated, and purified by flash chromatography to afford pure azidation product **1N** (120 mg, 0.488 mmol, 65% yield).

Preparative scale synthesis and one-pot derivatization of enzymatic azidation product 10: Under anaerobic conditions, to a 20 mL vial were added 5 mL of *Sav* HppD Az1 whole-cell suspension (OD_{600} = 20), ferrous ammonium sulfate (0.25 mL, 100 mM in water), sodium azide (0.25 mL, 1 M in water), and *N*-fluoroamide substrate **11NF** (0.125 mL, 1.5 M in DME)**.** The vial was capped and shaken at 680 rpm in an anaerobic chamber at room temperature for 48 hours. Afterwards, a DMF solution of the alkyne (0.188 mmol, 57.8 mg) was added to the reaction mixture, which is followed by the addition of $CuSO_4$ (0.02 mmol, 3.2 mg), BTTAA ligand (0.04 mmol, 17 mg), and sodium ascorbate (0.02 mmol, 4 mg). The reaction was left in an anerobic chamber and shaked overnight. The reaction mixture was then extracted with ethylacetate (3 ´ 20 mL). Removal of the organic solvent under vacuum and the crude was purified by Biotage flash chromatography to afford pure azidation product **19** as white solid (56 mg, 55% yield). **Characterization of 19: ^{1}H NMR (300 MHz, $CDCl_3$)** δ 7.92 (s, 1H), 7.45-7.35 (m, 4H), 7.22-7.19 (m, 1H), 6.81-6.73 (m, 2H), 5.97 (brs, 1H), 5.74 (s, 2H), 5.16 (s, 2H), 2.93-2.88 (m, 2H), 2.57-2.33 (m, 2H), 2.19-1.95 (m, 6H), 1.71-1.39 (m, 14H), 0.92 (s, 3H). **^{13}C NMR (75 MHz, $CDCl_3$)** δ 220.9, 168.4, 156.3, 144.2, 137.9, 136.9, 133.1, 133.0, 132.6, 130.7, 128.9, 127.2, 126.4, 124.0, 114.8, 112.4, 62.0, 52.2, 51.3, 50.4, 48.0, 44.0, 38.3, 35.9, 31.6, 29.7, 28.8, 26.5, 25.9, 21.6, 13.9.

X. Spectroscopic studies

Anaerobic Techniques Unless otherwise stated, spectroscopic samples were prepared in an MBraun UNIlab glovebox circulated under a positive pressure of N_2(g). *Sav* HppD Az1 was rendered anoxic by vacuuming and sparging the protein (~7 cycles) with Ar(g) in a round bottom flask connected to a Shlenk line. All buffers and compounds were prepared within the glovebox to render a uniform anaerobic environment.

UV-Vis Sample Preparation and Spectra Collection
UV-Vis Samples (final volume = 200 µL) contained 350 µM *Sav* HppD Az1, 320 µM Fe^{2+}, 70 mM azide, and 8.75 mM substrate in 50 mM potassium phosphate buffer pH 7.4. Stock solutions of anaerobic substrate (~100 mM), ferrous ammonium sulfate (40 mM), and 250 mM sodium azide were prepared in phosphate buffer and diluted as needed to yield the previously mentioned quantities. Reactions were initiated by spiking the respective anaerobic substrate into the generated *Sav* HppD Az1-Fe(II)-azide complex.

UV-Vis spectra were collected using an Agilent Cary 8454 spectrophotometer placed in the glovebox, which is equipped with a temperature controlled cuvette holder (set temperature 4 °C). All samples were collected within a micro quartz cuvette (12.5 mm width x 45 mm height; total size, 3 mm width x 4 mm height; optical window; 1 cm pathlength). Spectra (full traces and single wavelength) were collected and analyzed using the Agilent ChemStation software. All UV-Vis figures were created using the software SpectraGryph (https://www.effemm2.de/spectragryph/).

Mössbauer Sample Preparation and Spectral Analysis
Sav HppD Az1 Mössbaur samples (final volume = 300 µL) were comprised of 1 mM *Sav* HppD Az1, 0.9 mM ^{57}Fe, and varying concentrations of azide (0 – 200 mM). Specifically, samples were prepared by addition of each component to 20 mM potassium phosphate buffer pH 7.4, wherein azide was added as the final component of each sample. Following azide addition, each sample was incubated in the glovebox for 5 minutes prior to freezing under liquid nitrogen. Polyoxymethylene cups were used as sample holders for Mössbauer samples.

Mössbaur spectra were recorded with home-built Mössbauer spectrometers using Janis Research SuperVaritemp dewars. These dewars allow for studies in the temperature range of 1.5 to 200 K and applied magnetic fields up to 8 T. A LakeShore model 331A temperature controller was used to control the temperature in experiments. Spectral simulations were preformed using the WMOSS software package (SEE Co., Edina, MN). Isomer shifts are quoted relative to Fe metal at room temperature. All Mössbauer figures were prepared using the software SpinCount (*10*).

Regarding simulations, all Mössbaur spectra were analyzed with the following Hamiltonian:

$$H = H_Q = \frac{eQV_{ZZ}}{4I(2I-1)}\left[3\hat{I}_z^2 - I(I+1) + \eta\left(\hat{I}_x^2 - \hat{I}_y^2\right)\right] \text{ (Equation 1)}$$

Wherein the Hamiltonian reflects the electric quadrupole interactions. Within the quadrupole Hamiltonian, Q is the quadrupole moment, V_{zz} is the z component of the electric field gradient tensor $\tilde{V}$. The term I is the ^{57}Fe nuclear spin, which is I = 3/2 for the excited ^{57}Fe nuclear states, η is an asymmetry parameter (denoted by $\eta = \frac{(V_{xx}-V_{yy})}{V_{zz}}$). Spectra were fit directly with this

Hamiltonian, wherein isomer shift, quadrupole splitting, and relative area parameters were gleaned from the spectral fits.

Sav HppD Az1 Reaction EPR Sample Preparation

Typical enzymatic reaction EPR samples consisted of a 300 µL mixtures of 300 µM *Sav* HppD Az1, 270 µM Fe^{2+}, 7.5 mM non-ethyl substrate, and 60 mM sodium azide within 50 mM sodium phosphate pH 7.4. Stock solutions of anaerobic HppD (~1 mM protein), ~100 mM non-ethyl substrate, 25 mM ferrous ammonium sulfate, and 250 mM sodium azide were all diluted in phosphate buffer to yield the previously mentioned working concentrations. Following addition of the substrate analog, **18NF**, samples were incubated anaerobically at 4 °C prior to freezing in liquid $N_2(l)$.

X Band EPR spectra were collected with a Bruker ELEXYS-II E500 EPR spectrometer equipped with an Oxford ESR-910 liquid helium cryostat. The signal was quantified relative to a previously prepared Cu(II)(EDTA) spin standard. The microwave frequency was calibrated with a frequency counter, while the magnetic field was calibrated with an NMR gaussmeter. Unless specifically specified, the following standard parameters were used for each EPR spectrum: 100 kHz modulation frequency, 5 G modulation amplitude, 150 ms conversion time, 9.63 GHz microwave frequency. Each sample was analyzed at an appropriate microwave power and sample temperature to satisfy non saturating conditions. EPR spectra were simulated, and each signal was quantified using the software SpinCount (*10*). During simulations, all intensity factors both theoretical and experimental were considered to quantify each signal.

Sav HppD Az1 Reaction EPR Spectral Analysis

Analysis of the EPR spectra of the *Sav* HppD Az1 reaction with the substrate analog, **17NF**, displays that the mononuclear iron in *Sav* HppD Az1 is in the S = 5/2 high spin Fe(III) state. Simulations were therefore analyzed using the following spin Hamiltonian:

$$\widehat{H} = D\left[\vec{S}_z^2 - \frac{35}{12} + \left(\frac{E}{D}\right)\left(\vec{S}_x^2 - \vec{S}_y^2\right)\right] + \beta\vec{S}\cdot\tilde{\boldsymbol{g}}\cdot\vec{B} \quad \text{(Equation 2)}$$

Within equation 2, *D* and *E* correspond to the axial and rhombic zero-field splitting (ZFS) terms. The coordinates (x, y, and z) delineate the principal axes of the zero-field splitting tensor. The remaining terms have their usual definitions: β is the electron Bohr magneton, *S* is the spin vector, *B* is the magnetic field vector, and $\tilde{g}$ is the g tensor. The *E*/*D* parameter may be used to measure the characteristics of the electronic environment associated with the system in question. In this instance, we may use it to survey the iron in *Sav* HppD Az1 as its electronic characteristics lie between fully axial (E/D = 0) and fully rhombic (E/D = 0.333) symmetry. Spectral simulations allow for determination of the E/D parameter of each spectra recorded. Furthermore, the intensity of the observed EPR signals may be examined at multiple temperatures to determine saturation conditions as well as the value of *D*. Following the calculations of the *E*/*D* and *D* values, correlation of spectra features to spin quantifications were accomplished via simulations with double integration methods.

Sav HppD Az1 NO Adduct EPR Sample Preparation

Sav HppD Az1 NO containing EPR samples comprised 250 µL solutions of 250 µM *Sav* HppD Az1, 225 µM Fe^{2+}, 2.5 mM ascorbate, 2.5 mM NO(g), and variable amounts of azide (0-50 mM) and the substrate, **1NF** (0 or 6.25 mM). A saturated stock NO(g) containing solution was generated by dissolving DEA NONOate (Sigma Aldrich) powder in phosphate buffer and

incubating for ~10 minutes at room temperature. Samples were prepared by addition of all the previously mentioned components prior to NONOate solution addition. Each sample was incubated for ~15 minutes prior to DEA NONOate solution addition. Following NO addition, each sample was incubated for an additional 5 minutes prior to freezing in liquid N_2(l).

Sav HppD Az1 NO Adduct EPR Simulation Analysis

EPR spectra were collected in a manner identical to that which was described in the "_Sav_ HppD Az1 Reaction EPR Sample Preparation section." The $\{FeNO\}^7$ S = 3/2 species was analyzed by using the following spin Hamiltonian:

$$\widehat{H} = \vec{S} \cdot \widetilde{D} \cdot \vec{S} + \beta \vec{S} \cdot \tilde{g} \cdot \vec{B} = D\left[\vec{S}_z^2 - \frac{15}{4} + \left(\frac{E}{D}\right)\left(\vec{S}_x^2 - \vec{S}_y^2\right)\right] + \beta \vec{S} \cdot \tilde{g} \cdot \vec{B} \text{ (Equation 3)}$$

Where, in a similar manner to the previously discussed S = 5/2 Hamiltonian, E and D are the rhombic and axial ZFS terms, β is the electron Bohr magneton, S is the spin vector, B is the applied magnetic field vector, and $\tilde{g}$ is the g tensor. E/D, D, and species concentrations were obtained using methods identical to those described in the previous "_Sav_ HppD Az1 Reaction EPR Spectral Analysis" section utilizing the S = 3/2 Hamiltonian.

Comments on the Spectroscopic Analysis

Mössbauer spectroscopic measurements were carried out to provide spectroscopic evidence on the anion binding to the Fe(II) center of _Sav_ HppD Az1. The Mössbauer spectrum of the sample containing the _Sav_ HppD Az1•Fe(II) complex exhibited a major quadrupole splitting feature at 4.2 K. The spectral simulation suggested that this spectral feature can be best simulated by two quadrupole doublets with the parameters δ_1 = 1.30 mm/s $|\Delta E_{Q1}|$ = 3.41 mm/s, δ_2 = 1.32 mm/s $|\Delta E_{Q2}|$ = 3.02 mm/s (Fig. 4A and Fig. S5 left panel A). The parameters suggest that the two quadrupole doublets, which represent 55% (Species I) and 45% (Species 2) of the total iron in the sample, are typical high-spin ferrous species. Upon addition of 200 equivalents (relative to the protein concentration) of N_3^- in the form of NaN_3, clear spectral changes were observed (Fig. S5 left panel B). By taking a difference spectrum between that of the _Sav_ HppD Az1•Fe(II) complex and that of the putative _Sav_ HppD Az1•Fe(II)•N_3 complex, the spectral differences can be clearly visualized (Fig. S5 left panel C). The upward peaks and the downward peaks in the difference spectrum represent the disappeared and the appeared species upon N_3^- treatment. The spectral simulations suggested that the Species I (δ_1 = 1.31 mm/s $|\Delta E_{Q1}|$ = 3.41 mm/s, Fig. S5 left panel D, blue solid line) observed in the sample containing the _Sav_ HppD Az1•Fe(II) complex was mostly converted (-45%) to two new quadrupole doublets (Fig. S5 left panel D, purple and yellow lines) having the Mössbauer parameters of δ_3 = 1.20 mm/s $|\Delta E_{Q3}|$ = 2.29 mm/s, δ_4 = 1.17 mm/s $|\Delta E_{Q4}|$ = 2.97 mm/s, which represent 17% and 25% of the iron, respectively. The two new species are also typical of high-spin ferrous species and likely to be the _Sav_ HppD Az1•Fe(II)•N_3 complex. We also carried out the Mössbauer analysis on the same set of samples prepared by another batch of purified protein (Fig S5 right panel). The overall spectral results are the same. Namely the _Sav_ HppD Az1•Fe(II) complex is represented by two high-spin ferrous quadrupole doublets with isomer shift ~ 1.3 mm/s, and only one of the two ferrous quadrupole doublets can be converted to two new ferrous quadrupole doublets representing the putative _Sav_ HppD Az1•Fe(II)•N_3 complex. In addition, subtle changes of the Mössbauer simulation parameters could be observed between the two batches of protein, which might be due to certain batch-to-batch variation (Table S5). In summary, the Mössbauer spectra suggest that ~40% of iron centers in the sample containing the _Sav_ HppD Az1•Fe(II) complex can be converted to the putative azide bound species. We also incubated the _Sav_ HppD Az1•Fe(II) complex with 200 equivalents (relative to the protein concentration) of Cl^- or Br^- in

the form of NaCl or NaBr, no obvious spectral changes could be observed (Fig S6), which suggests that the binding of Cl^- and Br^- to the Fe(II) center may be much weaker than those induced by N_3^-. This could be a possible reason why only N_3^- can lead to the observed reactivity in *Sav* HppD Az1.

To further search for evidence to support the direct interactions between N_3^-, the substrate **1NF** and the iron center of *Sav* HppD Az1, we carried out EPR measurements on samples treated with nitric oxide (NO). The addition of NO to Fe(II) center can lead to the formation of $S = 3/2$ $\{FeNO\}^7$ species. The spectroscopic features of this $\{FeNO\}^7$ species is sensitive to the ligation change and the surrounding environment change of the iron center in protein (*11*). The addition of NO to the *Sav* HppD Az1•Fe(II) complex led to the formation of a $g \sim 4$ resonance in the EPR spectrum, which is a typical $S = 3/2$ $\{FeNO\}^7$ species with the rhombic zero field splitting parameter $E/D \sim 0.014$ based on the spectral simulation (Fig S7). The addition of N_3^- caused the $g \sim 4$ resonance to broaden with the corresponding increase of the E/D value to ~ 0.018 (Fig S7). The further addition of **1NF** caused the additional broadening of the g ~ 4 resonance with further increase of the E/D value to 0.024 (Fig S7). These spectroscopic changes observed upon N_3^- and 1NF treatment provide evidence that the iron center of *Sav* HppD Az1 interacts with N_3^- and **1NF**.

In order to demonstrate an Fe(III)-N_3 species in *Sav* HppD Az1 is formed and is involved in the reaction, we used **18NF** to incubate with the enzyme. We reasoned that **18NF** could still generate the *N*-centered radical via F• transfer to the Fe(II) center. However, the absence of the ethyl group would abolish the HAT step as well as the following N_3^- rebound step thus leave the iron center at the Fe(III) state with bound N_3^-. Indeed, the addition of **18NF** to the *Sav* HppD Az1•Fe(II)•N_3 complex under anaerobic condition resulted a slow accumulation of a red species with optical absorption features centered at 505 nm (Fig 4B and Scheme S5). This optical spectrum is reminiscent to that of the Fe(III)-N_3 complex found in the ferric superoxide dismutase (See ref 25 in the main text). Omission of N_3^- or the enzyme in the treatment did not generate such an optical spectrum, thus strongly suggesting the observed chromophore is likely to be originated from the Fe(III)-N_3 ligand-to-metal charge transfer band, which is generated by an enzyme bound Fe(III)-N_3 species. We further used EPR measurements to verify the iron oxidation state of this red species. The EPR signal of this red species was located at g ~ 4.3 (Fig 4A), thus confirming the iron oxidation state as high spin ($S = 5/2$) Fe(III). The simulation parameters are g = [1.96, 2.00, 2.03], D = 0.5 cm^{-1}, E/D = 0.26. Also consistent with the Mössbauer results that ~ 40% of the *Sav* HppD Az1•Fe(II) complex can be converted to the putative azide bound species, the amount of Fe(III)-N_3 generated is ~ 33% of the total Fe-loaded enzyme based on the spin quantification. In addition to generate Fe(III) species when **18NF** is used to react with the *Sav* HppD Az1•Fe(II) complex, an amidyl radical should also be formed simultaneously. Due to the instability of the amidyl radical, such species was not observed in EPR. However, a minor stable organic radical centered at g = 2 was observed instead (Scheme S6). This stable radical could be the secondary radical formed via the quench of the initial amidyl radical. This assertion is further supported by the fact that the stable radical could only be observed when the *Sav* HppD Az1•Fe(II) complex is incubated with **18NF** (Scheme S6).

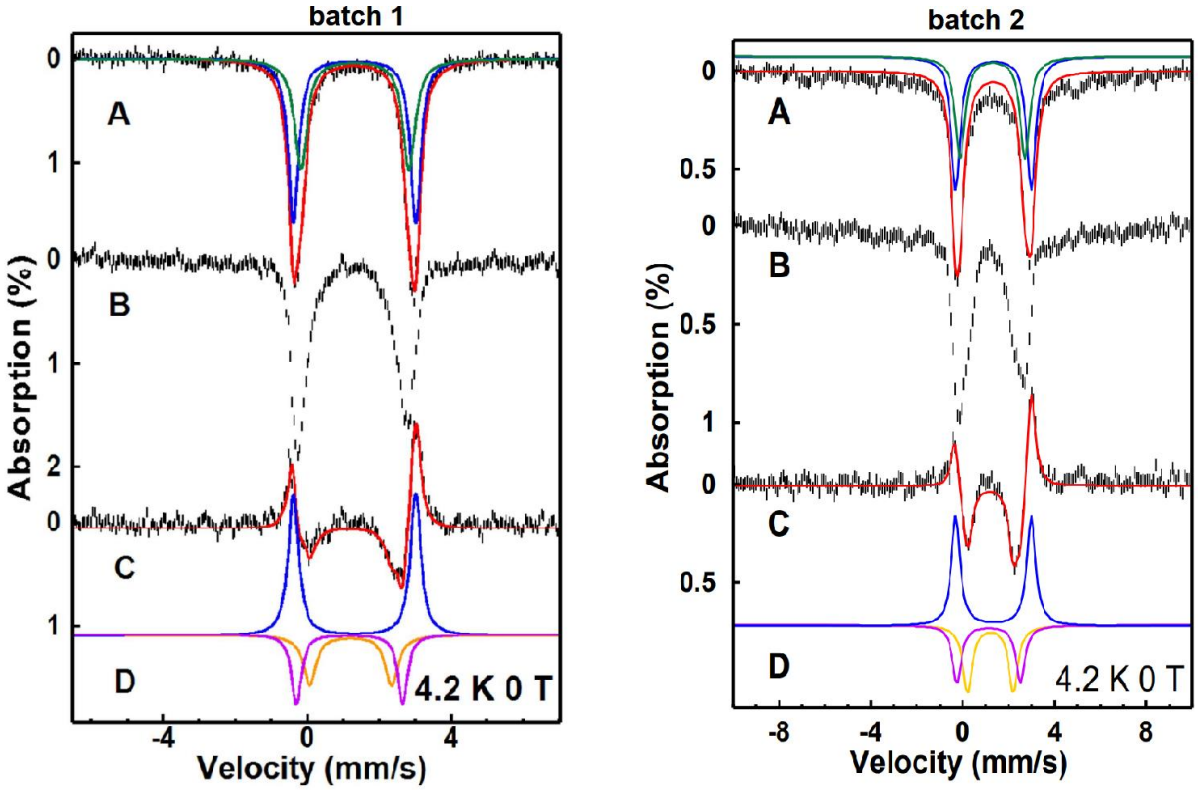

Figure S5. Left panel: Zero field 4.2 K Mössbauer spectra (black) and the corresponding simulations (colored lines) of the *Sav* HppD Az1•Fe(II) complex with and without NaN_3 prepared from batch 1 of the purified protein. (A) The spectrum of a sample containing the *Sav* HppD Az1•Fe(II) complex. The overall spectral simulation (red) and the simulated spectral components (blue and green) are overlaid with the experimental data. (B) The spectrum of a sample containing the *Sav* HppD Az1•Fe(II) complex treated with NaN_3. (C) The difference spectrum (black) obtained by subtracting spectrum (A) from spectrum (B). The overall simulation (red) is overlaid with the experimental data. (D) The simulated spectral components of the simulation shown in (C). The simulation parameters and detailed discussion are included in the SI section, "Comments on the Spectroscopic Analysis", and Table S5. **Right panel**: Zero field 4.2 K Mössbauer spectra (black) and the corresponding simulations (colored lines) of the *Sav* HppD Az1•Fe(II) complex with and without NaN_3 prepared from batch 2 of the purified protein. (A) The spectrum of a sample containing the *Sav* HppD Az1•Fe(II) complex. The overall spectral simulation (red) and the simulated spectral components (blue and green) are overlaid with the experimental data. (B) The spectrum of a sample containing the *Sav* HppD Az1•Fe(II) complex treated with NaN_3. (C) The difference spectrum (black) obtained by subtracting spectrum (A) from spectrum (B). The overall simulation (red) is overlaid with the experimental data. (D) The simulated spectral components of the simulation shown in (C). The simulation parameters and detailed discussion are included in the SI section, "Comments on the Spectroscopic Analysis", and Table S5. The broad absorption distributed in the baseline in (A) and (B) represents ~ 25% of the total absorption, which may be due to the mononuclear ferric impurity exist in this set of samples and generated by O_2 contaminant.

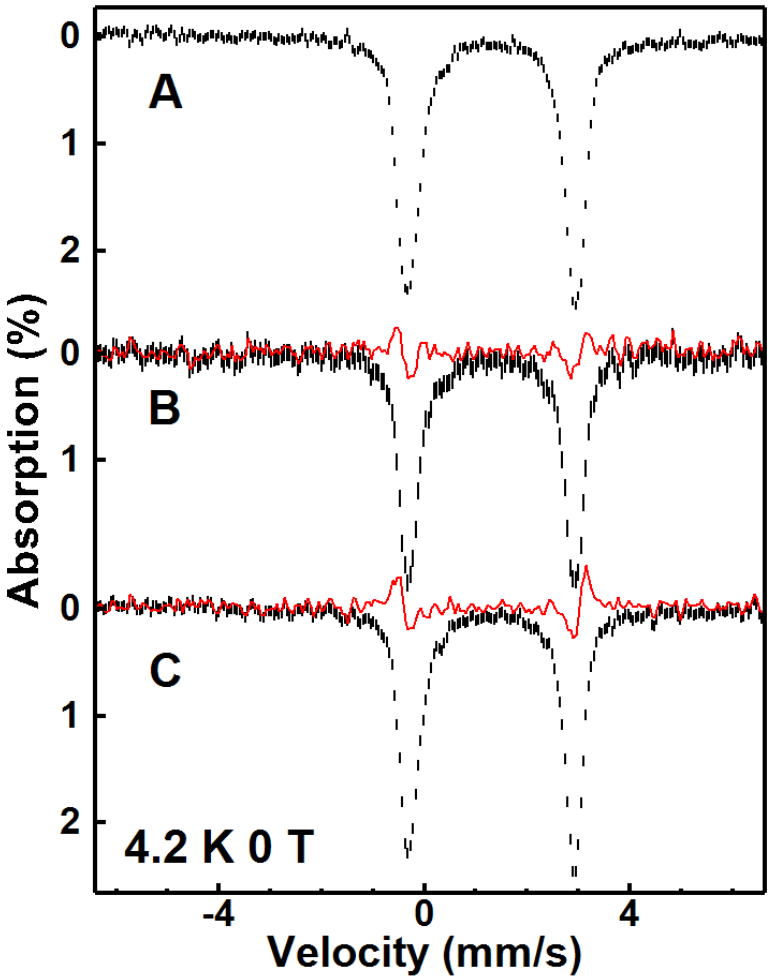

Figure S6. Zero field 4.2 K Mössbauer spectra (black) and the associated difference spectra (red) of the *Sav* HppD Az1•Fe(II) complex with and without the presence of anions chloride and bromide. (A) The spectrum of a sample comprised of *Sav* HppD Az1•Fe(II) complex. (B) The spectrum of a sample of *Sav* HppD AQAII•Fe(II) complex supplemented with 200 mM sodium chloride. The difference spectrum (red) displays the result of subtracting spectrum (A) from spectrum (B). (C) The spectrum of a sample of *Sav* HppD Az1•Fe(II) complex treated with 200 mM sodium bromide. The difference spectrum (red) conveys the results of subtracting spectrum (A) from spectrum (C).

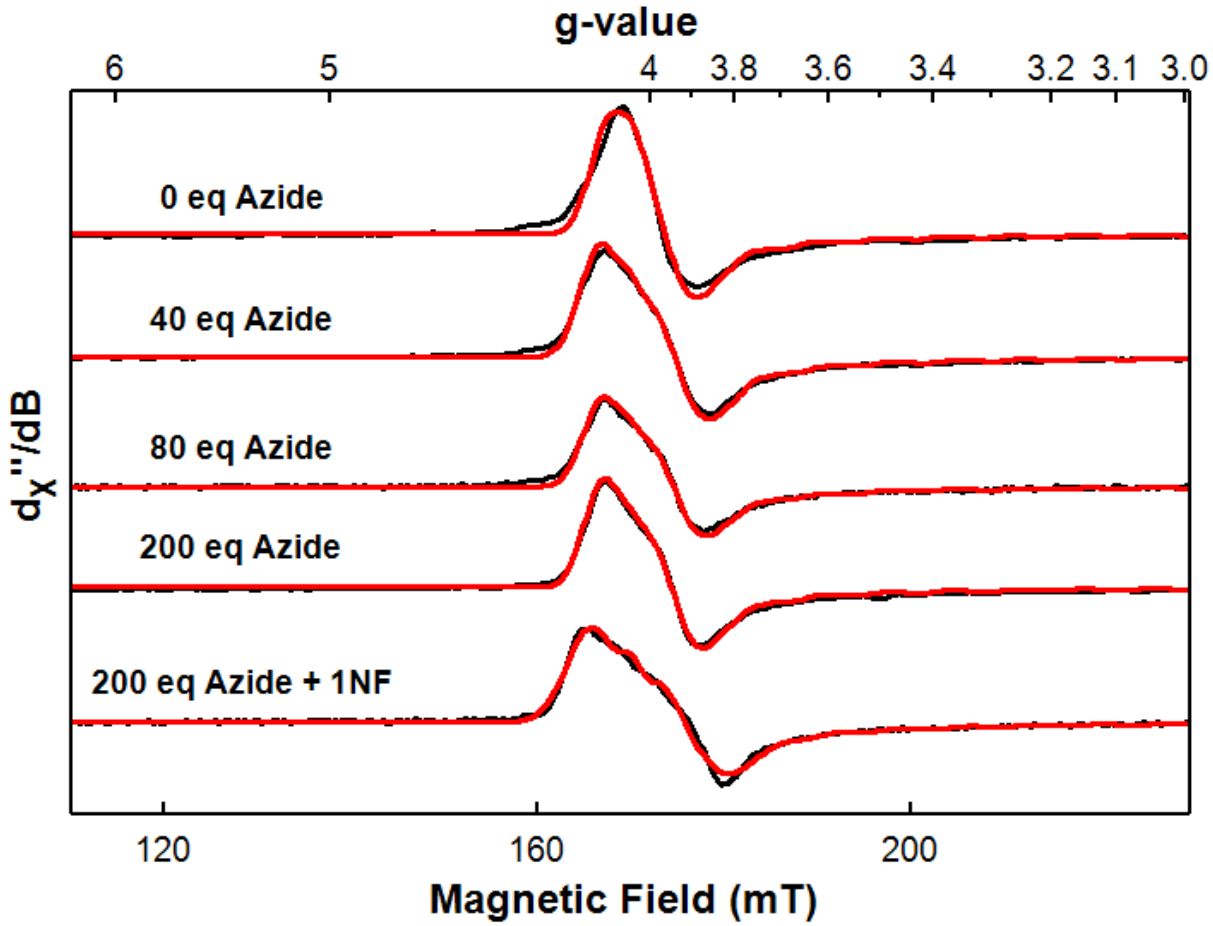

Figure S7. X-band EPR spectra (black solid lines) of samples containing the *Sav* HppD Az1•Fe complex with the addition of NO and different amounts of azide in the form of sodium azide with and without the presence of **1NF**. All spectra were measured at T = 12 K. The red solid lines are the spectral simulation. The measurement conditions as well as the simulation procedures were described in the SI section, "*Sav* HppD Az1 NO Adduct EPR Simulation Analysis". The simulation parameters can be found in Table S6.

Scheme S5. Optical absorption spectra of the *Sav* HppD Az1•Fe(II) complex with **18NF** (grey), the *Sav* HppD Az1•Fe(II)•N_3 complex with **18NF** (black), the *Sav* HppD Az1•Fe(II) complex incubated with **18NF** for 60 min (green), and the *Sav* HppD Az1•Fe(II)•N_3 complex incubated with **18NF** for 60 min (red).

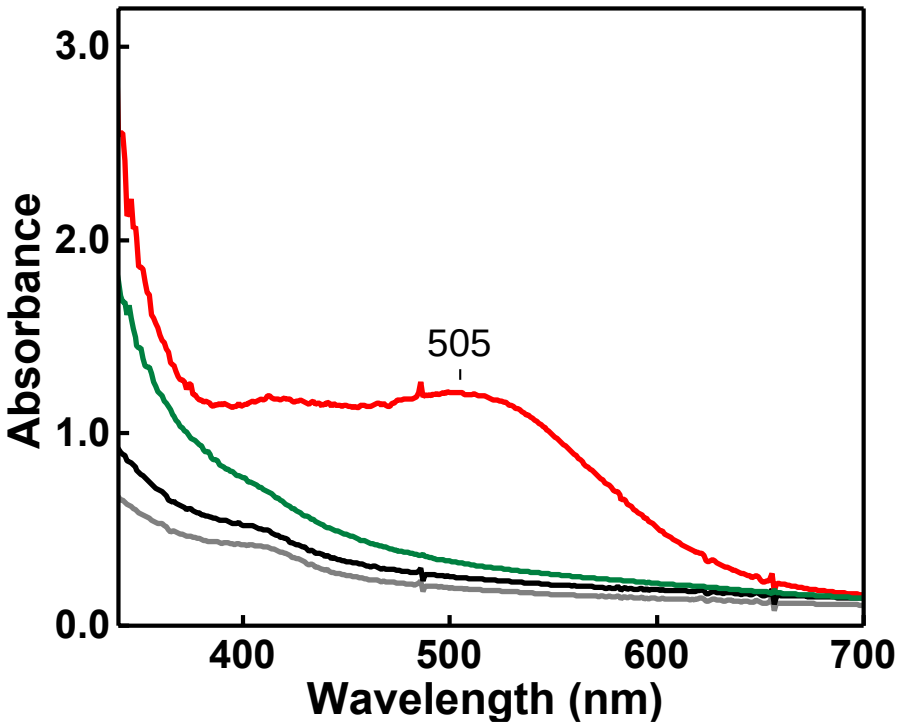

Scheme S6. X-band EPR spectra (black) of the *Sav* HppD Az1•Fe(II) complex incubated with **18NF** (top trace) or with **1NF** (middle traces) after 5 minutes, and the *Sav* HppD Az1•Fe(II) complex alone (bottom traces). The left panel shows the EPR spectra measured at the low field region, the right panel shows the EPR spectra measured at the high field region. The red traces are the spectral simulations of the g = 4.3 signal using the parameters listed in the SI section, "Comments on the Spectroscopic Analysis". The EPR signal at g ~ 2 showing nuclear hyperfine structure belongs to Mn^{2+} impurity, which has a spin concentration less than 2 μM. The sharp g = 2 signal belongs to a stable organic radical.

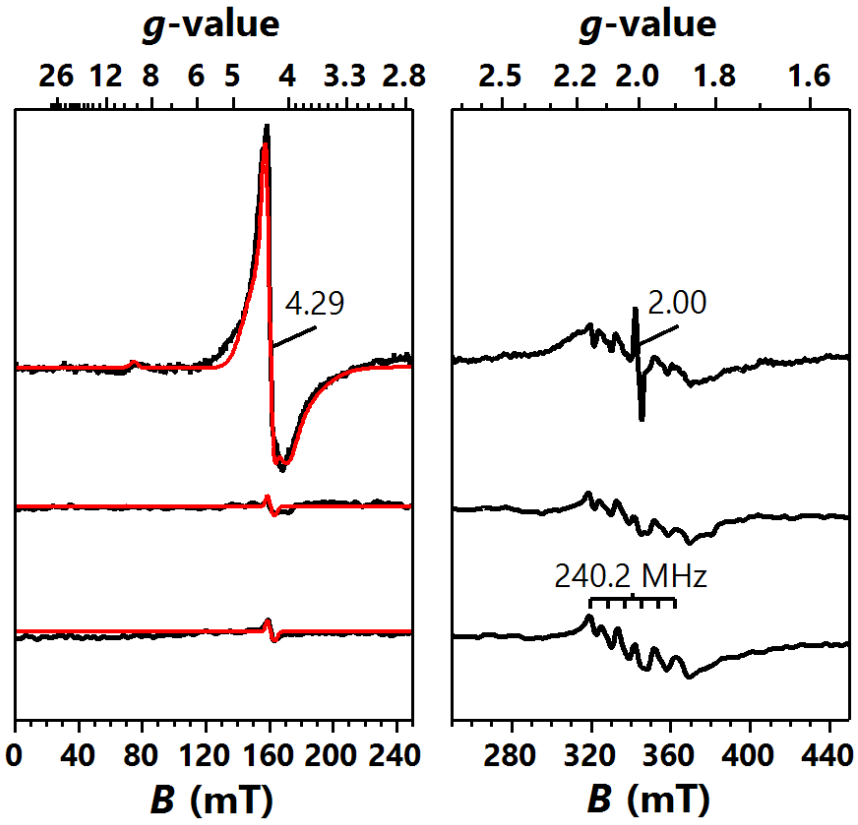

Table S5. Mössbauer simulation parameters of the *Sav* HppD Az1•Fe(II) complex and the *Sav* HppD Az1•Fe(II)•N3 complex prepared from two batches of purified protein.

Protein Batch	**Spectrum**	**Species**	**δ (mm/s)**	**ΔE_Q (mm/s)**	**Relative Area (%)**
Batch 1	*Sav* HppD Az1•Fe(II)	Species I	1.30	3.41	55
		Species II	1.32	3.02	45
	Difference spectrum after N_3^- addition	Species I	1.30	3.4	-45
		FeII-N3(I)	1.20	2.29	17
		FeII-N3(II)	1.17	2.97	25
Batch 2	*Sav* HppD Az1•Fe(II)	Species I	1.35	3.28	40
		Species II	1.31	2.82	35
	Difference spectrum after N_3^- addition	Species I	1.35	3.28	-35
		FeII-N3(I)	1.23	2.00	18
		FeII-N3(II)	1.15	2.76	13

Table S6. EPR simulation parameters of the S = 3/2 [7] species.

	0 eq Azide	**40 eq Azide**	**80 eq Azide**	**200 eq Azide**	**200 eq Azide + S**
g_z	2.00	2.00	2.00	2.00	2.00
g_x	2.015	2.017	2.016	2.016	2.017
g_y	2.015	2.017	2.016	2.016	2.017
D (cm^{-1})	6	6	6	6	6
E/D	0.0145	0.0184	0.0175	0.0168	0.0234
Conc. (mM)	0.20	0.24	0.17	0.20	0.27

Note: *D* and g_z values were fixed for the above simulations.

XI. Computational Modelling

Quantum Mechanics (QM) calculations. Density Functional Theory (DFT) calculations were employed to study the azidation mechanism of **1NF** to **1N** using a computational truncated model. The truncated model [Fe^{2+}(N_3^-)(H_2O)(Ac^-)($Im)_2$(**1NF**)] includes a ferrous metal center (Fe^{2+}) coordinated to an acetate (Ac^-) and two imidazoles (Im) to mimic the iron coordination sphere as observed in *Sav* HppD enzyme active site (Glu349, His187 and His270), an azide ion (N_3^-), and a coordinating water molecule as well as the substrate (**1NF**). The initial structure used to generate this truncated model was obtained from a representative snapshot of a MD trajectory. All DFT calculations were carried out using Gaussian09 software package (*12*). The (U)B3LYP functional was used (*13-15*), together with 6-31G(d) basis set for all atoms except for Fe, where SDD basis set and related SDD pseudopotential were used with an *ultrafine* integration grid. CPCM polarizable conductor model (diethyl ether, $\varepsilon = 4.3$) (*16, 17*) was used to provide an estimation of the dielectric permittivity of the enzyme active site (*18*). All the optimized stationary point geometries were characterized by frequency calculations, verifying that only transition states geometries had a single imaginary frequency consistent with the reaction coordinate. Enthalpies and entropies were calculated at 1 atm and 298.15 K. A correction to the harmonic oscillator approximation, as proposed by Truhlar and co-workers (*19, 20*), was also applied to the enthalpy by raising all frequencies below 100 cm^{-1} to 100 cm^{-1} using Goodvibes v.3.0.1 python script (*21*). Single point energy calculations were performed using the functional (U)B3LYP with the Def2TZVP basis set on all atoms and an *ultrafine* integration grid, and including CPCM polarizable conductor model corrections (diethyl ether, $\varepsilon = 4.3$) . All structures have a total neutral charge and calculations were performed considering the triplet (T) and quintet (Q) multiplicities, which are energetically accessible for the Fe species. Figures were rendered using CYLview (*22*).

Molecular Dynamics (MD) simulations. The available *Sav* HppD X-ray monomeric structure (chain B, PDB: 1T47) without the NTBC inhibitor was used as starting point. Variant Az2 was generated by introducing 7 mutations (V189A, N191A, S230L, P243G, N245F, Q255P, L367I) to the X-ray structure using PyMOL (*23*). Molecular Dynamics (MD) simulations in explicit water were performed using the AMBER18 package (*24*). Parameters for the **1NF** substrate were generated within the Antechamber module from AMBER18 package using the general AMBER force field (gaff2) (*25*), with partial charges set to fit the electrostatic potential generated at the HF/6-31G(d) level by the RESP model (*26*). The charges were calculated according to the Merz–Singh–Kollman scheme (*27, 28*) using Gaussian 09 (*12*). Parameters for the Fe^{2+} ion and its coordinating residues were obtained using the Metal Center Parameter Builder (MCPB.py) (*29*), following the protocols implemented in AMBER18 package. The coordination sphere of the ferrous metal center includes His187, His270, Glu349, and the azide ion (N_3^-). Two water molecules were added to fill the octahedral coordination of the metal, which were treated using a restrained nonbonded model.

The proteins were solvated in a pre-equilibrated cubic box with a 10-Å buffer of TIP3P (*30*) water molecules using the AMBER18 leap module, resulting in the addition of ~13,250 solvent molecules. Explicit counterions (Na^+ or Cl^-) were introduced to neutralize the system. All subsequent calculations were done using the Stony Brook modification of the Amber14 force field (*ff*14SB) (*31*). A two-stage geometry optimization approach was used. The first stage minimizes the positions of solvent molecules and ions imposing positional restraints on solute by a harmonic potential with a force constant of 500 kcal mol^{-1} $Å^{-2}$, and the second stage is an unrestrained minimization of all the atoms in the simulation cell. The system was gently heated

using six 50 ps steps, incrementing the temperature by 50 K for each step (0–300 K) under constant-volume and periodic-boundary conditions. Water molecules were treated using the SHAKE algorithm, where the angle between the hydrogen atoms was kept fixed. Long-range electrostatic effects were modelled using the particle-mesh-Ewald method (*32*). An 8 Å cutoff was applied to Lennard–Jones and electrostatic interactions. Harmonic restraints of 30 $kcal \cdot mol^{-1}$ were applied to the solute, and the Langevin scheme was used to control and equalize the temperature. The time step was kept at 1 fs during the heating stages, allowing potential inhomogeneities to self-adjust. Each system was then equilibrated for 2 ns with a 2 fs time step at a constant pressure of 1 atm and temperature of 300 K without restraints. Once the systems were equilibrated in the NPT ensemble, production trajectories were then run under the NVT ensemble and periodic-boundary conditions. In particular, a total of 4,500 ns (4.5 μs) in the absence of substrate were accumulated for *Sav* HppD, and Az2 variants from 6 independent replicas (3x 1,000 ns + 3x 500 ns) for each system. Cpptraj (*33*) module from Ambertools utilities was used to process and analyze the trajectories. Protein structures were rendered using PyMOL (*34*).

Docking and substrate-bound MD simulations. The most representative structures from the azide-bound simulations were characterized by clustering of the accumulated trajectories, considering the protein backbone RMSD. These structures were used for docking calculations with substrate **1NF**, which were performed using AutoDock Vina (*35*) after removing one water molecule bonded to the metal center to preserve its octahedral coordination. Docking results were used as starting points for constrained-MD simulations, in which the distance between the F atom from **1NF** substrate and the Fe center was kept restrained (3-3.2 Å, using a 50 $kcal \cdot mol^{-1} \cdot Å^{-2}$ force constant). This allowed to explore catalytically relevant binding poses of the substrate, largely refining the docking predictions, and preventing undesired unbinding events. The same protocol previously described for MD simulations was applied. A total of 6 independent replica of 1,000 ns of production trajectory each were accumulated for each system (6x 1,000 ns for each system). These simulations led to observe the spontaneous C-terminal α-helix open-to-close conformational change in the wt Sav HppD enzyme, which is believed to have an impact on the enzyme catalytic activity. Consequently, 6 additional and independent replicas of 500 ns each were carried out starting from the C-terminal α-helix closed state in all systems (additional 6x 500 ns for each system, in the closed state). Therefore, a total of 9 μs of MD simulation time for **1NF** substrate-bound in wt *Sav* HppD and Az2 variant were accumulated, allowing the exploration of the open-to-close state transitions and the full characterization of near attack conformations for N–F activation.

Figure S8. DFT model calculations exploring two possible azide coordination modes. DFT calculations using a computational truncated model [Fe(N_3^-)(Ac)(Im)$_2$(H_2O)$_2$] were used to study two different coordination modes for the azide ion (mode 1 and 2). **(A)** Computed relative energies in terms of electronic energy (ΔE), enthalpy (ΔH), and quasi-harmonic corrected Gibbs energy (ΔG). Energy values were obtained at the (U)B3LYP/Def2TZVP/PCM(dietyl-ether)//(U)B3LYP/6-31G(d)+SDD(Fe)/ PCM(dietylether) level. Energies are referred considering the lowest in energy quintet coordination mode 1 as zero. All energies are given in kcal·mol^{-1}. **(B)** Optimized geometries for the two coordination modes computationally explored. Distances and angles are given in Angstrom (Å) and degrees (^{o}), respectively.

A

Structure	Electronic State	ΔE	ΔH	ΔG
Coordination mode 1	triplet (T)	16.6	17.5	19.9
	quintet (Q)	0.0	0.0	0.0
Coordination mode 2	triplet (T)	16.3	16.5	17.6
	quintet (Q)	2.5	2.7	3.8

B

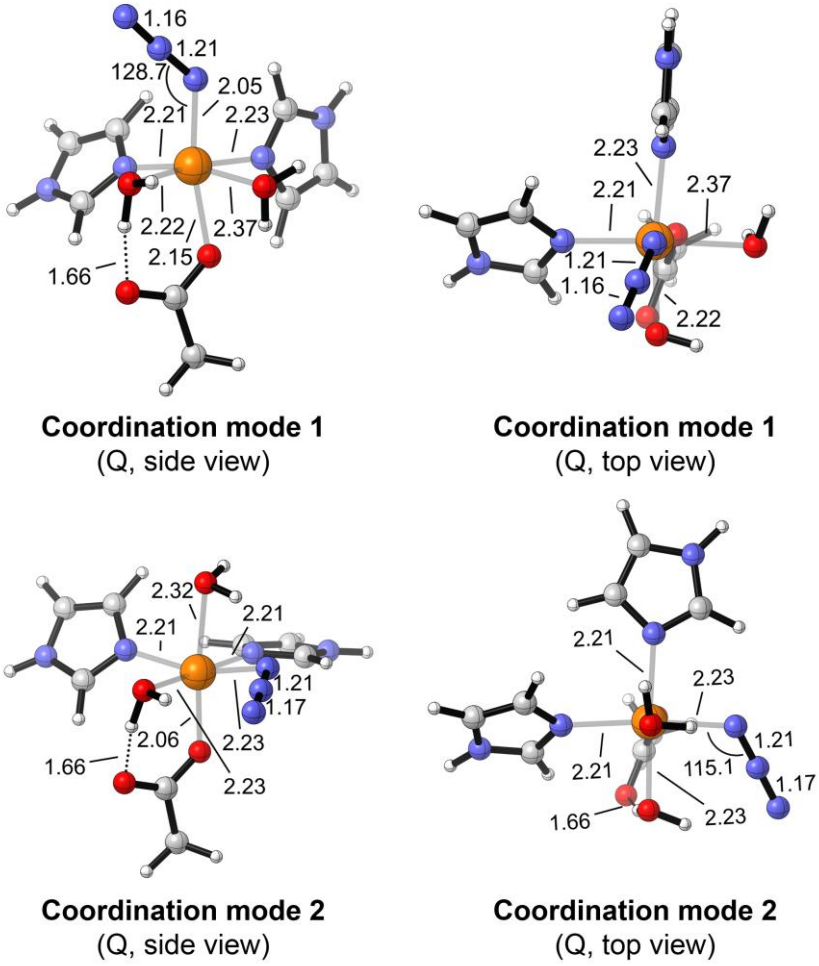

Azide coordination *trans* to the acetate (Aspartic) ligand (coordination mode 1) is intrinsically more favorable since it reduces the repulsion between the two anions. The quintet spin state is energetically much more stable than the triplet electronic state.

Figure S9. DFT relaxed scan calculations investigating the azide rotation when coordinated to Fe. **(A)** A computational truncated model [Fe(N_3^-)(Ac)(Im)$_2$(H_2O)$_2$] (as described in **Figure S8**) was used. The lowest in energy azide conformation is shown, with the ∠N(Im)-Fe-N1-N2 dihedral angle explored highlighted in blue. **(B)** Relaxed potential energy surface (PES) corresponding to the rotation of the ∠N(Im)-Fe-N1-N2 dihedral angle. Electronic energies were obtained at the (U)B3LYP/6-31G(d)+SDD(Fe)/PCM(diethyl ether) level and in the quintet electronic state. Energies and dihedrals are given in kcal·mol^{-1} and degrees (º), respectively.

A

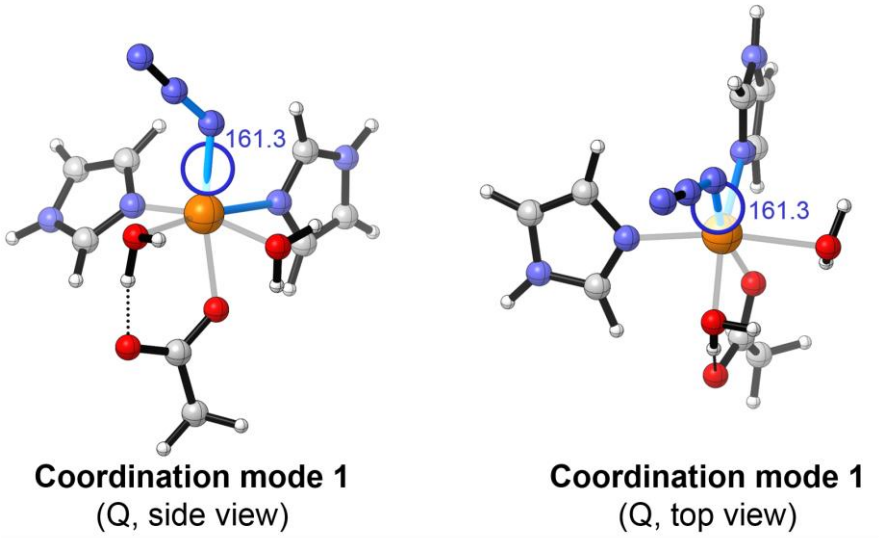

B

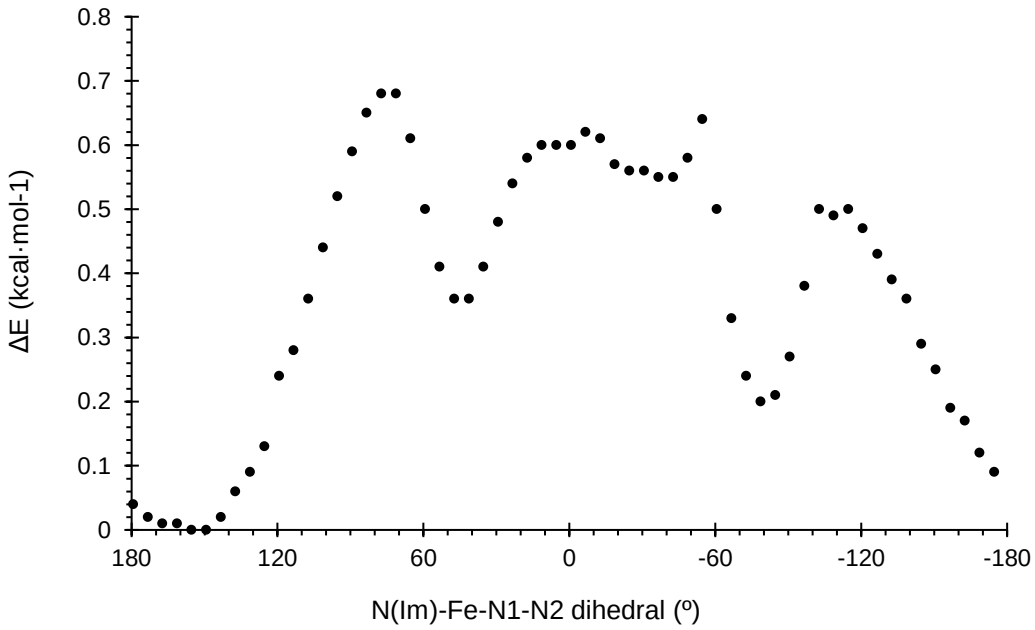

Relaxed scan calculations show that the azide can rotate freely when coordinated to the Fe center.

Figure S10. Exploration of azide coordination in wt *Sav* HppD and HppD Az2 intermediate variant from MD simulations. Representative structures of the most populated conformational states characterized from clustering analyses of MD simulations (3 replicas of 500 ns each, 1,500 ns for each system) of the Fe-N_3 complex in two different coordination modes in: **(A)** wt *Sav* HppD; and **(B)** HppD Az2 variant. Blue surfaces describe the solvent-accessible area in the active site cavity. Structures from coordination mode 1 were used for docking calculations.

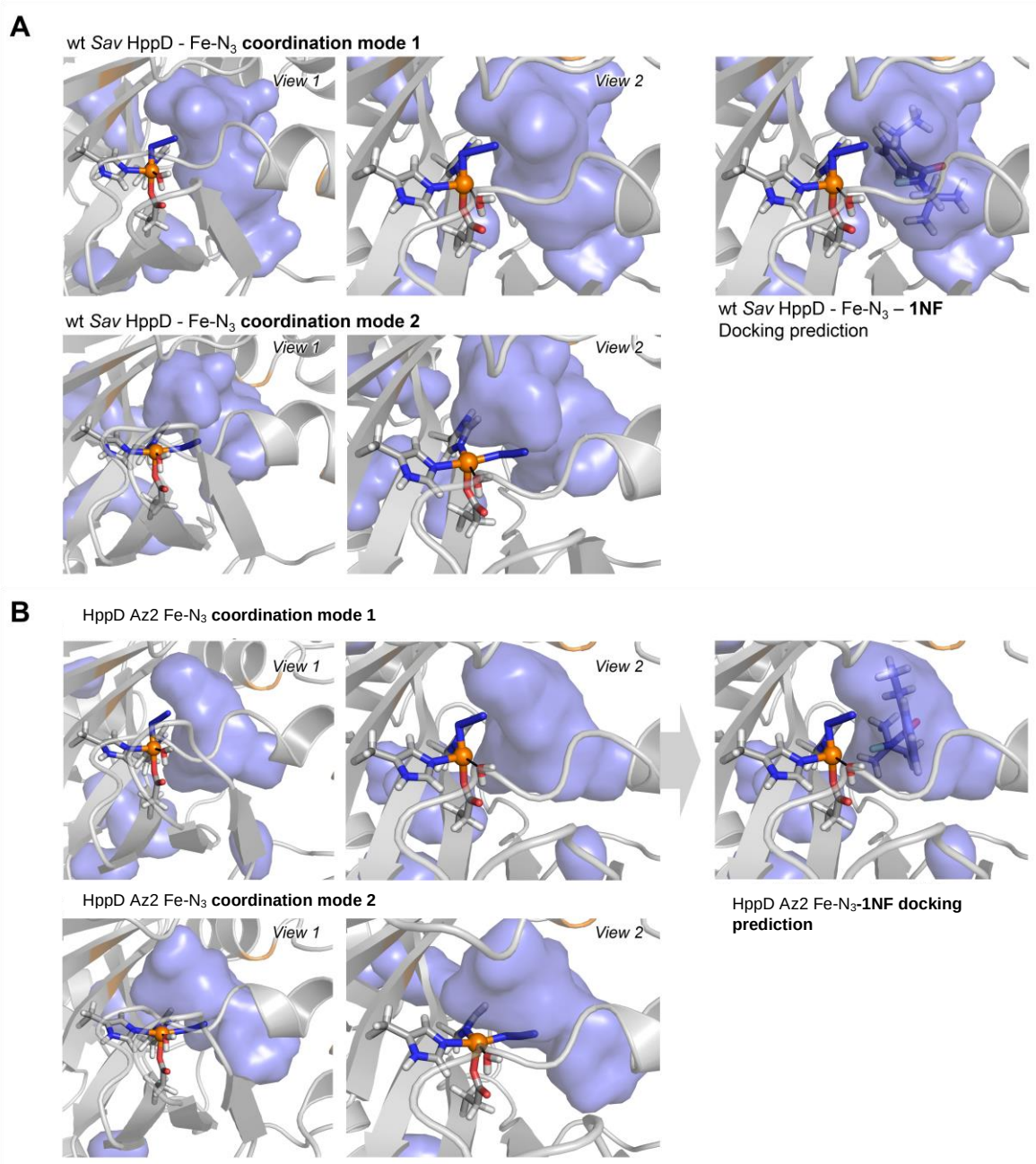

Coordination mode 1 of the Fe-N_3 complex in wt *Sav* HppD allows the effective approach of the **1NF** substrate to the Fe catalytic center in a near attack conformation for N-F activation. Coordination mode 2 does not allow it. Coordination mode 1 is intrinsically energetically more favorable than coordination mode 2 (**Figure S8**). In order to promote and improve the azide binding within this coordination mode, residues that are in proximity to the azide group in this region of the active site were selected for saturation mutagenesis (see **Figure 2** in the main text).

Figure S11. MD simulations on wt *Sav* HppD – Fe-N_3. 3 independent replicas (replica 1, 2 and 3) of MD simulations of 500 ns each were carried out to analyze the relative orientation of azide and the H-bond interactions occurring between active site residues in wt *Sav* HppD – Fe-N_3. Distances and dihedral angles explored along MD trajectories are all described in the included schematic figures. All distances, dihedral angles, and simulation time are given in Å, deg., and ns, respectively. **(A)** $\angle N_\varepsilon$(His270)-Fe-N1-N2 dihedral angle explored along MD trajectories, which describes the relative orientation of the azide in wt *Sav* HppD active site. **(B)** H-bond interactions analyzed as the distances between the donor and acceptor atoms of active site residues in wt *Sav* HppD–Fe-N_3.

A

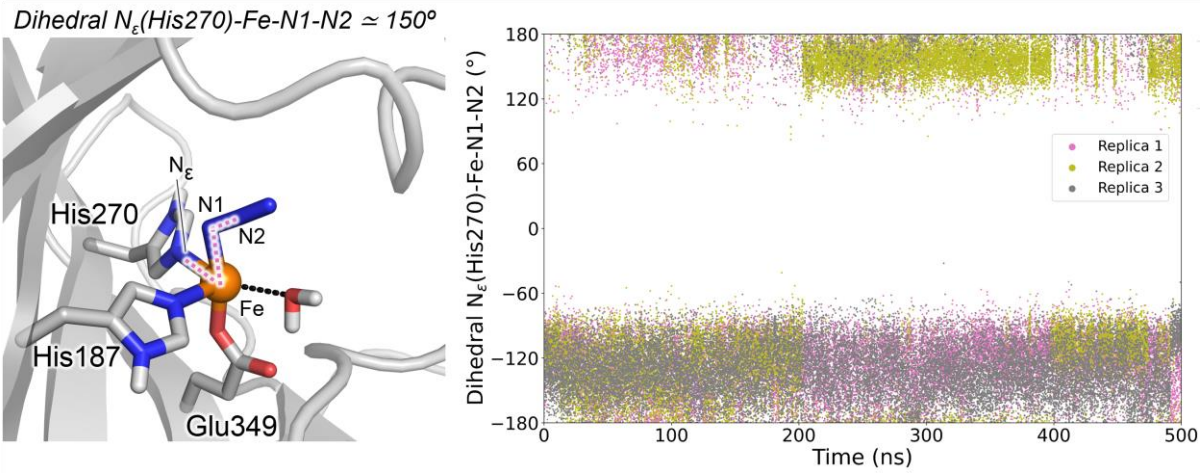

B

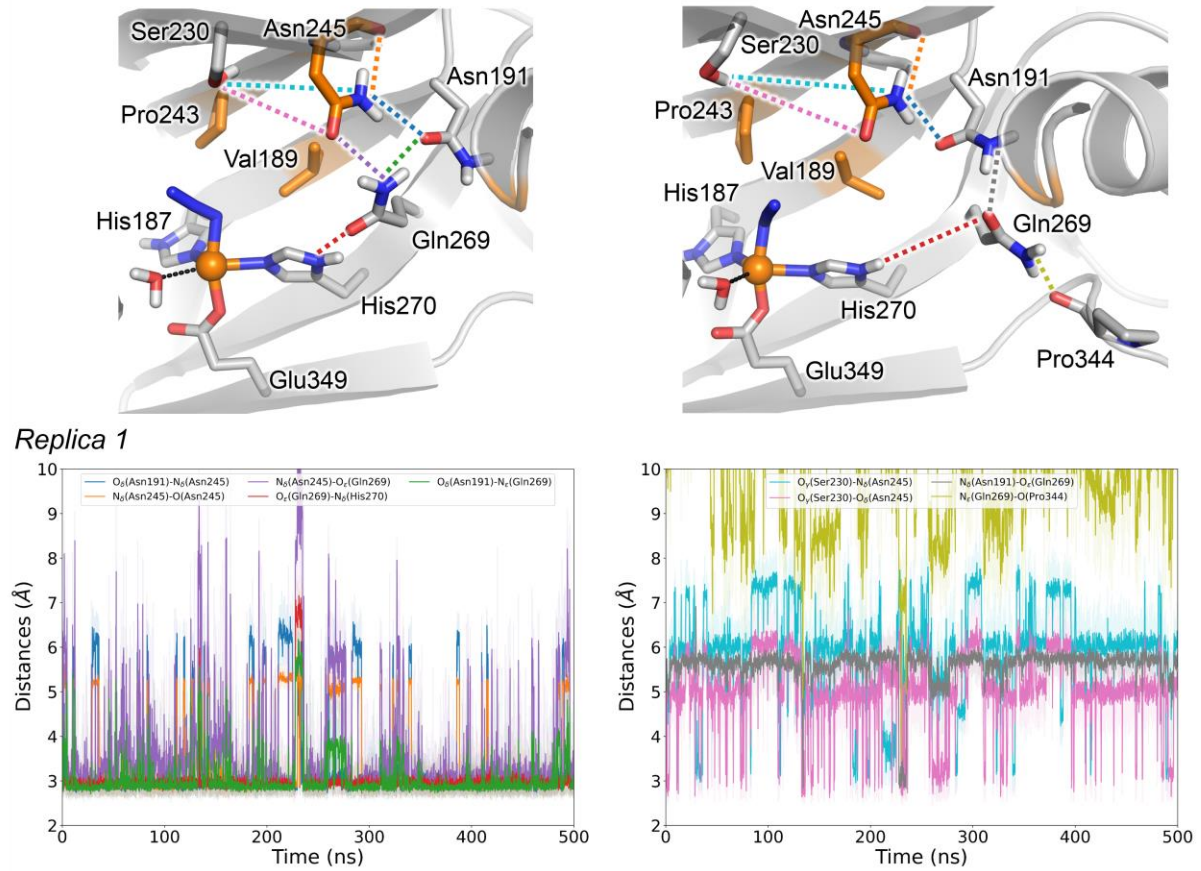

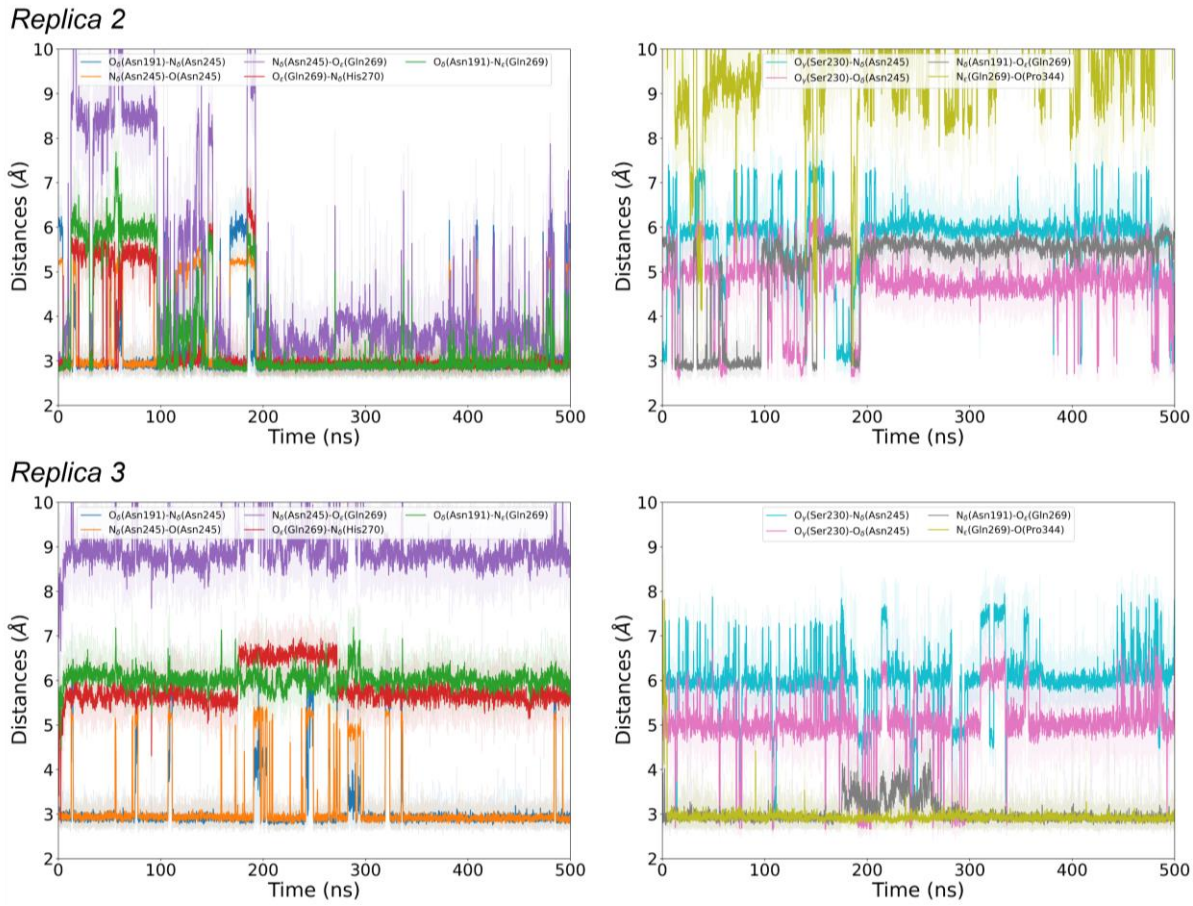

MD simulations describe that azide is predominantly oriented opposite to the catalytic His270 when coordinated to the Fe. Replicas 1 and 2 describe strong H-bond interactions between Gln269 and His270 (in red), while at the same time Gln269 interacts with Asn191 and Asn245 sidechains (in green and purple, respectively). In all replicas, Asn245 establishes H-bond interaction with Asn191 sidechain (in dark blue). No relevant interactions are observed involving Ser230. The apolar Pro243 and Val183 side chains are surrounding the azide anion.

Figure S12. MD simulations on HppD Az2 – Fe-N_3. 3 independent replicas (replica 1, 2 and 3) of MD simulations of 500 ns each were carried out to analyze the relative orientation of azide and the H-bond interactions occurring between active site residues in HppD Az2 – Fe-N_3. Distances and dihedral angles explored along MD trajectories are all described in the included schematic figures. All distances, dihedral angles, and simulation time are given in Å, deg., and ns, respectively. **(A)** $\angle N_\varepsilon$(His270)-Fe-N1-N2 dihedral angle explored along MD trajectories, which describes the relative orientation of the azide in HppD Az2 active site. **(B)** H-bond interactions analyzed as the distances between the donor and acceptor atoms of active site residues in HppD Az2 – Fe-N_3.

A

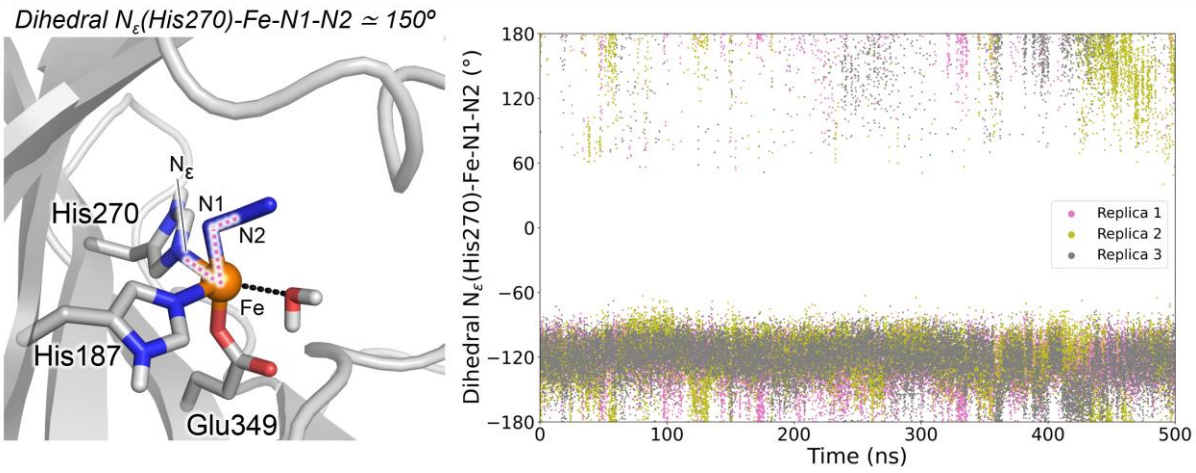

B

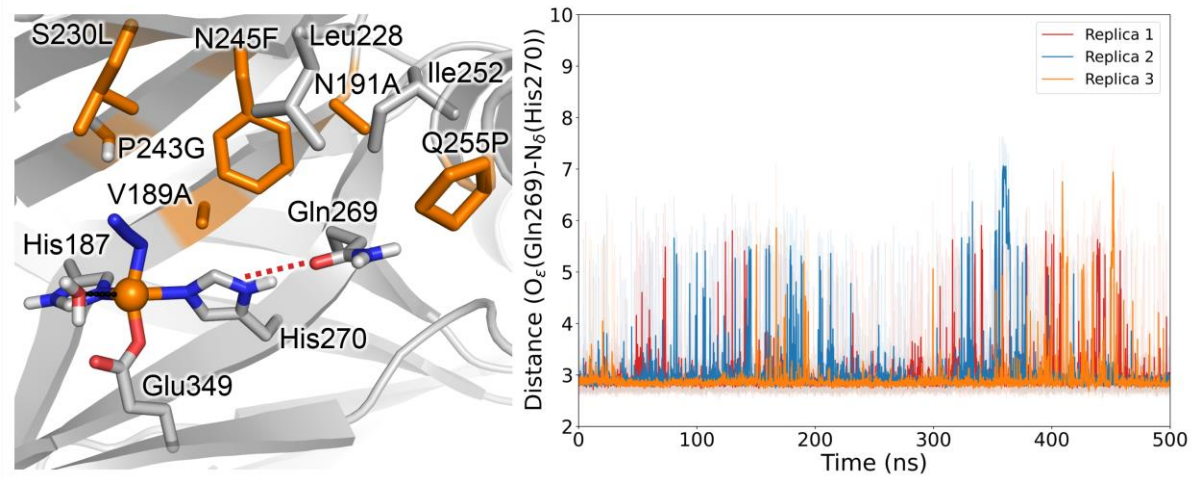

MD simulations describe that the coordinated azide in Az2 variant is oriented opposite to the catalytic His270, similarly to wt *Sav* HppD enzyme (see **Figure S11**). New introduced mutations (V189A, N191A, S230L, P243G, N245F, Q255P and L367I) increase the hydrophobicity of the active site, and disrupt the original active site H-bond network. The only persistent polar interaction observed in Az2 active site is a H-bond established by His270 and Gln269. Simulations showed that V189A and P243G generated more space to accommodate and stabilize the iron-bound azide in this region of the active site.

Figure S13. MD simulations on substrate-bound wt *Sav* HppD enzyme. 3 independent replicas (replica 1, 2 and 3) of constrained-MD simulations of 500 ns each were carried out to characterize catalytically relevant binding poses of **1NF** substrate bound in a near attack conformation for N–F activation in the closed state wt *Sav* HppD active site with the azide coordinated to the iron. Distances and dihedral angles explored along MD trajectories are all described in the included schematic figures. All distances, dihedral angles, and simulation time are given in Å, deg., and ns, respectively. **(A)** Distances explored along MD trajectories between **1NF** N-atom and pro-*R* H (H_R, red) and pro-*S* H (H_S, green) atoms, respectively, from **1NF** ethyl group. **(B)** Distances explored along MD trajectories between **1NF** C-atom from the ethyl group (C(Et)) and azide N1 (orange) and N3 (blue) atoms, respectively. **(C)** ∠N(Im)-Fe-N1-N2 dihedral angle explored along MD trajectories, which describes the relative orientation of the azide in wt *Sav* HppD active site. **(D)** Relative conformations explored by **1NF** substrate along MD trajectories as defined by ∠C(^{t}Bu)-N-C1(Ph)-C2(Ph) and ∠N_ε(His270)-Fe-N-C(^{t}Bu) dihedral angles. These two dihedrals describe: i) the relative orientation of **1NF** with respect to the Fe-azide active species (∠N_ε(His270)-Fe-N-C(^{t}Bu)); and ii) the relative orientation of **1NF** ethyl group (∠C(^{t}Bu)-N-C1(Ph)-C2(Ph)). **(E)** Representative selected snapshots that describe the geometries that **1NF** explores when bound in a near attack conformation for N–F activation in wt *Sav* HppD active site, as observed from MD trajectories. Star markers describe the positioning of each selected snapshot on the respective MD trajectory.

A

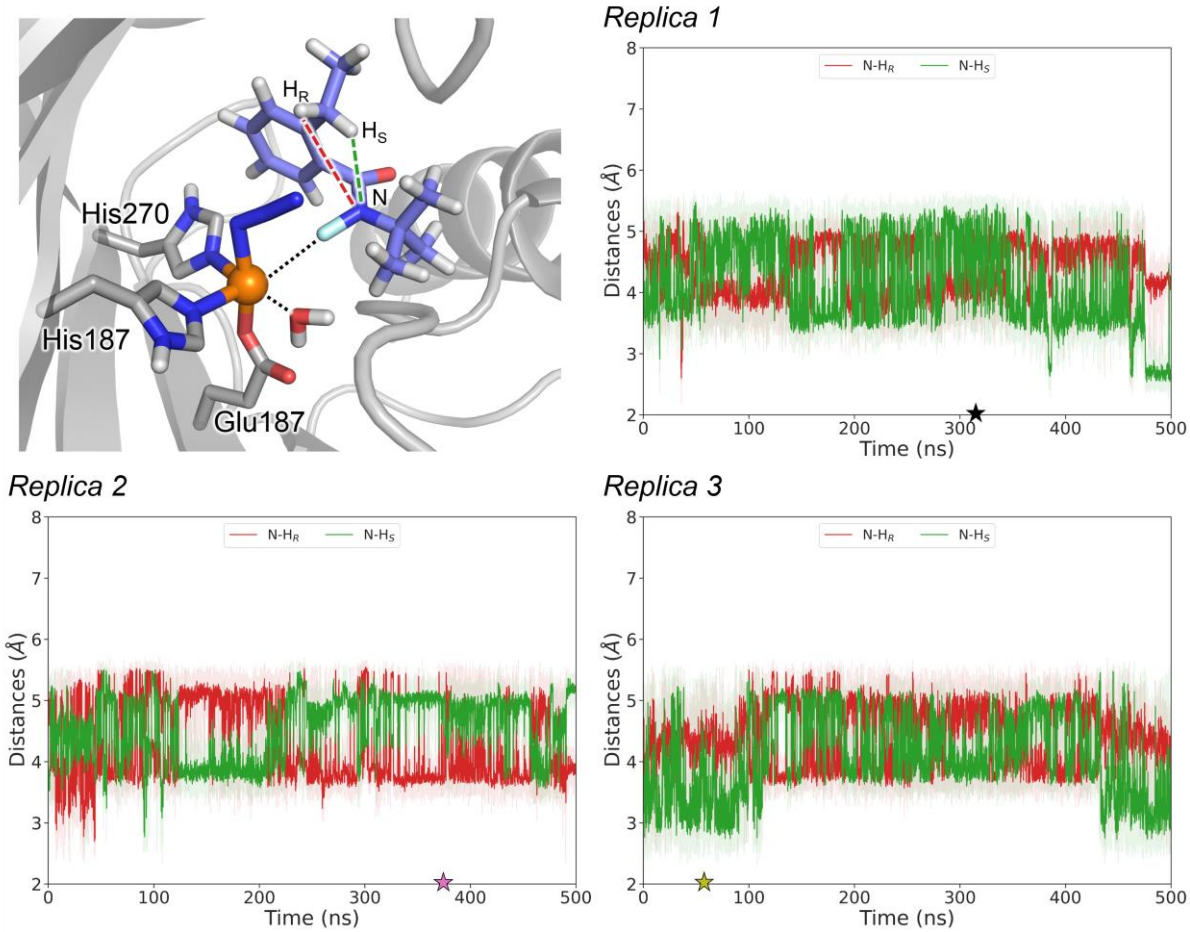

B

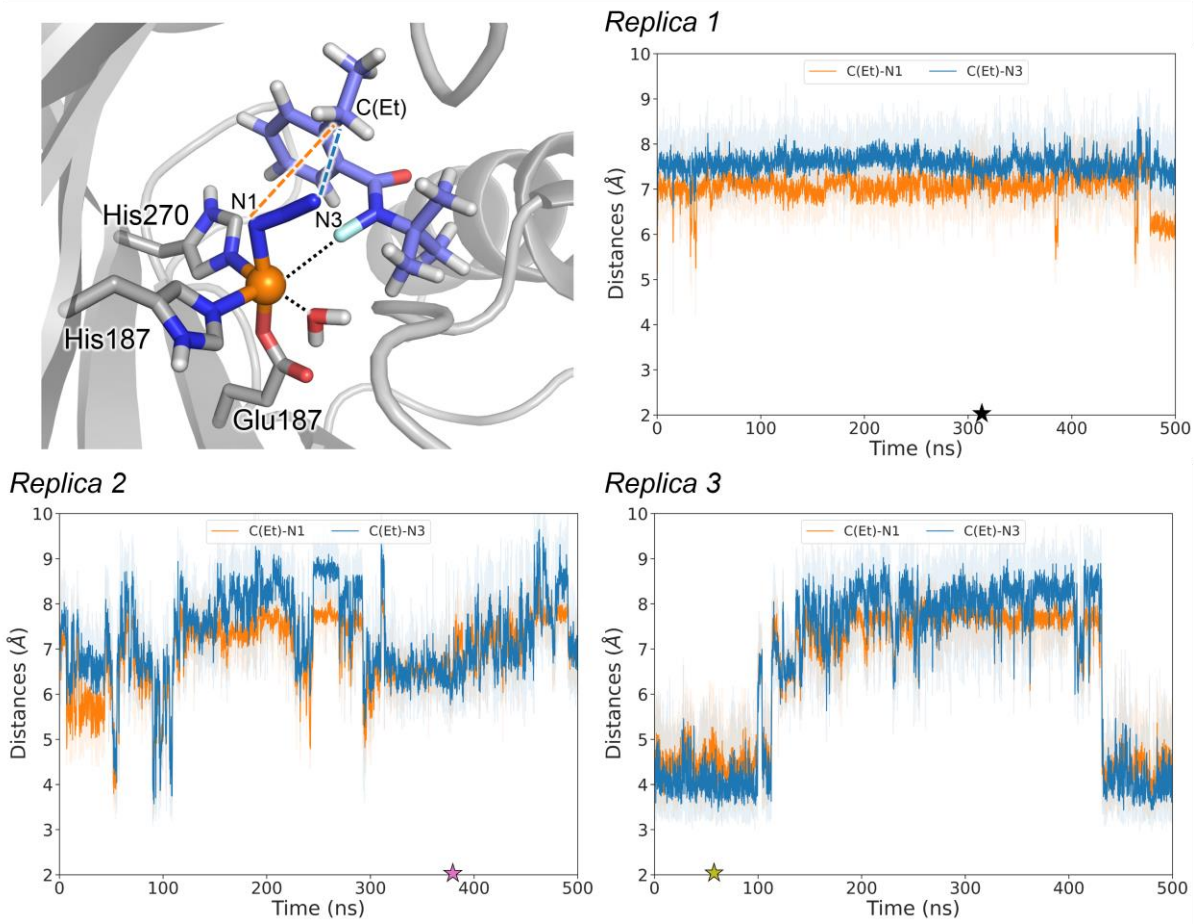
C(Et)
N1
N3
His270
His187
Glu187
Replica 1
C(Et)-N1
C(Et)-N3
Distances (Å)
Time (ns)
Replica 2
Replica 3

C

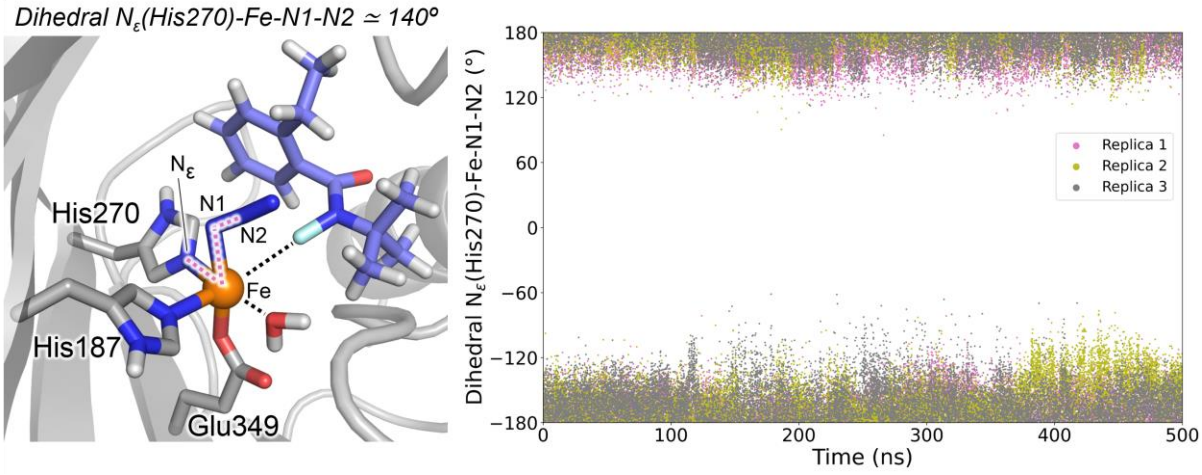
Dihedral Nε(His270)-Fe-N1-N2 ≃ 140°
Nε
N1
N2
Fe
His270
His187
Glu349
Dihedral Nε(His270)-Fe-N1-N2 (°)
Time (ns)
Replica 1
Replica 2
Replica 3

D

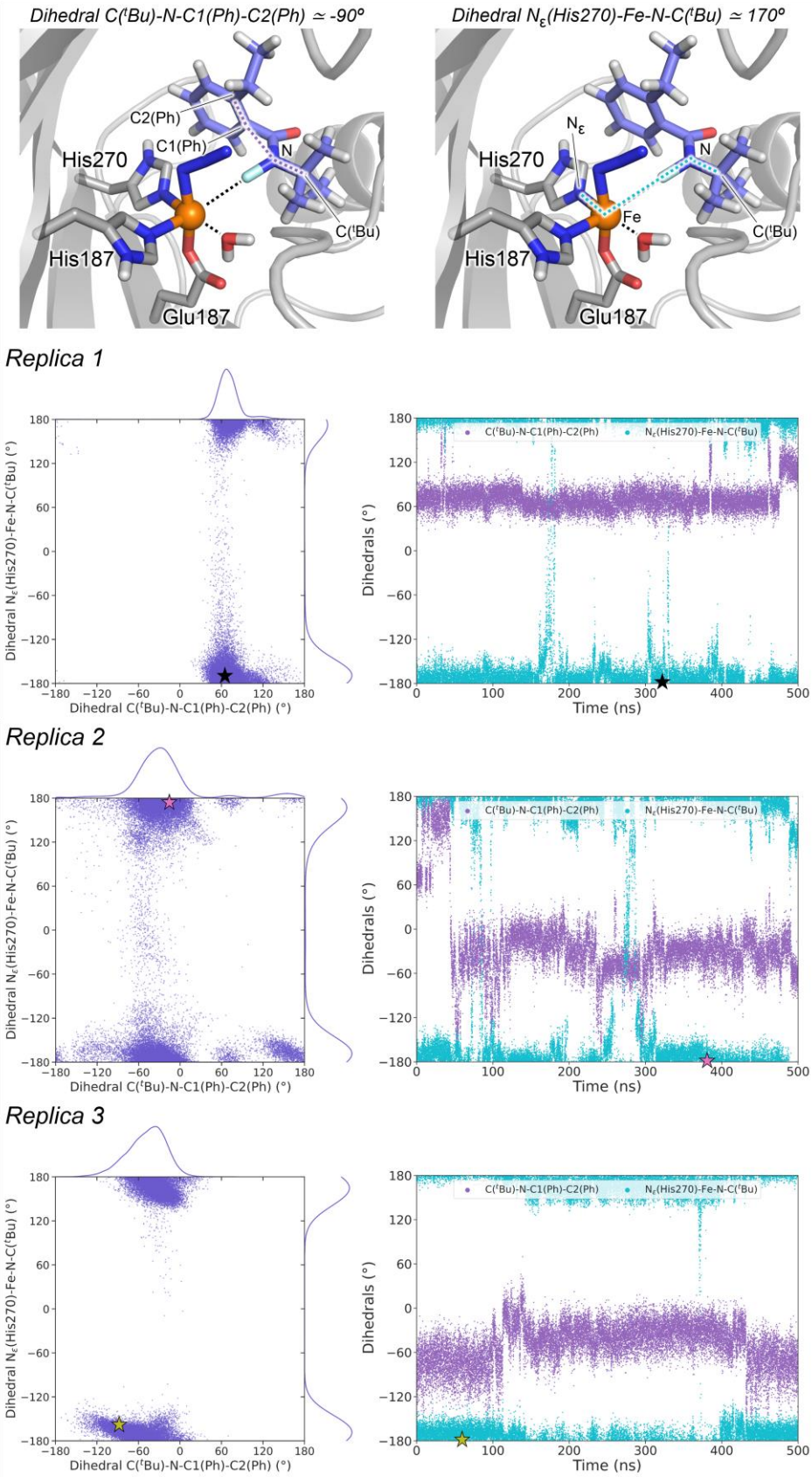
Dihedral C(tBu)-N-C1(Ph)-C2(Ph) ≃ -90°
Dihedral Nε(His270)-Fe-N-C(tBu) ≃ 170°
C2(Ph)
C1(Ph)
N
His270
His187
Glu187
C(tBu)
Nε
Fe
Replica 1
Replica 2
Replica 3
Dihedral Nε(His270)-Fe-N-C(tBu) (°)
Dihedral C(tBu)-N-C1(Ph)-C2(Ph) (°)
Dihedrals (°)
Time (ns)
C(tBu)-N-C1(Ph)-C2(Ph)
Nε(His270)-Fe-N-C(tBu)

E

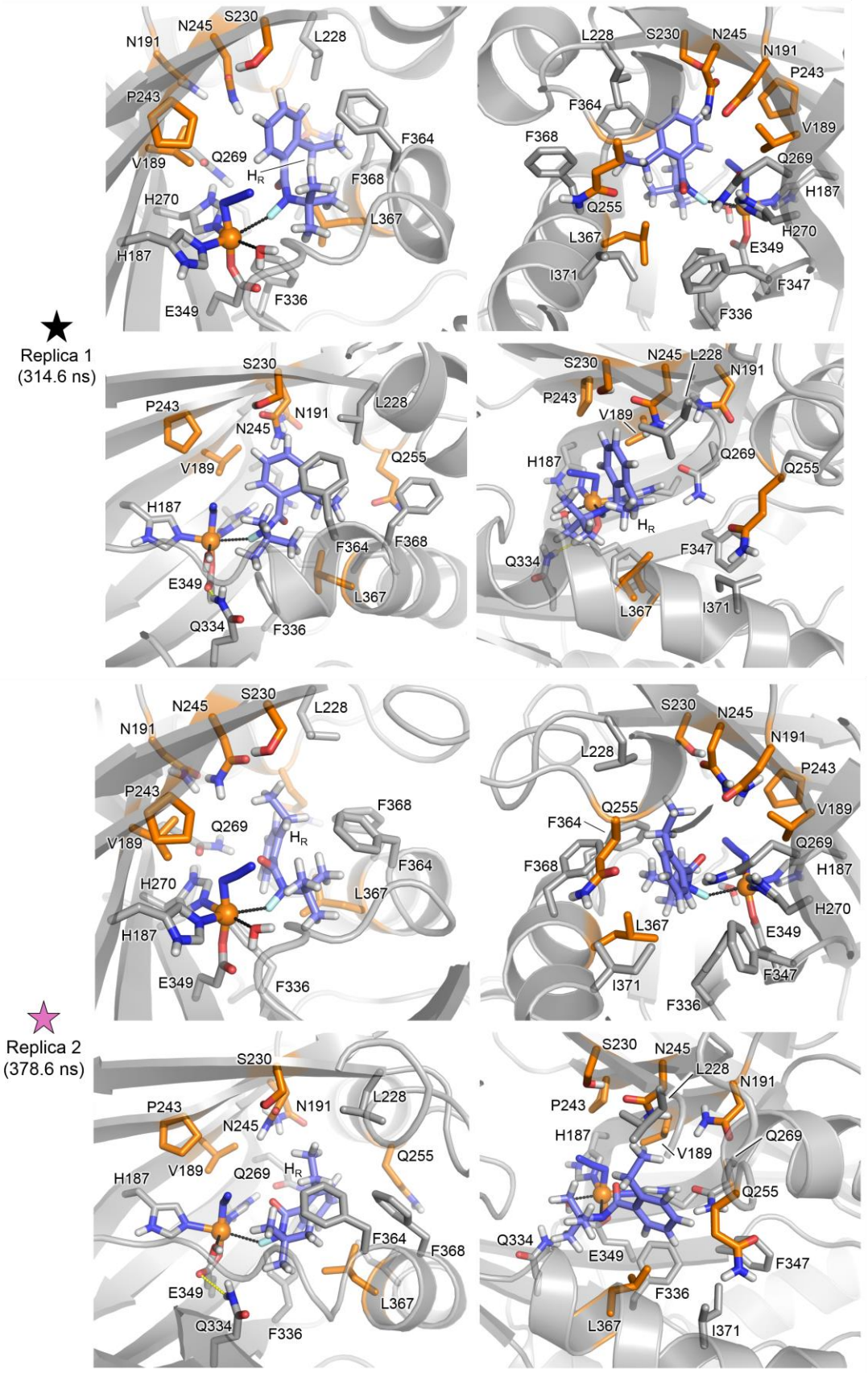
Replica 1
(314.6 ns)
Replica 2
(378.6 ns)
N245
S230
L228
N191
P243
V189
Q269
F364
F368
H270
H187
L367
E349
F336
Q255
I371
F347
Q334

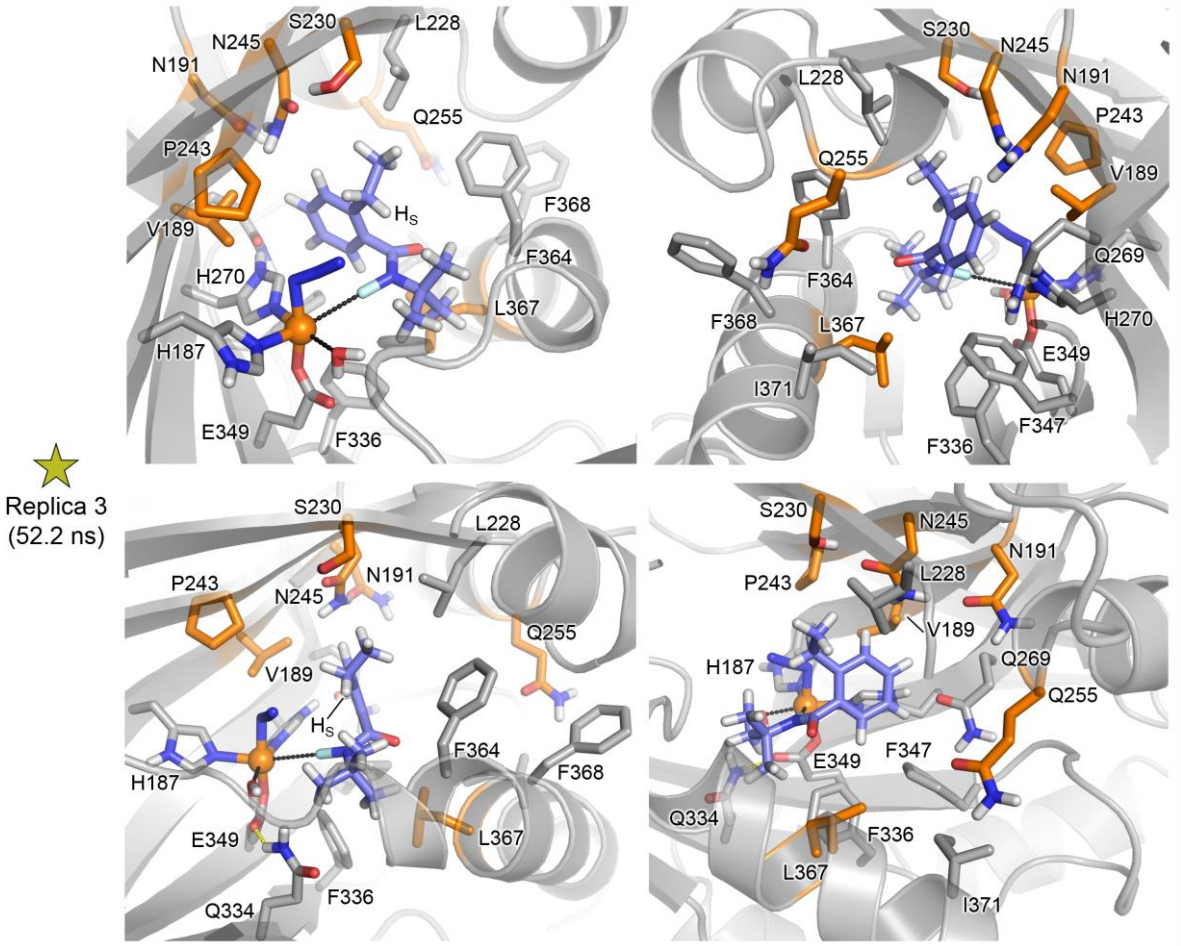

MD simulations show that when **1NF** binds in a catalytically competent pose for N–F activation in wt *Sav* HppD active site, it mainly explores conformations in which its relative orientation respect to the Fe-azide ($\angle N_\varepsilon$(His270)-Fe-N-C(^{t}Bu)) remains more less constant (**Figure S13-D** and **E**). However, the ethyl group and the phenyl ring ($\angle N_\varepsilon$(His270)-Fe-N-C(^{t}Bu)) are found to be quite flexible, exploring alternative conformations (**Figure S13-D**). Consequently, the ethyl group is not kept always close to the azide (**Figure S13-B**), and both H_R and H_S atoms can be equally oriented toward the substrate N-atom (**Figure S13-A**). This is indicating a lack of preorganization for the HAT step, which rapidly takes place once the fluorine atom is transferred to the Fe. The azide orientation is kept constant; it doesn't explore alternative conformations during the MD trajectories (**Figure S13-C**). This orientation is similar to the one observed for the azide in the MD simulations without the substrate.

Figure S14. H-bond network analysis in wt *Sav* HppD – Fe-N_3 – 1NF active site explored by MD simulations. H-bond interactions analyzed as the distances between the donor and acceptor atoms of active site residues in closed state wt *Sav* HppD – Fe-N_3 with substrate **1NF** bound in a near attack conformation for N-F activation. 3 independent replicas (replica 1, 2 and 3) of MD simulations of 500 ns each are analyzed. Distances explored along MD trajectories are all described in the included schematic figures. All distances and simulation time are given in Å and ns, respectively.

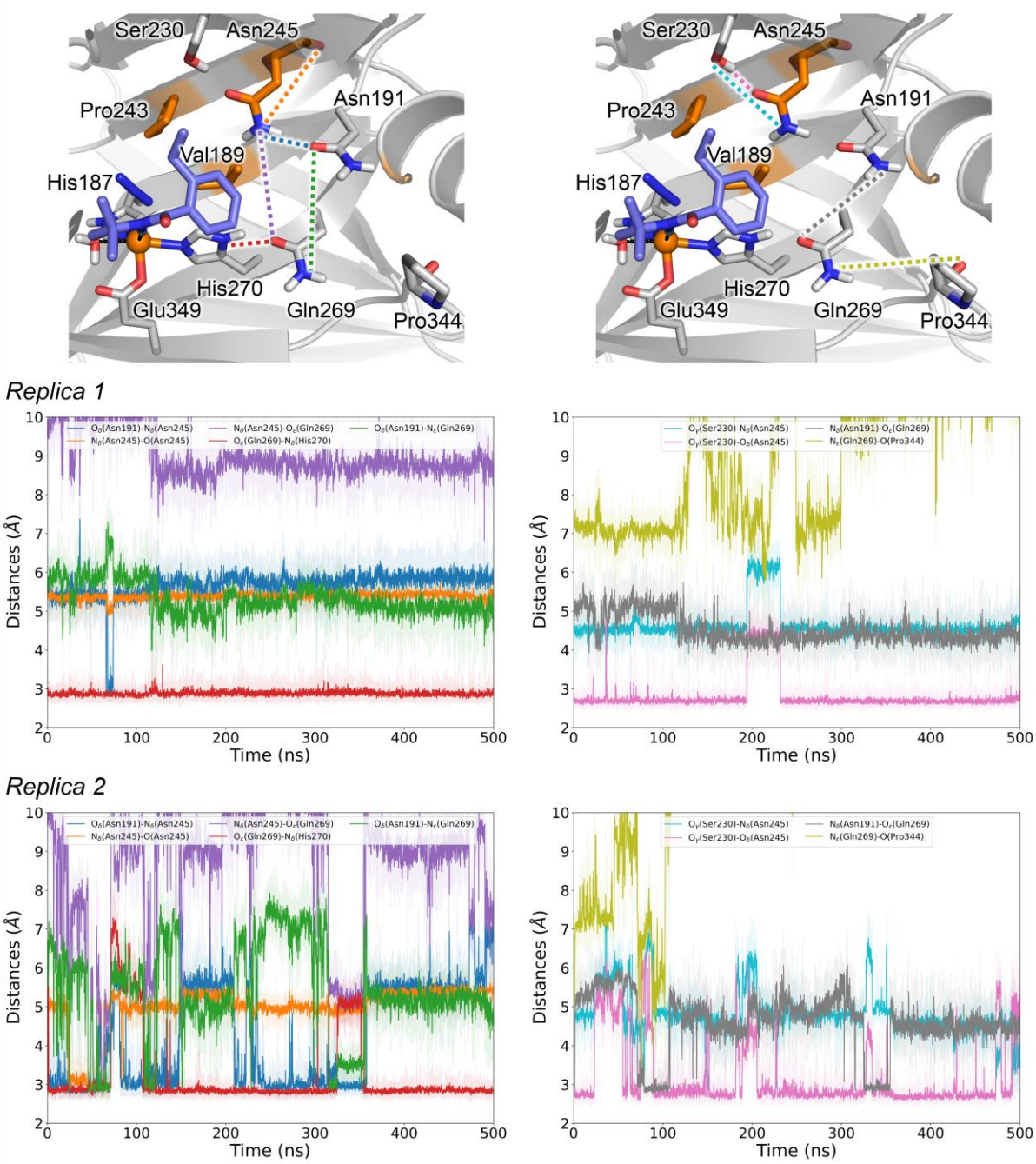

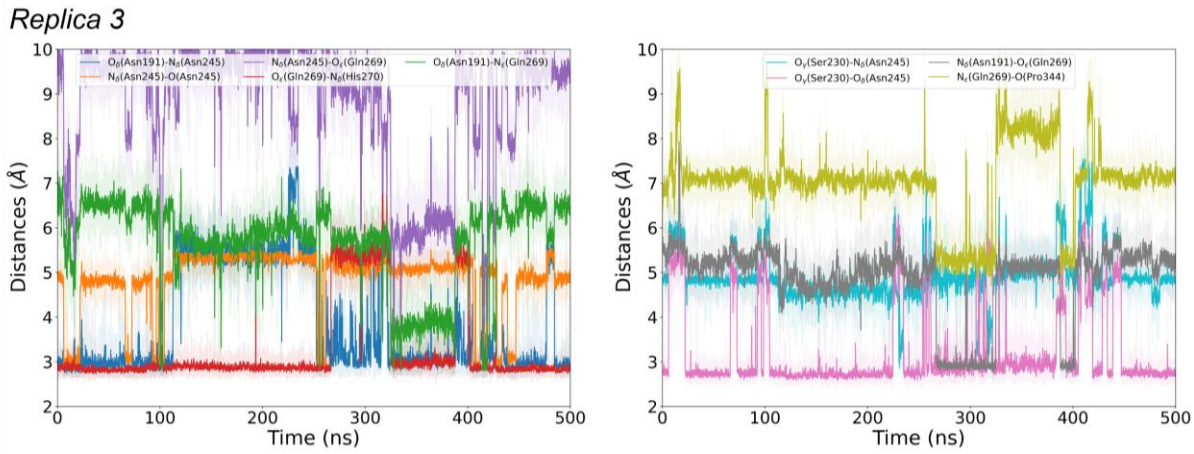

MD simulations of wt *Sav* HppD – Fe-N_3 with **1NF** bound in a near attack conformation of N-F activation describe that Gln269 establishes strong H-bond interactions with the protonated N_δ of His270 (in red), while Ser230 is also strongly interacting with Asn245 sidechain (in pink). Asn191 can also interact via H-bond with Asn245 (in dark blue).

MD simulations described that the catalytically relevant conformations that substrate **1NF** explores in wt *Sav* HppD (see **Fig. S13**), orient the ethyl group close to the azide and the benzylic C–Hs from the ethyl close to the substrate N atom. This substrate binding mode and conformation is important for an effective and selective HAT and to ensure a rapid and stereo-retentive azide recombination. Within this binding mode, the ethyl group of **1NF** is oriented toward the active site region where polar residues N191, S230 and N245 are placed (see **Fig. S13**), which establish the previously described H-bond network.

Consequently, it was hypothesized that a reshaping of this particular region of the active site would be required to control and restrict the accessible conformations of the ethyl group, preorganizing it for a selective HAT and azide recombination steps, in order to enhance the selectivity of the whole reaction. Therefore, positions N191, S230 and N245 were selected and prioritized to be revisited in additional rounds of evolution focused on enhanced enantioselectivity (see **Fig. S15** for computational modelling and discussions on reshaped Az2 active site).

Figure S15. MD simulations on substrate-bound HppD Az2 enzyme. 3 independent replicas (replica 1, 2 and 3) of constrained-MD simulations of 500 ns each were carried out to characterize catalytically relevant binding poses of **1NF** substrate bound in a near attack conformation for N–F activation in closed state Az2 active site with the azide coordinated to the iron. Distances and dihedral angles explored along MD trajectories are all described in the included schematic figures. All distances, dihedral angles, and simulation time are given in Å, deg., and ns, respectively. **(A)** Distances explored along MD trajectories between **1NF** N-atom and pro-*R* H (H_R, red) and pro-*S* H (H_S, green) atoms, respectively, from **1NF** ethyl group. **(B)** Distances explored along MD trajectories between **1NF** C-atom from the ethyl group (C(Et)) and azide N1 (orange) and N3 (blue) atoms, respectively. **(C)** ∠N(Im)-Fe-N1-N2 dihedral angle explored along MD trajectories, which describes the relative orientation of the azide in Az2 active site. **(D)** Relative conformations explored by **1NF** substrate along MD trajectories as defined by ∠C(^{t}Bu)-N-C1(Ph)-C2(Ph) and ∠N_ε(His270)-Fe-N-C(^{t}Bu) dihedral angles. These two dihedrals describe: i) the relative orientation of **1NF** with respect to the Fe-azide active species (∠N_ε(His270)-Fe-N-C(^{t}Bu)); and ii) the relative orientation of **1NF** ethyl group (∠C(^{t}Bu)-N-C1(Ph)-C2(Ph)). **(E)** Representative selected snapshots that describe the geometries that **1NF** explores when bound in a near attack conformation for N–F activation in Az2 active site, as observed from MD trajectories. Star markers describe the positioning of each selected snapshot on the respective MD trajectory.

A

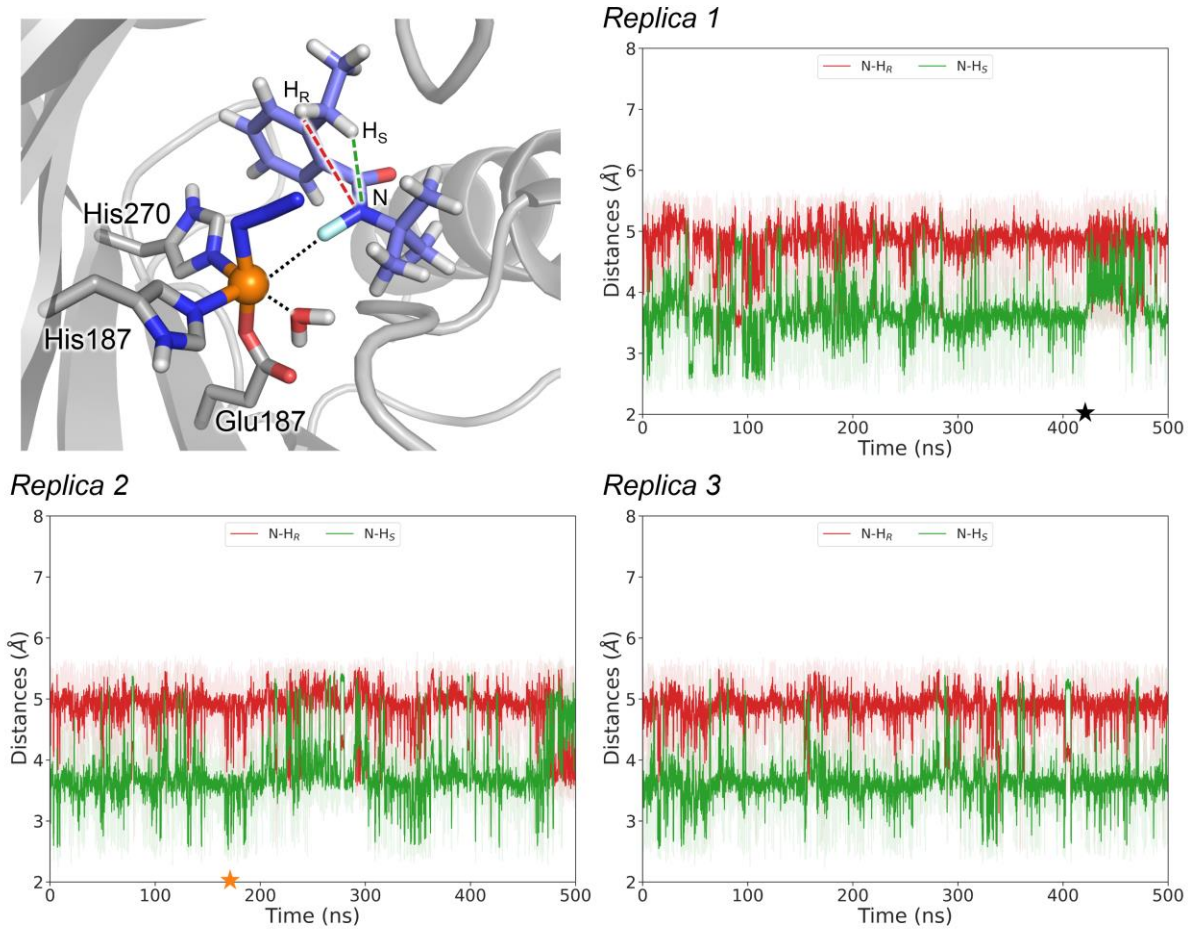

B

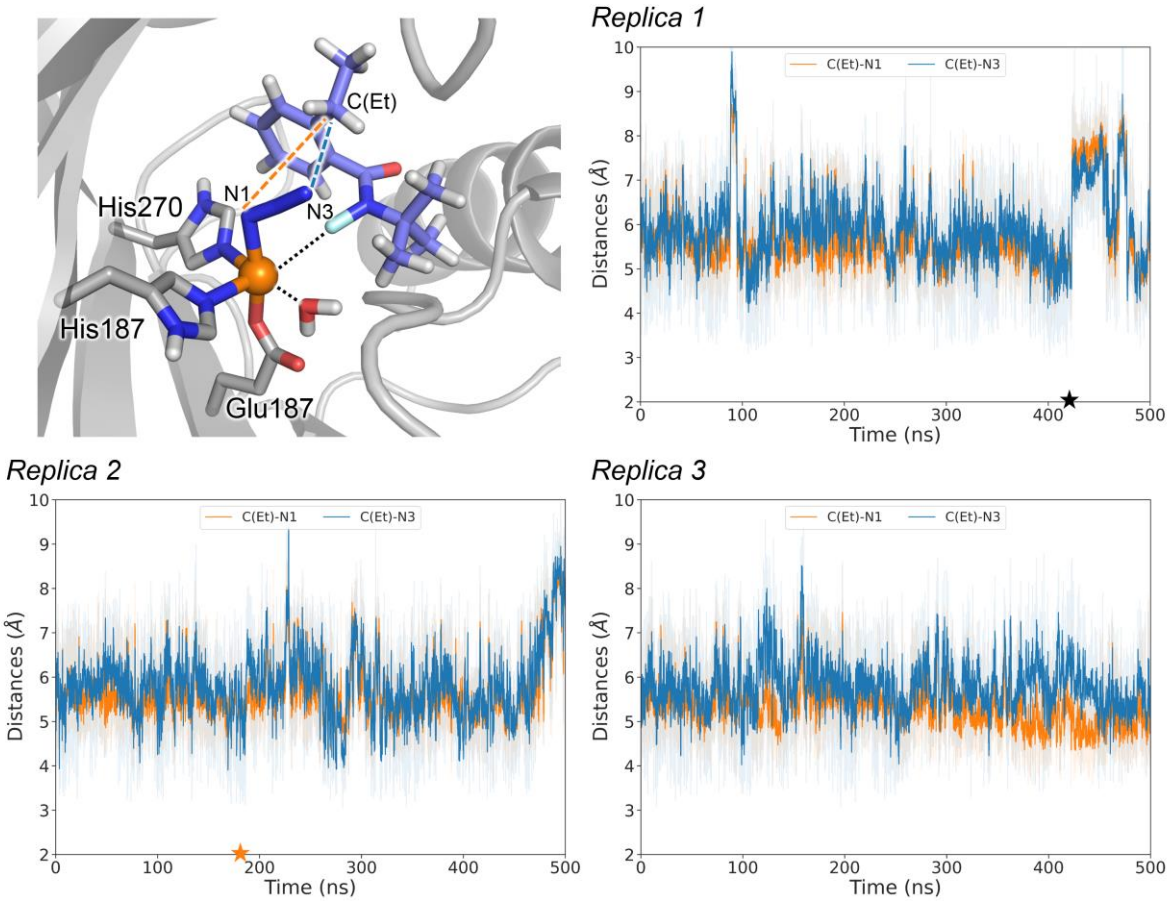
C(Et)
N1
N3
His270
His187
Glu187
Replica 1
Replica 2
Replica 3
C(Et)-N1
C(Et)-N3
Distances (Å)
Time (ns)

C

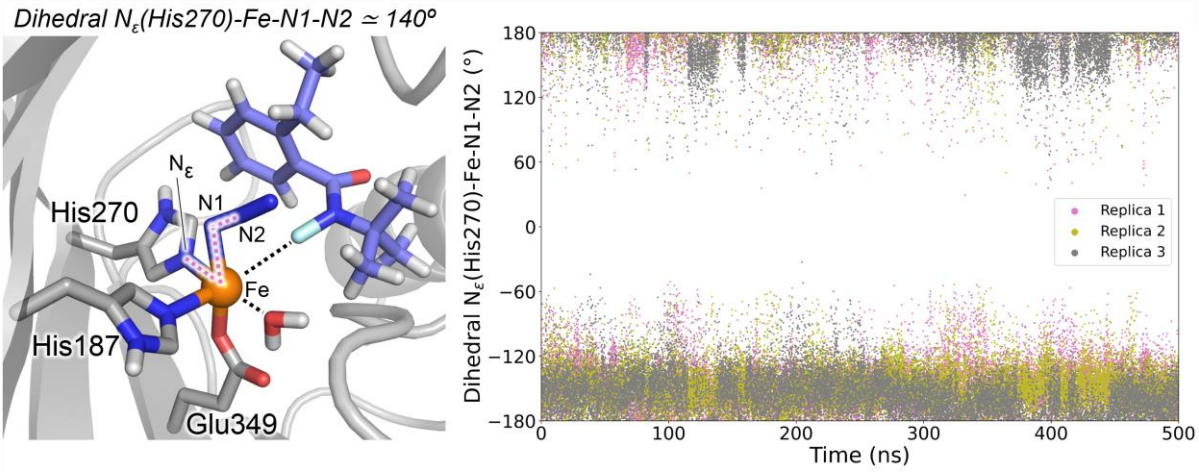
Dihedral Nε(His270)-Fe-N1-N2 ≃ 140°
Nε
N1
N2
Fe
His270
His187
Glu349
Dihedral Nε(His270)-Fe-N1-N2 (°)
Time (ns)
Replica 1
Replica 2
Replica 3

D

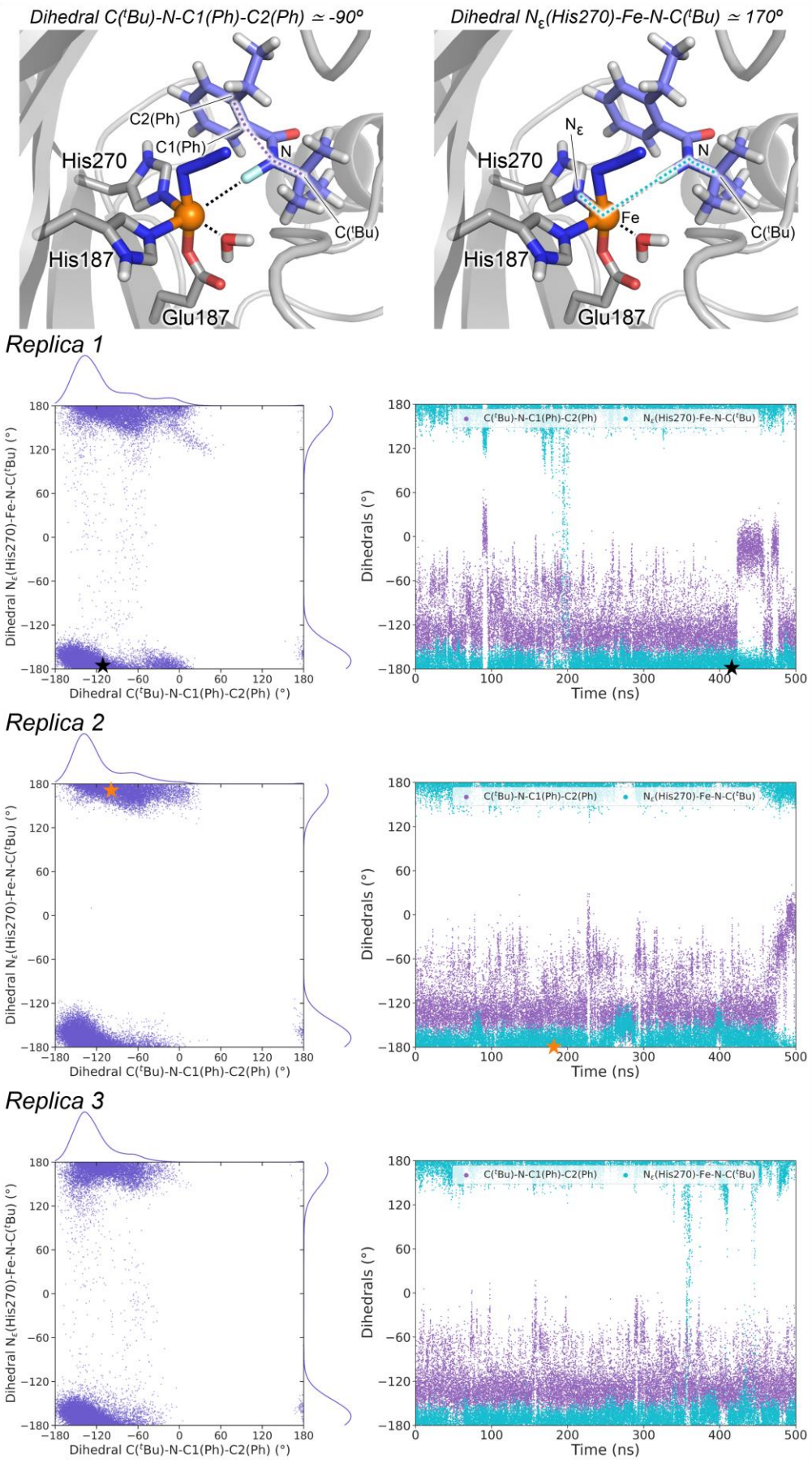
Dihedral C(tBu)-N-C1(Ph)-C2(Ph) ≃ -90°
Dihedral Nε(His270)-Fe-N-C(tBu) ≃ 170°
C2(Ph)
C1(Ph)
N
His270
C(tBu)
His187
Glu187
Nε
Fe
Replica 1
Replica 2
Replica 3
Dihedral Nε(His270)-Fe-N-C(tBu) (°)
Dihedral C(tBu)-N-C1(Ph)-C2(Ph) (°)
Dihedrals (°)
Time (ns)
C(tBu)-N-C1(Ph)-C2(Ph)
Nε(His270)-Fe-N-C(tBu)

E

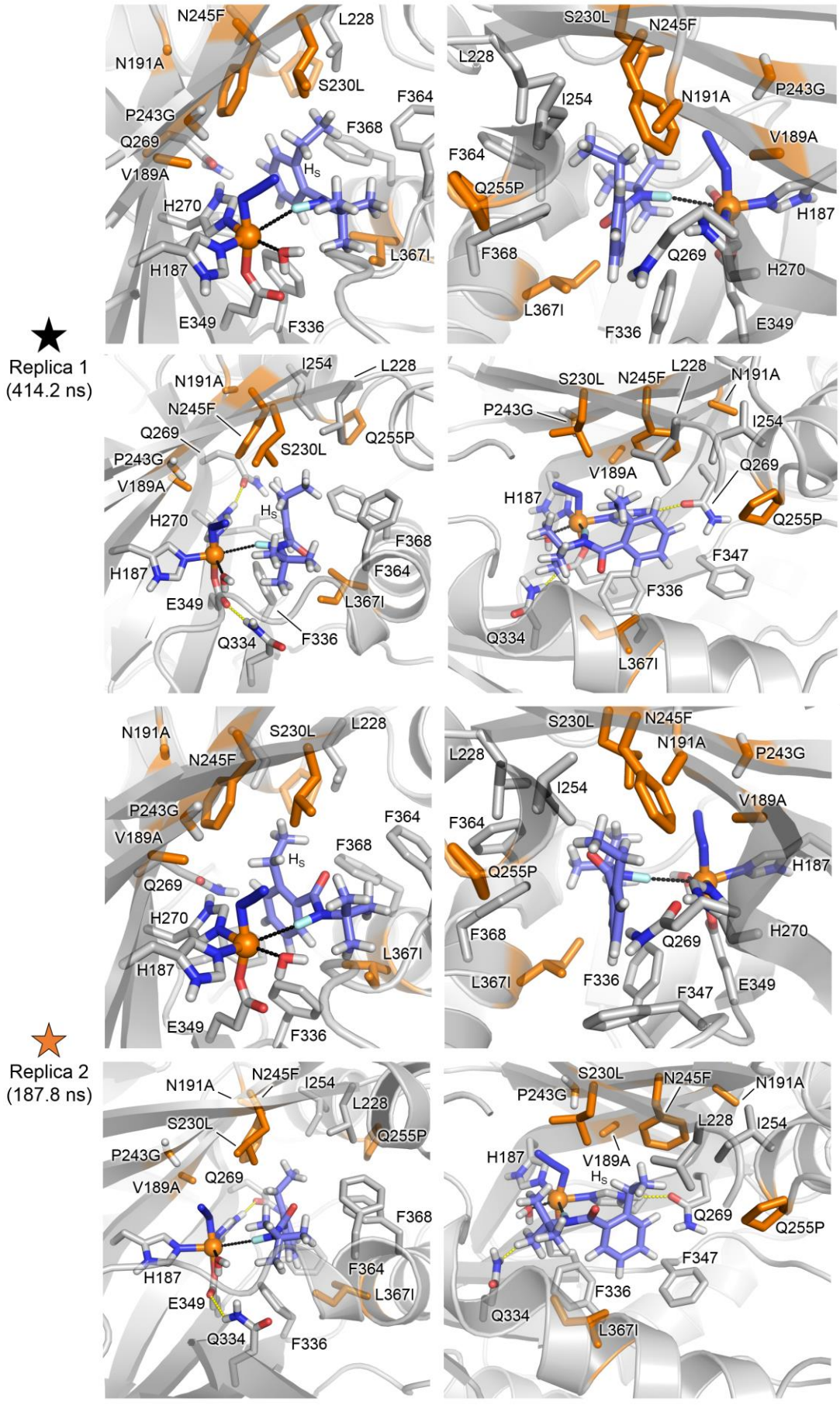
Replica 1
(414.2 ns)
Replica 2
(187.8 ns)
N245F
L228
N191A
S230L
F364
P243G
F368
Q269
V189A
Hs
H270
L367I
H187
E349
F336
I254
Q255P
F347
Q334

MD simulations show that when **1NF** binds in a catalytically competent pose for N–F activation in HppD Az2 active site, in the protein closed state, it preferentially explores a single orientation relative to the Fe-azide active species (**Fig. S15D** and **E**). Simulations describe that V189A and P243G generated more space to accommodate and stabilize the iron-bound azide in this region of the active site (see also **Fig. S11**). In wt *Sav* HppD, N191, N245 and S230 participate in a hydrogen bonding network with Q269, which is important for the binding and positioning of the native substrate 4-hydroxyphenylpyruvate (HPP). The newly introduced mutations disrupt the original hydrogen bonding network and create a hydrophobic environment to accommodate the *N*-fluoroamide substrate for N–F activation. V189A, N191A and P243G create space for bulkier S230L and N245F side chains that, together with L367I mutation and other active site residues, establish hydrophobic interactions with the substrate and help position the benzyl ethyl group closer to the azide in a restricted and preorganized conformation for the subsequent reaction steps.

The preferential orientation explored by the **1NF** substrate is characterized by ∠C(^{t}Bu)-N-C1(Ph)-C2(Ph) dihedral angle (**Fig. S15D**), which describes how the substrate is oriented in the active site relative to the iron species. Within this orientation, **1NF** adopts a single conformation defined by ∠N_ε(His270)-Fe-N-C(^{t}Bu) angle (**Fig. S15D**), in which the phenyl ethyl group is kept close to the azide (to both N1 and terminal N3, **Fig. S15B**), preorganizing it for the final radical recombination step. The recombination step is preceded by the HAT from the ethyl to the N-radical, which is formed by N–F activation.

This preferred near attack conformation for N–F activation characterized from restrained-MD simulations also describes that the H_S atom from the ethyl group is precisely positioned for an effective HAT once the N-radical is formed (**Fig. S15A**), thus explaining the origin of enantioselectivity for the azidation catalyzed by Az2 variant. The azide ligand explores a single orientation in Az2 active site in the presence of **1NF** substrate (**Fig. S15C**), which is equivalent to the one characterized by MD simulations in the absence of the substrate (**Fig. S12**).

The active site reshaping due to mutations in Az2 variant as compared to wt *Sav* HppD, has led to a highly complementarity between the active site and the *N*-fluoroamide substrate. This makes the substrate to be stabilized in a single preferential near attack conformation for N–F activation, which preorganizes it for the subsequent and enantioselective HAT and azide recombination steps.

Figure S16. H-bond network analysis in HppD Az2 – Fe-N_3 – 1NF active site explored by MD simulations. H-bond interactions analyzed as the distances between the donor and acceptor atoms of active site residues in closed state HppD Az2 – Fe-N_3 with substrate **1NF** bound in a near attack conformation for N-F activation. 3 independent replicas (replica 1, 2 and 3) of MD simulations of 500 ns each are analyzed. Distances explored along MD trajectories are all described in the included schematic figures. All distances and simulation time are given in Å and ns, respectively.

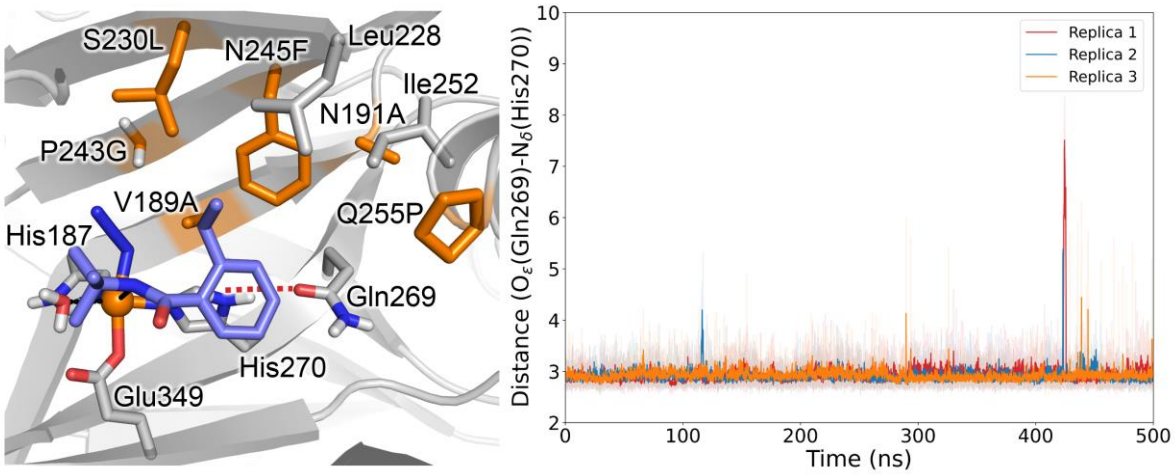

The new hydrophobic mutations introduced in HppD Az2 variant significantly reduce the extent of the H-bond network observed in wt *Sav* HppD (**Figure S14**). Only a single polar interaction between Gln269 and His270 is observed to be highly persistent along the 3 MD replicas, similar to the substrate-free MD simulations in Az2 (**Figure S12**).

The newly introduced mutations, specially S230L, N245F and N191A, largely reduce the polarity of this region of the active site where the azide is placed, making it highly hydrophobic. We hypothesize that this more hydrophobic environment might disfavor the coordination and stabilization of the azide anion, and thus might be contributing to the lower activity exhibited by the Az2 variant.

Figure S17. Conformational exploration of 1NF substrate using DFT calculations. DFT calculations were used to study **1NF** conformational flexibility. **(A)** Computed relative electronic energy (ΔE), enthalpy (ΔH), and quasi-harmonic corrected Gibbs energy (ΔG). Energy values were obtained at the (U)B3LYP/Def2TZVP/PCM(diethyl ether) // (U)B3LYP/6-31G(d)/PCM(diethyl ether) level. Energies are referred considering the lowest in energy conformer 1 as zero. **(B)** Optimized geometries for the lowest in energy conformers 1 and 2, and their interconverting transition state (TS). **(C)** Relaxed potential energy surface (PES) corresponding to the rotation along the ∠F-N-C-O dihedral angle. Electronic energies were obtained at the (U)B3LYP/6-31G(d)/PCM(diethyl ether) level. Energies and dihedrals are given in kcal·mol^{-1} and degrees (º), respectively.

A

Structure	Electronic State	ΔE	ΔH	ΔG
Conformer 1	close-shell singlet (CSS)	0.0	0.0	0.0
TS rotation 1-2	close-shell singlet (CSS)	9.6	8.9	10.2
Conformer 2	close-shell singlet (CSS)	4.8	4.8	4.7
Conformer 3	close-shell singlet (CSS)	0.6	0.6	0.6

B

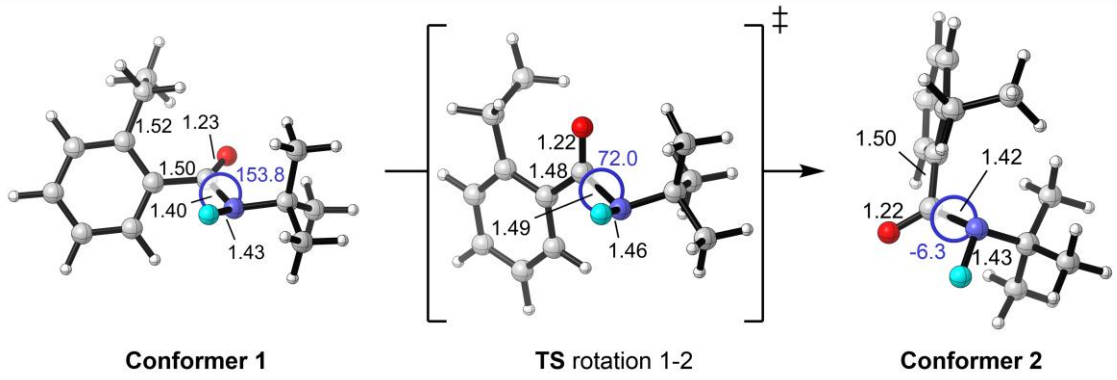

C

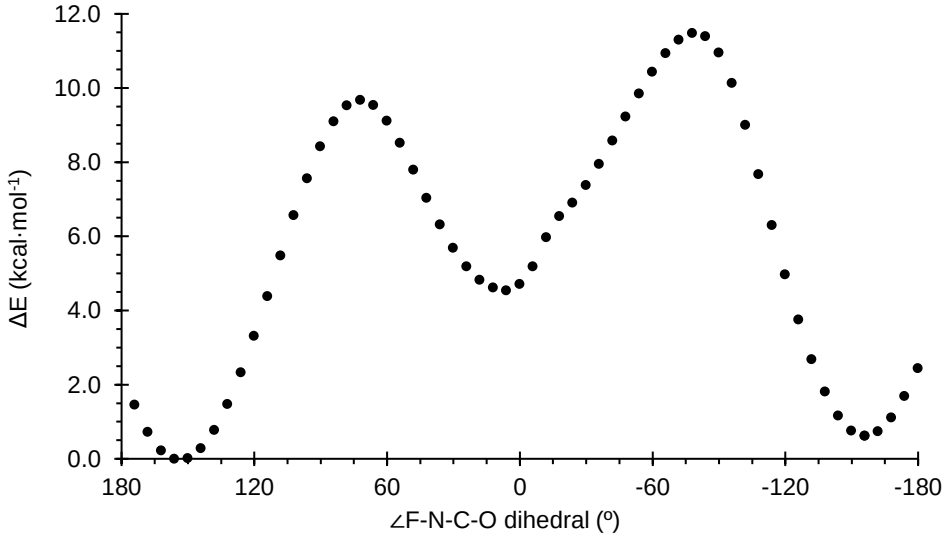

DFT calculations show that different conformers for **1NF** substrate are energetically accessible, with isomerization barriers lower than the rate-limiting step of the azidation reaction (**Figure S18)**.

Figure S18. Enzymatic non-heme iron Azidation mechanism explored by DFT calculations. (A) Proposed catalytic cycle for azidation reaction catalyzed by non-heme iron enzymes. **(B)** DFT calculated reaction mechanism for **1NF** azidation using a truncated computational model based on HppD Az2 active site [Fe(N_3^-)(Ac)(Im)$_2$(H_2O)$_2$]. Relative electronic energies (ΔE, in parenthesis) and quasi-harmonic corrected Gibbs energies (ΔG) of the lowest in energy electronic state (quintet) are reported. Energy values were obtained at the (U)B3LYP/Def2TZVP/PCM(diethyl ether) // (U)B3LYP/6-31G (d)/PCM(diethyl ether) level. All energies are referred considering the **[4 + 1NF]** reactant complex as zero. **(C)** Preferential near attack conformation for N–F activation explored by **1NF** in HppD Az2 active site as characterized from MD simulations (**Figure S15**, representative snapshot obtained from replica 1, at 414.2 ns). This structure was used as starting point to build the computational truncated model for the study of the azidation mechanism. **(D)** Optimized geometries for the stationary points (reactants and products, intermediates, and transition states (TSs)) reported in **A-B**. All energy values are given in kcal·mol^{-1}. Mulliken spin densities of key atoms are reported (ρ, a.u.). Distances and angles are given in Angstrom (Å) and degrees (º), respectively.

A

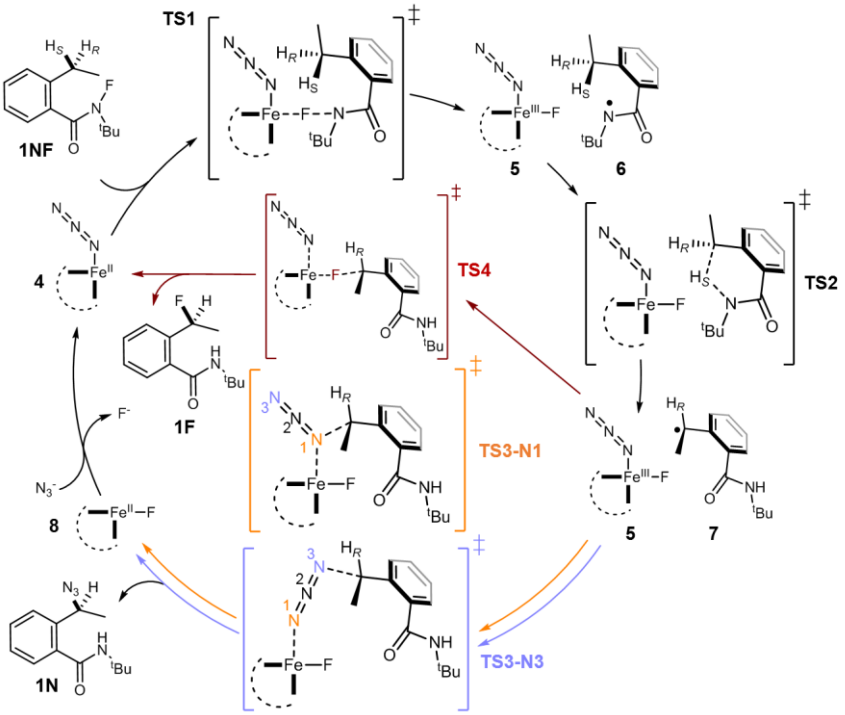

B

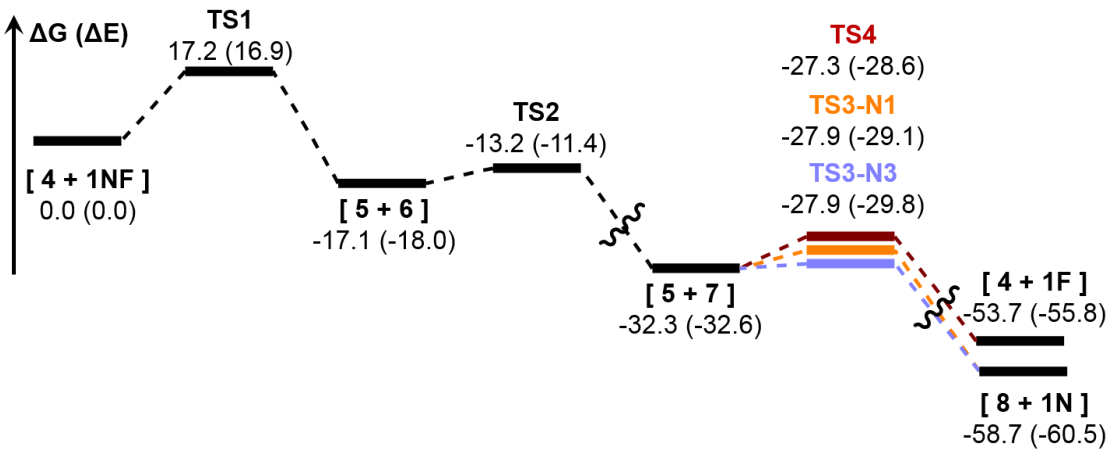

C

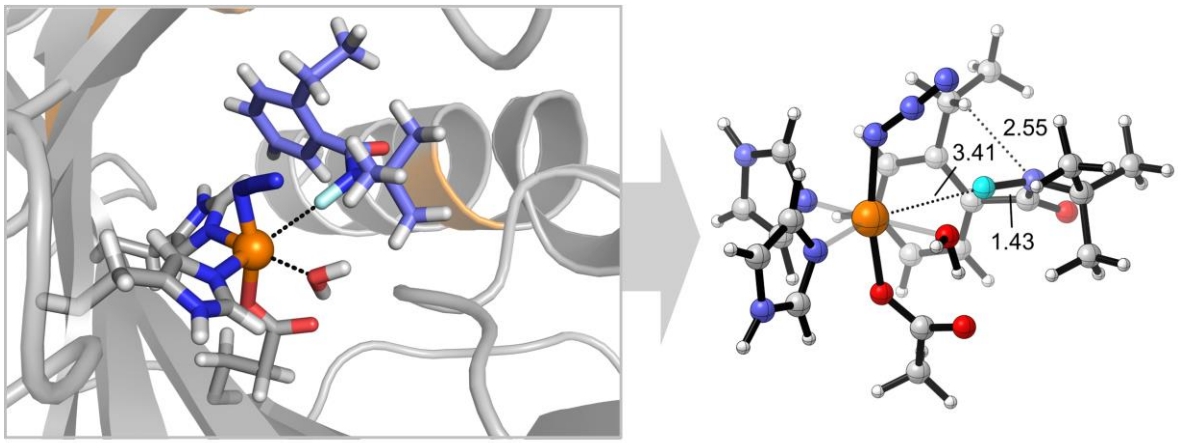

HppD *Az2* - Fe-N_3 – **1NF**, MD replica 1, at 414.2 ns

DFT optimized **[4 + 1NF] reactant complex**

D

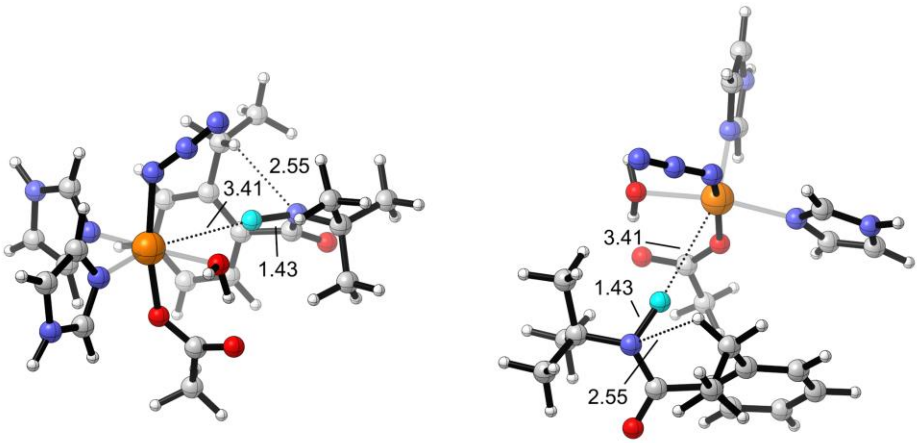

(view 1) (view 2)

[4 + 1NF]
(React. Complex, Q)
ΔG= 0.0 (ΔE= 0.0)

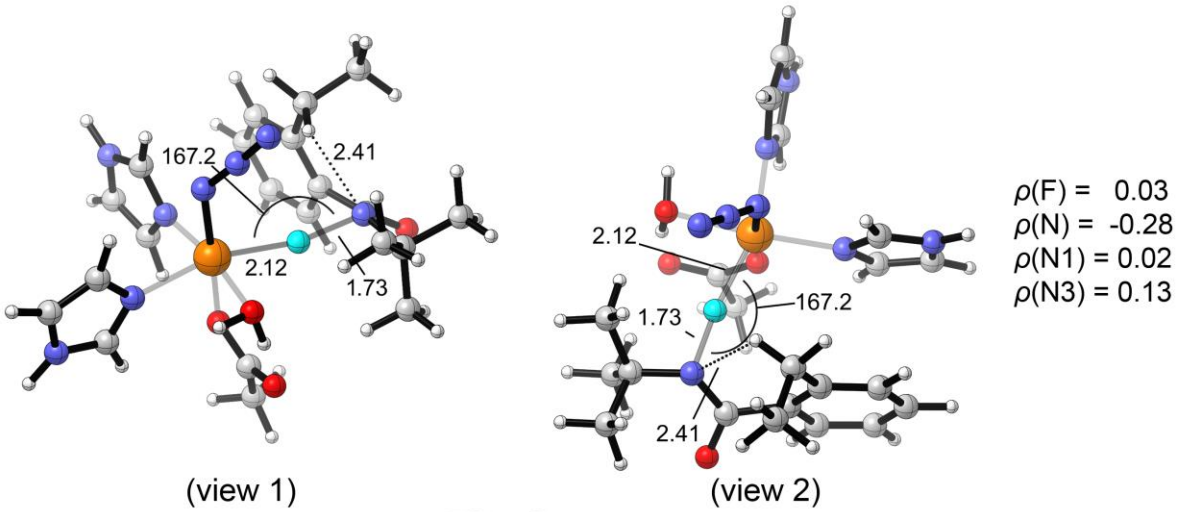

ρ(F) = 0.03
ρ(N) = -0.28
ρ(N1) = 0.02
ρ(N3) = 0.13

(view 1) (view 2)

TS1 (Q)
$\Delta G^{\ddagger}$= 17.2 ($\Delta E^{\ddagger}$= 16.9)

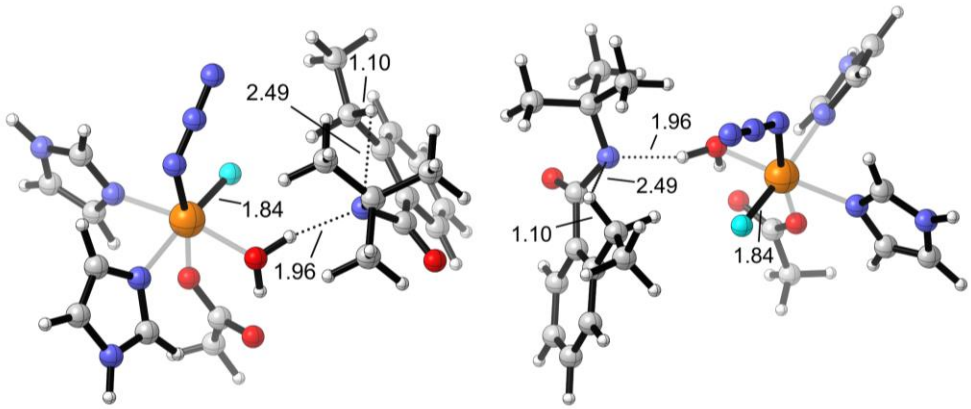

(view 1) (view 2)

[5 + 6]
(Int. Complex, Q)
ΔG_R= -17.1 (ΔE_R= -18.0)

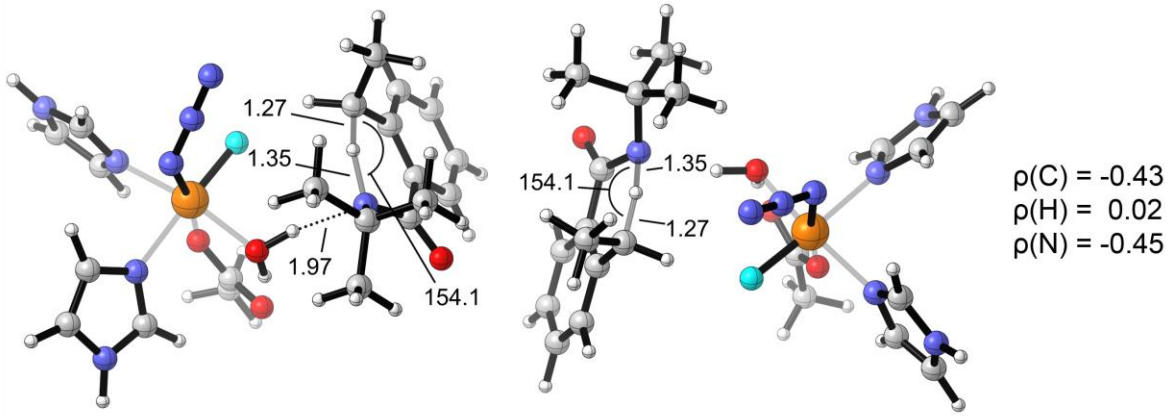

(view 1) (view 2)

TS2 (Q)
$\Delta G^{‡}$= 4.0 ($\Delta E^{‡}$= 6.6)

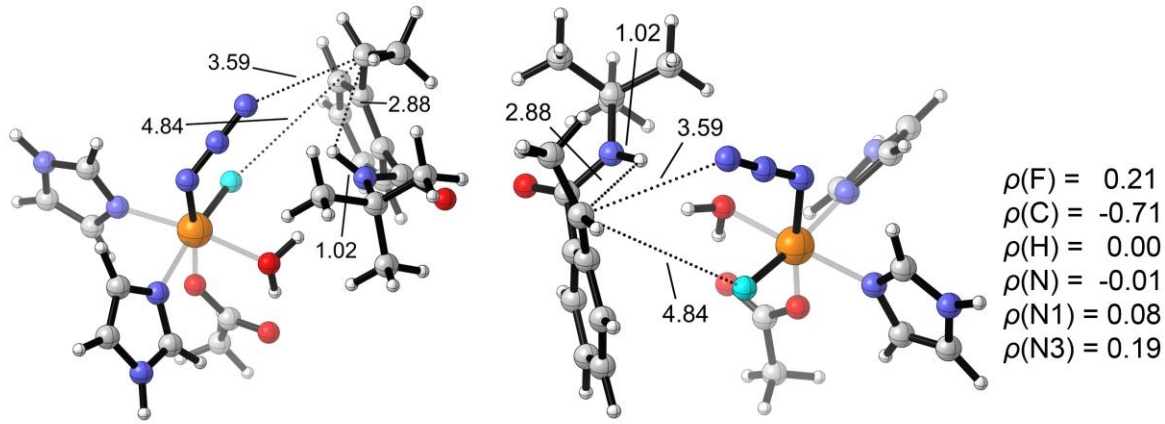

(view 1) (view 2)

[5 + 7]
(Int. Complex, Q)
ΔG_R= -15.1 (ΔE_R= -14.6)

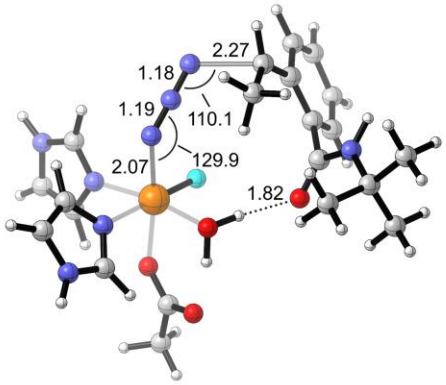

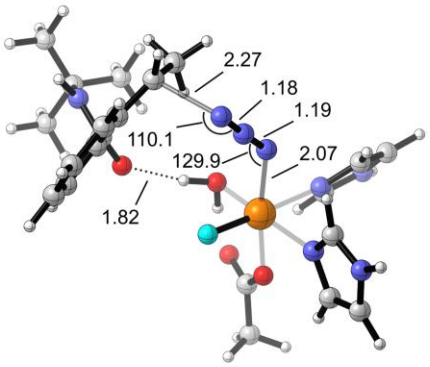

ρ(C) = -0.41
ρ(N1) = 0.05
ρ(N3) = 0.19

(view 1) (view 2)

TS3-N3 (Q)
$\Delta G^{\ddagger}$= 4.3 ($\Delta E^{\ddagger}$= 2.8)

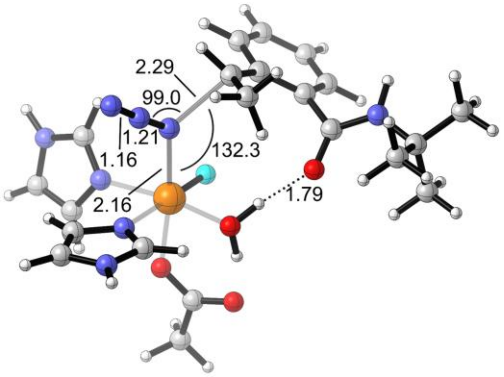

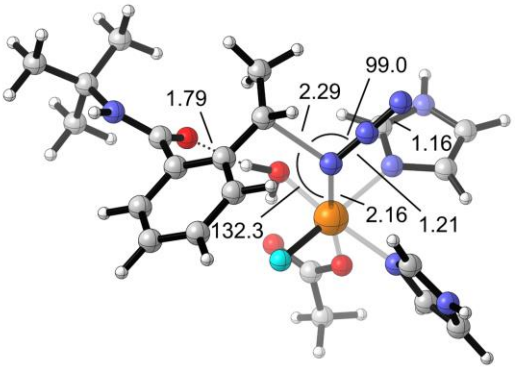

ρ(C) = -0.38
ρ(N1) = 0.06
ρ(N3) = 0.11

(view 1) (view 2)

TS3-N1 (Q)
$\Delta G^{\ddagger}$= 4.4 ($\Delta E^{\ddagger}$= 3.5)

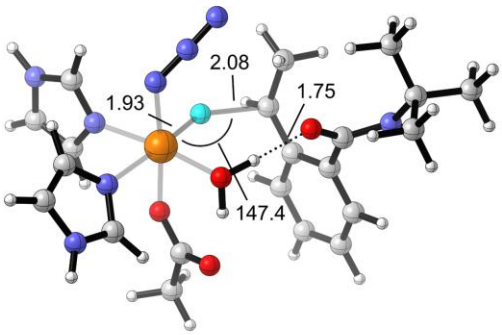

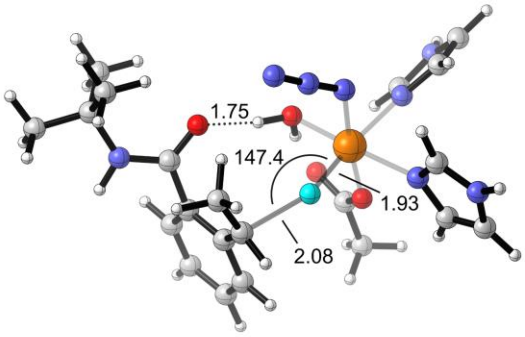

ρ(F) = 0.12
ρ(C) = -0.36

(view 1) (view 2)

TS4 (Q)
$\Delta G^{\ddagger}$= 5.0 ($\Delta E^{\ddagger}$= 4.0)

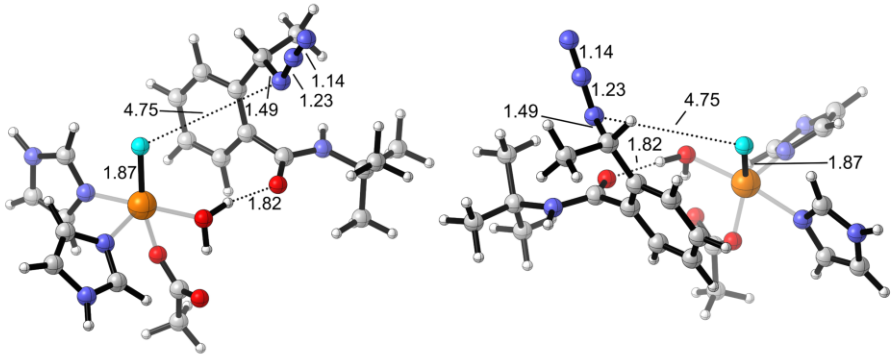

(view 1) (view 2)

[8 + 1N]
(Prod. Complex, Q)
ΔG_R= -26.4 (ΔE_R= -28.0)

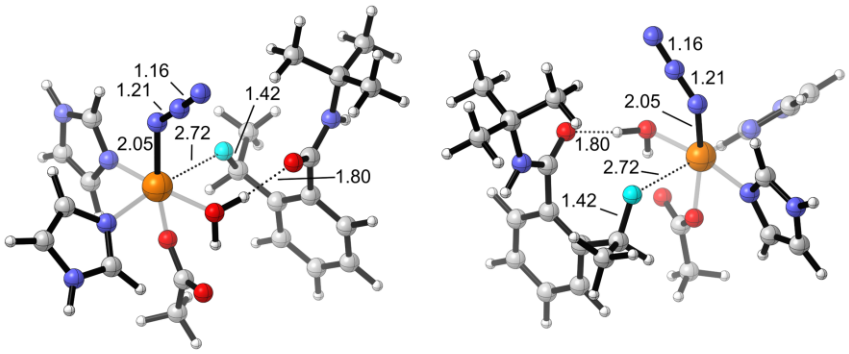

(view 1) (view 2)

[4 + 1F]
(Prod. Complex, Q)
ΔG_R= -21.4 (ΔE_R= -23.2)

The initial truncated model structure used for the DFT modelling was generated form a representative MD snapshot that describes the preferred binding mode of **1NF** in a near attack conformation for N–F activation in HppD Az2 variant (**Figure S15**). Quintet and triplet electronic states were considered for the entire reaction pathway (**Table S7**), being the quintet electronic state the energetically more favorable pathway. The N–F activation by the ferric azide corresponds to the rate-limiting step of the reaction (**TS1**, $\Delta G^{\ddagger}$ = 17.2 kcal·mol^{-1}). After fluorine abstraction, the iron is oxidized to its ferric form and a *N*-radical intermediate is formed (**[5 + 6]** intermediate complex). Due to substrate preorganization in Az2 active site (**Figure S15**), pro-*S* (H_S) benzylic hydrogen can rapidly be abstracted through a low in energy 1,5-HAT transition state (**TS2**, $\Delta G^{\ddagger}$ = 4.0 kcal·mol^{-1}), forming a much more stable benzylic C-radical intermediate (**[5 + 7]** intermediate complex, $\Delta\Delta G$ = 15.1 kcal·mol^{-1} more stable than the *N*-centered radical). The low barrier calculated for 1,5-HAT, and the formation of a thermodynamically much more stable benzylic C-radical intermediate, indicate that this stereo-determining step of the reaction mechanism is controlled by the geometric preorganization that the enzyme active site is imposing to the substrate. Once formed, the resulting C-radical can rapidly recombines with the iron-bound assize in a stereo-retentive manner though nitrogen N1 (N–Fe, **TS3-N1**, $\Delta G^{\ddagger}$ = 4.4 kcal·mol^{-1}) or terminal N3 (**TS3-N3**, $\Delta G^{\ddagger}$ = 4.3 kcal·mol^{-1}). The orientation of the azide in Az2 active site with respect to **1NF** substrate (**Figure S15-C**), and the isoenergetic transition state barriers calculated, indicate that both recombination pathways are possible. The possible fluorine transfer to the benzylic C-radical has also been explored. Model DFT calculations describe that the fluorine recombination has a low activation barrier (**TS4**, $\Delta G^{\ddagger}$ = 5.0 kcal·mol^{-1}), indicating that steric constraints imposed by Az2 active site prevent the radical intermediate **7** to repositioning for effective fluorine recombination.

Table S7. Relative energies of all the stationary points characterized for the azidation mechanism. DFT computed relative energies for all the stationary points described in **Figure S18** in their triplet (T) and quintet (Q) electronic states in terms of electronic energy (ΔE), enthalpy (ΔH), and quasi-harmonic corrected Gibbs energy (ΔG). Energy values were obtained at the (U)B3LYP/Def2TZVP/PCM(diethyl ether)//(U)B3LYP/6-31G(d)/PCM(diethyl ether) level. Energies are referred considering the lowest in energy **[4 + 1NF]** (reactant complex) in the quintet electronic state as zero. All energies are given in kcal·mol^{-1}.

Structure	Electronic State	ΔE	ΔH	ΔG
4 + 1NF	triplet (T)	15.5	14.5	-0.5
(Separated React.)	quintet (Q)	-3.8	-5.0	-21.6
[4 + 1NF]	triplet (T)	17.5	17.8	19.1
(React. Complex)	quintet (Q)	0.0	0.0	0.0
TS1	triplet (T)	31.5	30.5	34.6
	quintet (Q)	16.9	15.4	17.2
[5 + 6]	triplet (T)	4.0	3.7	6.4
(Int. Complex)	quintet (Q)	-18.0	-18.6	-17.1
TS2	triplet (T)	0.9	-3.2	0.0
	quintet (Q)	-11.4	-15.8	-13.2
[5 + 7]	triplet (T)	-16.8	-17.4	-14.6
(Int. Complex)	quintet (Q)	-32.6	-33.4	-32.3
TS3-N3	triplet (T)	-11.1	-12.0	-8.5
	quintet (Q)	-29.8	-31.0	-27.9
TS3-N1	triplet (T)	-6.9	-7.8	-3.8
	quintet (Q)	-29.1	-30.1	-27.9
TS4	triplet (T)	-11.9	-12.4	-8.1
	quintet (Q)	-28.6	-29.6	-27.3
[8 + 1N]	triplet (T)	-40.4	-39.0	-36.8
(Prod. Complex)	quintet (Q)	-60.5	-59.5	-58.7
[4 + 1F]	triplet (T)	-38.8	-37.3	-34.8
(Prod. Complex)	quintet (Q)	-55.8	-54.6	-53.7

Figure S19. DFT exploration of N–F activation step. A) Thermodynamic cycle explored for alternative N–F activation via a first outer sphere electron transfer. **B**) Relative energies for all the species involved in terms of electronic energy (ΔE), enthalpy (ΔH), and quasi-harmonic corrected Gibbs energy (ΔG). Energy values were obtained at the (U)B3LYP/Def2TZVP/PCM(diethyl ether) // (U)B3LYP/6-31G(d)/PCM(diethyl ether) level. Energies are referred considering the lowest in energy **[4 + 1NF]** (independent reactants) in the quintet electronic state as zero. The electronic state reported in each case refers only to the spin state of the Fe-containing species. **C**) Optimized geometries for the studied species, including key geometric parameters and the charge and spin density of key atoms (charge / spin density, in a.u.). All energies are given in kcal·mol^{-1}. Distances are given in Angstrom (Å).

A

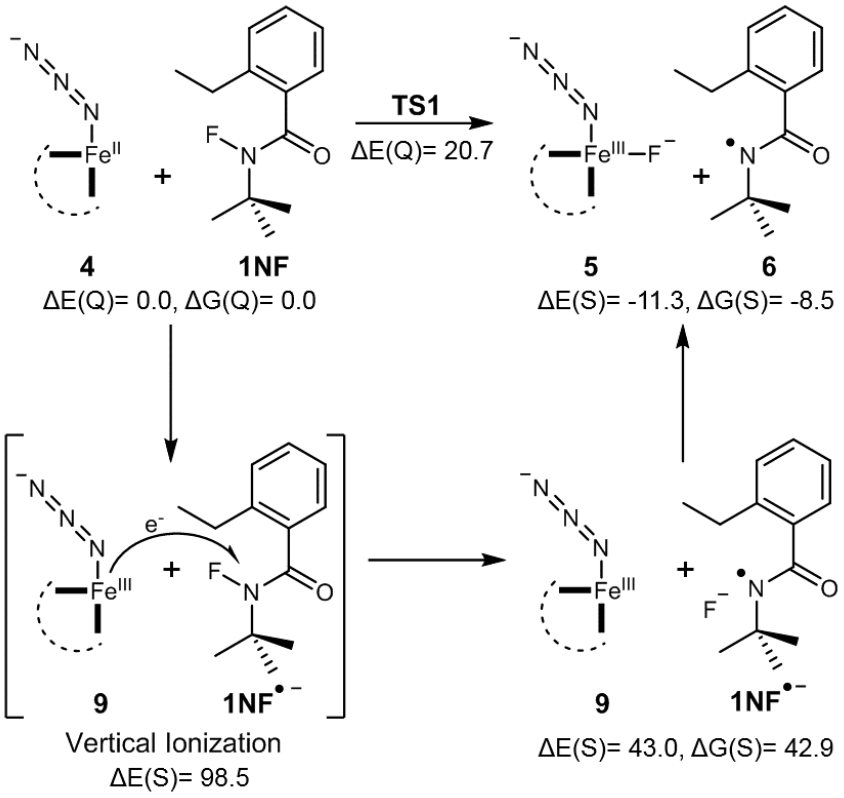

B

Structure	Electronic State	ΔE	ΔH	ΔG
4 + 1NF (Separated React.)	triplet (T)	19.3	19.5	21.1
	quintet (Q)	0.0	0.0	0.0
TS1	triplet (T)	35.3	35.5	56.2
	quintet (Q)	20.7	20.3	38.7
9 + 1NF•- (Separated Int.)	doublet (D)	115.4	-	-
	quartet (Qu)	115.8	-	-
Vertical Ionization	sextet (S)	98.5	-	-
9 + 1NF•- (Separated Int.)	doublet (D)	61.4	60.7	65.0
	quartet (Qu)	52.1	50.4	52.7
	sextet (S)	43.0	41.9	42.9
5 + 6 (Separated Int.)	doublet (D)	0.0	-0.3	7.1
	quartet (Qu)	0.9	0.0	4.6
	sextet (S)	-11.3	-12.5	-8.5

C

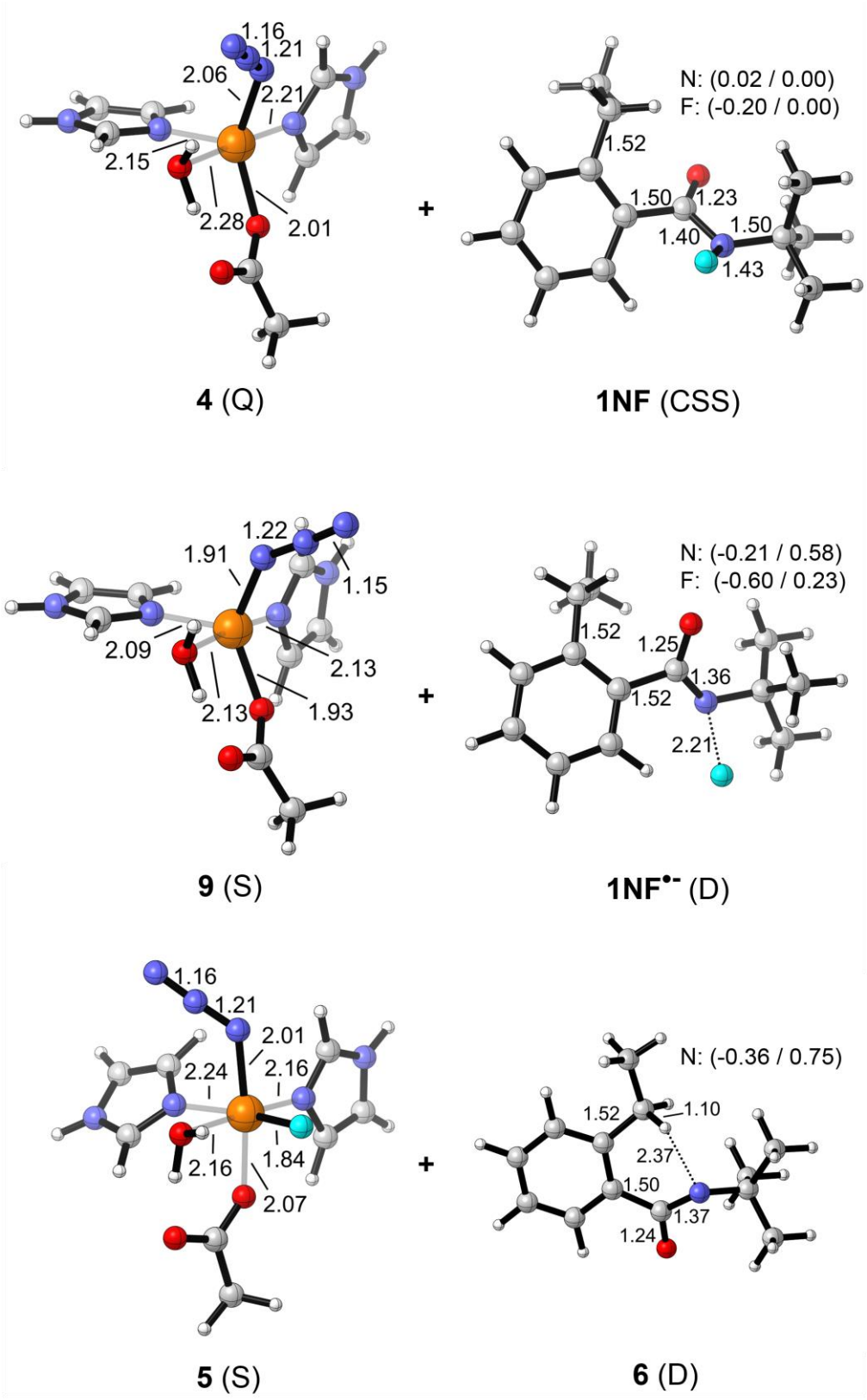

DFT calculations indicate that the fluorine abstraction process is expected to occur through a concerted homolytic cleavage of the N–F bond (**TS1)**, as described in **Figure S18**. The alternative N–F bond activation thought a first electron transfer (ET) from the ferrous metal center to the *N*–fluoroamide substrate is energetically highly unfavorable.

Figure S20. Frontier Molecular Orbital (FMO) analysis of the radical recombination step. Frontier Molecular Orbitals (FMO), β-HOMO and β-LUMO orbitals, at the transition states (TSs) corresponding to the azide recombination from the terminal N3-atom (**TS3-N3**) and the Fe-bound N-atom (**TS3-N1**), and for the fluorine recombination (**TS4**).

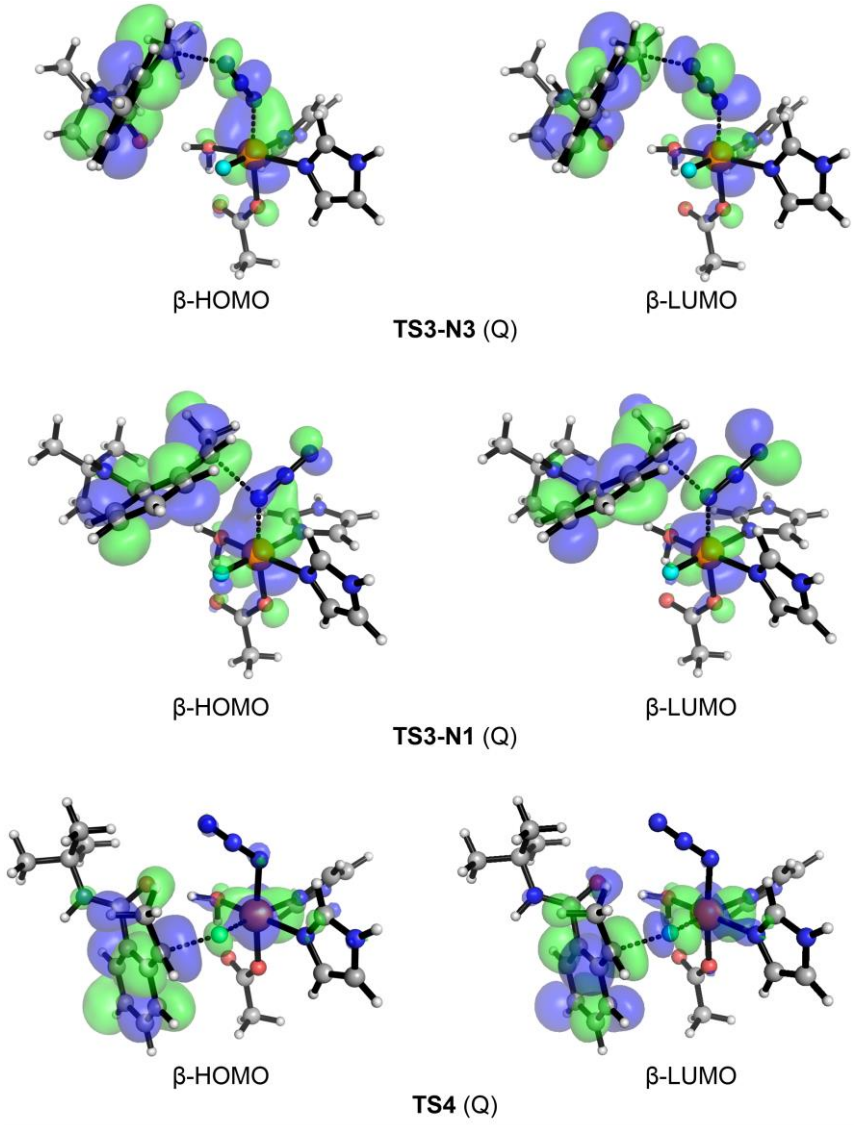

The FMO orbitals (β-HOMO and β-LUMO) from **TS3-N3** (Q) and **TS3-N1** (Q) optimized geometries show a clear contribution on the electron-donor β-HOMOs of the substrate C-radical p-orbital, and a β-dπ (Fe-N_3) character. On the other hand, the electron-acceptor β-LUMOs show a strong β-dπ* contribution on the Fe-N3 bond that is being cleaved. An equivalent scenario is observed for fluorine recombination and **TS4** (Q).

These observations are consistent with previous works (*36, 37*) describing that the radical recombination step is initiated by a β-electron transfer from the C-radical to the iron center through a superexchange mediating anionic ligand, which after the TS is followed by the anion recombination (N_3 in this case). This mechanism implies the electron transfer from β-HOMO to β-LUMO right after the TS.

Table S8. Energies and thermochemistry parameters (at T = 298.15 K and P = 1 atm) of all computationally characterized stationary points reported in **Figures S8**, **S17**, and **S19**. Electronic energies (E), enthalpy (H), free energy (G), quasi harmonic corrected free energy (qh-G), and electronic energies from high level single point calculations (E (SP)) are given in a.u. Imaginary frequencies are given in cm^{-1}.

Structure	Electronic State	E	H	G	G-qh	E (SP)	Imag. Freq.
Coordination mode 1	triplet (T)	-1122.026010	-1121.737867	-1121.821620	-1121.821043	-2262.300598	-
	quintet (Q)	-1122.055944	-1121.769148	-1121.857088	-1121.856131	-2262.327085	-
Coordination mode 2	triplet (T)	-1122.022898	-1121.735772	-1121.821130	-1121.821130	-2262.301045	-
	quintet (Q)	-1122.054018	-1121.767010	-1121.852429	-1121.852163	-2262.323029	-
1NF (conformer 1)	close-shell singlet (CSS)	-735.994954	-735.689196	-735.750719	-735.757740	-736.279217	-
TS rotation 1-2	close-shell singlet (CSS)	-735.979492	-735.674972	-735.734416	-735.741402	-736.263866	58.0i
1NF (conformer 2)	close-shell singlet (CSS)	-735.984940	-735.679249	-735.741165	-735.747982	-736.271531	-
1NF (conformer 3)	close-shell singlet (CSS)	-735.993922	-735.688108	-735.749723	-735.756719	-736.278276	-
1NF$^{\bullet-}$ (Vertical Ionization)	doublet (D)	-736.022072	-	-	-	-736.323991	-
1NF$^{\bullet-}$	doublet (D)	-736.091347	-733.057767	-733.681827	-733.752937	-736.397493	-
4	triplet (T)	-1045.597718	-1045.338074	-1045.416433	-1045.415738	-2185.827167	-
	quintet (Q)	-1045.630385	-1045.371148	-1045.452334	-1045.451339	-2185.857862	-
5	doublet (D)	-1145.461681	-1145.197343	-1145.274016	-1145.273493	-2285.735355	-
	quartet (Qu)	-1145.461466	-1145.198074	-1145.279280	-1145.278771	-2285.733871	-
	sextet (S)	-1145.482406	-1145.219431	-1145.301551	-1145.300993	-2285.753410	-
6	doublet (D)	-636.165573	-635.865403	-635.926212	-635.926212	-636.401728	-
9 (Vertical Ionization)	doublet (D)	-1045.403312	-	-	-	-2185.629110	-
	quartet (Qu)	-1045.405259	-	-	-	-2185.628565	-
	sextet (S)	-1045.432835	-	-	-	-2185.656157	-
9	doublet (D)	-1045.417367	-1045.156783	-1045.229440	-1045.229205	-2185.641777	
	quartet (Qu)	-1045.431412	-1045.172437	-1045.249116	-1045.248058	-2185.656618	-
	sextet (S)	-1045.447041	-1045.187260	-1045.265757	-1045.264796	-2185.671032	-

Table S9. Energies and thermochemistry parameters (at T = 298.15 K and P = 1 atm) of all computationally characterized stationary points reported in **Figure S18** and **Table S7**. Electronic energies (E), enthalpy (H), free energy (G), quasi harmonic corrected free energy (qh-G), and electronic energies from high level single point calculations (E (SP)) are given in a.u. Imaginary frequencies are given in cm^{-1}.

Structure	Electronic State	E	H	G	G-qh	E (SP)	Imag. Freq.
[4 + 1NF]	triplet (T)	-1781.579139	-1781.011646	-1781.135785	-1781.132641	-2922.100758	-
(React. Complex)	quintet (Q)	-1781.613318	-1781.046421	-1781.171299	-1781.168713	-2922.131042	-
TS1	triplet (T)	-1781.560523	-1780.995458	-1781.112601	-1781.111215	-2922.076167	693.0i
	quintet (Q)	-1781.589261	-1781.024786	-1781.145692	-1781.143766	-2922.101400	790.5i
[5 + 6]	triplet (T)	-1781.623539	-1781.057204	-1781.177048	-1781.175107	-2922.124602	-
(Int. Complex)	quintet (Q)	-1781.646034	-1781.080142	-1781.202235	-1781.200093	-2922.159664	-
TS2	triplet (T)	-1781.610331	-1781.049991	-1781.169258	-1781.167125	-2922.129568	1480.4i
	quintet (Q)	-1781.632922	-1781.073025	-1781.192842	-1781.191173	-2922.149161	1493.2i
[5 + 7]	triplet (T)	-1781.643864	-1781.077886	-1781.197885	-1781.195840	-2922.157803	-
(Int. Complex)	quintet (Q)	-1781.663351	-1781.097857	-1781.220354	-1781.218251	-2922.182944	-
TS3-N3	triplet (T)	-1781.626411	-1781.060912	-1781.180334	-1781.177588	-2922.148771	533.5i
	quintet (Q)	-1781.659684	-1781.094597	-1781.213677	-1781.212048	-2922.178558	312.1i
TS3-N1	triplet (T)	-1781.622400	-1781.056958	-1781.174761	-1781.172867	-2922.142079	661.8i
	quintet (Q)	-1781.658003	-1781.092738	-1781.213404	-1781.211515	-2922.177373	385.6i
TS4	triplet (T)	-1781.628168	-1781.061968	-1781.179413	-1781.177424	-2922.150028	619.8i
	quintet (Q)	-1781.657144	-1781.091841	-1781.212057	-1781.21048	-2922.176560	527.2i
[8 + 1N]	triplet (T)	-1781.673073	-1781.103961	-1781.225614	-1781.222735	-2922.195358	-
(Prod. Complex)	quintet (Q)	-1781.708619	-1781.140001	-1781.263901	-1781.261051	-2922.227506	-
[4 + 1F]	triplet (T)	-1781.671151	-1781.101818	-1781.222246	-1781.220075	-2922.192948	-
(Prod. Complex)	quintet (Q)	-1781.701630	-1781.132868	-1781.255756	-1781.253647	-2922.219965	-

Table S10. Cartesian coordinates (xyz, in Å) of all DFT optimized structures.

Coordination mode 1 (T)

C	-0.729283	3.478590	1.793803
N	0.624942	3.327813	2.012094
H	1.216421	3.949978	2.545540
C	1.032250	2.203366	1.374958
H	2.047152	1.833708	1.381012
N	0.012130	1.620498	0.761794
C	-1.093225	2.410217	1.018361
H	-2.065148	2.158455	0.620948
C	-2.819606	-2.290124	1.778051
N	-3.623574	-1.752880	0.792549
H	-4.623545	-1.871639	0.706618
C	-2.842933	-1.042614	-0.052877
H	-3.193443	-0.515162	-0.925845
N	-1.576157	-1.095054	0.340090
C	-1.549739	-1.873271	1.484434
H	-0.619743	-2.081232	1.988381
C	3.016411	-2.174752	1.846758
H	4.053925	-1.928265	2.079652
H	2.957500	-3.180658	1.419388
C	2.420786	-1.158875	0.885221
O	1.258088	-1.467895	0.403158
O	3.049450	-0.110888	0.620095
Fe	-0.014635	-0.167204	-0.537199
N	-1.196402	0.319277	-2.066900
N	-0.932996	1.150456	-2.907060
N	-0.748429	1.931359	-3.742755
O	1.635610	0.555717	-1.545312
H	2.295804	0.494368	-0.798249
H	1.858879	-0.225386	-2.107623
H	-3.214201	-2.904792	2.571622
H	2.431715	-2.181750	2.774435
H	-1.287938	4.309301	2.195636
O	1.949233	-2.072019	-2.380866
H	1.678670	-2.229730	-1.453910
H	1.180855	-2.344709	-2.907952

Coordination mode 1 (Q)

C	-1.062423	-2.364318	2.889568
N	-2.251902	-1.724789	2.604121
H	-3.121565	-1.828688	3.108562
C	-2.059246	-0.942992	1.514896
H	-2.824535	-0.323322	1.069867
N	-0.808113	-1.040726	1.088577
C	-0.177361	-1.927480	1.940510
H	0.860268	-2.191835	1.803058
C	3.364290	1.807523	1.576985
N	3.971291	0.680279	1.060483
H	4.929389	0.395713	1.211012
C	3.058133	0.017736	0.309388
H	3.250575	-0.905262	-0.216819
N	1.898062	0.657737	0.316210
C	2.078074	1.777805	1.105892
H	1.268948	2.473567	1.266312
C	-2.301318	3.566161	0.361391
H	-3.355140	3.829233	0.252476
H	-1.675963	4.319129	-0.129010
C	-2.017839	2.189472	-0.222005
O	-0.777624	1.853839	-0.296033
O	-2.979227	1.465452	-0.577600
Fe	0.054900	-0.088806	-0.703781
N	1.107714	-1.694002	-1.433615
N	0.687592	-2.740465	-1.862111
N	0.333531	-3.763556	-2.281806
O	-1.787981	-0.530070	-1.852942
H	-2.365377	0.187897	-1.449318
H	-1.604845	-0.242841	-2.762780
H	3.889860	2.503595	2.211881
H	-2.037730	3.569759	1.425718
H	-0.962836	-3.051847	3.714771
O	0.619888	1.310075	-2.531313
H	0.273284	2.033446	-1.971258
H	1.586734	1.381291	-2.475809

Coordination mode 2 (T)

C	-0.647011	-3.803131	-0.888708
N	-1.883890	-3.391077	-0.433778
H	-2.701300	-3.973772	-0.314958
C	-1.822543	-2.061918	-0.187860
H	-2.657208	-1.467031	0.154246
N	-0.607571	-1.601525	-0.451997
C	0.137595	-2.680844	-0.894333
H	1.161257	-2.547898	-1.215621
C	2.599605	-0.637077	2.801477
N	3.244043	0.449719	2.247372
H	4.097974	0.872981	2.583803
C	2.530863	0.867464	1.176731
H	2.797160	1.700369	0.545328
N	1.460982	0.098304	1.011584
C	1.492404	-0.843463	2.024044
H	0.721913	-1.592543	2.116227
C	-3.047651	1.787511	2.580590
H	-4.137687	1.819059	2.529723
H	-2.664690	2.792447	2.791157
C	-2.453916	1.285786	1.272295
O	-1.182541	1.138332	1.251728
O	-3.226731	1.048527	0.304425
Fe	-0.011762	0.425300	-0.304873
O	-1.534298	0.805439	-1.626423
H	-2.308761	0.922924	-0.972822
H	-1.431335	1.650838	-2.097724
H	2.978078	-1.149656	3.671602
H	-2.732159	1.142614	3.407516
H	-0.449419	-4.826769	-1.165426
O	2.877626	-0.949764	-1.926925
H	2.381281	-0.103020	-1.913419
H	3.192268	-1.023650	-1.013226
N	1.286947	1.502771	-1.455332
N	0.864505	2.196177	-2.354003

N	0.470687	2.874071	-3.207784

Coordination mode 2 (Q)

C	-1.062423	-2.364318	2.889568
N	-2.251902	-1.724789	2.604121
H	-3.121565	-1.828688	3.108562
C	-2.059246	-0.942992	1.514896
H	-2.824535	-0.323322	1.069867
N	-0.808113	-1.040726	1.088577
C	-0.177361	-1.927480	1.940510
H	0.860268	-2.191835	1.803058
C	3.364290	1.807523	1.576985
N	3.971291	0.680279	1.060483
H	4.929389	0.395713	1.211012
C	3.058133	0.017736	0.309388
H	3.250575	-0.905262	-0.216819
N	1.898062	0.657737	0.316210
C	2.078074	1.777805	1.105892
H	1.268948	2.473567	1.266312
C	-2.301318	3.566161	0.361391
H	-3.355140	3.829233	0.252476
H	-1.675963	4.319129	-0.129010
C	-2.017839	2.189472	-0.222005
O	-0.777624	1.853839	-0.296033
O	-2.979227	1.465452	-0.577600
Fe	0.054900	-0.088806	-0.703781
N	1.107714	-1.694002	-1.433615
N	0.687592	-2.740465	-1.862111
N	0.333531	-3.763556	-2.281806
O	-1.787981	-0.530070	-1.852942
H	-2.365377	0.187897	-1.449318
H	-1.604845	-0.242841	-2.762780
H	3.889860	2.503595	2.211881
H	-2.037730	3.569759	1.425718
H	-0.962836	-3.051847	3.714771
O	0.619888	1.310075	-2.531313
H	0.273284	2.033446	-1.971258
H	1.586734	1.381291	-2.475809

1NF (Conformer 1, CSS)

C	-1.029394	-0.371469	-0.191572
C	-1.211214	-1.707668	-0.588410
C	-2.456845	-2.318246	-0.491628
C	-3.533622	-1.598680	0.031133
C	-3.352823	-0.278850	0.438782
C	-2.113838	0.369779	0.327316
H	-0.367072	-2.261596	-0.985240
H	-2.584844	-3.347173	-0.815144
H	-4.510443	-2.065488	0.125207
H	-4.192302	0.272073	0.856790
C	-2.016813	1.817074	0.772651
H	-0.993235	2.064293	1.065574
H	-2.643146	1.943107	1.664927
C	-2.480427	2.807931	-0.310301
H	-2.430033	3.836567	0.065088
H	-3.514967	2.608168	-0.612474
H	-1.840650	2.730528	-1.193446
C	0.302139	0.280114	-0.410725
O	0.426695	1.397477	-0.901437
N	1.431191	-0.502850	-0.146911
C	2.816649	0.030041	0.035808
C	3.729719	-1.175567	0.322983
C	3.257182	0.674274	-1.291904
C	2.857163	1.034521	1.199281
H	3.496974	-1.644337	1.281096
H	3.639534	-1.929181	-0.466256
H	4.767878	-0.830498	0.352280
H	2.679243	1.568711	-1.520125
H	4.315354	0.944685	-1.209505
H	3.150490	-0.036162	-2.118532
H	3.884818	1.374610	1.365478
H	2.236382	1.908041	0.982016
H	2.499314	0.564953	2.121493
F	1.151949	-1.415634	0.913352

TS rotation 1-2 (CSS)

C	1.012447	-0.350332	-0.157672
C	0.970749	-1.739205	0.088120
C	2.132767	-2.477439	0.279065
C	3.368185	-1.833781	0.210612
C	3.424407	-0.464277	-0.047938
C	2.272989	0.310939	-0.233056
H	0.004157	-2.224102	0.123984
H	2.074023	-3.544492	0.471809
H	4.288451	-2.394708	0.350215
H	4.393258	0.024799	-0.111674
C	2.462771	1.793975	-0.485398
H	1.742330	2.153636	-1.222336
H	3.464696	1.936892	-0.907719
C	2.340192	2.643082	0.793763
H	2.518058	3.699930	0.565144
H	3.073519	2.329838	1.545616
H	1.340741	2.554859	1.228517
C	-0.263899	0.382287	-0.343024
O	-0.365064	1.587143	-0.470000
N	-1.457835	-0.500363	-0.383817
C	-2.672935	-0.063934	0.362567
C	-3.696321	-1.198970	0.178755
C	-2.241360	0.017146	1.838271
C	-3.282678	1.269061	-0.110488
H	-3.966015	-1.307772	-0.875545
H	-3.286695	-2.151425	0.530633
H	-4.606817	-0.978983	0.746139
H	-1.538513	0.838221	2.012386
H	-3.125901	0.198692	2.457019
H	-1.780657	-0.919316	2.170557
H	-4.237334	1.427693	0.403440
H	-2.626895	2.114620	0.098882
H	-3.475486	1.239674	-1.186126
F	-1.788161	-0.435998	-1.799520

1NF (Conformer 2, CSS)

C	-0.974534	-0.572106	0.427218

C	-1.518127	-1.798703	0.010738
C	-2.772133	-1.854947	-0.587612
C	-3.510400	-0.677857	-0.739471
C	-2.993674	0.530393	-0.278671
C	-1.723509	0.617283	0.314525
H	-0.939672	-2.707182	0.153577
H	-3.175216	-2.806663	-0.921330
H	-4.496014	-0.705827	-1.196081
H	-3.594718	1.433182	-0.360200
C	-1.272037	1.957302	0.872897
H	-0.398059	1.830246	1.516365
H	-2.076539	2.336911	1.516495
C	-0.960610	3.018323	-0.195626
H	-0.728890	3.978618	0.278216
H	-1.811022	3.172205	-0.869310
H	-0.097567	2.727332	-0.803016
C	0.360509	-0.629094	1.114449
O	0.519369	-1.241195	2.155801
N	1.379977	0.168188	0.538185
C	2.030823	-0.112943	-0.797854
C	2.751196	-1.472105	-0.747949
C	0.982880	-0.104859	-1.920755
C	3.031789	1.029996	-1.040310
H	3.473979	-1.501534	0.070688
H	2.038016	-2.292667	-0.612533
H	3.286470	-1.640997	-1.688155
H	0.397534	0.817957	-1.925703
H	1.519876	-0.170878	-2.872682
H	0.297166	-0.951712	-1.864228
H	3.514184	0.887520	-2.012541
H	2.518875	1.997331	-1.047303
H	3.806172	1.053058	-0.271325
F	2.450844	0.190138	1.478433

1NF (Conformer 3, CSS)

C	1.172390	-0.469398	0.196140
C	1.826950	-1.703886	0.317939
C	3.170280	-1.841384	-0.022667
C	3.878259	-0.723838	-0.463490
C	3.237585	0.512410	-0.554238
C	1.882383	0.674598	-0.235743
H	1.264477	-2.559642	0.678735
H	3.657140	-2.808698	0.060653
H	4.928279	-0.809120	-0.730058
H	3.802744	1.382819	-0.878916
C	1.278944	2.066124	-0.290310
H	0.326777	2.046887	-0.825268
H	1.950042	2.707828	-0.873045
C	1.076658	2.692899	1.101541
H	0.659479	3.702115	1.009816
H	2.027189	2.765211	1.641799
H	0.388942	2.099808	1.713953
C	-0.261143	-0.476449	0.649246
O	-0.591917	-0.965480	1.724323
N	-1.208985	0.131393	-0.172045
C	-2.676678	-0.160415	-0.150656
C	-2.928195	-1.653092	-0.419871
C	-3.225320	0.273511	1.221295
C	-3.328678	0.709913	-1.239514
H	-2.494744	-1.946301	-1.381736
H	-2.490076	-2.270445	0.369270
H	-4.004648	-1.851335	-0.455069
H	-2.975774	1.320823	1.421856
H	-4.316455	0.180578	1.201159
H	-2.830891	-0.342590	2.028119
H	-4.415146	0.595804	-1.174681
H	-3.084413	1.767070	-1.092258
H	-3.012377	0.414657	-2.241874
F	-0.755882	0.111406	-1.524527

1NF radical anion (D)

C	-1.107100	-0.313417	0.185858
C	-1.267166	-1.689760	-0.043898
C	-2.533307	-2.240978	-0.244088
C	-3.660323	-1.419576	-0.231393
C	-3.504682	-0.049702	-0.016790
C	-2.246047	0.529927	0.200441
H	-0.360605	-2.293625	-0.049374
H	-2.637597	-3.311369	-0.410101
H	-4.653259	-1.836273	-0.387475
H	-4.382130	0.595100	-0.016754
C	-2.169928	2.036865	0.372856
H	-1.523718	2.276491	1.219246
H	-3.175772	2.414379	0.599427
C	-1.638682	2.758265	-0.878810
H	-1.608400	3.843399	-0.719911
H	-2.274864	2.560437	-1.750055
H	-0.624416	2.425880	-1.122073
C	0.287772	0.231819	0.449473
O	0.443542	1.116364	1.323017
N	1.254539	-0.209696	-0.391157
C	2.668067	0.136876	-0.184320
C	3.455537	-0.688612	-1.219199
C	2.858079	1.642252	-0.487394
C	3.179203	-0.200589	1.230639
H	3.226413	-1.740859	-1.044714
H	3.145657	-0.425937	-2.238655
H	4.534725	-0.509185	-1.127863
H	2.328141	2.253629	0.246520
H	3.925983	1.896703	-0.460213
H	2.478148	1.885615	-1.487384
H	4.261431	-0.026120	1.302636
H	2.674144	0.410411	1.982189
H	2.959945	-1.253613	1.416669
F	1.494170	-2.336479	0.155733

4 (T)

C	1.200840	1.925866	3.079051
N	2.357985	1.305625	2.653563
H	3.252111	1.322363	3.124585
C	2.090980	0.676008	1.483342
H	2.818645	0.103540	0.926615
N	0.825866	0.854911	1.135490
C	0.260649	1.633872	2.126376

H	-0.776261	1.932439	2.081338
C	-3.377238	-1.814662	1.197974
N	-3.977099	-0.678973	0.690506
H	-4.950902	-0.425108	0.783140
C	-3.039850	0.037498	0.029888
H	-3.217085	0.973707	-0.475215
N	-1.866188	-0.579847	0.087450
C	-2.065701	-1.740026	0.815597
H	-1.253943	-2.428154	0.986258
C	1.978103	-3.721061	-0.407361
H	3.008371	-4.021011	-0.607201
H	1.291829	-4.326646	-1.008225
C	1.771161	-2.246383	-0.715824
O	0.565357	-1.819501	-0.603433
O	2.761950	-1.545675	-1.046681
Fe	-0.131311	0.077226	-0.712054
N	-1.108479	1.620033	-1.512070
N	-0.587861	2.633470	-1.919762
N	-0.153704	3.627584	-2.328925
O	1.586697	0.653089	-1.700470
H	2.174883	-0.159596	-1.533433
H	1.431866	0.692750	-2.658457
H	-3.925177	-2.551020	1.764387
H	1.741657	-3.912056	0.645721
H	1.158755	2.501315	3.990540

4 (Q)

C	-0.033884	3.553158	1.862771
N	1.313262	3.476953	1.567669
H	2.019682	4.152646	1.825450
C	1.530344	2.340006	0.869306
H	2.491875	2.017044	0.501154
N	0.392627	1.678366	0.698437
C	-0.591504	2.429449	1.316036
H	-1.621124	2.105774	1.321787
C	-4.035316	-0.798890	0.627087
N	-4.106642	-0.405151	-0.694056
H	-4.948901	-0.314746	-1.245462
C	-2.846418	-0.171111	-1.132487
H	-2.596180	0.143651	-2.134217
N	-1.969825	-0.389773	-0.163867
C	-2.701916	-0.784418	0.940570
H	-2.216326	-1.041084	1.869828
C	1.233813	-3.559973	2.185127
H	2.138427	-4.138590	2.380489
H	0.452733	-4.217497	1.788601
C	1.510096	-2.436752	1.197706
O	0.487413	-1.710893	0.890568
O	2.667256	-2.276893	0.753735
Fe	0.222420	-0.175314	-0.385059
N	-0.031357	0.198298	-2.392491
N	0.903926	0.262761	-3.150885
N	1.797065	0.322805	-3.892881
O	2.484320	-0.086437	-0.675530
H	2.690699	-0.943003	-0.182834
H	2.721240	-0.238512	-1.606733
H	-4.913844	-1.049244	1.200876
H	0.857062	-3.139629	3.124209
H	-0.454861	4.376510	2.418023

5 (D)

C	-0.491444	-0.553393	3.647917
N	-1.789790	-0.408701	3.199874
H	-2.622384	-0.392742	3.773016
C	-1.766558	-0.307409	1.853498
H	-2.643896	-0.189508	1.235572
N	-0.515644	-0.375589	1.416140
C	0.290425	-0.532533	2.526289
H	1.358977	-0.633791	2.429210
C	2.758798	2.718184	0.355364
N	3.605671	1.662288	0.081759
H	4.615778	1.693505	0.067308
C	2.854988	0.570170	-0.179654
H	3.244564	-0.404583	-0.423466
N	1.568440	0.873928	-0.082746
C	1.491922	2.213418	0.247355
H	0.538607	2.702641	0.357995
C	-2.856000	2.699313	-1.374964
H	-3.938170	2.681396	-1.515199
H	-2.377440	3.077759	-2.284937
C	-2.330879	1.306105	-1.076934
O	-1.083394	1.241610	-0.777265
O	-3.114806	0.324666	-1.126526
Fe	0.066350	-0.357704	-0.517035
N	1.244006	-1.860685	-0.117256
N	1.108889	-2.874411	-0.772109
N	1.037326	-3.867612	-1.357687
O	-1.412556	-1.594923	-1.074758
H	-2.203889	-0.951599	-1.124300
H	-1.130307	-1.720161	-2.002086
H	3.125568	3.704611	0.590943
H	-2.595545	3.383634	-0.561159
H	-0.251766	-0.658113	4.694055
F	0.502338	-0.387914	-2.281631

5 (Qu)

C	1.065030	1.885844	3.006826
N	2.123631	1.016609	2.831066
H	2.915085	0.906350	3.450636
C	1.935514	0.343834	1.675752
H	2.612684	-0.400224	1.284374
N	0.807001	0.738547	1.099857
C	0.254379	1.702917	1.920881
H	-0.671426	2.191218	1.662024
C	-3.850038	-1.217190	0.963930
N	-4.163149	0.033058	0.466490
H	-5.076653	0.465710	0.469999
C	-3.034810	0.576282	-0.046507
H	-2.983712	1.548082	-0.512555
N	-2.014471	-0.255531	0.098152
C	-2.511806	-1.381044	0.725702
H	-1.869388	-2.219550	0.942592
C	1.362196	-3.913530	0.193445
H	2.342265	-4.393529	0.184247

H	0.697488	-4.423047	-0.512407
C	1.481425	-2.448631	-0.194765
O	0.369207	-1.792840	-0.138917
O	2.592313	-1.978935	-0.521218
Fe	0.011498	0.050318	-0.729399
N	-0.533877	1.877985	-1.096327
N	0.282717	2.664575	-1.539513
N	0.985642	3.475838	-1.960244
O	2.100009	0.399729	-1.560412
H	2.443083	-0.484513	-1.239213
H	1.878497	0.250708	-2.496070
H	-4.589499	-1.853866	1.423834
H	0.912756	-4.003799	1.187872
H	0.991343	2.537495	3.862900
F	-0.335276	-0.511265	-2.416382

5 (S)

C	-0.578957	-2.552448	2.562587
N	-1.858328	-2.078355	2.355066
H	-2.684607	-2.341486	2.874778
C	-1.824114	-1.206497	1.322070
H	-2.688365	-0.676018	0.951061
N	-0.588961	-1.093657	0.854194
C	0.197030	-1.931870	1.621696
H	1.256858	-2.028347	1.442673
C	3.300735	1.907531	1.412076
N	3.952720	0.897576	0.731070
H	4.943612	0.699152	0.762287
C	3.041010	0.223228	-0.002431
H	3.267315	-0.613802	-0.644856
N	1.835454	0.746639	0.176713
C	1.983939	1.802581	1.055818
H	1.133803	2.398102	1.347655
C	-2.483761	3.308047	0.875062
H	-3.553601	3.523309	0.859884
H	-1.935445	4.139925	0.419842
C	-2.177241	2.027423	0.118272
O	-0.944828	1.668005	0.103702
O	-3.113528	1.395974	-0.433898
Fe	0.054774	0.158151	-0.892265
N	0.955129	-1.479821	-1.631939
N	0.606615	-2.634122	-1.548510
N	0.310924	-3.750864	-1.494481
O	-1.832518	-0.400327	-1.779667
H	-2.456790	0.274952	-1.336841
H	-1.732429	-0.111697	-2.703806
H	3.821853	2.588404	2.066322
H	-2.138834	3.219431	1.910926
H	-0.348736	-3.269417	3.334678
F	0.396835	1.228514	-2.343611

6 (D)

C	0.415937	-1.045754	0.146949
O	0.828013	-2.207913	-0.000618
N	1.304444	-0.075399	0.542566
H	-0.029242	1.778742	-0.795849
C	2.643818	0.078728	-0.028098
C	3.070046	1.537278	0.236212
C	3.578317	-0.869228	0.772453
C	2.715250	-0.237025	-1.533346
H	2.436486	2.239585	-0.315442
H	3.001941	1.774009	1.302587
H	4.105312	1.683675	-0.089651
H	3.304426	-1.910514	0.594088
H	4.612608	-0.702473	0.450099
H	3.508939	-0.663176	1.845040
H	3.739250	-0.096015	-1.895846
H	2.416855	-1.268385	-1.735052
H	2.061870	0.435188	-2.101668
C	-1.046151	-0.721576	0.080003
C	-1.894356	-1.840102	0.030890
C	-1.595296	0.586856	0.045207
C	-3.276063	-1.699888	-0.031267
H	-1.437487	-2.823542	0.049013
C	-2.990838	0.700139	-0.019615
C	-3.824785	-0.418350	-0.054392
H	-3.914895	-2.577892	-0.059856
H	-3.443346	1.684972	-0.048383
H	-4.902060	-0.282977	-0.103636
C	-0.722897	1.832690	0.054350
C	-1.449072	3.181186	0.000735
H	-2.112033	3.321878	0.861657
H	-0.714355	3.993020	0.013633
H	-2.047199	3.290096	-0.910899
H	-0.085749	1.805178	0.946656

9 (D)

C	-1.097120	-0.747171	3.229862
N	-2.233030	-1.150843	2.559160
H	-3.080309	-1.507732	2.982928
C	-2.039945	-0.993028	1.238650
H	-2.767980	-1.221039	0.477798
N	-0.817806	-0.503942	1.027366
C	-0.216212	-0.345585	2.266435
H	0.783575	0.043355	2.368469
C	3.881779	0.630098	0.564490
N	3.911320	-0.724825	0.300545
H	4.714350	-1.333429	0.395976
C	2.694666	-1.110845	-0.120336
H	2.429936	-2.114999	-0.407952
N	1.873546	-0.060608	-0.139962
C	2.607955	1.037169	0.287308
H	2.162631	2.015829	0.344580
C	-0.663229	4.073818	-0.180774
H	-1.547728	4.710253	-0.223771
H	0.099015	4.446355	-0.872686
C	-1.019828	2.650254	-0.534552
O	-0.012203	1.820590	-0.563323
O	-2.198593	2.327778	-0.781976
Fe	-0.018999	-0.089353	-0.700715
N	0.241071	-1.798862	-1.428763
N	-0.668323	-2.604365	-1.591962
N	-1.458249	-3.415708	-1.772442
O	-1.862850	-0.062122	-1.455444

H	-2.165423	0.910430	-1.242376
H	-1.869369	-0.163514	-2.424175
H	4.749325	1.169000	0.910532
H	-0.233609	4.103865	0.826378
H	-1.019367	-0.779359	4.304756

9 (Qu)

C	-1.505679	1.493086	-3.079484
N	-2.671946	1.256382	-2.381347
H	-3.612177	1.416731	-2.719571
C	-2.354172	0.769818	-1.165938
H	-3.074474	0.496535	-0.410820
N	-1.032269	0.681406	-1.045766
C	-0.490431	1.132209	-2.237826
H	0.575732	1.159676	-2.401218
C	3.886961	0.052253	-0.865499
N	3.834737	1.234529	-0.150617
H	4.582923	1.910658	-0.061930
C	2.625440	1.343228	0.420964
H	2.302305	2.166473	1.037073
N	1.885896	0.277214	0.107471
C	2.668416	-0.539108	-0.698463
H	2.292299	-1.475804	-1.073147
C	-0.031009	-4.164485	-0.474831
H	-0.717850	-4.988217	-0.277407
H	0.970858	-4.419854	-0.114447
C	-0.508418	-2.906814	0.207734
O	0.252971	-1.865143	0.052258
O	-1.567318	-2.911540	0.875805
Fe	-0.012854	-0.036900	0.657677
N	0.083989	1.585634	1.649806
N	-0.936797	2.108886	2.081928
N	-1.839563	2.669189	2.515706
O	-1.662685	-0.563896	1.570116
H	-1.747500	-1.615011	1.381523
H	-1.739410	-0.382730	2.523012
H	4.766010	-0.252320	-1.410770
H	0.042375	-3.990956	-1.553454
H	-1.505604	1.885044	-4.084078

9 (S)

C	-3.440730	-2.063360	-0.514752
N	-2.663146	-3.127767	-0.103465
H	-2.956716	-4.095119	-0.051381
C	-1.440387	-2.671729	0.216915
H	-0.626163	-3.283777	0.569182
N	-1.387229	-1.351257	0.031261
C	-2.637779	-0.962506	-0.428323
H	-2.861738	0.065156	-0.662284
C	-1.364636	3.174177	-1.784649
N	-1.747664	3.474987	-0.492066
H	-2.263989	4.294743	-0.199244
C	-1.300319	2.503278	0.324885
H	-1.455343	2.486769	1.392443
N	-0.647547	1.581495	-0.380677
C	-0.680635	1.993989	-1.703428
H	-0.201834	1.420475	-2.480781
C	3.377752	-0.089632	-2.594743
H	4.275935	-0.668818	-2.811576
H	3.642783	0.956873	-2.411589
C	2.667536	-0.651436	-1.387384
O	1.572999	-0.014827	-1.043768
O	3.105430	-1.643900	-0.783797
Fe	0.292359	-0.163913	0.399065
N	0.277416	0.484419	2.190760
N	1.017743	1.104024	2.928811
N	1.675550	1.688220	3.668004
O	1.289316	-1.953336	0.982819
H	2.106446	-1.977198	0.366084
H	1.601899	-1.936805	1.903264
H	-1.603841	3.814475	-2.618800
H	2.705302	-0.109570	-3.458858
H	-4.466704	-2.184489	-0.823693

[4 + 1NF] (React. Complex, T)

Fe	1.737812	-0.218659	-0.309367
N	3.952510	-0.481704	0.091749
C	4.562938	-0.299916	1.251394
C	4.932443	-0.871673	-0.801122
H	4.085753	0.010088	2.168883
C	6.145218	-0.923314	-0.164779
H	4.694039	-1.078570	-1.834063
N	5.890308	-0.556528	1.140818
H	6.570297	-0.492461	1.886053
H	7.136115	-1.177957	-0.507110
N	1.777293	1.795113	-0.517046
C	1.974858	2.447582	-1.655263
C	1.627642	2.755472	0.467909
H	2.113480	1.979043	-2.616552
N	1.962060	3.782368	-1.437597
C	1.741997	3.998892	-0.091258
H	1.441550	2.464870	1.488445
H	2.085558	4.492645	-2.145560
H	1.684559	4.990295	0.329763
O	1.422639	-2.222399	-0.110874
H	1.238122	-2.295820	0.891988
H	2.243377	-2.709254	-0.289970
O	0.904329	-2.004413	2.386734
C	0.948572	-0.756213	2.538077
C	0.553920	-0.163510	3.882044
H	1.309386	0.554501	4.216897
H	-0.388020	0.385371	3.767015
H	0.423617	-0.946461	4.631432
O	1.292126	0.092105	1.638588
C	-2.711034	2.971001	2.008314
C	-3.087675	1.640587	1.836640
C	-3.185247	1.076469	0.556054
C	-2.944760	1.865614	-0.591617
C	-2.584042	3.205580	-0.391668
C	-2.455159	3.756415	0.884167
H	-2.626462	3.388835	3.007425
H	-3.310075	1.019554	2.699239
H	-2.404810	3.830485	-1.263412
H	-2.165772	4.797909	0.996658

C	-3.140575	1.360295	-2.009175
C	-4.624294	1.236881	-2.403990
H	-2.645204	0.396010	-2.142362
H	-2.647813	2.059617	-2.694807
H	-4.717336	0.886090	-3.438071
H	-5.153506	0.526496	-1.759449
H	-5.134543	2.203630	-2.324617
C	-3.653382	-0.352609	0.533471
O	-4.657281	-0.707184	1.145330
N	-2.938339	-1.260996	-0.236388
C	-2.945147	-2.747489	-0.055262
C	-4.367927	-3.243159	-0.378609
C	-2.527653	-3.117547	1.378158
H	-4.366460	-4.338128	-0.349128
H	-5.098968	-2.870000	0.337932
H	-4.665518	-2.929133	-1.384852
H	-1.529263	-2.731602	1.608652
H	-3.240991	-2.719183	2.105534
H	-2.503360	-4.207723	1.484720
F	-1.599993	-0.805420	-0.416702
C	-1.967262	-3.343223	-1.083544
H	-2.206865	-3.001501	-2.095934
H	-0.929357	-3.085606	-0.864614
H	-2.065329	-4.433528	-1.059059
N	1.737887	-0.391300	-2.296410
N	1.517345	-1.416876	-2.896948
N	1.320299	-2.366685	-3.533190

[4 + 1NF] (React. Complex, Q)

Fe	1.797284	-0.314573	-0.254941
N	3.947691	-0.644276	0.017737
C	4.608742	-0.596805	1.164552
C	4.884959	-0.921342	-0.960119
H	4.171963	-0.397075	2.131356
C	6.123485	-1.041266	-0.387177
H	4.598022	-1.011369	-1.997155
N	5.927842	-0.831710	0.962274
H	6.640827	-0.850254	1.678654
H	7.097254	-1.250567	-0.801316
N	1.841655	1.893697	-0.452597
C	1.833653	2.550375	-1.602189
C	1.890042	2.851109	0.542090
H	1.791017	2.089361	-2.577227
N	1.878759	3.887460	-1.385822
C	1.915772	4.099307	-0.021712
H	1.887768	2.565379	1.582294
H	1.883534	4.600714	-2.101762
H	1.951872	5.089457	0.405084
O	1.390247	-2.486590	0.024503
H	1.081410	-2.450757	0.985733
H	2.230348	-2.972854	0.029269
O	0.621722	-2.027088	2.488417
C	0.837693	-0.799557	2.621670
C	0.436888	-0.109592	3.916633
H	1.268122	0.491949	4.298535
H	-0.393202	0.576437	3.711165
H	0.125222	-0.836939	4.668700
O	1.375564	-0.040534	1.731920
C	-2.579610	2.998304	2.042797
C	-3.040175	1.700361	1.830783
C	-3.083299	1.150548	0.540985
C	-2.701853	1.924777	-0.578151
C	-2.257814	3.232890	-0.338853
C	-2.182093	3.766586	0.948475
H	-2.539157	3.404549	3.049413
H	-3.371444	1.093910	2.668416
H	-1.968208	3.846336	-1.188744
H	-1.823731	4.782373	1.092444
C	-2.831405	1.441339	-2.010828
C	-4.289159	1.414707	-2.507407
H	-2.389270	0.448525	-2.119610
H	-2.249367	2.111744	-2.654048
H	-4.332707	1.074935	-3.548389
H	-4.905600	0.736777	-1.907050
H	-4.741455	2.411686	-2.454653
C	-3.650435	-0.240625	0.470134
O	-4.719870	-0.523677	1.003060
N	-2.947883	-1.195620	-0.253929
C	-3.069493	-2.678328	-0.080113
C	-4.497080	-3.075268	-0.502729
C	-2.776151	-3.072529	1.377435
H	-4.574114	-4.167483	-0.472170
H	-5.248723	-2.647895	0.160073
H	-4.700166	-2.747344	-1.527909
H	-1.777392	-2.739127	1.677765
H	-3.516234	-2.636643	2.054910
H	-2.817840	-4.162535	1.480503
F	-1.571150	-0.835216	-0.334628
C	-2.066373	-3.341769	-1.040501
H	-2.194523	-2.970389	-2.062364
H	-1.030717	-3.176215	-0.738101
H	-2.255586	-4.420325	-1.042394
N	1.555745	-0.467051	-2.264029
N	1.162986	-1.396537	-2.926031
N	0.795203	-2.258355	-3.608910

TS1 (T)

Fe	-1.233925	-0.040894	-0.241202
N	-3.299966	-0.811928	-0.365266
C	-4.431405	-0.132015	-0.489480
C	-3.654848	-2.144431	-0.281487
H	-4.511301	0.940788	-0.587369
C	-5.016954	-2.262841	-0.354276
H	-2.902754	-2.912595	-0.188126
N	-5.492393	-0.973483	-0.485967
H	-6.461934	-0.700558	-0.572548
H	-5.674335	-3.117790	-0.329974
N	-0.810524	-0.995660	1.467713
C	-0.122988	-2.123674	1.579199
C	-1.152899	-0.606439	2.750497
H	0.303983	-2.671479	0.755257
N	-0.019500	-2.475457	2.879700
C	-0.666503	-1.522802	3.642256
H	-1.706282	0.302215	2.920345
H	0.477140	-3.284164	3.226111
H	-0.718823	-1.583406	4.717796

O	-1.557346	0.982875	-1.956701
H	-2.158362	1.732500	-1.619593
H	-2.076399	0.450200	-2.583091
O	-2.908784	2.766195	-0.685826
C	-2.508946	2.545848	0.486847
C	-2.867351	3.526624	1.590949
H	-3.454499	3.016656	2.362814
H	-1.953486	3.894440	2.068991
H	-3.438119	4.367690	1.193450
O	-1.810035	1.533123	0.851311
C	3.493510	-2.870569	1.477900
C	3.370379	-1.484758	1.505061
C	3.087818	-0.747520	0.341605
C	2.950474	-1.415944	-0.899568
C	3.090853	-2.812965	-0.900691
C	3.349930	-3.540142	0.261013
H	3.709480	-3.418474	2.391226
H	3.496658	-0.942908	2.436796
H	2.996763	-3.339879	-1.847112
H	3.448023	-4.621636	0.211834
C	2.750720	-0.720414	-2.232713
C	4.047297	-0.096339	-2.780650
H	1.981075	0.045900	-2.147597
H	2.383158	-1.461692	-2.951956
H	3.865927	0.362243	-3.759603
H	4.427740	0.682453	-2.110787
H	4.833201	-0.851476	-2.899952
C	3.068044	0.739340	0.553838
O	3.840325	1.253841	1.368156
N	2.260424	1.526670	-0.254453
C	1.975194	2.948160	0.011727
C	3.317647	3.703115	-0.185258
C	1.399260	3.198091	1.415316
H	3.108905	4.778564	-0.160388
H	4.032618	3.455916	0.598600
H	3.757623	3.463944	-1.159232
H	0.444300	2.677495	1.528186
H	2.090811	2.855621	2.188896
H	1.228207	4.271752	1.556281
F	0.738624	0.732315	-0.238636
C	1.001749	3.437202	-1.075830
H	1.399977	3.224354	-2.073398
H	0.027491	2.957826	-0.985606
H	0.870084	4.520452	-0.979257
N	-0.601578	-1.651715	-1.233134
N	-0.781729	-1.723968	-2.423876
N	-0.939250	-1.839594	-3.569725

TS1 (Q)

Fe	1.220613	-0.395748	-0.302538
N	3.469851	-0.575504	-0.365714
C	4.290926	-0.517868	0.672106
C	4.269844	-0.631571	-1.492337
H	3.986552	-0.455489	1.705371
C	5.587730	-0.610666	-1.119675
H	3.832207	-0.676818	-2.478028
N	5.580368	-0.537161	0.258913
H	6.393276	-0.504858	0.859089
H	6.503816	-0.641534	-1.688388
N	1.347268	1.775178	-0.089363
C	1.423526	2.621952	-1.105731
C	1.578671	2.513482	1.055343
H	1.301379	2.354575	-2.143873
N	1.696939	3.869393	-0.659768
C	1.799204	3.821326	0.716933
H	1.563426	2.041019	2.024234
H	1.803345	4.691268	-1.238235
H	2.007580	4.698886	1.308579
O	1.373110	-2.611426	-0.338518
H	1.246108	-2.759267	0.654996
H	2.316847	-2.772517	-0.502401
O	1.087174	-2.639868	2.266145
C	1.143679	-1.428333	2.581356
C	0.964446	-1.033169	4.039404
H	1.719957	-0.297402	4.332286
H	-0.016874	-0.559519	4.161364
H	1.018732	-1.907640	4.690723
O	1.337215	-0.455681	1.760487
C	-2.151816	3.181210	2.053099
C	-2.463904	1.830828	1.938550
C	-2.562906	1.205489	0.683458
C	-2.365619	1.957602	-0.498900
C	-2.072355	3.322713	-0.355196
C	-1.957833	3.933298	0.893144
H	-2.070023	3.642226	3.033367
H	-2.646693	1.234499	2.827077
H	-1.938133	3.919905	-1.254267
H	-1.724464	4.992851	0.958248
C	-2.544817	1.407618	-1.902074
C	-4.023760	1.313585	-2.320953
H	-2.083935	0.423604	-1.992683
H	-2.022250	2.073353	-2.599725
H	-4.106836	0.944780	-3.349606
H	-4.576919	0.625866	-1.671887
H	-4.514675	2.292404	-2.267805
C	-3.029219	-0.218896	0.734599
O	-3.924673	-0.543040	1.518903
N	-2.527316	-1.119447	-0.196460
C	-2.752852	-2.574981	-0.116544
C	-4.259555	-2.772135	-0.442049
C	-2.400211	-3.184329	1.250657
H	-4.448027	-3.848447	-0.524314
H	-4.894690	-2.356218	0.340135
H	-4.514279	-2.306748	-1.399886
H	-1.348661	-3.009090	1.494274
H	-3.024236	-2.762687	2.041550
H	-2.566540	-4.267267	1.218643
F	-0.814179	-0.939260	-0.092365
C	-1.936607	-3.240840	-1.239628
H	-2.120759	-2.748183	-2.199488
H	-0.866961	-3.201884	-1.031360
H	-2.240241	-4.290353	-1.323104
N	1.107269	-0.216236	-2.312750
N	0.383606	-0.736833	-3.126247
N	-0.283469	-1.202862	-3.951057

[5 + 6] (Int. Complex, T)

C	-4.597106	2.860264	0.948074
N	-4.026091	2.601639	2.179198
H	-4.278414	3.034033	3.057563
C	-3.050977	1.683911	2.013502
H	-2.414105	1.319211	2.805154
N	-2.967088	1.339999	0.733767
C	-3.925500	2.070348	0.057211
H	-4.041429	1.980642	-1.010479
C	-4.688678	-3.077570	-0.979117
N	-4.823574	-2.253005	-2.078277
H	-5.436594	-2.404643	-2.867542
C	-3.973326	-1.210265	-1.926337
H	-3.869087	-0.412473	-2.645413
N	-3.304194	-1.318268	-0.789088
C	-3.741671	-2.482893	-0.188722
H	-3.331985	-2.798940	0.757113
C	-1.303956	-2.197027	3.627480
H	-0.927873	-1.971930	4.627133
H	-0.751915	-3.049974	3.217195
C	-1.126594	-0.999329	2.707161
O	-1.684273	-1.119867	1.552379
O	-0.478057	-0.003494	3.099957
Fe	-1.620174	0.023199	-0.072134
N	-1.725893	1.036378	-1.731152
N	-1.120619	0.629514	-2.706772
N	-0.579294	0.321001	-3.676161
O	-0.078154	1.313006	0.839997
H	-0.085930	0.918487	1.760644
H	0.810465	1.122609	0.462130
H	-5.260690	-3.985539	-0.868975
H	-2.358989	-2.484302	3.679837
H	-5.403947	3.565006	0.824370
C	3.710902	0.791324	0.649820
O	4.293572	1.510881	1.472099
N	2.716631	1.364988	-0.129134
H	1.846783	-0.641291	-1.406146
C	2.899624	2.647549	-0.823114
C	1.881066	2.678050	-1.980955
C	2.530004	3.761002	0.197635
C	4.328769	2.856494	-1.356056
H	2.084476	1.889617	-2.711726
H	0.860874	2.547632	-1.608039
H	1.942877	3.644403	-2.493038
H	3.255373	3.784893	1.012677
H	2.529730	4.726234	-0.321864
H	1.533428	3.583065	0.611961
H	4.394919	3.824953	-1.863329
H	5.061823	2.842658	-0.545995
H	4.592244	2.078953	-2.082548
C	3.935573	-0.685436	0.599901
C	4.618652	-1.212425	1.710050
C	3.546228	-1.535499	-0.468052
C	4.906920	-2.568746	1.803849
H	4.911493	-0.528059	2.498827
C	3.855833	-2.898063	-0.349717
C	4.518768	-3.414616	0.764387
H	5.425668	-2.959972	2.674265
H	3.576240	-3.575687	-1.148344
H	4.734687	-4.478762	0.813958
C	2.833994	-1.011540	-1.704155
C	2.638598	-2.006899	-2.853798
H	1.998650	-2.845060	-2.557183
H	2.143596	-1.501062	-3.688903
H	3.590441	-2.411587	-3.218009
F	-0.310335	-1.024804	-0.758711
H	3.388153	-0.144787	-2.087821

[5 + 6] (Int. Complex, Q)

C	-4.721877	2.903746	0.510141
N	-4.126125	2.861146	1.755345
H	-4.373054	3.427068	2.555734
C	-3.137519	1.939039	1.719445
H	-2.489978	1.713472	2.553869
N	-3.067278	1.386134	0.517060
C	-4.050503	1.982881	-0.247635
H	-4.188953	1.716079	-1.283535
C	-4.692100	-3.182869	-0.605864
N	-4.727054	-2.566633	-1.841507
H	-5.313402	-2.826952	-2.622810
C	-3.828553	-1.557430	-1.835739
H	-3.641882	-0.906710	-2.675444
N	-3.220967	-1.490695	-0.659189
C	-3.750839	-2.503391	0.118332
H	-3.404008	-2.656116	1.127281
C	-1.413791	-1.718040	3.986708
H	-0.959436	-1.383432	4.921022
H	-0.968000	-2.672509	3.685704
C	-1.200483	-0.695534	2.882924
O	-1.766559	-0.962544	1.759488
O	-0.514625	0.329861	3.111641
Fe	-1.579814	-0.141597	-0.135608
N	-1.685603	0.735879	-1.958402
N	-0.991618	0.427995	-2.901324
N	-0.355445	0.177356	-3.834340
O	-0.161211	1.224678	0.679802
H	-0.181610	0.986709	1.662849
H	0.760901	1.067742	0.363237
H	-5.321023	-4.025771	-0.366416
H	-2.484917	-1.891528	4.135393
H	-5.541561	3.568353	0.287073
C	3.634729	0.854677	0.691239
O	4.145902	1.613699	1.524527
N	2.637289	1.369057	-0.128089
H	1.872965	-0.784518	-1.381329
C	2.788762	2.648143	-0.838984
C	1.806573	2.617258	-2.027698
C	2.342006	3.763366	0.148497
C	4.224462	2.906733	-1.330720
H	2.064617	1.828471	-2.740483
H	0.782047	2.448209	-1.683338
H	1.842008	3.578141	-2.552282
H	3.034177	3.827064	0.989703
H	2.327509	4.719043	-0.388067
H	1.336637	3.557745	0.527323
H	4.265962	3.866859	-1.855984
H	4.931156	2.940726	-0.498080
H	4.543808	2.127128	-2.032082

C	3.949188	-0.605628	0.661457
C	4.641995	-1.077706	1.790662
C	3.636389	-1.489295	-0.404338
C	5.016179	-2.411120	1.903695
H	4.874503	-0.368919	2.577911
C	4.033644	-2.827145	-0.266990
C	4.706531	-3.289365	0.864601
H	5.541597	-2.759894	2.788000
H	3.815737	-3.528357	-1.064455
H	4.991537	-4.336320	0.928407
C	2.905543	-1.029887	-1.655109
C	2.866535	-2.018224	-2.826808
H	2.315270	-2.929570	-2.571236
H	2.348753	-1.553228	-3.671785
H	3.871560	-2.305695	-3.157796
F	-0.261294	-1.319259	-0.633503
H	3.362218	-0.096920	-2.008459

TS2 (T)

C	4.353646	2.951032	-1.195274
N	3.830137	2.514816	-2.397020
H	4.060113	2.872602	-3.314216
C	2.936069	1.536738	-2.143591
H	2.347584	1.037199	-2.898052
N	2.859029	1.323181	-0.835446
C	3.737121	2.202760	-0.231531
H	3.840567	2.237150	0.840675
C	4.876687	-2.738911	1.390470
N	4.931806	-1.779973	2.382279
H	5.537316	-1.791372	3.191631
C	4.016253	-0.825182	2.093117
H	3.840079	0.043472	2.708649
N	3.381013	-1.116477	0.968821
C	3.908474	-2.312005	0.521233
H	3.541783	-2.767877	-0.384447
C	1.550380	-2.623385	-3.356483
H	1.155544	-2.550929	-4.371522
H	1.091540	-3.479720	-2.849817
C	1.245063	-1.357287	-2.571131
O	1.802276	-1.296246	-1.411211
O	0.504926	-0.479072	-3.067755
Fe	1.610659	-0.009632	0.087344
N	1.584290	1.177627	1.629382
N	0.956534	0.842572	2.617518
N	0.384921	0.607227	3.590223
O	0.002718	1.060840	-0.981527
H	0.031185	0.555698	-1.846410
H	-0.898361	0.938427	-0.605789
H	5.511497	-3.611077	1.399189
H	2.630224	-2.800902	-3.386539
H	5.093512	3.733640	-1.139937
C	-3.718940	0.550539	-0.775387
O	-4.362768	1.117605	-1.663531
N	-2.810471	1.211689	0.031074
H	-1.600036	-0.950056	1.771412
C	-2.960617	2.640919	0.414639
C	-1.933141	2.917538	1.526217
C	-2.617078	3.510542	-0.817251
C	-4.382830	2.949006	0.917852
H	-2.139987	2.320260	2.421100
H	-0.917024	2.691354	1.187622
H	-1.974325	3.974403	1.810766
H	-3.340666	3.348361	-1.617505
H	-2.631582	4.567702	-0.526282
H	-1.617305	3.265620	-1.188724
H	-4.460135	4.005759	1.197651
H	-5.126167	2.742966	0.143678
H	-4.621555	2.348070	1.803164
C	-3.827009	-0.932033	-0.557128
C	-4.471299	-1.692110	-1.543241
C	-3.338042	-1.553107	0.609657
C	-4.620596	-3.066750	-1.389206
H	-4.847238	-1.180822	-2.423458
C	-3.496737	-2.938802	0.753212
C	-4.129960	-3.690180	-0.236853
H	-5.114092	-3.651875	-2.160031
H	-3.118324	-3.429397	1.646206
H	-4.241492	-4.763640	-0.108645
C	-2.668142	-0.731923	1.674482
C	-3.396544	-0.591597	2.998191
H	-3.481950	-1.571679	3.489948
H	-2.848856	0.068880	3.678096
H	-4.413142	-0.204596	2.864746
F	0.408962	-1.117750	0.878496
H	-2.621084	0.388084	1.081828

TS2 (Q)

C	-4.521280	2.917654	1.024710
N	-3.927677	2.623345	2.236471
H	-4.141740	3.052027	3.126589
C	-2.990920	1.670672	2.027811
H	-2.356632	1.265648	2.802435
N	-2.952223	1.336330	0.746014
C	-3.902294	2.110428	0.109209
H	-4.057443	2.038380	-0.955760
C	-4.851325	-2.787526	-1.227868
N	-4.815686	-1.955773	-2.329921
H	-5.400598	-2.027018	-3.151453
C	-3.848836	-1.032693	-2.131307
H	-3.598777	-0.255076	-2.835818
N	-3.264654	-1.225768	-0.957030
C	-3.881001	-2.321687	-0.382996
H	-3.567931	-2.681343	0.583678
C	-1.532149	-2.455573	3.566507
H	-1.071585	-2.335196	4.548690
H	-1.145320	-3.363547	3.090749
C	-1.234620	-1.259023	2.678380
O	-1.795481	-1.271975	1.520647
O	-0.489509	-0.342830	3.100878
Fe	-1.542671	-0.118611	-0.178587
N	-1.552651	1.103972	-1.797062
N	-0.855008	0.930463	-2.770792
N	-0.208934	0.812185	-3.723380
O	-0.066497	0.983926	0.890081
H	-0.095390	0.557085	1.806547
H	0.860254	0.912099	0.555692

H	-5.543160	-3.611615	-1.152550
H	-2.614632	-2.581230	3.676122
H	-5.303367	3.654529	0.931224
C	3.617350	0.543938	0.854242
O	4.201291	1.091377	1.793345
N	2.736509	1.219152	0.023725
H	1.667104	-0.909775	-1.847927
C	2.894480	2.662117	-0.309579
C	1.921674	2.965291	-1.462308
C	2.484245	3.494028	0.927866
C	4.337660	2.993504	-0.731520
H	2.172266	2.392930	-2.361991
H	0.891226	2.728186	-1.179367
H	1.972113	4.029587	-1.715763
H	3.165725	3.310997	1.759814
H	2.509728	4.559041	0.668195
H	1.466998	3.238003	1.240016
H	4.419369	4.057988	-0.978595
H	5.043129	2.772645	0.073438
H	4.626185	2.419138	-1.619551
C	3.770283	-0.926111	0.588305
C	4.380562	-1.709077	1.578499
C	3.358667	-1.512596	-0.625166
C	4.571589	-3.072842	1.381091
H	4.697285	-1.224326	2.496185
C	3.559305	-2.887589	-0.812215
C	4.158061	-3.662020	0.181348
H	5.038151	-3.676098	2.154660
H	3.240533	-3.351648	-1.741888
H	4.302909	-4.726833	0.019047
C	2.722940	-0.667911	-1.692420
C	3.509115	-0.462585	-2.973501
H	3.641719	-1.422205	-3.494350
H	2.977114	0.209032	-3.654781
H	4.508460	-0.057599	-2.778049
F	-0.319192	-1.279382	-0.912297
H	2.621286	0.430801	-1.061606

[5 + 7] (Int. Complex, T)

C	-3.649499	3.730405	0.211829
N	-4.185458	3.038076	1.280796
H	-4.869429	3.388880	1.937479
C	-3.631489	1.808673	1.313222
H	-3.859944	1.047866	2.041319
N	-2.767505	1.675860	0.314669
C	-2.767865	2.870117	-0.381330
H	-2.135469	3.006265	-1.243498
C	-5.205621	-2.097110	-1.757289
N	-4.712048	-1.452790	-2.874339
H	-5.080370	-1.518665	-3.813265
C	-3.633113	-0.725544	-2.496782
H	-3.041048	-0.125593	-3.170936
N	-3.411148	-0.865764	-1.200233
C	-4.385010	-1.722202	-0.726658
H	-4.412205	-2.004553	0.314219
C	-2.529599	-2.326236	3.369721
H	-2.029433	-2.530020	4.318269
H	-2.566494	-3.247776	2.777146
C	-1.775415	-1.267175	2.584069
O	-2.424433	-0.791177	1.562921
O	-0.637648	-0.915270	2.941772
Fe	-1.661828	-0.005714	-0.064773
N	-0.985659	0.864259	-1.688248
N	0.073714	0.482292	-2.139754
N	1.078457	0.176396	-2.621516
O	-0.021614	0.907742	1.160499
H	-0.103046	0.248481	1.917283
H	0.852071	0.744552	0.758833
H	-6.066426	-2.745842	-1.802002
H	-3.561790	-2.009910	3.548996
H	-3.935269	4.744552	-0.018070
C	3.705662	0.186670	0.748300
O	4.402523	0.526053	1.707069
N	3.063552	1.080159	-0.071365
H	2.641202	0.699758	-0.915273
C	3.243375	2.561568	-0.025745
C	2.340933	3.147839	-1.123174
C	2.798951	3.099493	1.347924
C	4.710304	2.946602	-0.296657
H	2.608832	2.759140	-2.112479
H	1.285766	2.919458	-0.934615
H	2.451468	4.236845	-1.146921
H	3.433463	2.701537	2.141898
H	2.869716	4.193331	1.354480
H	1.761017	2.819115	1.554245
H	4.823292	4.035442	-0.240857
H	5.371998	2.492789	0.445006
H	5.024334	2.624618	-1.295137
C	3.378268	-1.267567	0.497959
C	2.717556	-1.902500	1.552876
C	3.650728	-1.988837	-0.714774
C	2.234498	-3.207817	1.439613
H	2.549096	-1.344896	2.469634
C	3.106778	-3.309436	-0.807479
C	2.417378	-3.902235	0.234551
H	1.703374	-3.664484	2.268937
H	3.277931	-3.865668	-1.725763
H	2.030168	-4.911281	0.121129
C	4.460675	-1.546732	-1.789817
C	5.377109	-0.367796	-1.848109
H	5.660707	0.001321	-0.858922
H	6.296619	-0.638908	-2.382519
H	4.936958	0.475490	-2.402652
F	-0.687899	-1.480001	-0.391977
H	4.465949	-2.192565	-2.665759

[5 + 7] (Int. Complex, Q)

C	-4.098954	3.418765	-0.623518
N	-3.858206	3.440853	0.736098
H	-4.177808	4.144313	1.387945
C	-3.104554	2.362799	1.049036
H	-2.749271	2.143405	2.044654
N	-2.848550	1.649046	-0.037722
C	-3.462474	2.300580	-1.089574
H	-3.389747	1.924968	-2.098165
C	-4.955609	-2.616296	-1.366451

N	-4.416707	-2.252491	-2.585344
H	-4.743893	-2.548130	-3.495142
C	-3.361148	-1.441548	-2.357085
H	-2.744081	-1.008343	-3.128722
N	-3.197104	-1.262285	-1.053250
C	-4.185936	-1.993684	-0.422214
H	-4.250971	-2.014522	0.653682
C	-2.784483	-1.244526	3.963197
H	-2.494193	-0.915157	4.962343
H	-2.533304	-2.304085	3.841465
C	-2.066380	-0.436281	2.896965
O	-2.415313	-0.679130	1.682462
O	-1.201098	0.406795	3.234911
Fe	-1.573149	-0.168229	-0.127824
N	-0.946117	0.512565	-1.942445
N	0.138858	0.217039	-2.383246
N	1.178186	-0.028874	-2.833132
O	-0.154326	1.051738	0.950479
H	-0.432443	0.865286	1.911596
H	0.747703	0.698828	0.836037
H	-5.810790	-3.268885	-1.288327
H	-3.868419	-1.150633	3.839526
H	-4.682039	4.180377	-1.116694
C	3.740303	0.290944	0.745824
O	4.469715	0.759651	1.624009
N	3.030620	1.066437	-0.134154
H	2.585526	0.586571	-0.912187
C	3.160086	2.548094	-0.256109
C	2.200549	2.985735	-1.373840
C	2.740780	3.217745	1.066719
C	4.603763	2.943590	-0.621857
H	2.453374	2.511896	-2.328937
H	1.164200	2.731933	-1.125070
H	2.262519	4.070869	-1.506491
H	3.394542	2.907165	1.883669
H	2.799994	4.307349	0.962480
H	1.708383	2.952902	1.317693
H	4.682114	4.034454	-0.695130
H	5.304817	2.596511	0.140701
H	4.893730	2.517904	-1.588434
C	3.452183	-1.190780	0.690152
C	3.010219	-1.734982	1.900213
C	3.542032	-2.024764	-0.477287
C	2.563419	-3.053961	1.995791
H	2.994233	-1.092499	2.775852
C	3.030888	-3.355974	-0.351884
C	2.556825	-3.858623	0.846040
H	2.209912	-3.442600	2.946110
H	3.061275	-3.996072	-1.230039
H	2.192062	-4.881030	0.896329
C	4.160938	-1.686432	-1.706221
C	5.061961	-0.535347	-2.016307
H	5.475505	-0.062411	-1.121697
H	5.901568	-0.880820	-2.633575
H	4.552399	0.245369	-2.601586
F	-0.401987	-1.572345	-0.105485
H	4.027717	-2.408629	-2.509179

TS3-N3 (T)

C	4.148753	-1.703604	-2.997060
N	3.948985	-2.790186	-2.167410
H	4.280990	-3.731655	-2.324888
C	3.218760	-2.383909	-1.104940
H	2.892799	-3.031555	-0.305376
N	2.938430	-1.093318	-1.211587
C	3.510999	-0.656750	-2.389244
H	3.416844	0.368975	-2.708278
C	5.301462	2.555492	1.221320
N	4.753855	3.300384	0.195697
H	5.077380	4.201346	-0.128043
C	3.686093	2.617629	-0.288685
H	3.066326	2.979411	-1.095310
N	3.521087	1.479826	0.363673
C	4.523745	1.430854	1.311065
H	4.592445	0.593731	1.987633
C	3.217873	-2.364352	3.508113
H	3.035981	-3.375859	3.877417
H	2.934163	-1.643001	4.282899
C	2.402737	-2.092710	2.248525
O	2.688845	-0.998103	1.645340
O	1.536902	-2.926887	1.890757
Fe	1.789994	-0.040859	0.127704
N	1.047793	0.980816	-1.314100
N	0.239879	1.860821	-1.235550
N	-0.540398	2.745149	-1.250343
O	0.326568	-1.710883	-0.115858
H	0.613913	-2.246198	0.677923
H	-0.548390	-1.321697	0.084579
H	6.164711	2.890088	1.775409
H	4.285748	-2.226518	3.309457
H	4.708994	-1.776298	-3.915745
C	-3.410473	-0.240251	0.080487
O	-2.261461	-0.692456	0.020091
N	-4.518913	-1.016338	-0.022355
H	-5.409182	-0.537295	0.002742
C	-4.558219	-2.497460	-0.140941
C	-6.045060	-2.879840	-0.211044
C	-3.840577	-2.946103	-1.427590
C	-3.908281	-3.140419	1.098213
H	-6.579146	-2.561900	0.692589
H	-6.530816	-2.423482	-1.082073
H	-6.148048	-3.965752	-0.298265
H	-2.785805	-2.664576	-1.401915
H	-3.909536	-4.034851	-1.531006
H	-4.305635	-2.488452	-2.308223
H	-3.960550	-4.232294	1.022616
H	-2.858954	-2.849166	1.183114
H	-4.431213	-2.834224	2.011188
C	-3.692569	1.220238	0.331538
C	-4.445310	1.510603	1.478528
C	-3.207816	2.285697	-0.482802
C	-4.714331	2.821452	1.870471
H	-4.803215	0.687079	2.090175
C	-3.511268	3.605397	-0.062762
C	-4.237287	3.876822	1.088119
H	-5.284947	3.013447	2.774251
H	-3.154883	4.429866	-0.674564
H	-4.436756	4.906271	1.372257

C	-2.467551	2.176646	-1.731550
F	0.735590	0.843693	1.313944
H	-2.525423	3.087840	-2.318173
C	-2.284305	0.935229	-2.551721
H	-1.643608	0.198973	-2.058970
H	-3.249861	0.441031	-2.732921
H	-1.850594	1.188393	-3.523350

TS3-N3 (Q)

C	4.066358	-2.081070	-2.924662
N	3.789371	-3.091992	-2.025259
H	4.072276	-4.058757	-2.106458
C	3.061717	-2.565580	-1.011199
H	2.697572	-3.133035	-0.166463
N	2.857384	-1.272841	-1.210604
C	3.478669	-0.959734	-2.402731
H	3.451876	0.043310	-2.799983
C	5.265908	2.511837	0.908587
N	4.713246	3.196882	-0.155825
H	5.066050	4.051068	-0.564665
C	3.601435	2.530966	-0.549366
H	2.967517	2.852223	-1.361540
N	3.413122	1.456787	0.200622
C	4.446240	1.435065	1.117395
H	4.501488	0.650304	1.854826
C	3.201514	-2.324602	3.604359
H	2.993526	-3.324833	3.990239
H	2.939232	-1.581154	4.365511
C	2.404059	-2.047853	2.334677
O	2.646961	-0.934456	1.755720
O	1.578121	-2.911034	1.936493
Fe	1.669125	0.074514	0.156192
N	0.926650	0.917805	-1.583387
N	0.138688	1.799603	-1.729211
N	-0.643657	2.658839	-1.917665
O	0.213942	-1.539232	0.136995
H	0.614780	-2.152665	0.825442
H	-0.633471	-1.213314	0.513978
H	6.162623	2.849298	1.404326
H	4.273655	-2.219948	3.405434
H	4.637330	-2.251574	-3.823883
C	-3.267941	-0.278384	0.477573
O	-2.374305	-0.978403	0.974376
N	-4.372916	-0.793395	-0.111860
H	-5.086465	-0.129700	-0.384657
C	-4.725387	-2.235401	-0.228109
C	-6.062966	-2.288057	-0.983108
C	-3.643967	-2.986727	-1.025596
C	-4.888856	-2.845941	1.176549
H	-6.849911	-1.753340	-0.436843
H	-5.971627	-1.847368	-1.983007
H	-6.384025	-3.327574	-1.100380
H	-2.671233	-2.911451	-0.535333
H	-3.915003	-4.045490	-1.103839
H	-3.556736	-2.582210	-2.039789
H	-5.180038	-3.899122	1.094665
H	-3.951619	-2.786792	1.734535
H	-5.667081	-2.318045	1.739372
C	-3.258215	1.229307	0.594856
C	-3.460688	1.711781	1.891727
C	-3.132655	2.144933	-0.492986
C	-3.599352	3.075823	2.148085
H	-3.528983	0.998604	2.708062
C	-3.307082	3.526040	-0.200880
C	-3.538607	3.985519	1.085256
H	-3.762789	3.423223	3.163779
H	-3.216170	4.236497	-1.017773
H	-3.657249	5.049791	1.267339
C	-2.756184	1.821198	-1.843037
F	0.641537	1.147374	1.257730
H	-2.956822	2.603710	-2.566782
C	-2.481458	0.470510	-2.414767
H	-1.850635	-0.144620	-1.764312
H	-3.413799	-0.086386	-2.581967
H	-1.981557	0.571010	-3.382472

TS3-N1 (T)

C	-4.366730	-1.569045	2.618385
N	-3.280432	-2.391754	2.835549
H	-3.216509	-3.127452	3.525509
C	-2.304414	-2.044921	1.967800
H	-1.339200	-2.520067	1.900398
N	-2.708947	-1.040018	1.201079
C	-3.996793	-0.733179	1.600906
H	-4.560154	0.056555	1.131088
C	-4.675965	2.308257	-1.594762
N	-3.800882	3.211144	-1.024077
H	-3.904501	4.216260	-1.010107
C	-2.766115	2.520078	-0.493613
H	-1.919087	2.968331	0.001014
N	-2.936931	1.221824	-0.687500
C	-4.123966	1.073815	-1.381261
H	-4.458982	0.096497	-1.689749
C	-2.911007	-3.214168	-3.379308
H	-2.486367	-4.173539	-3.683615
H	-2.888927	-2.528535	-4.234940
C	-2.117783	-2.601412	-2.227845
O	-2.642760	-1.595856	-1.648797
O	-1.002520	-3.117069	-1.936272
Fe	-1.558245	-0.238793	-0.283951
N	-0.557751	1.065545	1.280376
N	-1.129643	1.221953	2.340041
N	-1.644292	1.392568	3.365306
O	-0.189004	-1.685260	0.038263
H	-0.401388	-2.302206	-0.759111
H	0.700165	-1.288300	-0.116271
H	-5.581212	2.620005	-2.091368
H	-3.959653	-3.344358	-3.092987
H	-5.275283	-1.649577	3.193858
C	3.297649	-0.031898	-0.093383
O	2.472522	-0.954130	-0.011361
N	4.635430	-0.242560	-0.039872
H	5.221396	0.581018	-0.072436
C	5.330794	-1.554204	0.043686
C	6.835060	-1.238902	0.042420
C	4.947566	-2.273676	1.350046

C	4.973357	-2.416458	-1.180758
H	7.130130	-0.716786	-0.875799
H	7.110039	-0.615820	0.902117
H	7.411137	-2.167321	0.101600
H	3.876427	-2.484825	1.375451
H	5.492687	-3.221163	1.426667
H	5.205740	-1.658566	2.219554
H	5.505590	-3.372946	-1.130215
H	3.900320	-2.616734	-1.215882
H	5.265250	-1.910128	-2.107610
C	2.907728	1.407997	-0.316985
C	3.416741	2.002957	-1.478903
C	2.038073	2.154923	0.536522
C	3.080860	3.305364	-1.849457
H	4.068549	1.418766	-2.122440
C	1.725807	3.480928	0.132712
C	2.225025	4.048033	-1.029534
H	3.479334	3.730085	-2.765863
H	1.073768	4.068051	0.774543
H	1.954711	5.065981	-1.296009
C	1.469887	1.729396	1.792368
F	-0.514359	0.419713	-1.615328
C	1.919431	0.582305	2.643681
H	1.904152	-0.366895	2.108063
H	2.949644	0.752027	2.995588
H	1.283866	0.502629	3.530839
H	1.028963	2.550696	2.351513

TS3-N1 (Q)

C	-4.124803	-2.251503	2.568510
N	-2.975906	-3.016426	2.580268
H	-2.821429	-3.854826	3.122866
C	-2.084946	-2.449464	1.731887
H	-1.099059	-2.837586	1.529484
N	-2.598214	-1.362824	1.175691
C	-3.872361	-1.229485	1.692814
H	-4.514959	-0.414958	1.396785
C	-5.247130	2.125932	-1.082279
N	-4.525762	3.039361	-0.338428
H	-4.811063	3.981118	-0.108133
C	-3.355760	2.457342	0.018095
H	-2.587956	2.952398	0.592729
N	-3.288261	1.222241	-0.451610
C	-4.463218	1.004689	-1.146114
H	-4.634440	0.065156	-1.647349
C	-2.916877	-2.634414	-3.746172
H	-2.457729	-3.449387	-4.309768
H	-3.080515	-1.779704	-4.412383
C	-2.032281	-2.204694	-2.579749
O	-2.525209	-1.303867	-1.814021
O	-0.906635	-2.746004	-2.444758
Fe	-1.500917	-0.118818	-0.385989
N	-0.682750	1.015674	1.263530
N	-1.179884	1.003394	2.369867
N	-1.615874	1.028098	3.442550
O	-0.022703	-1.661064	-0.240533
H	-0.224875	-2.137813	-1.112076
H	0.883340	-1.281580	-0.303341
H	-6.219784	2.356603	-1.487885
H	-3.898413	-2.949902	-3.375872
H	-4.986414	-2.497896	3.169076
C	3.408637	0.017436	-0.117299
O	2.640474	-0.956229	-0.142985
N	4.751800	-0.112098	-0.010214
H	5.283898	0.747185	0.031812
C	5.527666	-1.381219	0.019725
C	7.005395	-0.973559	0.127748
C	5.123720	-2.218682	1.246903
C	5.291894	-2.168514	-1.282122
H	7.314339	-0.369071	-0.733527
H	7.192111	-0.398922	1.043018
H	7.637254	-1.866411	0.155907
H	4.069650	-2.499241	1.194766
H	5.726987	-3.132449	1.287173
H	5.292852	-1.655473	2.171656
H	5.882646	-3.091226	-1.270910
H	4.237559	-2.431662	-1.391846
H	5.597485	-1.576408	-2.151948
C	2.934857	1.442761	-0.262325
C	3.425689	2.134122	-1.376035
C	2.019950	2.091147	0.624407
C	3.027719	3.440066	-1.666689
H	4.115999	1.627440	-2.044353
C	1.647015	3.424760	0.303551
C	2.128601	4.087646	-0.814000
H	3.414301	3.941451	-2.548733
H	0.955005	3.933465	0.969089
H	1.809504	5.104917	-1.021114
C	1.465090	1.566305	1.842423
F	-0.598502	0.901265	-1.641178
C	1.871986	0.335776	2.585605
H	1.884930	-0.553396	1.955546
H	2.885825	0.464897	2.998495
H	1.200094	0.169897	3.433045
H	0.994701	2.327945	2.457563

TS4 (T)

C	4.886540	-2.313008	2.032938
N	4.187080	-1.728196	3.070530
H	4.396563	-1.812586	4.055514
C	3.153113	-1.031159	2.540993
H	2.430340	-0.476617	3.122005
N	3.155853	-1.134645	1.221038
C	4.231264	-1.933989	0.892041
H	4.442053	-2.186918	-0.135290
C	4.698459	1.654330	-2.247436
N	4.490433	0.545699	-3.044088
H	4.962921	0.336440	-3.912305
C	3.535823	-0.219217	-2.464860
H	3.163730	-1.151398	-2.858601
N	3.124552	0.341289	-1.336930
C	3.840700	1.513847	-1.189990
H	3.664404	2.158836	-0.345012
C	1.305396	3.231129	2.358433
H	1.052220	3.384394	3.409819
H	0.602928	3.802013	1.739613

C	1.197543	1.758168	1.984986
O	1.750791	1.425594	0.879278
O	0.581107	0.978803	2.756679
Fe	1.673316	-0.350137	-0.119173
N	1.700415	-2.070381	-1.159474
N	0.664265	-2.652779	-1.373350
N	-0.298690	-3.254488	-1.617503
O	0.224514	-1.017660	1.094090
H	0.255655	-0.336163	1.833948
H	-0.661602	-0.906322	0.668427
H	5.415344	2.419244	-2.501251
H	2.310770	3.611245	2.153542
H	5.756345	-2.928600	2.200877
C	-3.264786	-0.076408	0.086613
O	-2.415285	-0.955484	0.297583
N	-4.592106	-0.338454	0.022703
H	-5.194428	0.441261	-0.205457
C	-5.250765	-1.654064	0.239504
C	-6.759040	-1.404926	0.081804
C	-4.771035	-2.666497	-0.816834
C	-4.948041	-2.161964	1.661212
H	-7.120753	-0.679995	0.821083
H	-6.995893	-1.028685	-0.920927
H	-7.309115	-2.339332	0.228847
H	-3.693873	-2.829662	-0.740234
H	-5.281355	-3.625172	-0.670603
H	-5.000454	-2.307688	-1.826612
H	-5.457485	-3.117068	1.830920
H	-3.875035	-2.311033	1.799698
H	-5.303219	-1.445712	2.410842
C	-2.899391	1.378571	-0.053536
C	-3.463567	2.260093	0.876650
C	-1.953052	1.863890	-1.005834
C	-3.102376	3.607856	0.921731
H	-4.175823	1.873834	1.600561
C	-1.598534	3.234736	-0.925145
C	-2.155022	4.092804	0.013838
H	-3.547723	4.265550	1.662183
H	-0.876258	3.619844	-1.639994
H	-1.859685	5.138169	0.034285
C	-1.357980	1.103856	-2.078718
F	0.296124	0.369976	-1.283446
C	-1.908952	-0.151104	-2.676587
H	-1.750079	-1.017418	-2.028418
H	-2.990955	-0.059859	-2.849976
H	-1.427011	-0.354574	-3.636386
H	-0.753295	1.709752	-2.743904

TS4 (Q)

C	4.649557	-1.542822	2.965559
N	3.980377	-0.533128	3.629121
H	4.161167	-0.214573	4.570877
C	3.020660	-0.051721	2.802340
H	2.337899	0.743646	3.064774
N	3.040155	-0.694241	1.645149
C	4.051799	-1.628400	1.736496
H	4.268429	-2.297262	0.917943
C	4.970907	0.387348	-2.730869
N	4.784505	-0.970260	-2.902065
H	5.307791	-1.571699	-3.522961
C	3.766144	-1.358651	-2.095816
H	3.394075	-2.369474	-2.025109
N	3.294205	-0.325994	-1.417128
C	4.036600	0.771219	-1.805115
H	3.829371	1.745921	-1.391675
C	1.811119	3.953446	0.926396
H	1.423696	4.579067	1.733038
H	1.434579	4.323104	-0.033782
C	1.389583	2.500581	1.109507
O	1.840798	1.678776	0.235752
O	0.650280	2.196571	2.079036
Fe	1.551794	-0.381033	-0.021030
N	1.446718	-2.443986	-0.209069
N	0.504994	-3.053355	-0.649489
N	-0.379424	-3.684698	-1.062193
O	0.035769	-0.305852	1.471612
H	0.114361	0.642701	1.789492
H	-0.873061	-0.436117	1.102784
H	5.727939	0.935333	-3.269859
H	2.903915	4.024717	0.895903
H	5.461292	-2.089581	3.419250
C	-3.309479	-0.030203	0.137914
O	-2.493160	-0.850026	0.590975
N	-4.637038	-0.270872	0.072743
H	-5.204418	0.449112	-0.355266
C	-5.345748	-1.487288	0.557509
C	-6.836995	-1.252153	0.271074
C	-4.850680	-2.727949	-0.208159
C	-5.119787	-1.652145	2.071349
H	-7.207867	-0.365596	0.799613
H	-7.018772	-1.120604	-0.802480
H	-7.421017	-2.113958	0.607711
H	-3.783777	-2.892441	-0.041503
H	-5.397381	-3.614477	0.132188
H	-5.023610	-2.612401	-1.284005
H	-5.664699	-2.530767	2.433898
H	-4.058715	-1.785911	2.292545
H	-5.485226	-0.773526	2.614920
C	-2.879133	1.339740	-0.317820
C	-3.375639	2.426222	0.408438
C	-1.929331	1.559054	-1.364559
C	-2.939663	3.730722	0.162662
H	-4.095103	2.243540	1.201858
C	-1.499198	2.896116	-1.579567
C	-1.986676	3.960477	-0.835278
H	-3.333537	4.553842	0.751046
H	-0.774918	3.079568	-2.368369
H	-1.634335	4.968241	-1.035330
C	-1.425529	0.570947	-2.274799
F	0.422465	-0.062570	-1.557758
C	-1.993632	-0.784992	-2.525318
H	-1.856692	-1.454879	-1.672846
H	-3.073740	-0.720494	-2.724642
H	-1.512991	-1.240718	-3.393525
H	-0.833680	0.988374	-3.080044

[8 + 1N] (Prod. Complex, T)

C	3.757959	-1.062680	-3.479698
N	3.678964	-2.266930	-2.808349
H	3.965692	-3.168489	-3.164197
C	3.148280	-2.038223	-1.585543
H	2.959082	-2.802422	-0.844266
N	2.885593	-0.746960	-1.432767
C	3.261600	-0.128193	-2.611198
H	3.148078	0.936486	-2.747412
C	4.923193	3.065020	0.266222
N	3.841371	3.663988	0.880258
H	3.813718	4.598568	1.262982
C	2.819255	2.777399	0.898367
H	1.847195	2.947551	1.331704
N	3.186676	1.641120	0.321676
C	4.501290	1.808021	-0.074334
H	5.044546	1.017054	-0.567092
C	3.952599	-2.974873	2.971362
H	3.807414	-4.052308	3.078525
H	3.748989	-2.487310	3.931702
C	3.028161	-2.392738	1.903480
O	3.184549	-1.162810	1.627409
O	2.177814	-3.163966	1.366365
Fe	1.967768	0.040485	0.254345
N	-0.100447	2.407823	-1.944479
N	-1.232856	2.311128	-2.059503
N	-2.443068	2.324639	-2.301720
O	0.609832	-1.473517	0.125824
H	1.101290	-2.210022	0.617996
H	-0.166681	-1.226529	0.673986
H	5.865871	3.572608	0.135582
H	4.997866	-2.765317	2.719435
H	4.146680	-0.987129	-4.482940
C	-2.920527	-0.658614	0.792459
O	-1.946838	-1.245468	1.282517
N	-3.894142	-1.292699	0.090846
H	-4.722302	-0.751758	-0.120582
C	-3.959573	-2.748803	-0.209158
C	-5.263805	-2.966156	-0.992537
C	-2.754456	-3.153361	-1.077818
C	-3.992589	-3.561577	1.098800
H	-6.139237	-2.683591	-0.394765
H	-5.270951	-2.382406	-1.920771
H	-5.366876	-4.022795	-1.257710
H	-1.811767	-2.943432	-0.568030
H	-2.800917	-4.225535	-1.299316
H	-2.765260	-2.607387	-2.028160
H	-4.078391	-4.629876	0.870552
H	-3.081197	-3.399663	1.677708
H	-4.854224	-3.272231	1.711282
C	-3.122135	0.823985	1.003921
C	-3.066473	1.258140	2.337954
C	-3.324564	1.762124	-0.029072
C	-3.260900	2.596272	2.664293
H	-2.868521	0.526042	3.114355
C	-3.505888	3.110094	0.317837
C	-3.488499	3.526353	1.646592
H	-3.226394	2.913151	3.702593
H	-3.635742	3.842795	-0.473611
H	-3.635641	4.575942	1.885768
C	-3.302857	1.386743	-1.510393
C	-4.686310	1.452913	-2.165637
H	-5.105011	2.460895	-2.084497
H	-4.617522	1.187903	-3.225185
H	-5.377692	0.758555	-1.678203
F	0.743994	0.959109	1.302647
H	-2.900073	0.376311	-1.628276

[8 + 1N] (Prod. Complex, Q)

C	5.583192	-1.038814	-2.661680
N	5.191061	-2.285639	-2.217428
H	5.636512	-3.165364	-2.438604
C	4.094263	-2.129782	-1.437025
H	3.571918	-2.939166	-0.946526
N	3.764244	-0.849306	-1.352818
C	4.688145	-0.158978	-2.113512
H	4.638852	0.914960	-2.214800
C	4.396869	2.759949	2.272886
N	3.865262	3.591361	1.306595
H	4.004743	4.589624	1.235399
C	3.116935	2.832575	0.466993
H	2.570877	3.211772	-0.382953
N	3.140773	1.563301	0.840384
C	3.935771	1.505688	1.967598
H	4.107811	0.570300	2.477958
C	2.389549	-2.930976	2.985640
H	2.266621	-4.014505	3.040488
H	1.731655	-2.445764	3.714343
C	2.085200	-2.415293	1.583573
O	2.094071	-1.137167	1.450385
O	1.860704	-3.240847	0.665599
Fe	2.027222	-0.022988	-0.303158
N	-2.399978	2.412438	-3.460936
N	-3.144999	2.531287	-2.603906
N	-3.997026	2.789529	-1.746918
O	0.758308	-1.616142	-1.176851
H	1.086367	-2.351441	-0.590404
H	-0.176755	-1.476062	-0.906949
H	5.032374	3.129630	3.062579
H	3.419346	-2.670135	3.256797
H	6.435219	-0.900395	-3.308610
C	-2.714388	-0.808065	0.246904
O	-1.903370	-1.577380	-0.288069
N	-3.994872	-1.164396	0.516846
H	-4.525925	-0.525040	1.093220
C	-4.619985	-2.488676	0.251271
C	-6.077150	-2.376048	0.726308
C	-4.583607	-2.789530	-1.257782
C	-3.889630	-3.586948	1.046850
H	-6.129795	-2.158386	1.800236
H	-6.611892	-1.587741	0.183301
H	-6.599851	-3.321300	0.551358
H	-3.555104	-2.837471	-1.620963
H	-5.069185	-3.751750	-1.454371
H	-5.118872	-2.015277	-1.818967
H	-4.367805	-4.556786	0.869494
H	-2.842914	-3.653562	0.741957
H	-3.929824	-3.377213	2.121796

C	-2.310345	0.580010	0.681760
C	-1.172503	0.658257	1.501903
C	-2.971115	1.761715	0.286835
C	-0.708219	1.885317	1.965852
H	-0.649432	-0.254948	1.768871
C	-2.480481	2.990526	0.755117
C	-1.369812	3.057699	1.591747
H	0.170234	1.925559	2.602830
H	-2.965924	3.906364	0.430571
H	-1.013544	4.023286	1.939906
C	-4.170762	1.773234	-0.660532
C	-5.480233	2.143438	0.043747
H	-5.409142	3.138658	0.493650
H	-6.308880	2.142638	-0.671004
H	-5.706545	1.427599	0.840302
F	1.331697	1.325603	-1.390096
H	-4.283306	0.789638	-1.125882

[4 + 1F] (Prod. Complex, T)

C	-5.510026	-0.876972	-2.007815
N	-5.022159	0.230316	-2.672522
H	-5.476746	0.718997	-3.431291
C	-3.811312	0.536888	-2.142772
H	-3.196794	1.362389	-2.472448
N	-3.497458	-0.307774	-1.173404
C	-4.551300	-1.195163	-1.081984
H	-4.540366	-2.002401	-0.364638
C	-3.228638	-0.222916	3.851203
N	-2.971442	-1.572641	3.709778
H	-3.157890	-2.292215	4.394240
C	-2.418709	-1.773192	2.491052
H	-2.107583	-2.728729	2.099428
N	-2.307978	-0.622244	1.841107
C	-2.810741	0.354588	2.682750
H	-2.815649	1.388463	2.378547
C	-1.628513	3.971365	0.090420
H	-1.306598	4.744749	-0.609790
H	-1.103033	4.085752	1.043084
C	-1.390158	2.581843	-0.487727
O	-1.477883	1.612970	0.352244
O	-1.159725	2.465621	-1.715352
Fe	-1.543741	-0.375487	-0.028968
N	-1.198195	-2.343315	-0.079939
N	-0.789818	-2.956052	-1.036750
N	-0.393433	-3.608031	-1.911777
O	-0.565902	-0.103746	-1.800464
H	-0.688966	0.882762	-1.924081
H	0.405459	-0.263778	-1.701564
H	-3.671565	0.187942	4.744855
H	-2.699791	4.098689	0.289871
H	-6.462152	-1.321205	-2.253005
C	2.898804	-0.145428	-0.715788
O	2.110211	-0.690071	-1.500783
N	3.936567	-0.787625	-0.137350
H	4.566819	-0.217508	0.411115
C	4.305372	-2.219610	-0.304150
C	5.515641	-2.453528	0.613813
C	3.136033	-3.121846	0.128497
C	4.692469	-2.491876	-1.769437
H	6.357282	-1.806672	0.336012
H	5.259428	-2.261985	1.662816
H	5.850443	-3.492000	0.531937
H	2.277046	-3.000836	-0.534415
H	3.452638	-4.170609	0.098760
H	2.824765	-2.882929	1.151013
H	4.983686	-3.541320	-1.890211
H	3.849474	-2.288167	-2.433711
H	5.539254	-1.864311	-2.070427
C	2.825369	1.338635	-0.417206
C	3.391023	2.190453	-1.377935
C	2.193862	1.887755	0.713318
C	3.361781	3.574167	-1.217864
H	3.858012	1.756231	-2.257840
C	2.163794	3.282404	0.855514
C	2.746987	4.122603	-0.090928
H	3.808018	4.217580	-1.970492
H	1.667676	3.714406	1.721833
H	2.708822	5.199700	0.044616
C	1.556098	1.060023	1.812332
C	2.483403	0.765488	2.985627
H	2.821114	1.699162	3.446886
H	1.956244	0.173798	3.740889
H	3.361712	0.205267	2.650290
F	1.121225	-0.178812	1.293319
H	0.651864	1.570025	2.156318

[4 + 1F] (Prod. Complex, Q)

C	5.461406	-0.996760	2.061980
N	4.966637	0.083641	2.764855
H	5.420451	0.551660	3.537060
C	3.752936	0.399809	2.252650
H	3.134386	1.212236	2.606764
N	3.444276	-0.415387	1.254680
C	4.504476	-1.292180	1.127930
H	4.497642	-2.073011	0.382416
C	3.411327	-0.101045	-3.877342
N	3.125470	-1.449615	-3.794789
H	3.319005	-2.145914	-4.501167
C	2.533966	-1.680612	-2.596739
H	2.195712	-2.647401	-2.255812
N	2.426643	-0.556149	-1.906585
C	2.971088	0.437786	-2.696997
H	2.991030	1.461020	-2.355548
C	1.751625	3.993924	0.118427
H	1.521928	4.760201	0.861451
H	1.176106	4.175824	-0.794518
C	1.455123	2.600449	0.660169
O	1.509688	1.647824	-0.201238
O	1.205345	2.462201	1.881205
Fe	1.549380	-0.404288	0.137562
N	1.149416	-2.414659	0.061004
N	0.592864	-3.103783	0.878043
N	0.061699	-3.809644	1.632392
O	0.424236	-0.100113	1.985169
H	0.603103	0.875159	2.093868
H	-0.544493	-0.200475	1.829261

H	3.886141	0.333556	-4.743205
H	2.813557	4.060583	-0.147728
H	6.417568	-1.441483	2.289180
C	-2.987288	-0.088154	0.646767
O	-2.263530	-0.609746	1.504480
N	-3.987040	-0.741538	0.013203
H	-4.566502	-0.183901	-0.600611
C	-4.406827	-2.154525	0.222966
C	-5.572178	-2.397028	-0.749540
C	-3.244559	-3.108609	-0.102985
C	-4.881966	-2.348772	1.674784
H	-6.410143	-1.718884	-0.545105
H	-5.255356	-2.256911	-1.790129
H	-5.938086	-3.422750	-0.643666
H	-2.411442	-2.977331	0.590502
H	-3.592015	-4.145550	-0.030781
H	-2.881548	-2.938317	-1.122580
H	-5.215837	-3.381866	1.822621
H	-4.070087	-2.143929	2.376273
H	-5.721658	-1.681479	1.901162
C	-2.879256	1.384822	0.301550
C	-3.577845	2.267017	1.139031
C	-2.094537	1.897801	-0.748054
C	-3.526233	3.644914	0.936101
H	-4.166130	1.862348	1.958297
C	-2.046097	3.286479	-0.933997
C	-2.757884	4.156920	-0.110217
H	-4.075812	4.311519	1.594281
H	-1.435332	3.689824	-1.738386
H	-2.701279	5.228704	-0.277447
C	-1.324063	1.036307	-1.728212
C	-2.133363	0.596034	-2.941086
H	-2.485474	1.470897	-3.497395
H	-1.512804	-0.013871	-3.605279
H	-3.001059	0.006764	-2.629922
F	-0.864139	-0.138395	-1.080296
H	-0.422984	1.570963	-2.037453

XII. X-ray Crystallography and the Assignments of Absolute Configuration

For azidation product **1N**, 10 mg of pure compound was dissolved in 0.5 mL dichloromethane and Crystals of compound **1N** were obtained via slow evaporation of a dichloromethane solution of **1N** at room temperature. A suitable crystal was selected and mounted in a nylon loop in immersion oil.

All reflection intensities were measured at 110(2) K using a SuperNova diffractometer (equipped with Atlas detector) with Cu *K*α radiation (λ = 1.54178 Å) under the program CrysAlisPro (Version CrysAlisPro 1.171.39.29c, Rigaku OD, 2017). The same program was used to refine the cell dimensions and for data reduction. The structure was solved with the program SHELXS-2018/3 and was refined on F^2 with SHELXL-2018/3 (*38*). Analytical numeric absorption correction using a multifaceted crystal model was applied using CrysAlisPro. The temperature of the data collection was controlled using the system Cryojet (manufactured by Oxford Instruments). The H atoms were placed at calculated positions (unless otherwise specified) using the instructions AFIX 13, AFIX 43 or AFIX 137 with isotropic displacement parameters having values 1.2 or 1.5 U_{eq} of the attached C atoms. The H atoms attached to N1X (X = A, B, C, D) were found from difference Fourier maps, and their coordinates were refined pseudofreely using the DFIX instruction in order to keep the N-H bond distances within an acceptable range.

The asymmetric unit contains four crystallographically independent molecules, and the structure is mostly ordered. The fragment C12D ® N4D of molecule D is slightly disordered over two orientations, and the occupancy factor of the major component (major component: C12D has the S configuration; minor component: C12 has the R configuration) refines to 0.911(4). This observation is consistent with what has been observed from chiral HPLC which shows an enantiomeric ratio of 93:7 (almost pure). Computer programs: CrysAlis PRO 1.171.39.29c (Rigaku OD, 2017), SHELXS 2018/3 (Sheldrick, 2018), SHELXL 2018/3 (Sheldrick, 2018), SHELXTL v6.10 (Sheldrick, 2008).

The absolute configuration has been established by anomalous dispersion effects in diffraction measurements on the crystal, and the Flack and Hooft parameters refine to -0.06(6) and -0.05(6), respectfully.

791_ALERT_4_G Model has Chirality at C12A	(Sohnke SpGr)	S Verify
791_ALERT_4_G Model has Chirality at C12B	(Sohnke SpGr)	S Verify
791_ALERT_4_G Model has Chirality at C12C	(Sohnke SpGr)	S Verify
791_ALERT_4_G Model has Chirality at C12D	(Sohnke SpGr)	S Verify

	xs2607a
Crystal data	
Chemical formula	$C_{13}H_{18}N_4O$
M_r	246.31
Crystal system, space group	Triclinic, *P*1
Temperature (K)	110
a, *b*, *c* (Å)	9.61890 (17), 10.20786 (19), 15.2906 (2)
α, β, γ (°)	102.6118 (14), 99.7985 (14), 106.3256 (16)
V (Å^3)	1362.40 (4)
Z	4
Radiation type	Cu *K*α
μ (mm^{-1})	0.64
Crystal size (mm)	0.32 × 0.12 × 0.06
Data collection	
Diffractometer	SuperNova, Dual, Cu at zero, Atlas
Absorption correction	Analytical *CrysAlis PRO* 1.171.39.46 (Rigaku Oxford Diffraction, 2018) Analytical numeric absorption correction using a multifaceted crystal model based on expressions derived by R.C. Clark & J.S. Reid. (Clark, R. C. & Reid, J. S. (1995). Acta Cryst. A51, 887-897) Empirical absorption correction using spherical harmonics, implemented in SCALE3 ABSPACK scaling algorithm.
T_{min}, T_{max}	0.844, 0.966
No. of measured, independent and observed [$I > 2\sigma(I)$] reflections	35563, 10306, 9894
R_{int}	0.022
$(\sin \theta/\lambda)_{max}$ (Å^{-1})	0.616
Refinement	
$R[F^2 > 2\sigma(F^2)]$, $wR(F^2)$, *S*	0.034, 0.094, 1.06
No. of reflections	10306
No. of parameters	715
No. of restraints	134

H-atom treatment	H atoms treated by a mixture of independent and constrained refinement
$\Delta\rho_{max}$, $\Delta\rho_{min}$ (e Å^{-3})	0.29, -0.21
Absolute structure	Flack x determined using 4583 quotients [(I+)-(I-)]/[(I+)+(I-)] (Parsons, Flack and Wagner, Acta Cryst. B69 (2013) 249-259).
Absolute structure parameter	-0.06 (6)

XIII. NMR Spectra

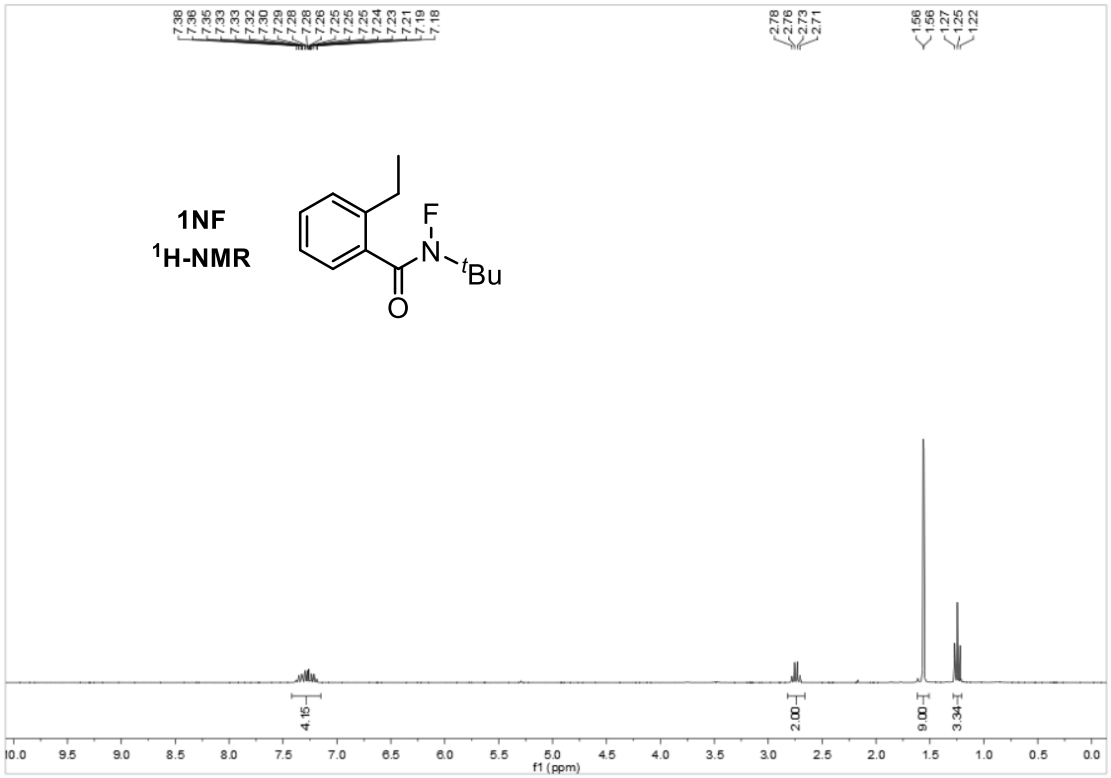

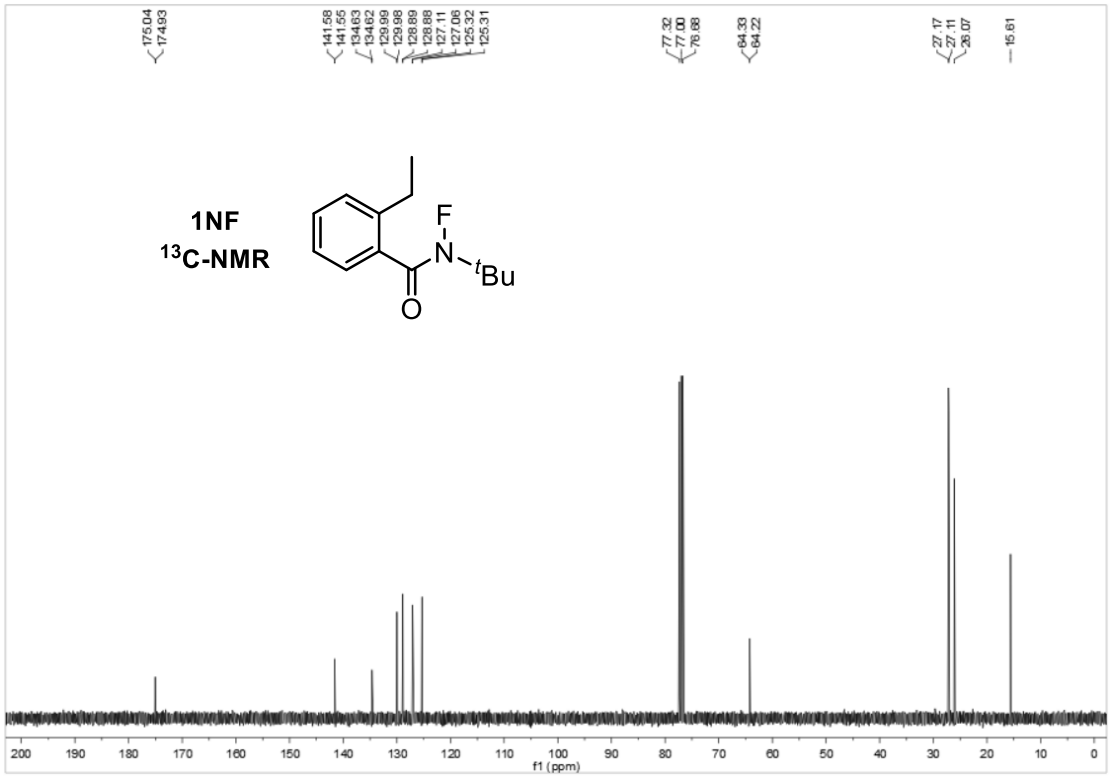

1NF
^{19}F-NMR

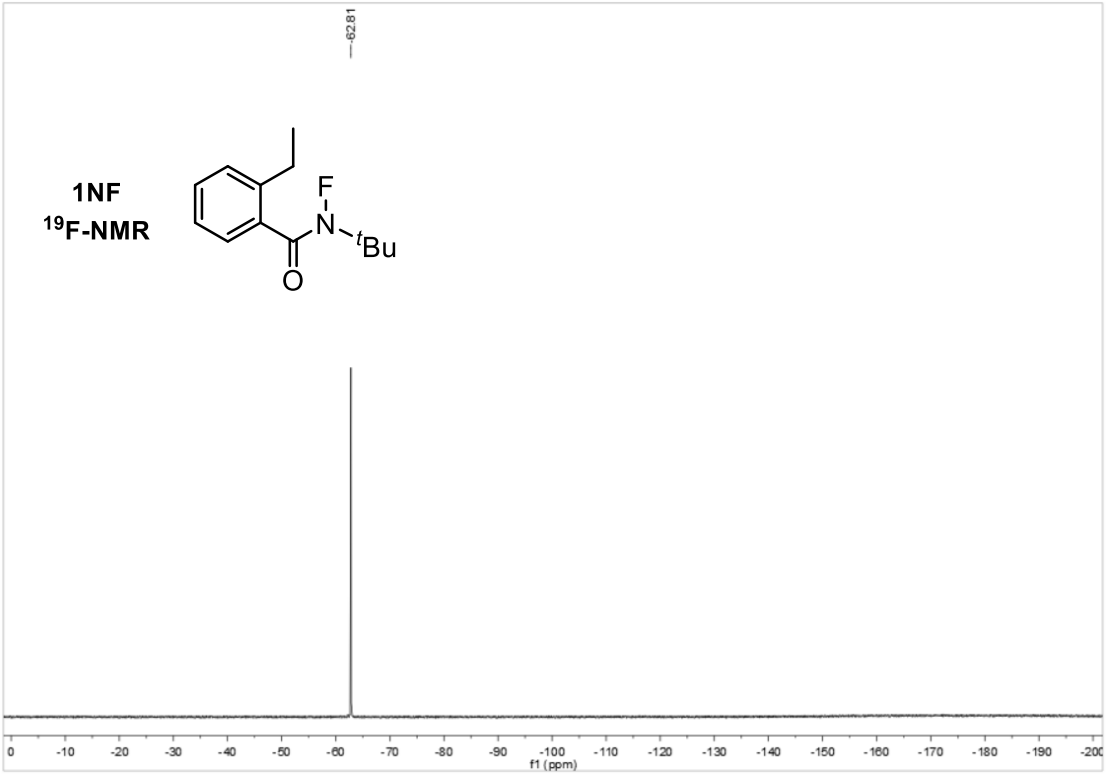

2NF
^{1}H-NMR

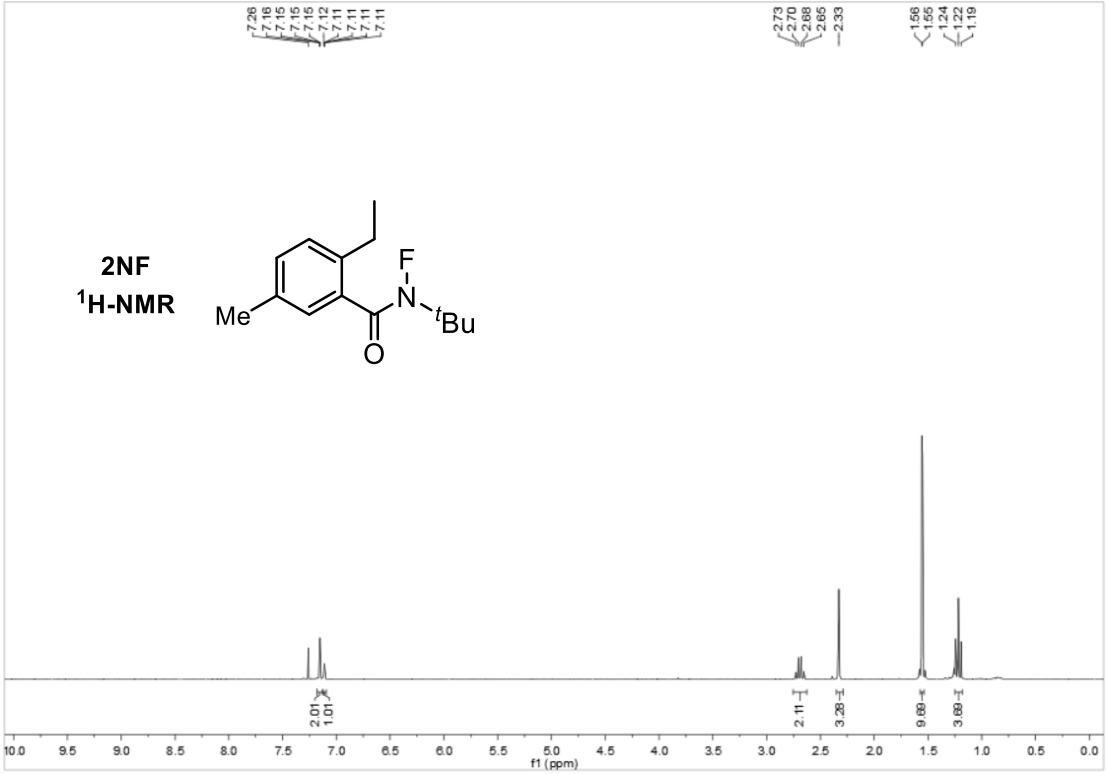

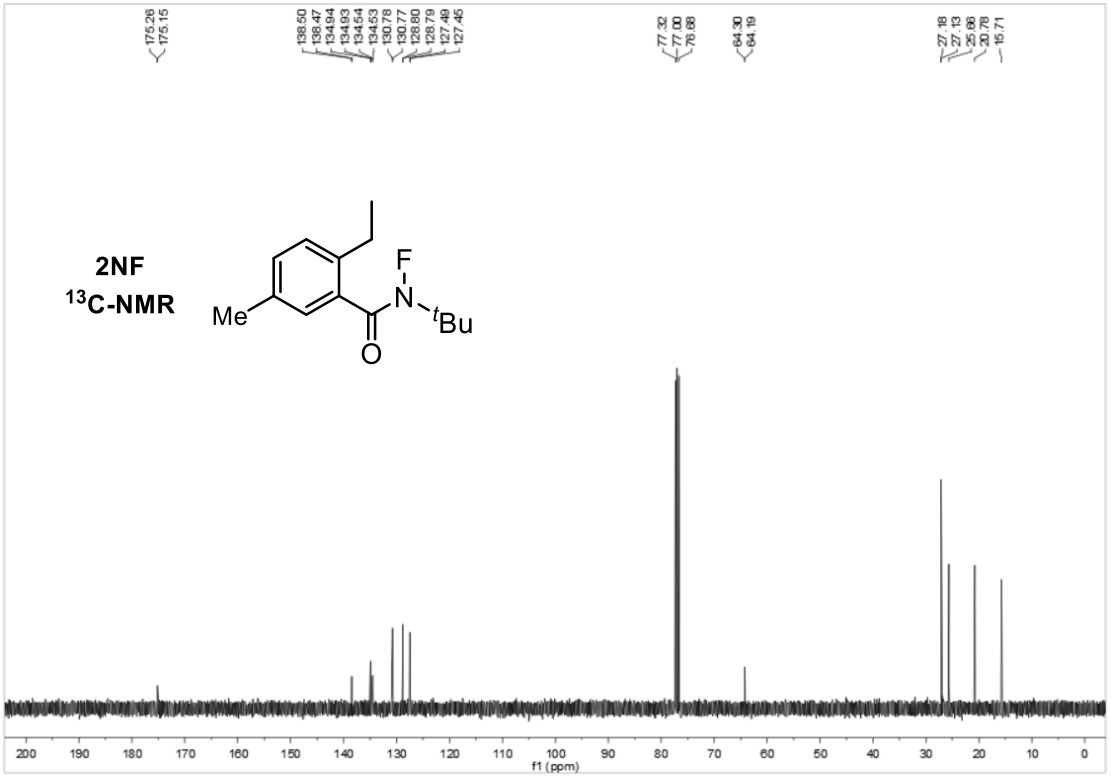
175.26
175.15
138.50
138.47
134.94
134.63
134.54
134.53
130.78
130.77
128.80
128.79
127.49
127.45
77.32
77.00
76.68
64.30
64.19
27.18
27.13
25.66
20.78
15.71
2NF
13C-NMR
Me
F
N
tBu
O
200 190 180 170 160 150 140 130 120 110 100 90 80 70 60 50 40 30 20 10 0
f1 (ppm)

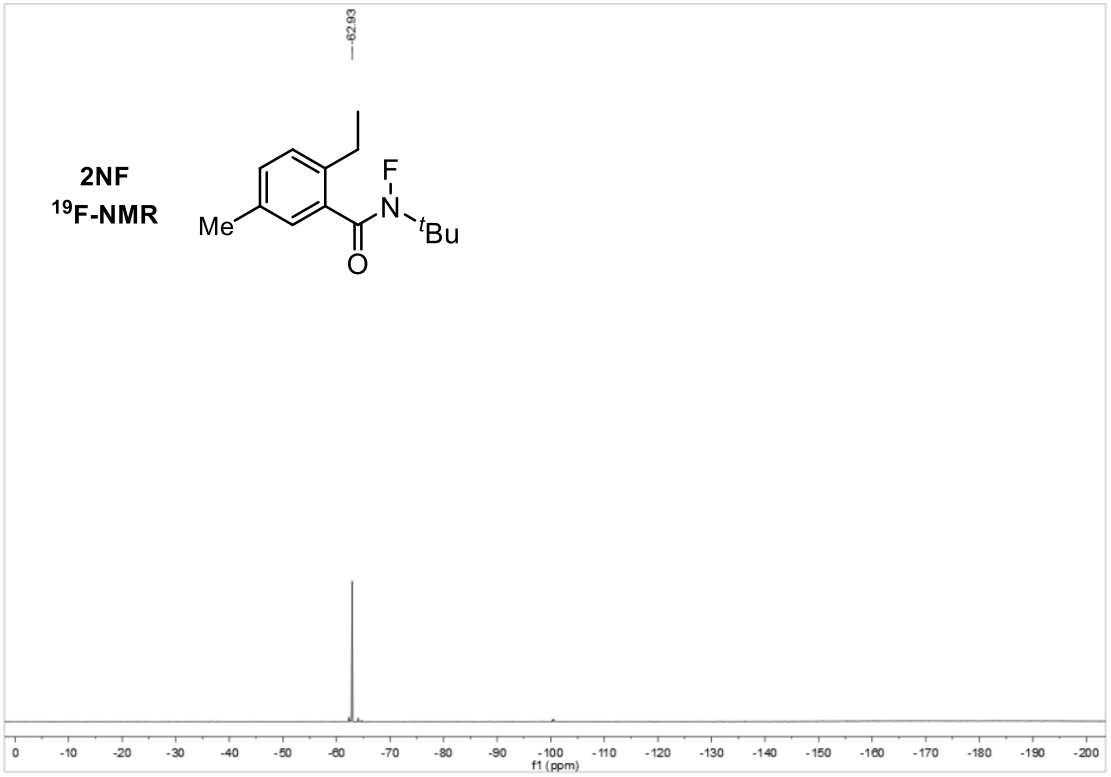
-62.93
2NF
19F-NMR
Me
F
N
tBu
O
0 -10 -20 -30 -40 -50 -60 -70 -80 -90 -100 -110 -120 -130 -140 -150 -160 -170 -180 -190 -200
f1 (ppm)

3NF
^{1}H-NMR

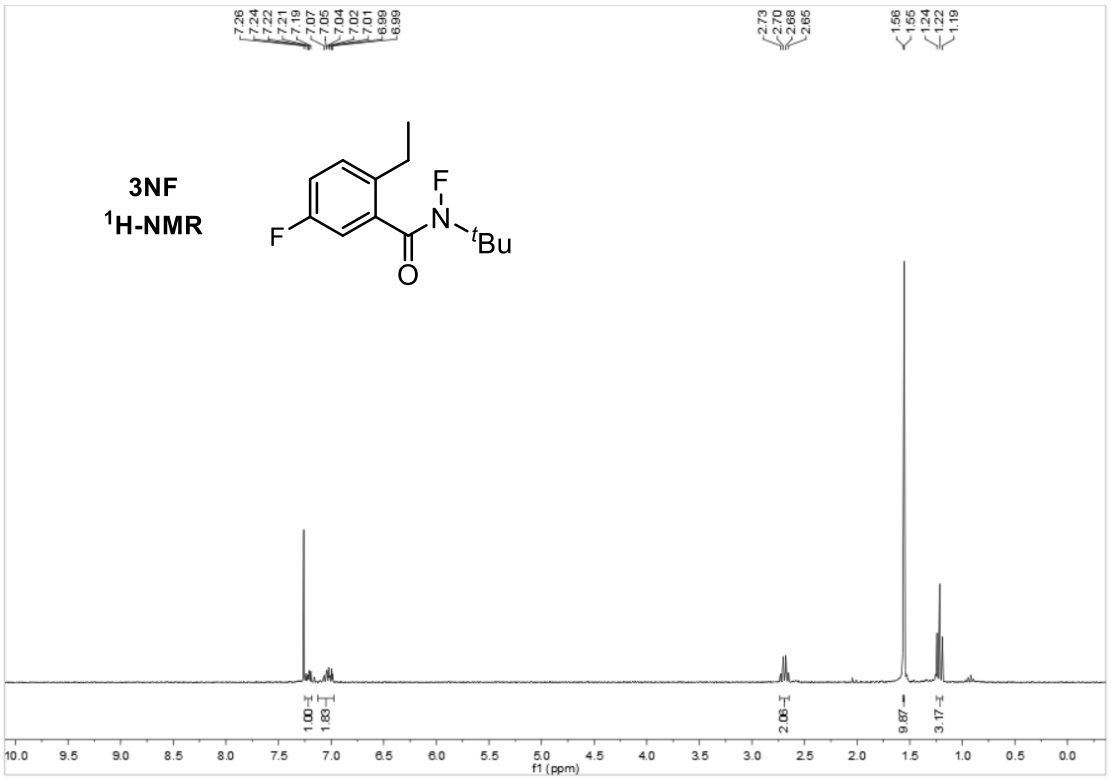

3NF
^{13}C-NMR

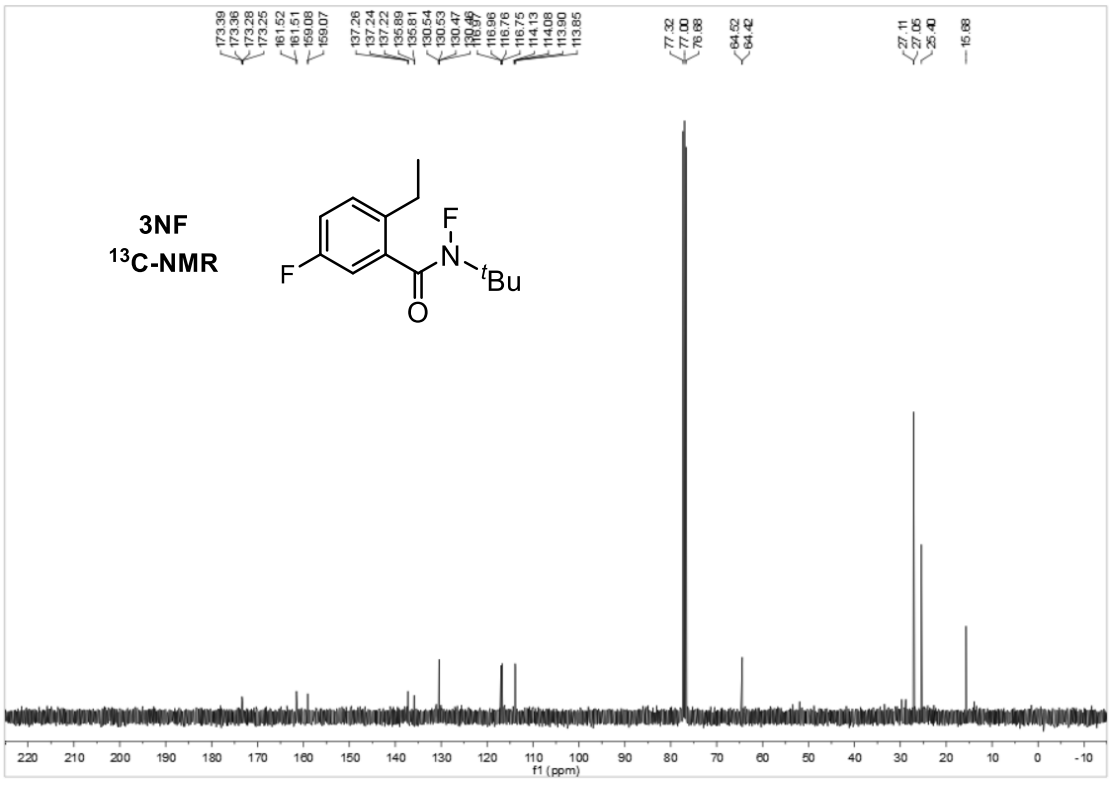

3NF
^{19}F-NMR

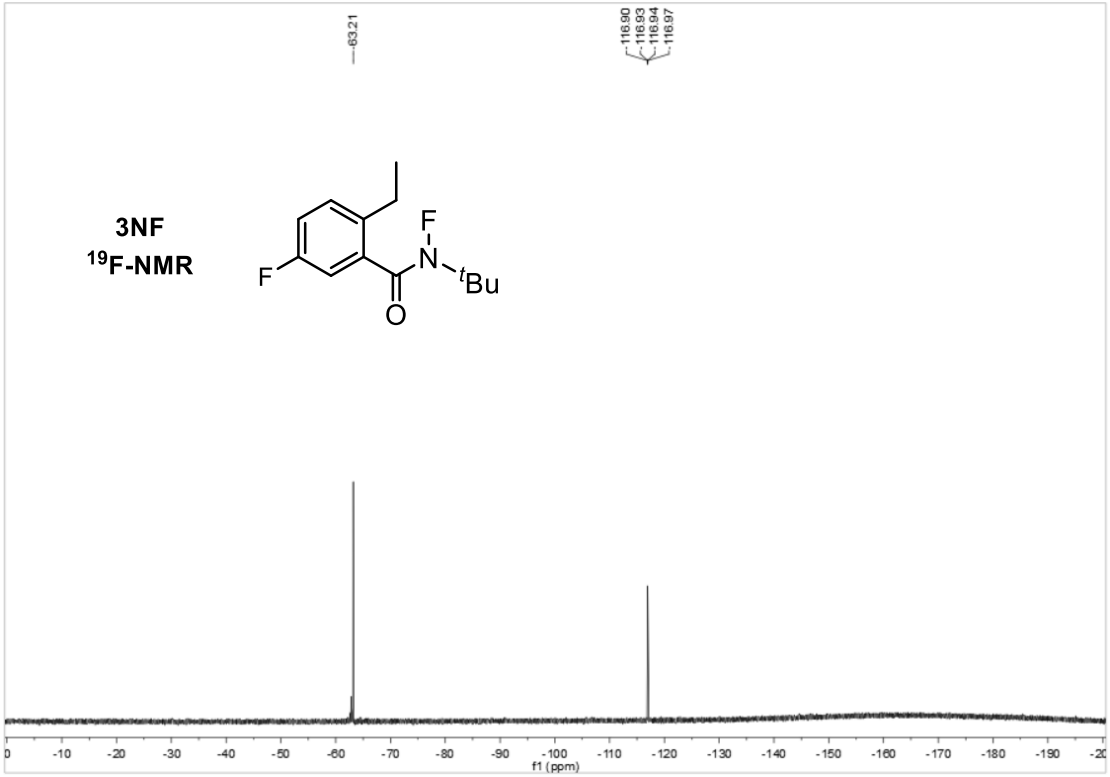

4NF
^{1}H-NMR

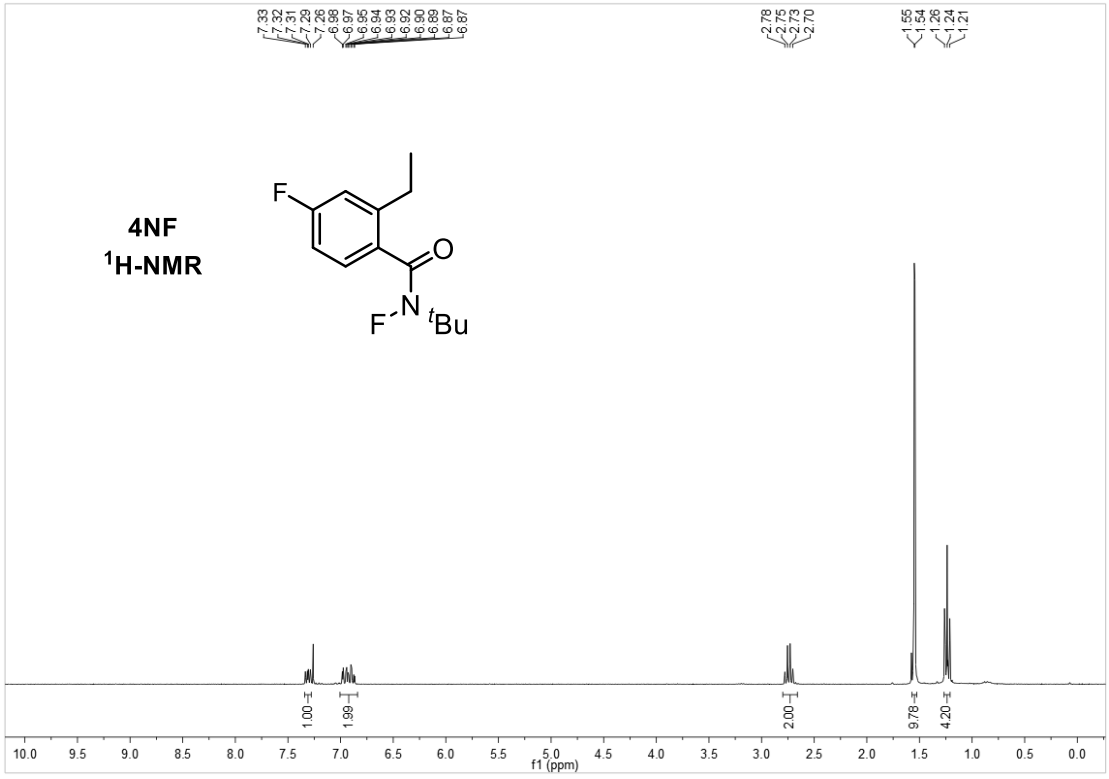

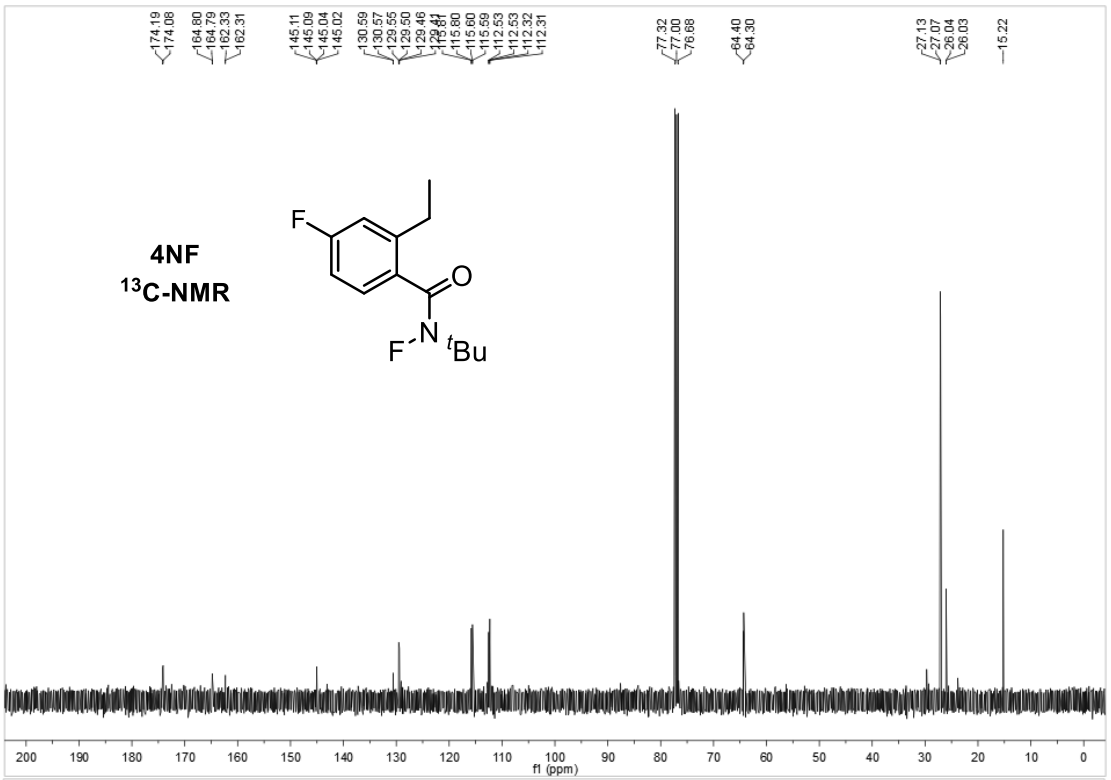
174.19
174.08
164.80
164.79
162.33
162.31
145.11
145.09
145.04
145.02
130.59
130.57
129.55
129.50
129.46
115.80
115.60
115.59
112.53
112.53
112.32
112.31
77.32
77.00
76.68
64.40
64.30
27.13
27.07
26.04
26.03
15.22
4NF
13C-NMR
F
O
F
N
tBu
200
190
180
170
160
150
140
130
120
110
100
90
80
70
60
50
40
30
20
10
0
f1 (ppm)

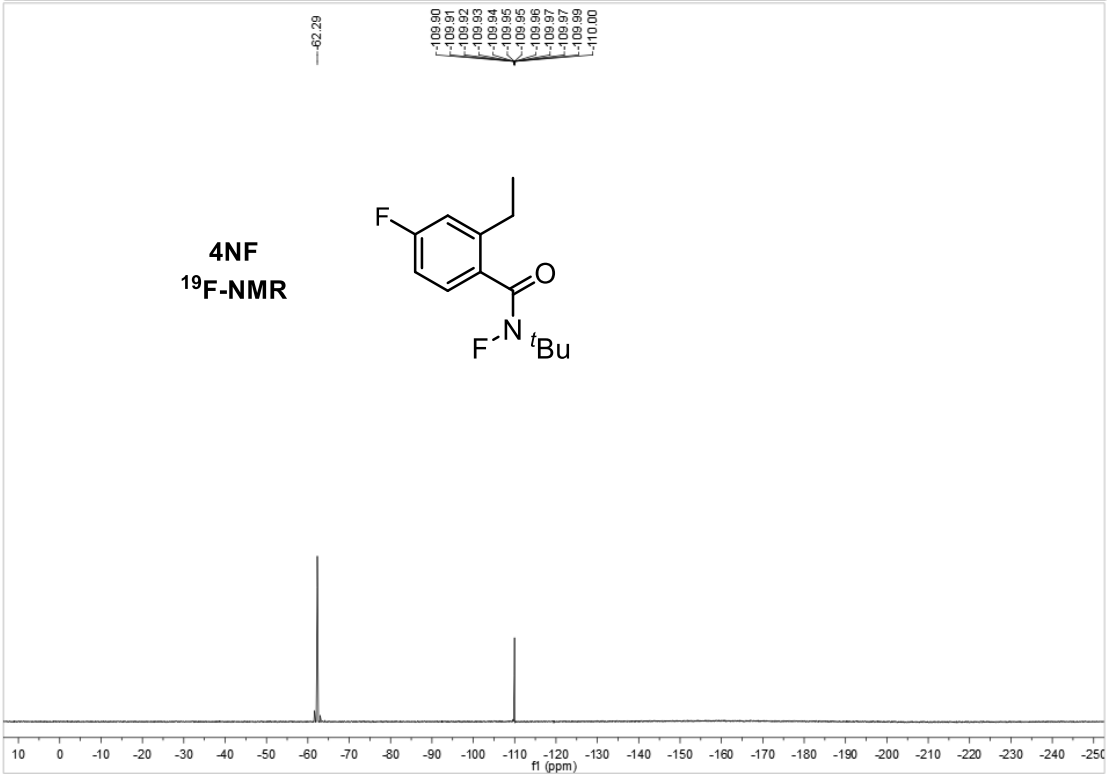
62.29
109.90
109.91
109.92
109.93
109.94
109.95
109.95
109.96
109.97
109.97
109.99
110.00
4NF
19F-NMR
F
O
F
N
tBu
10
0
-10
-20
-30
-40
-50
-60
-70
-80
-90
-100
-110
-120
-130
-140
-150
-160
-170
-180
-190
-200
-210
-220
-230
-240
-250
f1 (ppm)

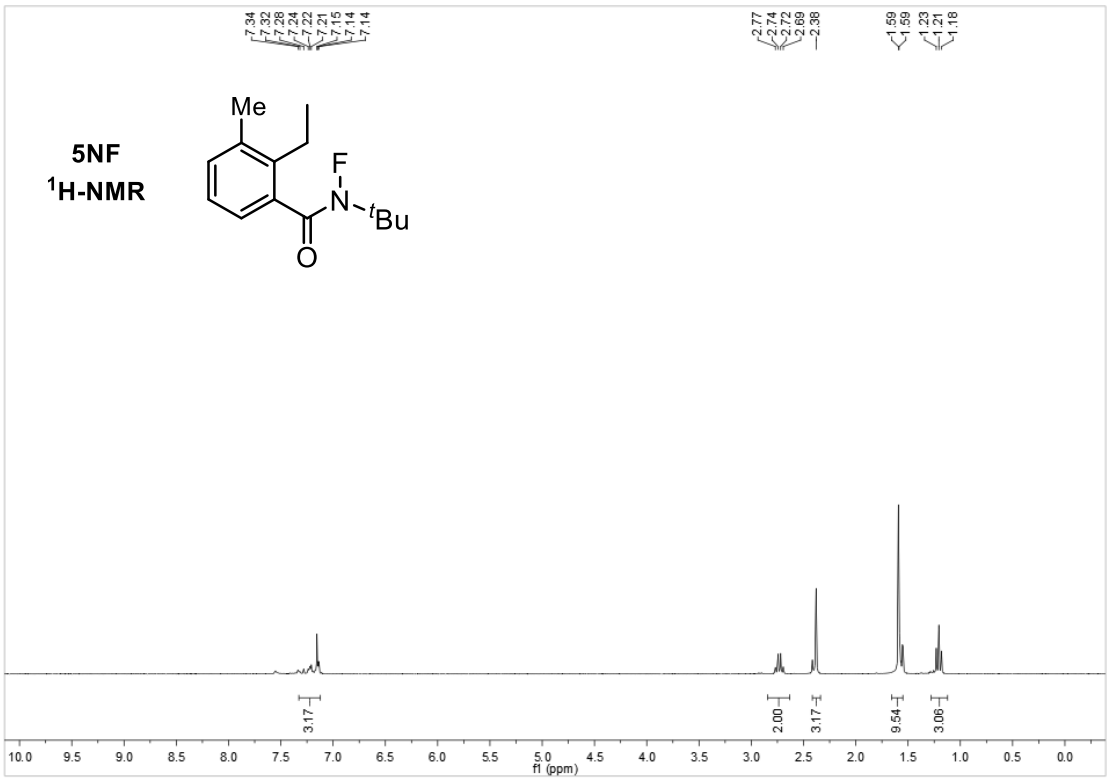
7.34
7.32
7.28
7.24
7.22
7.21
7.15
7.14
7.14
2.77
2.74
2.72
2.69
2.38
1.59
1.59
1.23
1.21
1.18
5NF
1H-NMR
Me
F
N
tBu
O
3.17
2.00
3.17
9.54
3.06
10.0
9.5
9.0
8.5
8.0
7.5
7.0
6.5
6.0
5.5
5.0
4.5
4.0
3.5
3.0
2.5
2.0
1.5
1.0
0.5
0.0
f1 (ppm)

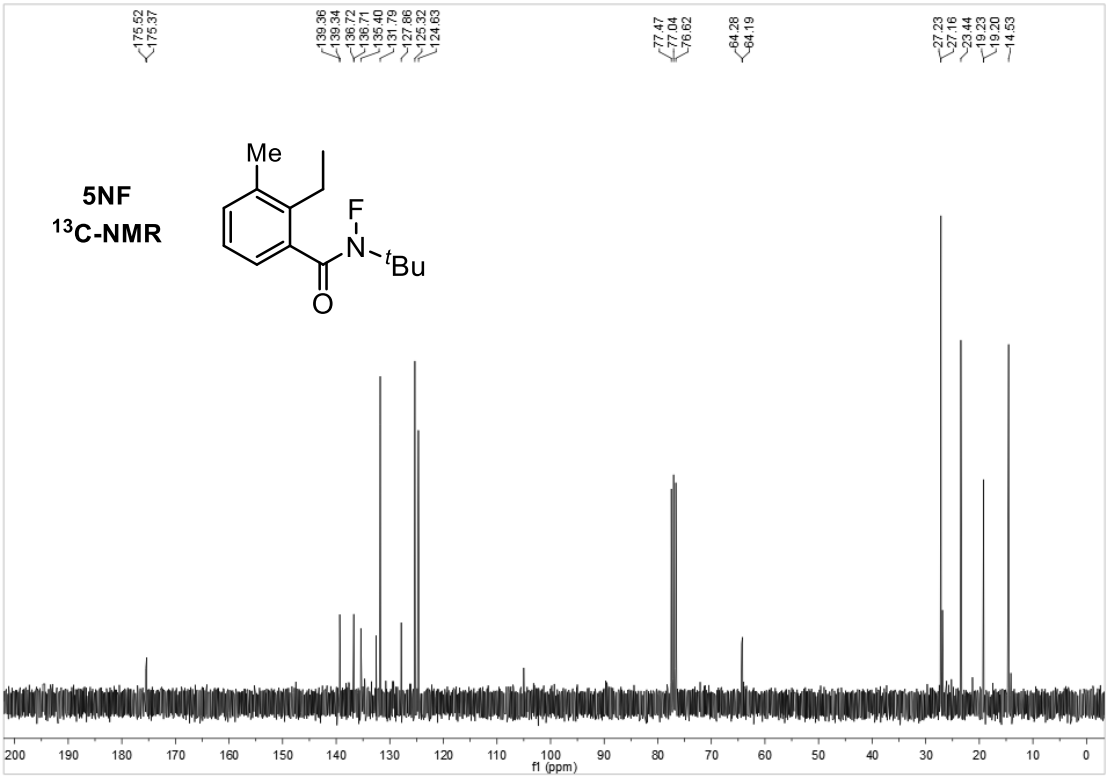
175.52
175.37
139.36
139.34
136.72
136.71
135.40
131.79
127.86
125.32
124.63
77.47
77.04
76.62
64.28
64.19
27.23
27.16
23.44
19.23
19.20
14.53
5NF
13C-NMR
Me
F
N
tBu
O
200
190
180
170
160
150
140
130
120
110
100
90
80
70
60
50
40
30
20
10
0
f1 (ppm)

5NF
^{19}F-NMR

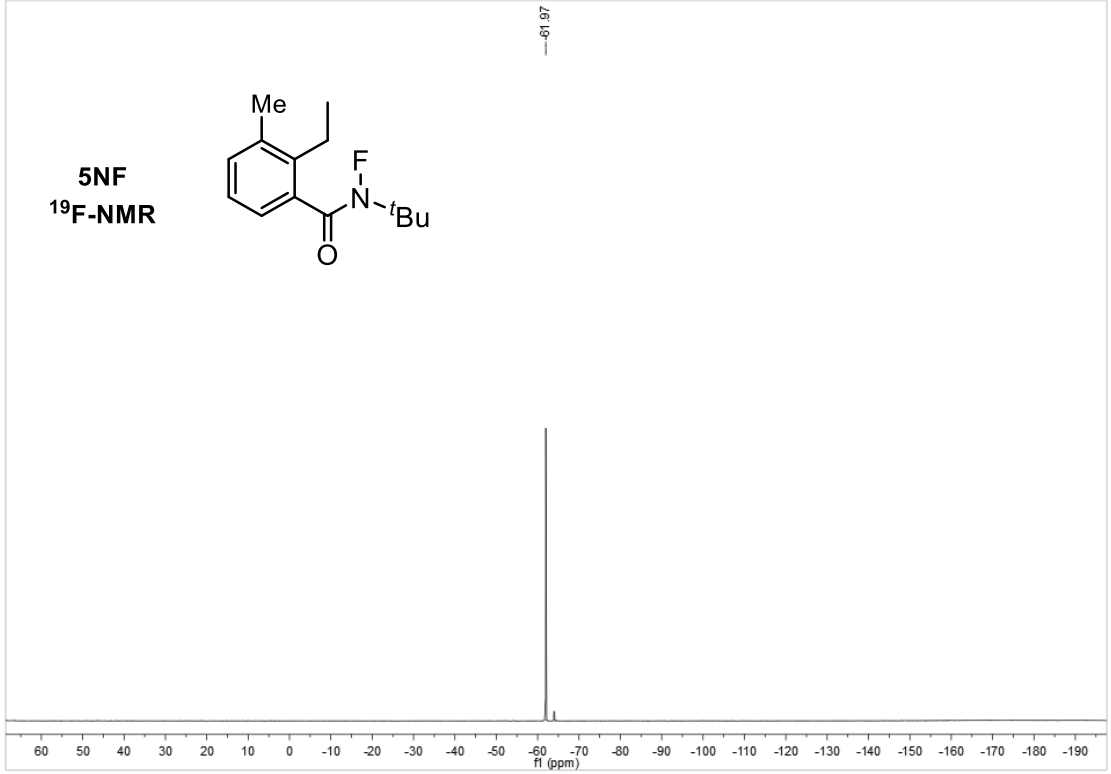

6NF
^{1}H-NMR

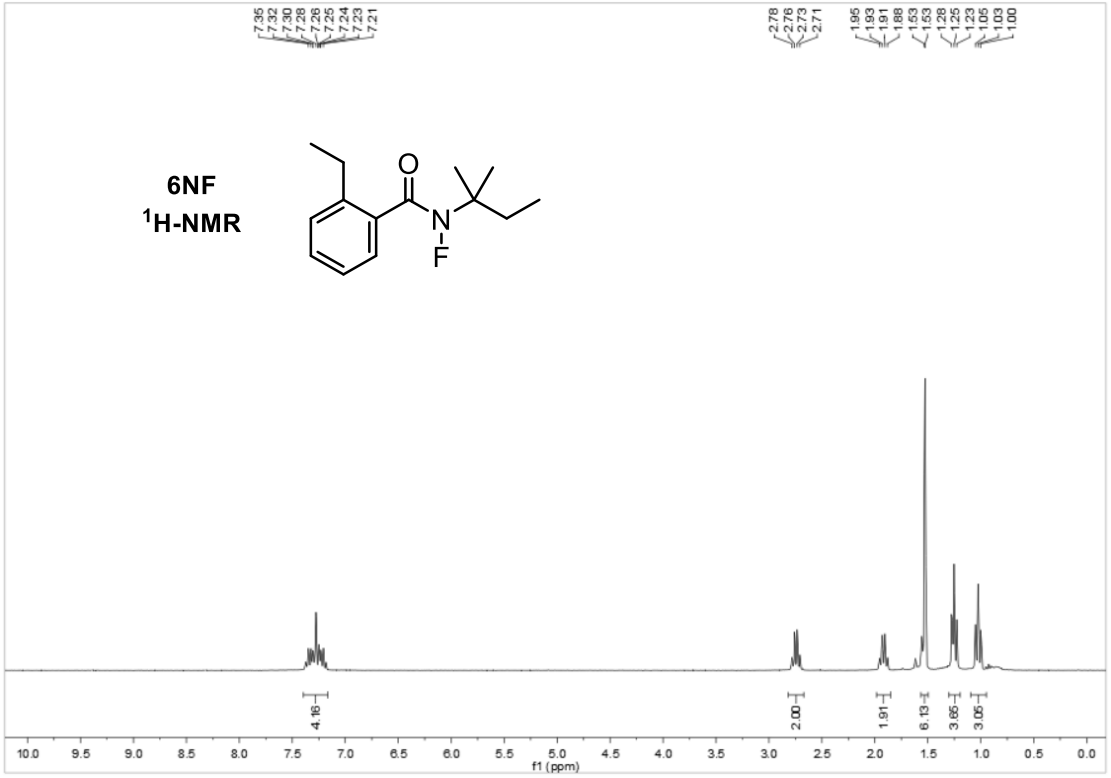

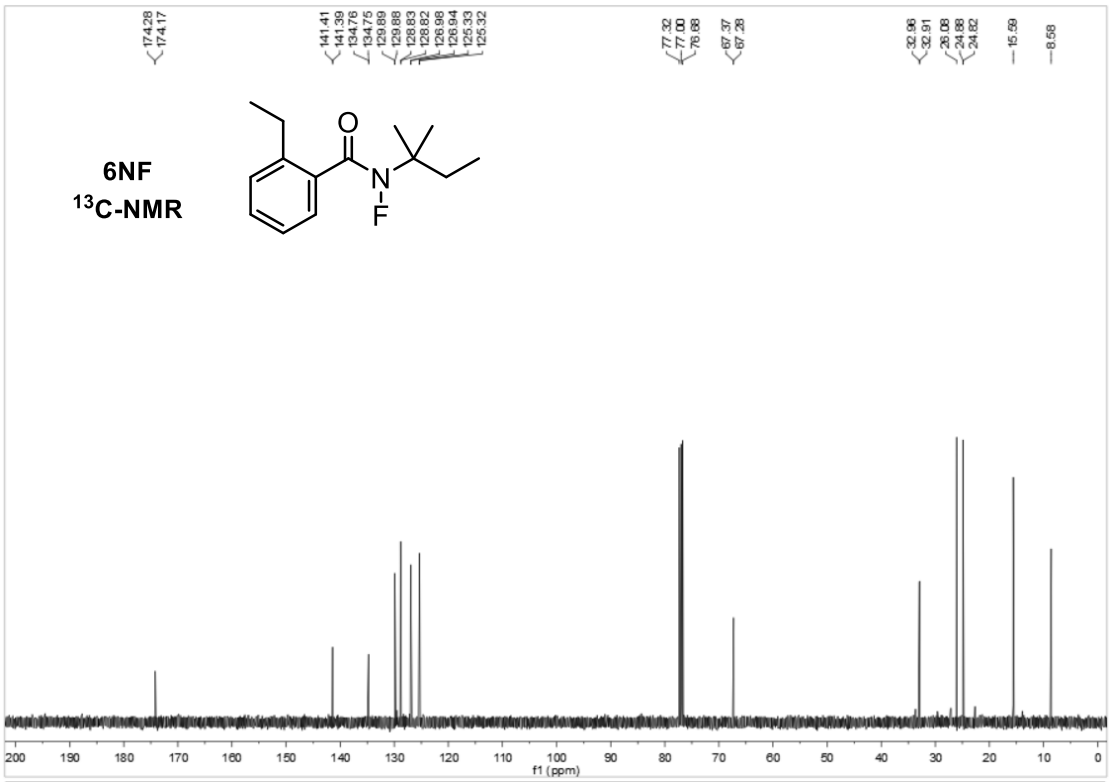
174.28
174.17
141.41
141.39
134.76
134.75
129.89
129.88
128.83
128.82
126.98
126.94
125.33
125.32
77.32
77.00
76.68
67.37
67.28
32.96
32.91
26.08
24.88
24.62
15.59
8.58
6NF
13C-NMR
O
N
F
200 190 180 170 160 150 140 130 120 110 100 90 80 70 60 50 40 30 20 10 0
f1 (ppm)

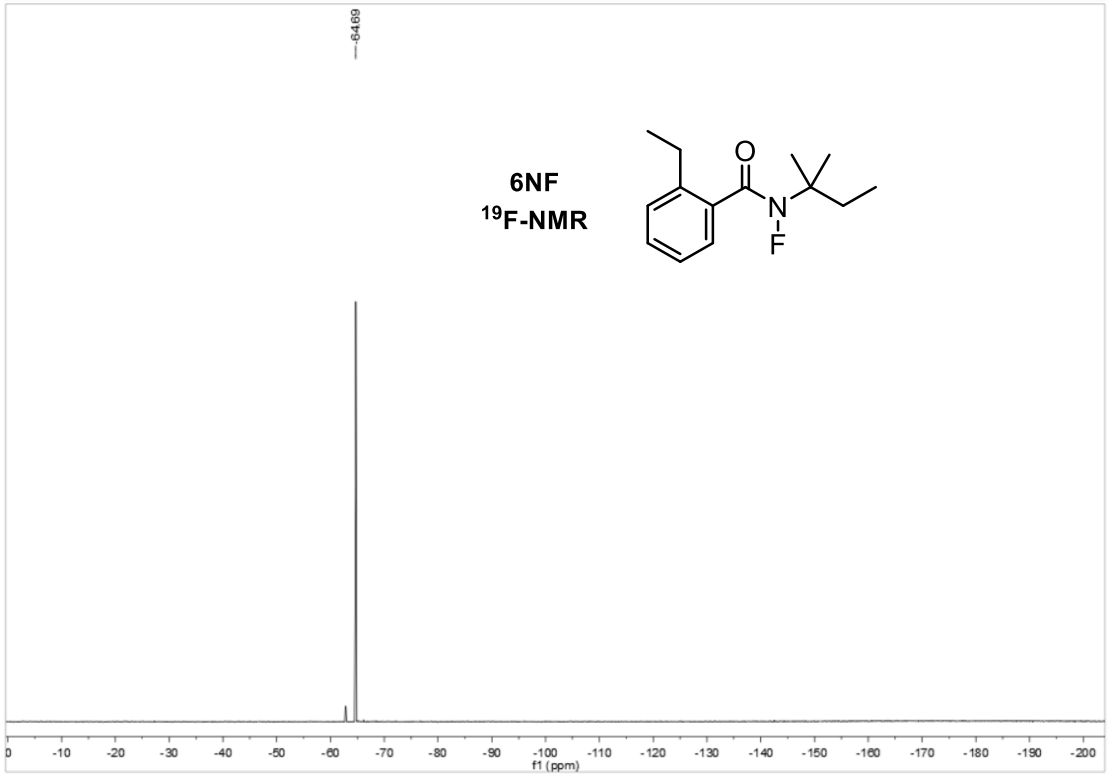
-64.69
6NF
19F-NMR
O
N
F
0 -10 -20 -30 -40 -50 -60 -70 -80 -90 -100 -110 -120 -130 -140 -150 -160 -170 -180 -190 -200
f1 (ppm)

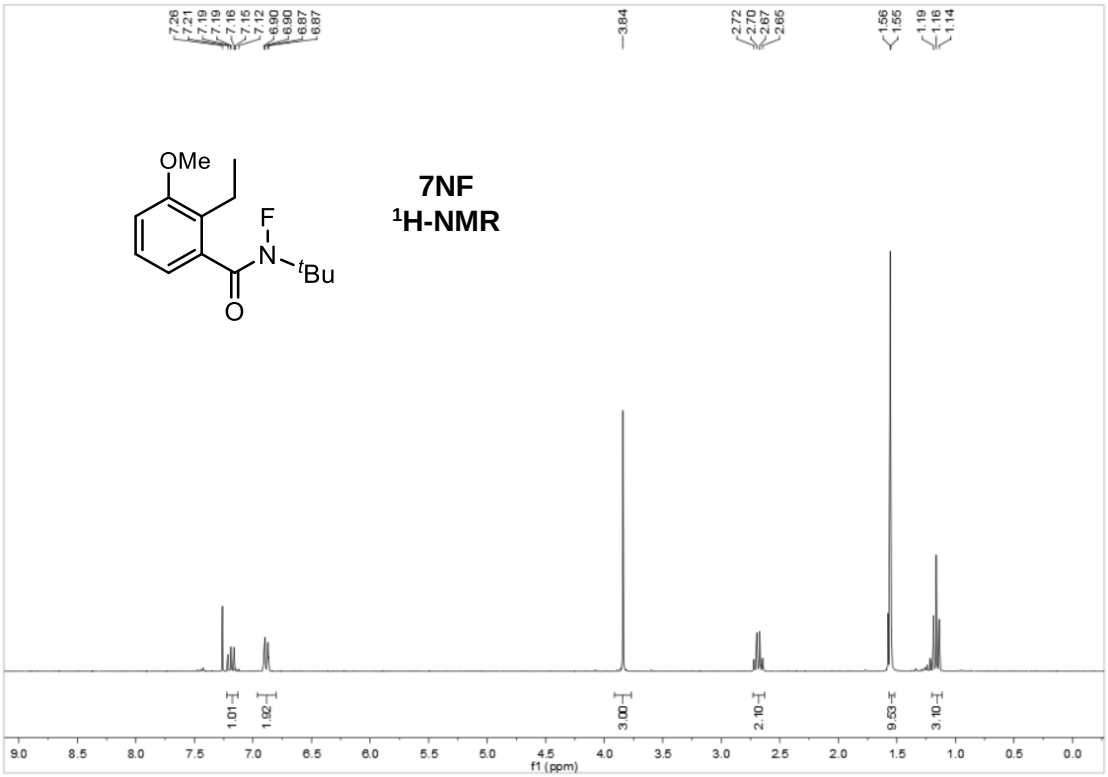
OMe
F
N
tBu
O
7NF
1H-NMR
f1 (ppm)

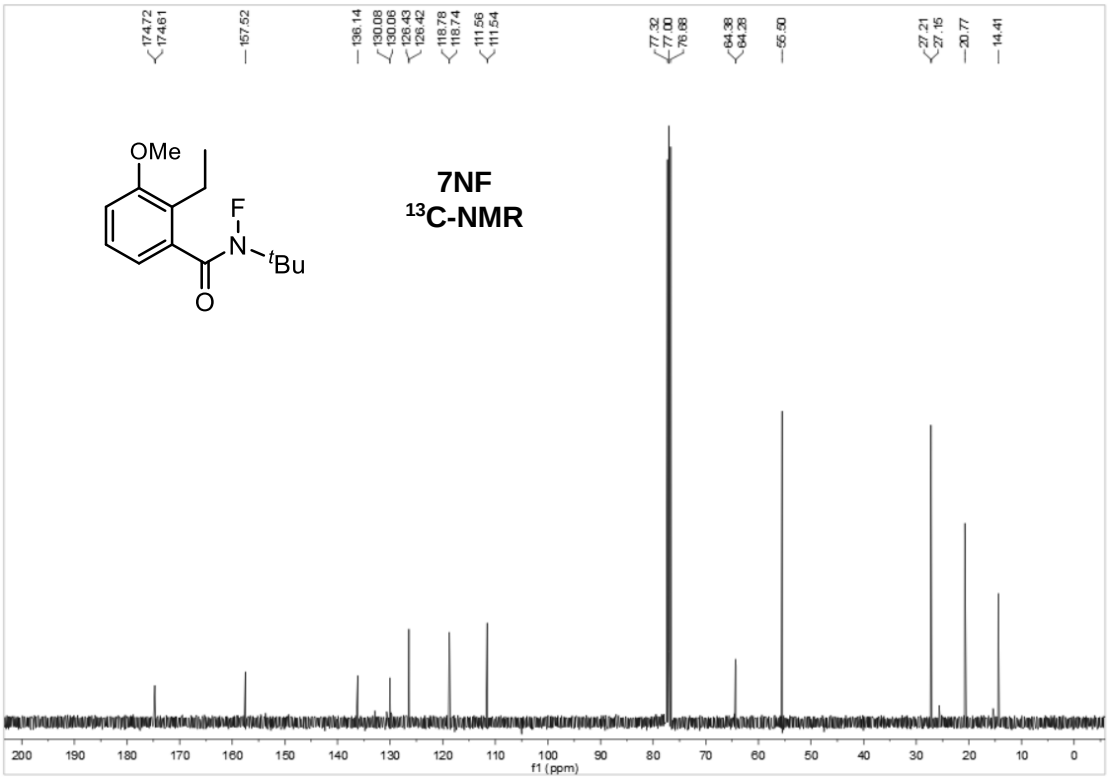
OMe
F
N
tBu
O
7NF
13C-NMR
f1 (ppm)

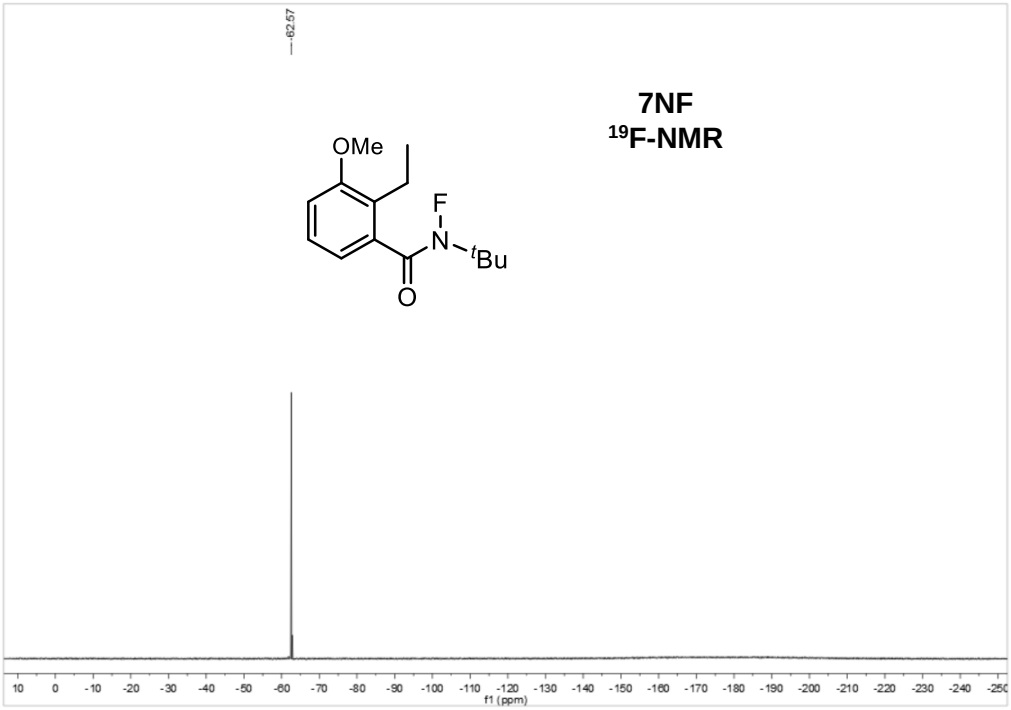
-62.57
7NF
19F-NMR
OMe
F
N
tBu
O
10 0 -10 -20 -30 -40 -50 -60 -70 -80 -90 -100 -110 -120 -130 -140 -150 -160 -170 -180 -190 -200 -210 -220 -230 -240 -250
f1 (ppm)

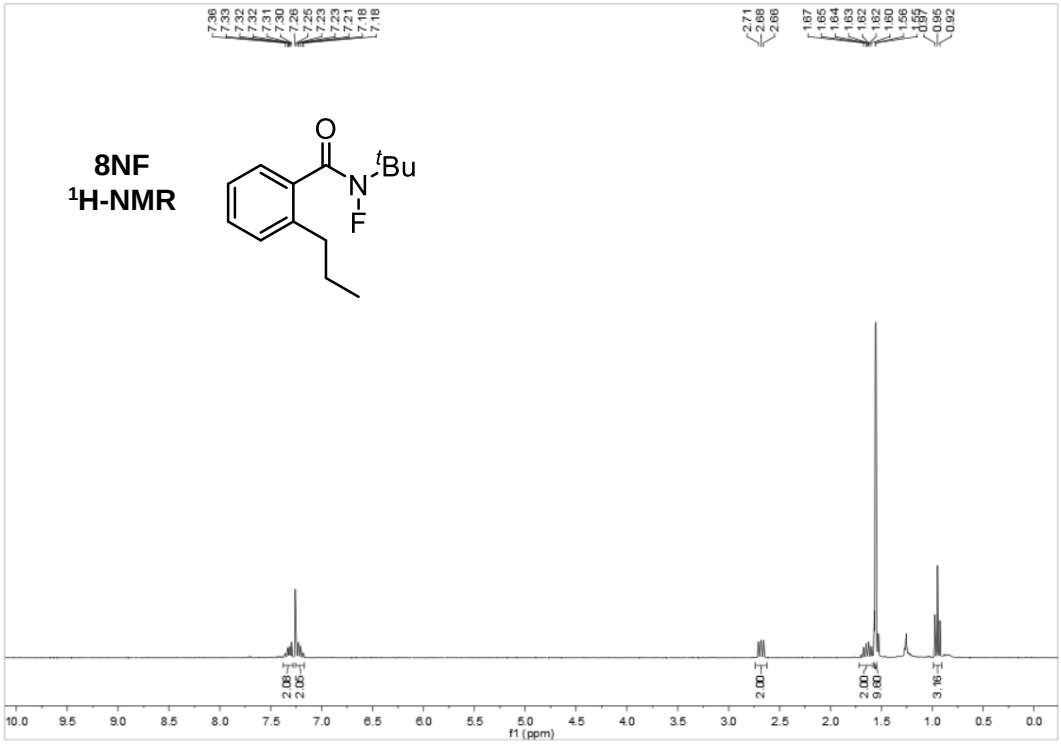
7.36
7.33
7.32
7.32
7.31
7.30
7.26
7.25
7.23
7.23
7.21
7.18
7.18
2.71
2.68
2.66
1.67
1.65
1.64
1.63
1.62
1.62
1.60
1.56
1.55
0.97
0.95
0.92
8NF
1H-NMR
O
tBu
N
F
2.08
2.05
2.00
2.00
9.60
3.16
10.0 9.5 9.0 8.5 8.0 7.5 7.0 6.5 6.0 5.5 5.0 4.5 4.0 3.5 3.0 2.5 2.0 1.5 1.0 0.5 0.0
f1 (ppm)

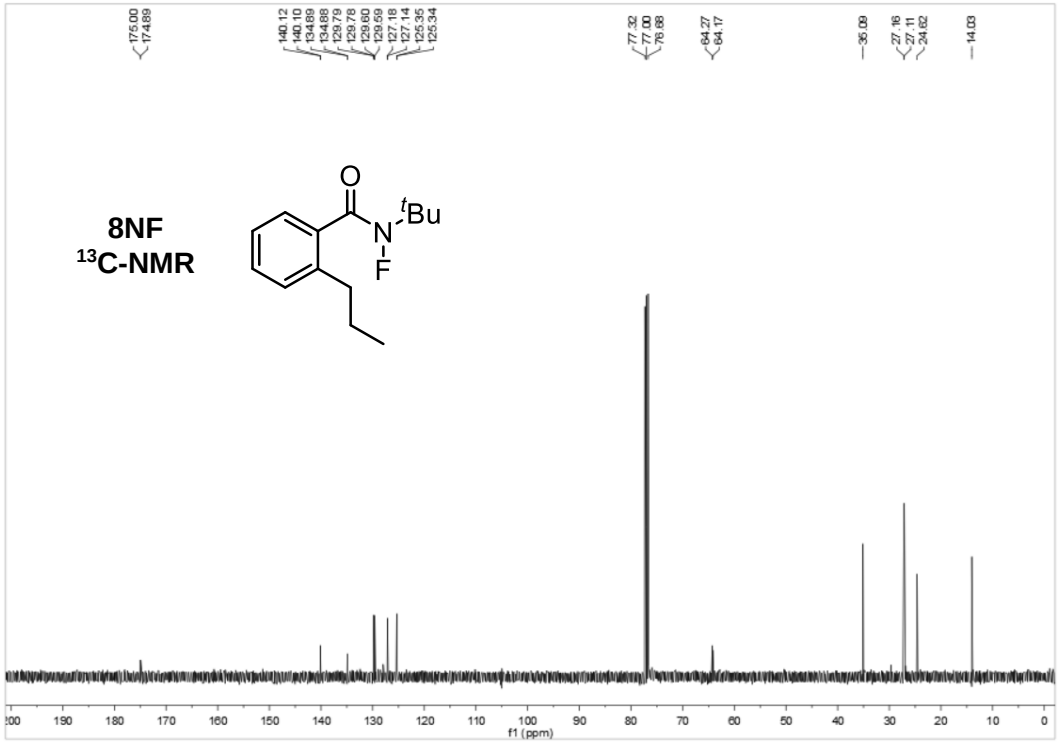
175.00
174.89
140.12
140.10
134.89
134.88
129.79
129.78
129.60
129.59
127.18
127.14
125.35
125.34
77.32
77.00
76.68
64.27
64.17
36.09
27.16
27.11
24.62
14.03
8NF
13C-NMR
O
tBu
N
F
f1 (ppm)

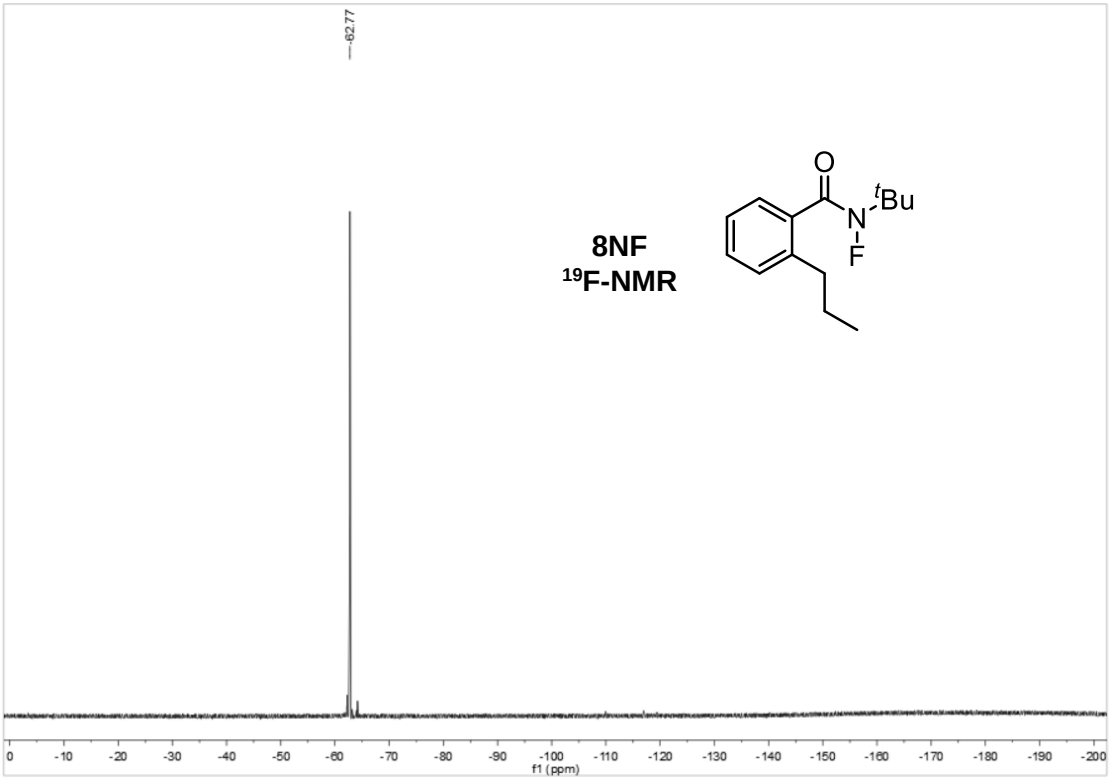
62.77
8NF
19F-NMR
O
tBu
N
F
f1 (ppm)

9NF
^{1}H-NMR

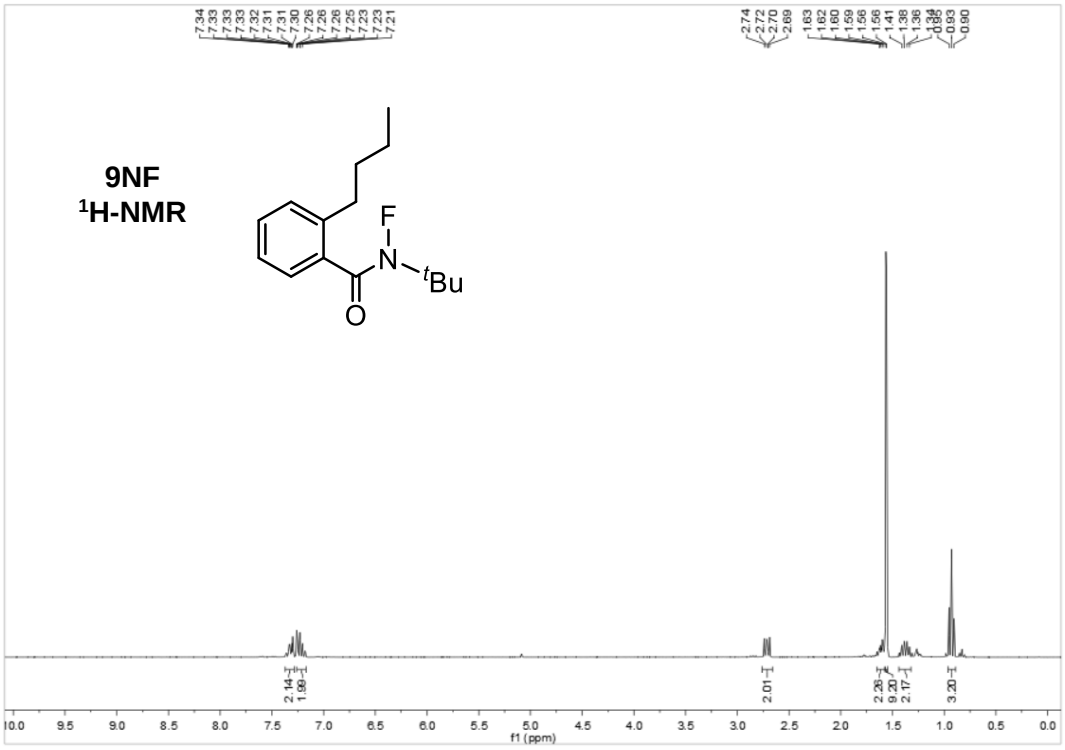

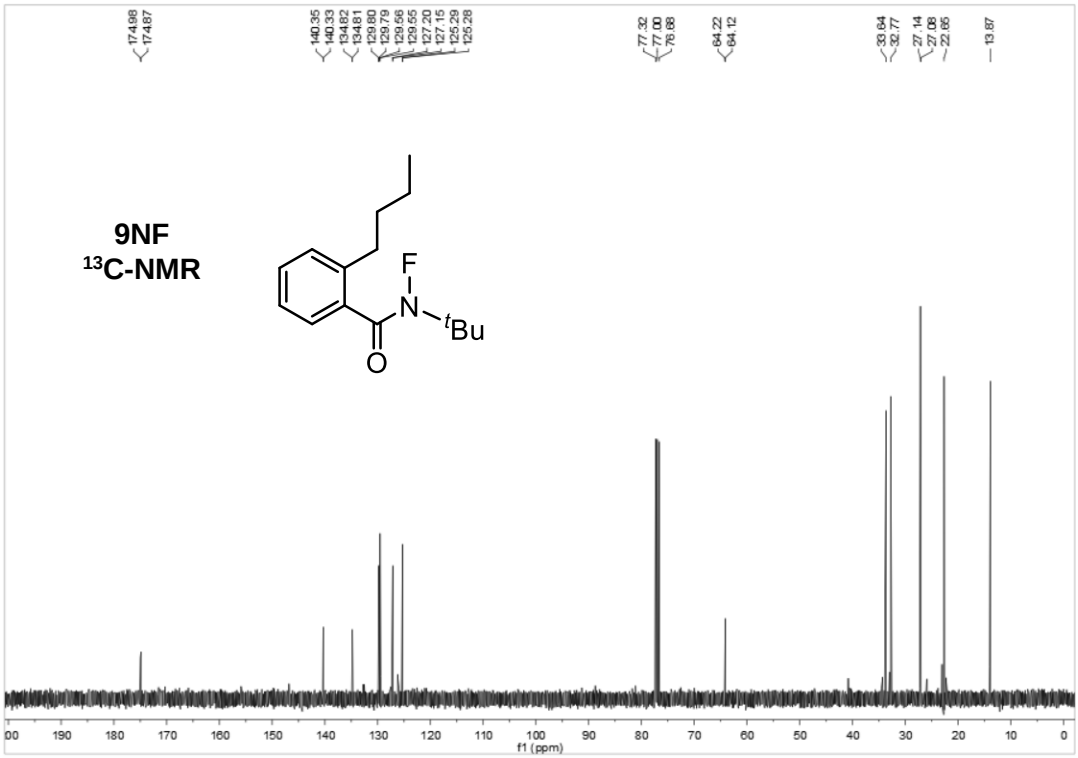
174.98
174.87
140.35
140.33
134.62
134.61
129.80
129.79
129.66
129.55
127.20
127.15
125.29
125.28
77.32
77.00
76.68
64.22
64.12
33.64
32.77
27.14
27.08
22.65
13.87
9NF
13C-NMR
F
N
tBu
O
f1 (ppm)

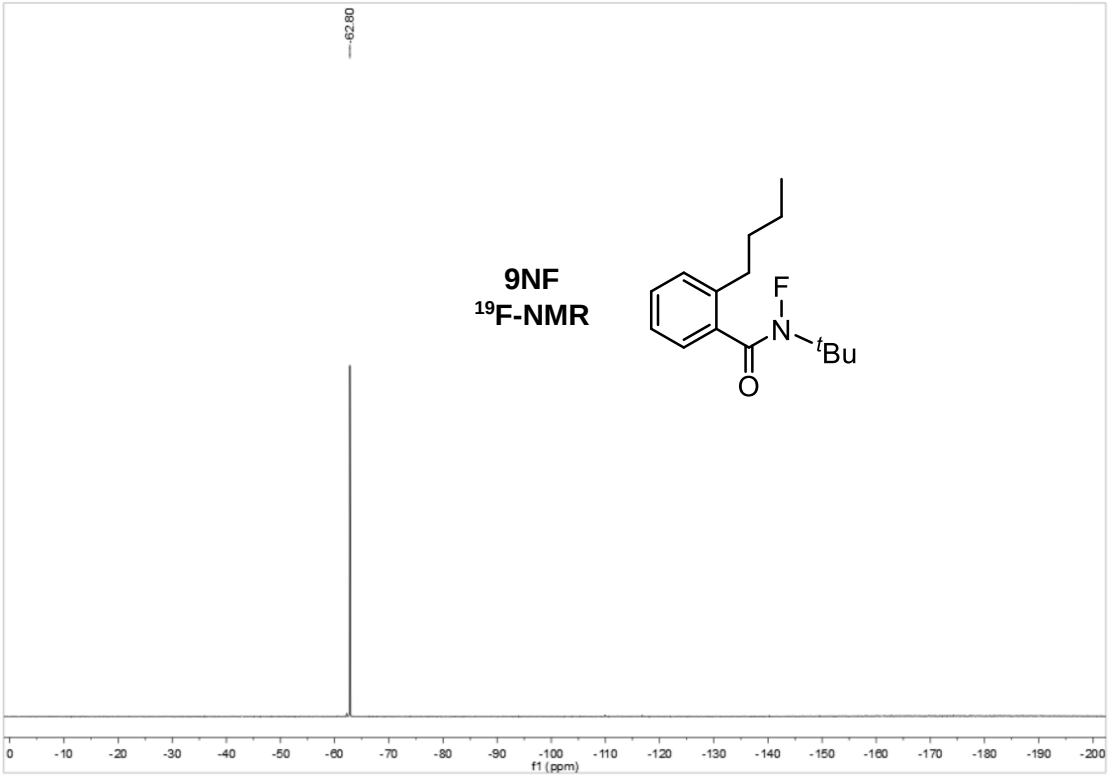
-62.80
9NF
19F-NMR
F
N
tBu
O
f1 (ppm)

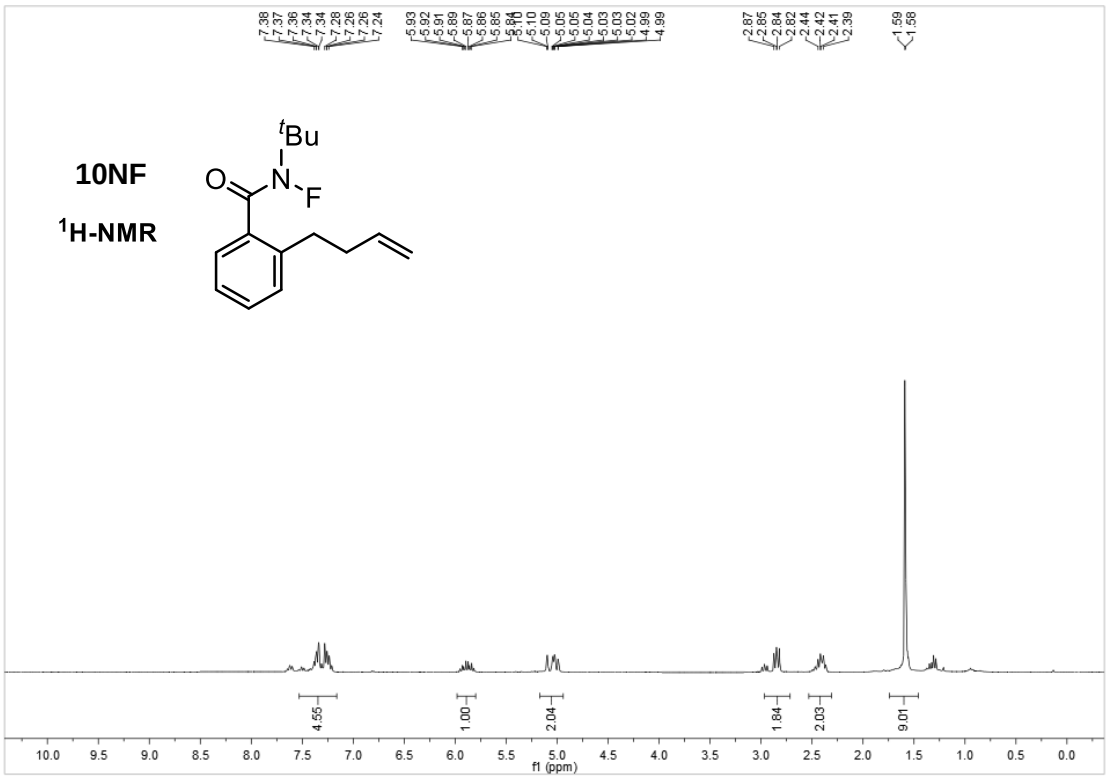
10NF
1H-NMR
tBu
O
N
F
f1 (ppm)

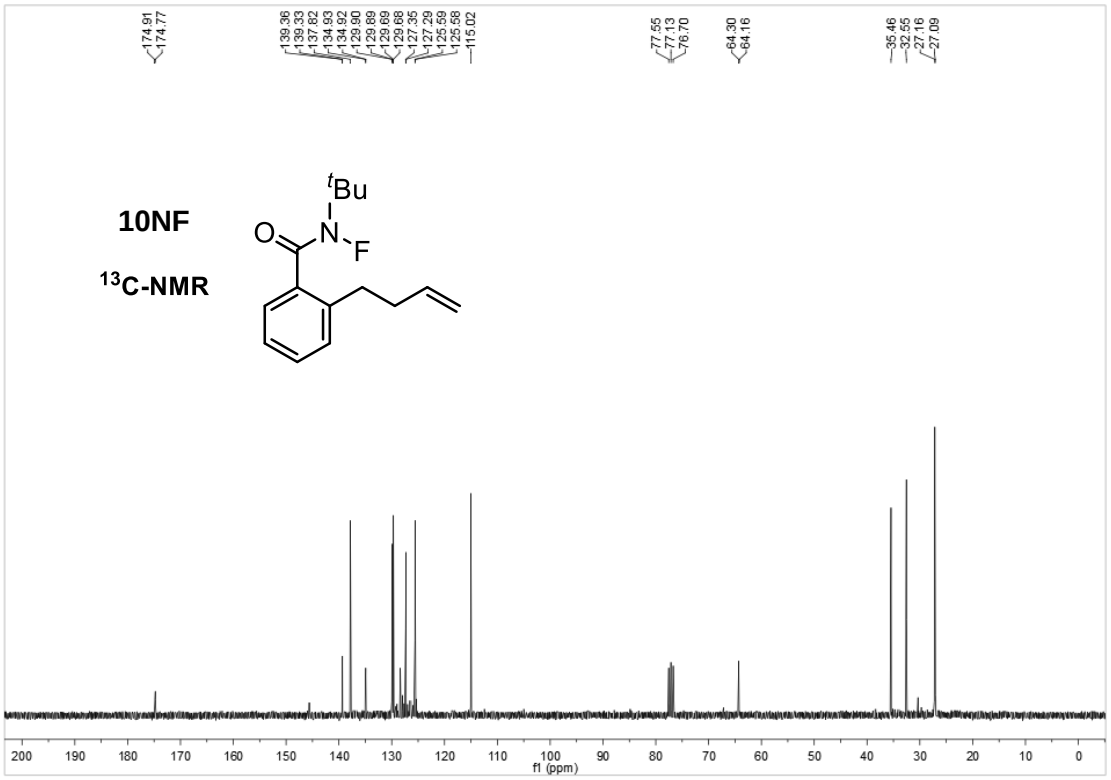
10NF
13C-NMR
tBu
O
N
F
f1 (ppm)

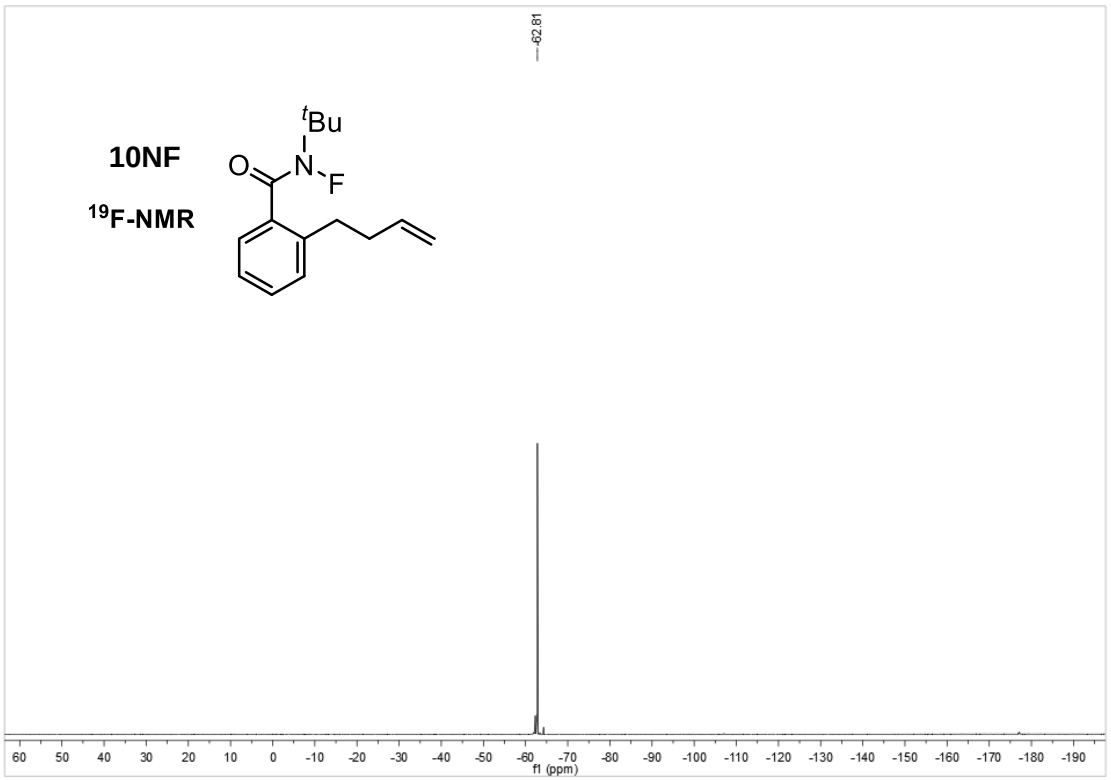
10NF
19F-NMR
tBu
O
N
F
-62.81
f1 (ppm)

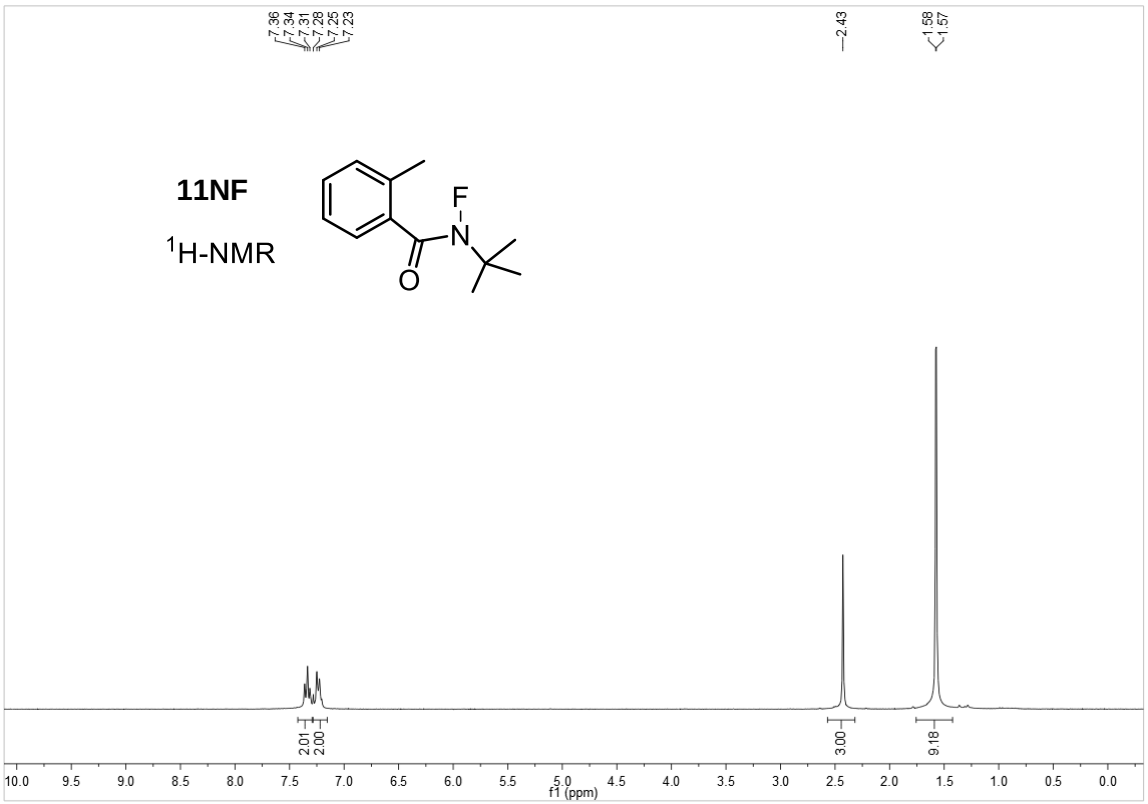
11NF
1H-NMR
F
N
O
7.36
7.34
7.31
7.28
7.25
7.23
2.43
1.58
1.57
2.01
2.00
3.00
9.18
f1 (ppm)

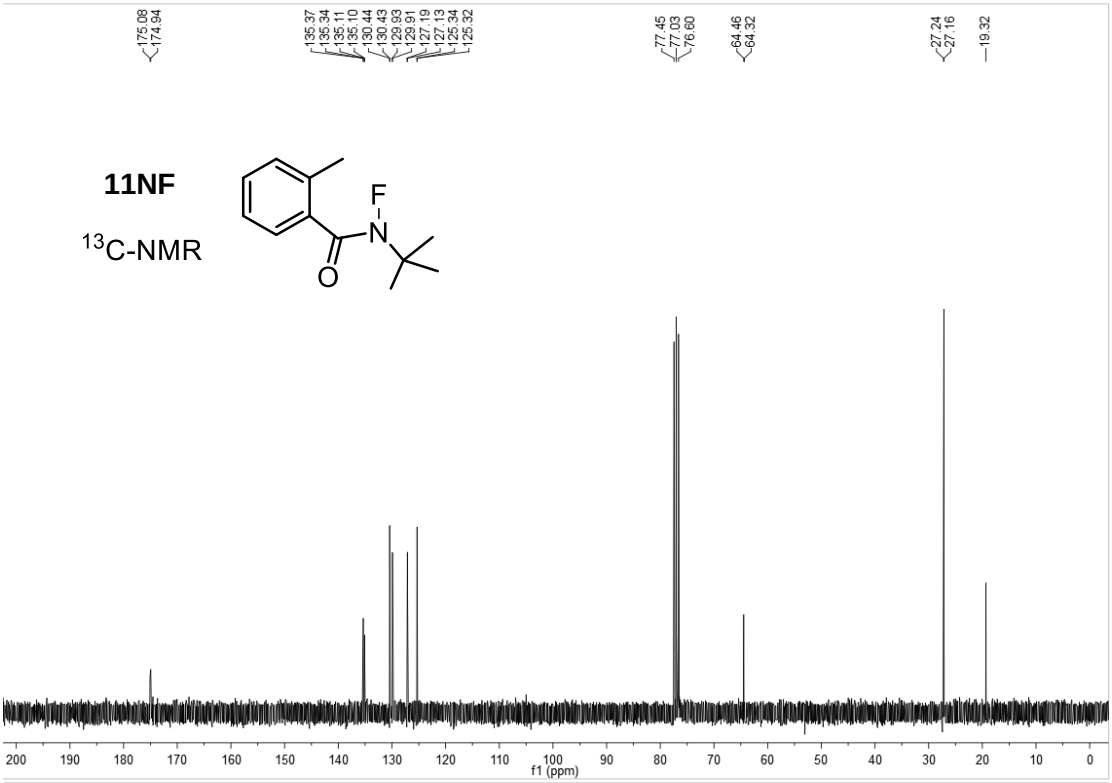
175.08
174.94
135.37
135.34
135.11
135.10
130.44
130.43
129.93
129.91
127.19
127.13
125.34
125.32
77.45
77.03
76.60
64.46
64.32
27.24
27.16
19.32
11NF
13C-NMR
F
N
O
200 190 180 170 160 150 140 130 120 110 100 90 80 70 60 50 40 30 20 10 0
f1 (ppm)

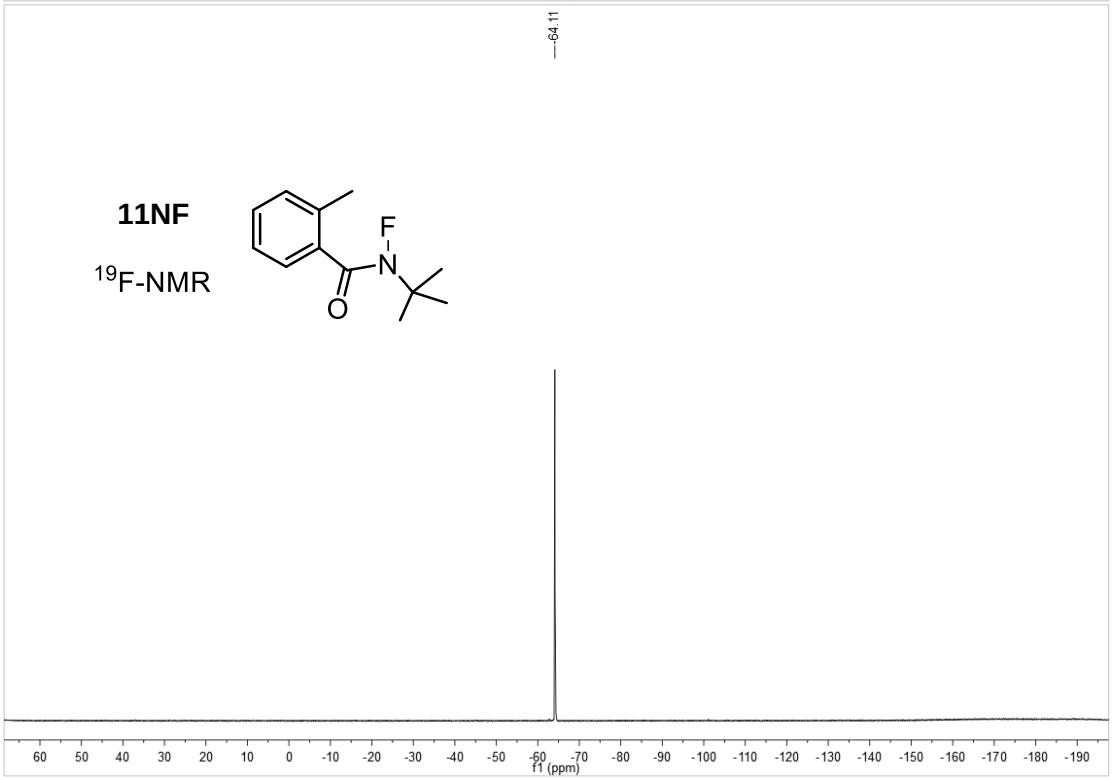
-64.11
11NF
19F-NMR
F
N
O
60 50 40 30 20 10 0 -10 -20 -30 -40 -50 -60 -70 -80 -90 -100 -110 -120 -130 -140 -150 -160 -170 -180 -190
f1 (ppm)

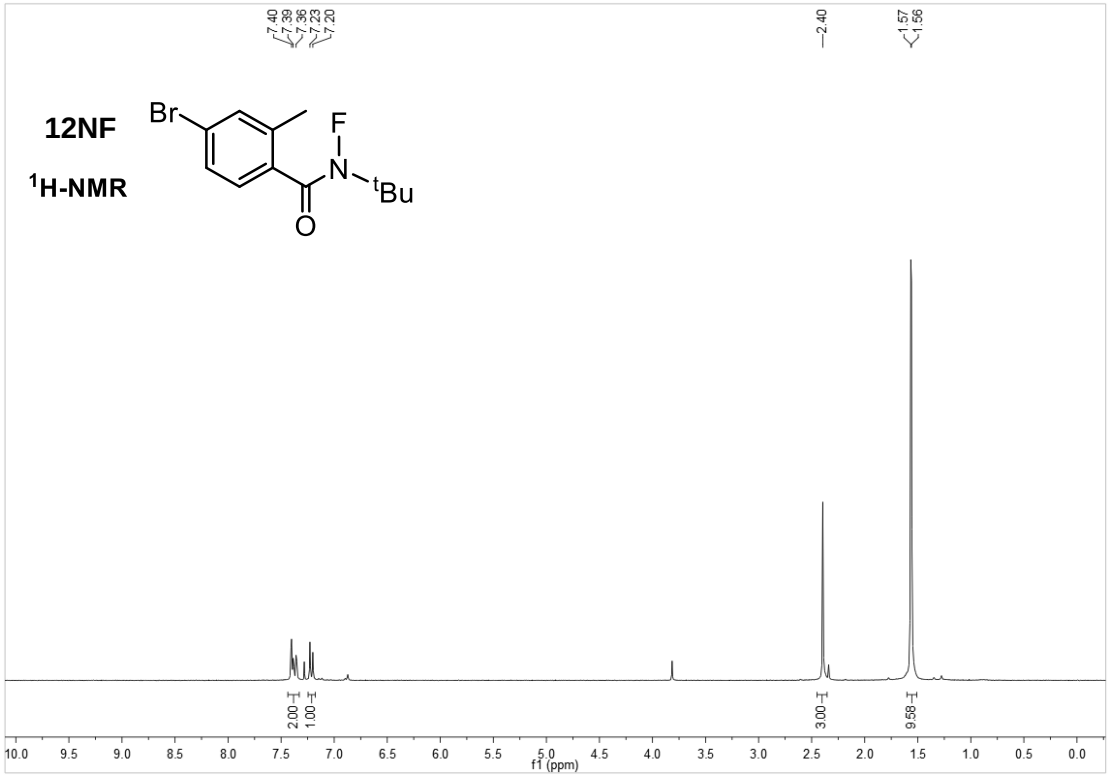
7.40
7.39
7.36
7.23
7.20
2.40
1.57
1.56
12NF
1H-NMR
Br
F
N
tBu
O
2.00
1.00
3.00
9.58
f1 (ppm)

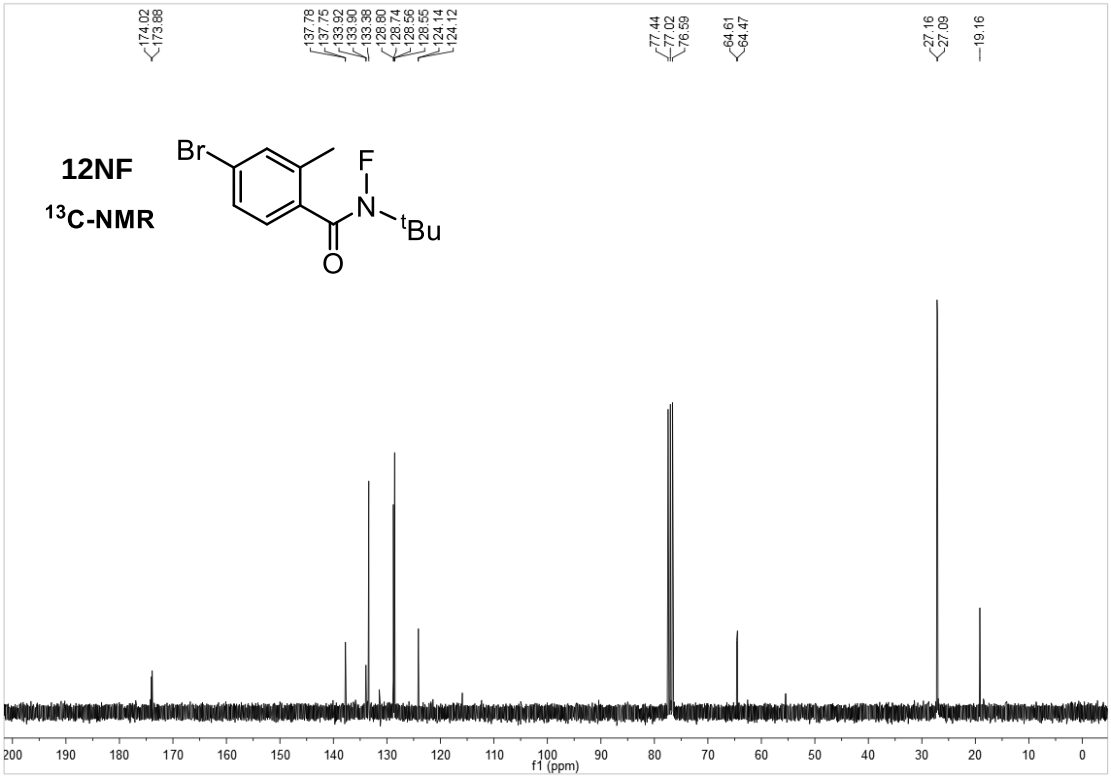
174.02
173.88
137.78
137.75
133.92
133.90
133.38
128.80
128.74
128.56
128.55
124.14
124.12
77.44
77.02
76.59
64.61
64.47
27.16
27.09
19.16
12NF
13C-NMR
Br
F
N
tBu
O
f1 (ppm)

12NF

^{19}F-NMR

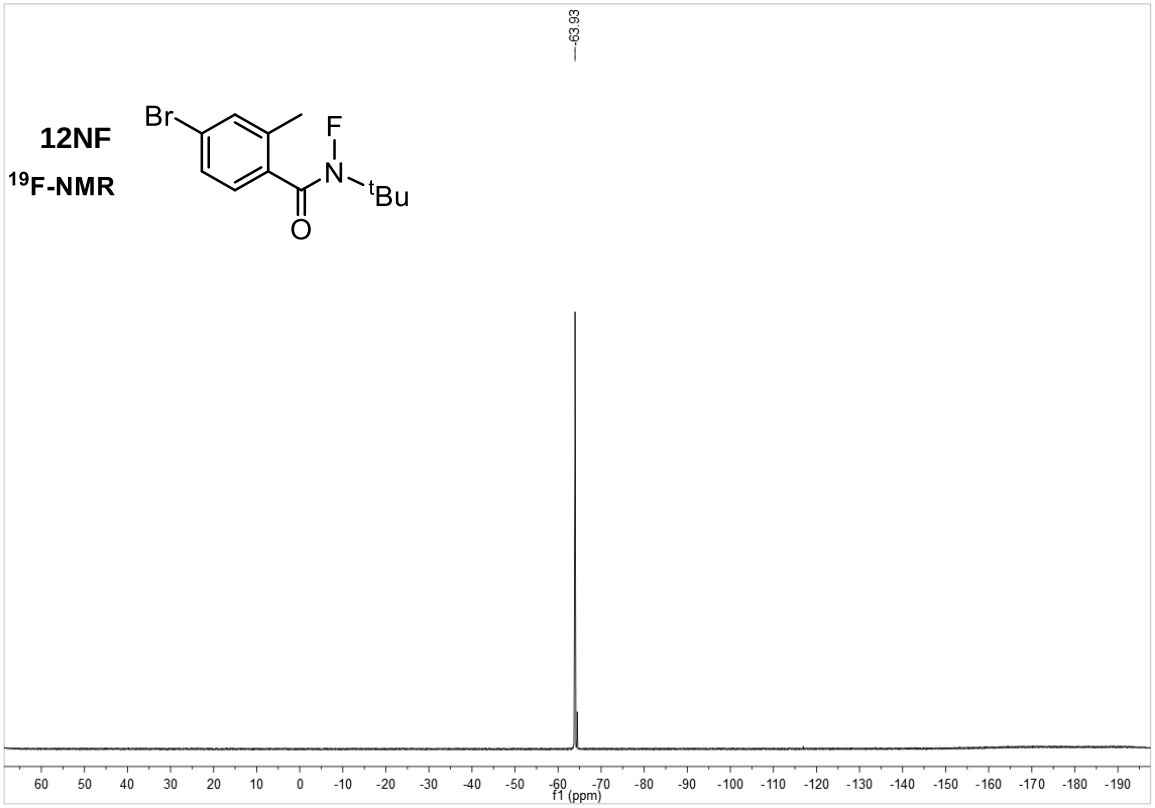

13NF

^{1}H-NMR

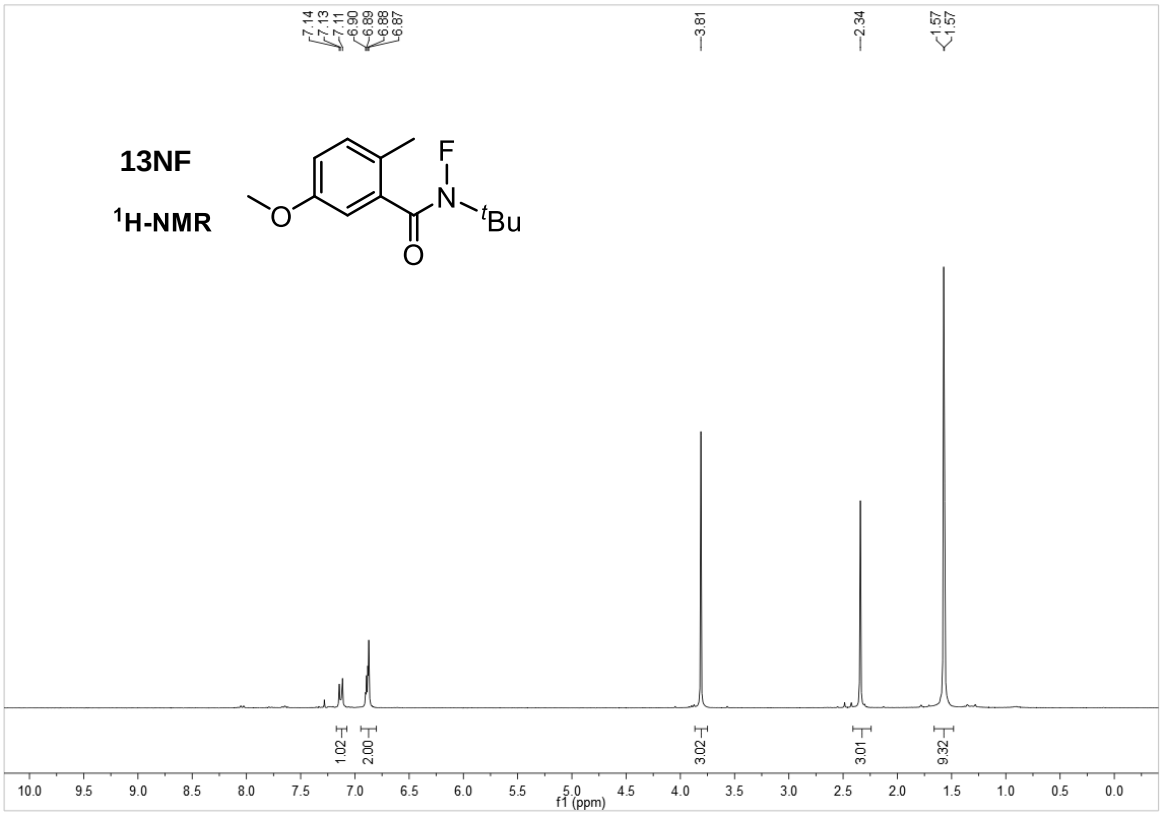

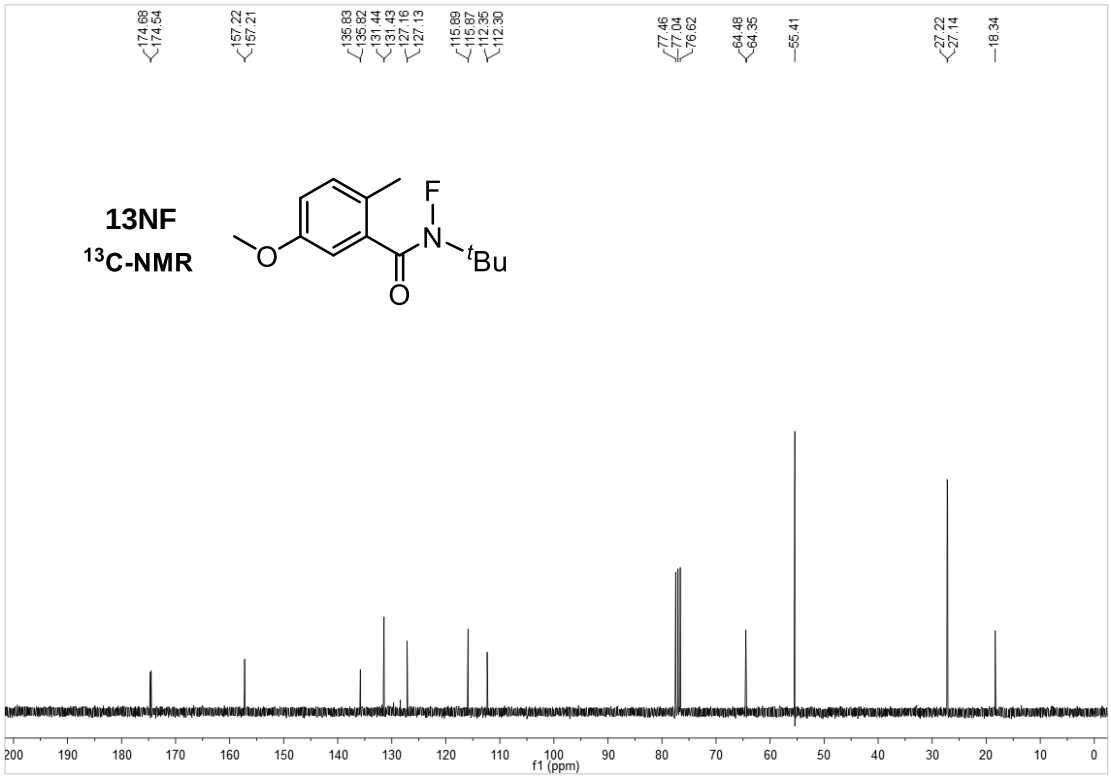
174.68
174.54
157.22
157.21
135.83
135.82
131.44
131.43
127.16
127.13
115.89
115.67
112.35
112.30
77.46
77.04
76.62
64.48
64.35
55.41
27.22
27.14
18.34
13NF
13C-NMR
F
N
tBu
O
O
f1 (ppm)

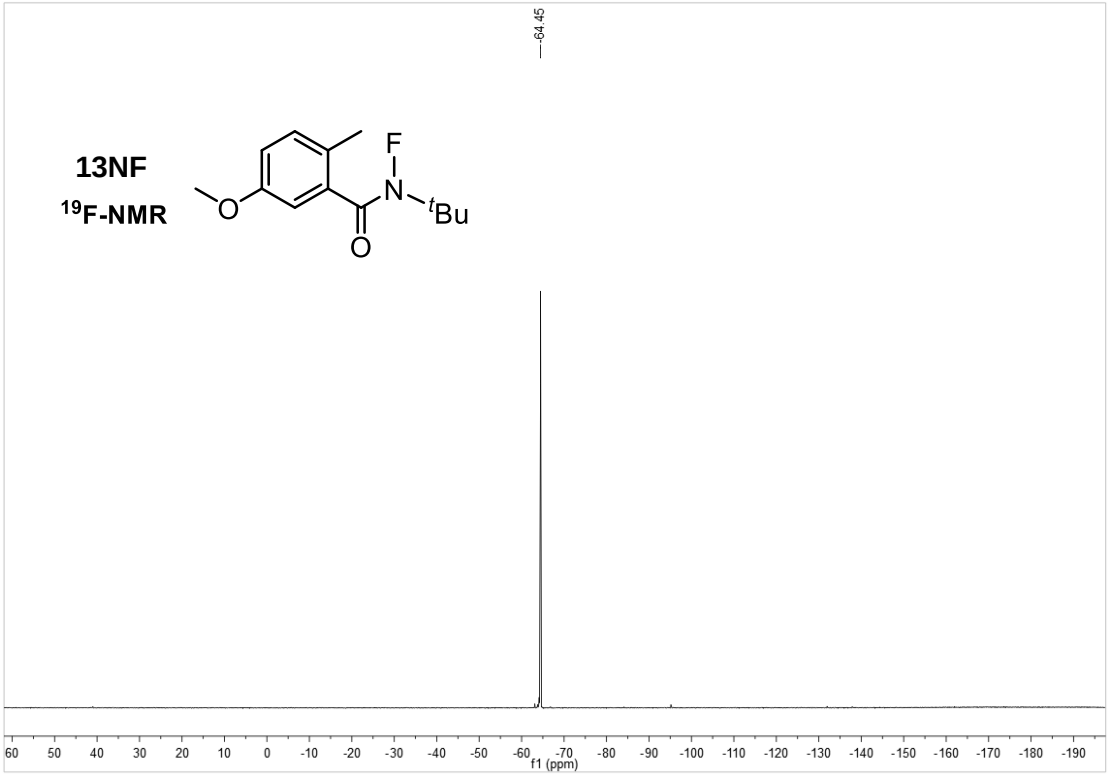
64.45
13NF
19F-NMR
F
N
tBu
O
O
f1 (ppm)

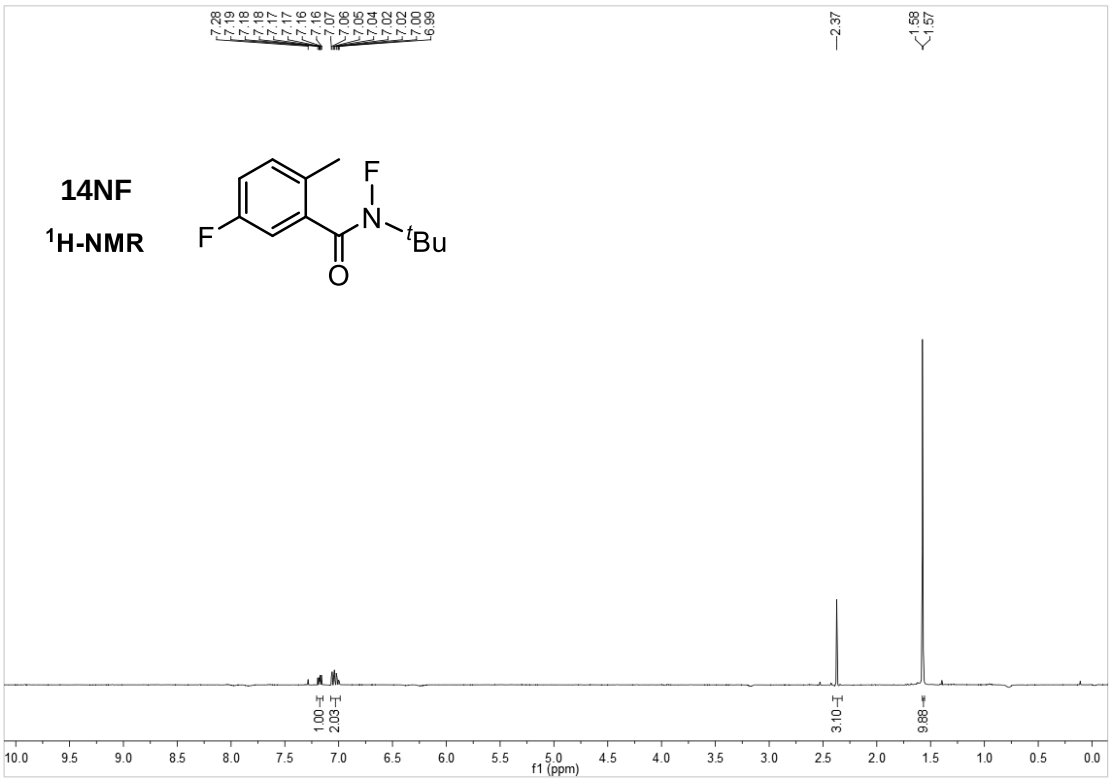
14NF
1H-NMR
F
N
tBu
O
7.28
7.19
7.18
7.18
7.17
7.17
7.16
7.16
7.07
7.06
7.05
7.04
7.02
7.02
7.00
6.99
2.37
1.58
1.57
1.00
2.03
3.10
9.88
f1 (ppm)

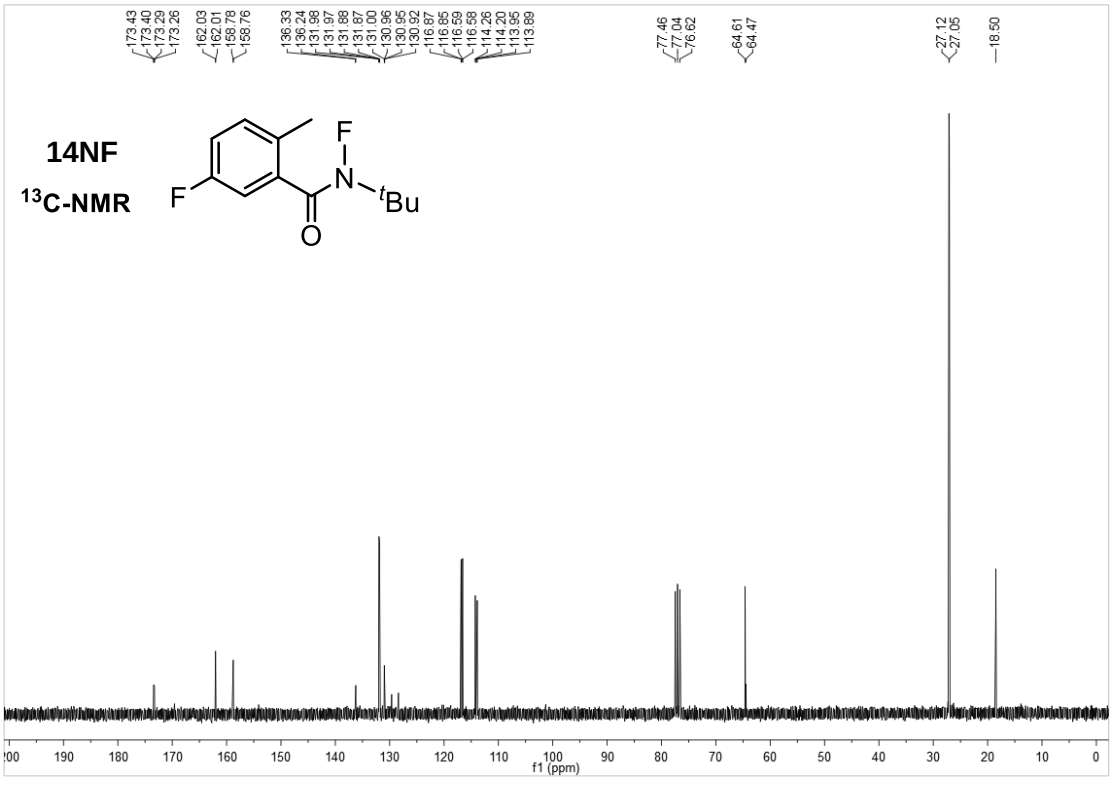
14NF
13C-NMR
F
N
tBu
O
173.43
173.40
173.29
173.26
162.03
162.01
158.78
158.76
136.33
136.24
131.98
131.97
131.88
131.87
131.00
130.96
130.95
130.92
116.87
116.85
116.59
116.58
114.26
114.20
113.95
113.89
77.46
77.04
76.62
64.61
64.47
27.12
27.05
18.50
f1 (ppm)

14NF

^{19}F-NMR

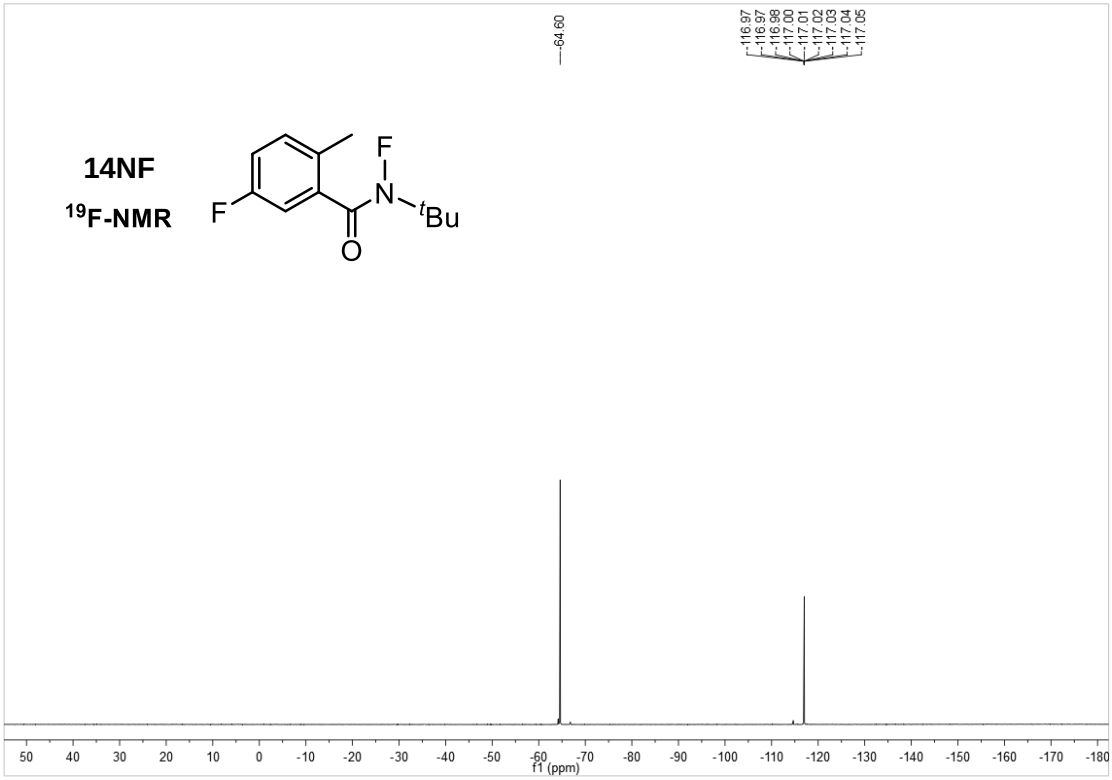

15NF

^{1}H-NMR

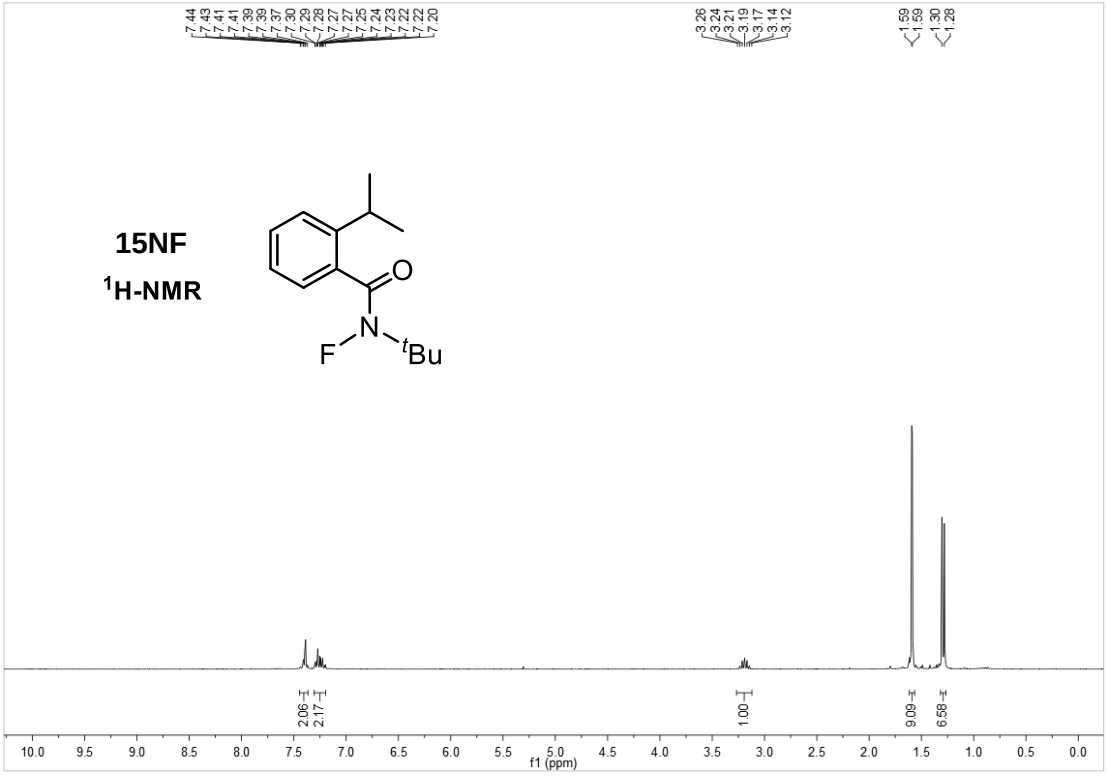

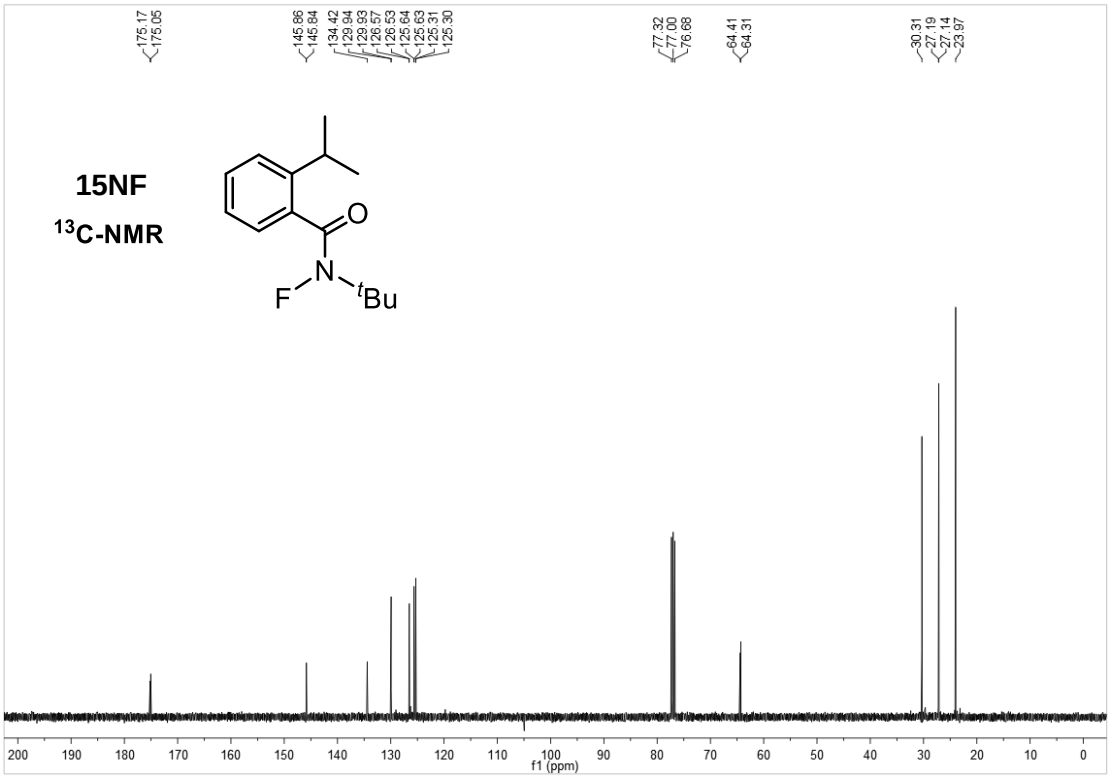
175.17
175.05
145.86
145.84
134.42
129.94
129.93
126.57
126.53
125.64
125.63
125.31
125.30
77.32
77.00
76.68
64.41
64.31
30.31
27.19
27.14
23.97
15NF
13C-NMR
O
N
F
tBu
200 190 180 170 160 150 140 130 120 110 100 90 80 70 60 50 40 30 20 10 0
f1 (ppm)

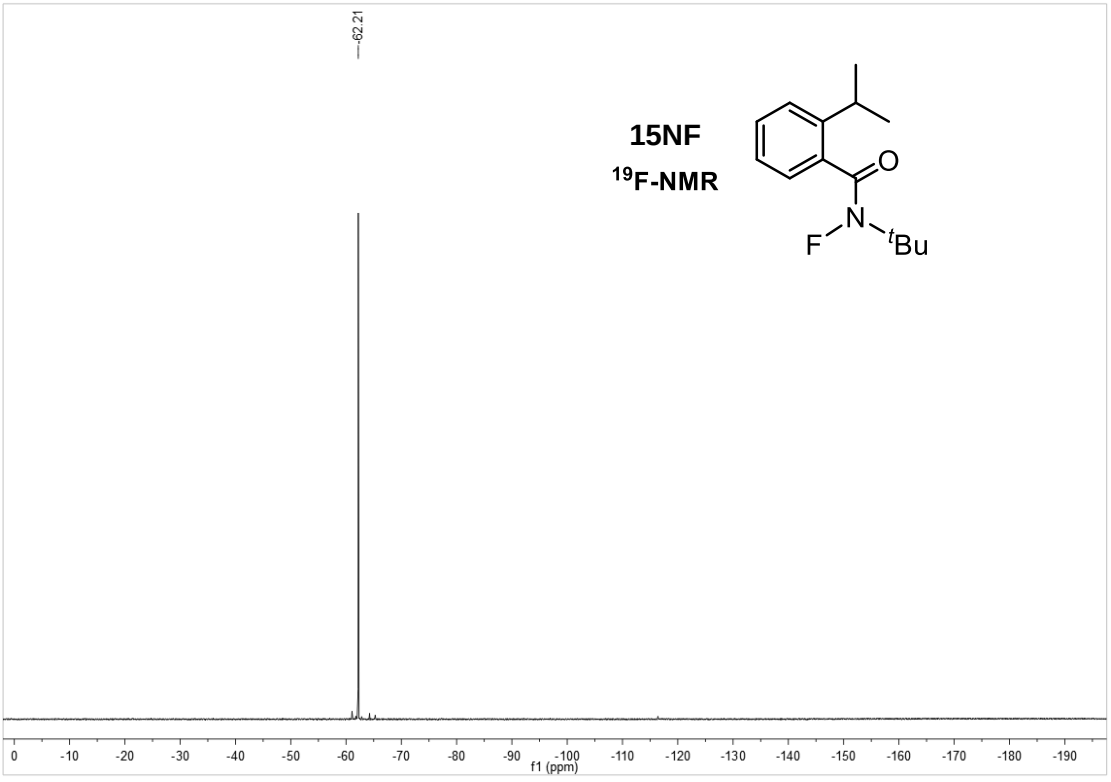
-62.21
15NF
19F-NMR
O
N
F
tBu
0 -10 -20 -30 -40 -50 -60 -70 -80 -90 -100 -110 -120 -130 -140 -150 -160 -170 -180 -190
f1 (ppm)

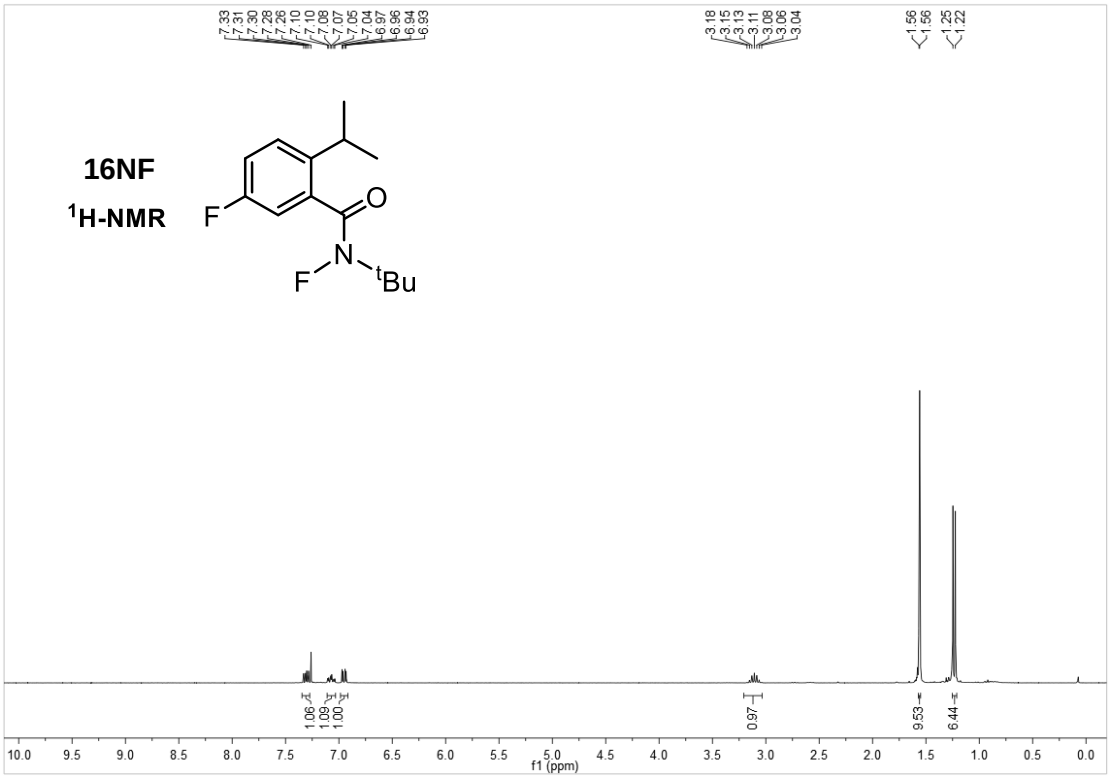
16NF
1H-NMR
F
O
N
F
tBu
7.33
7.31
7.30
7.28
7.26
7.10
7.08
7.07
7.05
7.04
6.97
6.96
6.94
6.93
3.18
3.15
3.13
3.11
3.08
3.06
3.04
1.56
1.56
1.25
1.22
1.06
1.09
1.00
0.97
9.53
6.44
f1 (ppm)

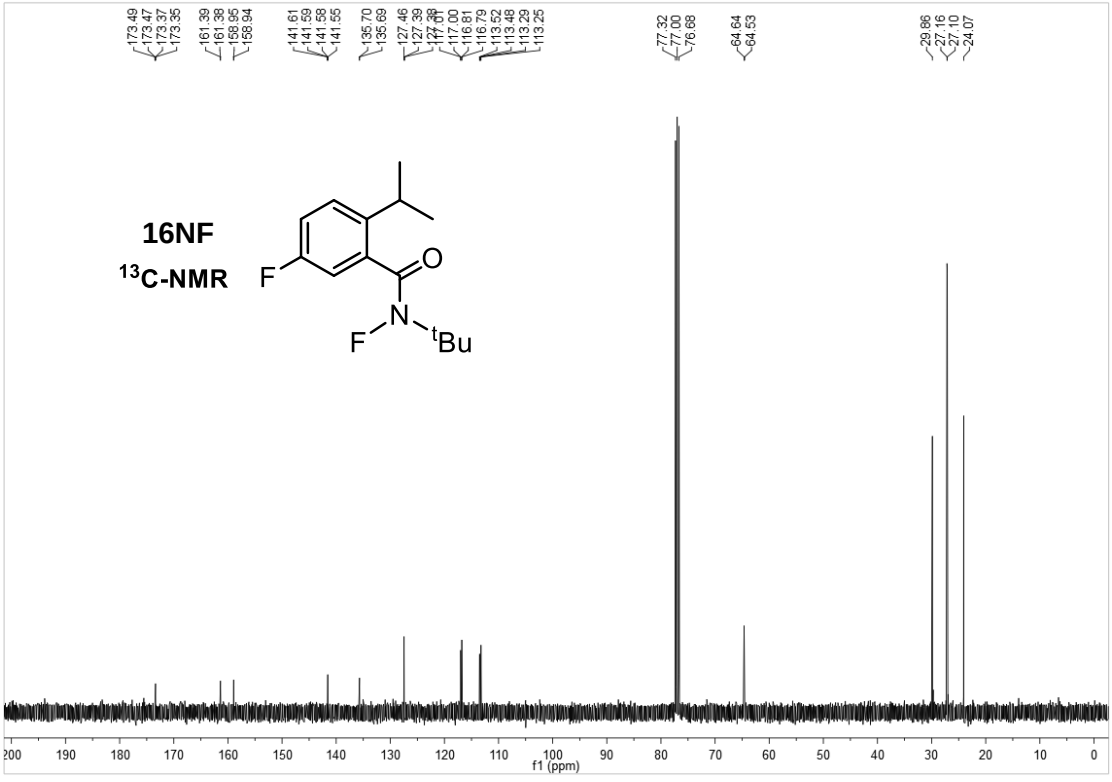
16NF
13C-NMR
F
O
N
F
tBu
173.49
173.47
173.37
173.35
161.39
161.38
158.95
158.94
141.61
141.59
141.58
141.55
135.70
135.69
127.46
127.39
117.00
116.81
116.79
113.52
113.48
113.29
113.25
77.32
77.00
76.68
64.64
64.53
29.86
27.16
27.10
24.07
f1 (ppm)

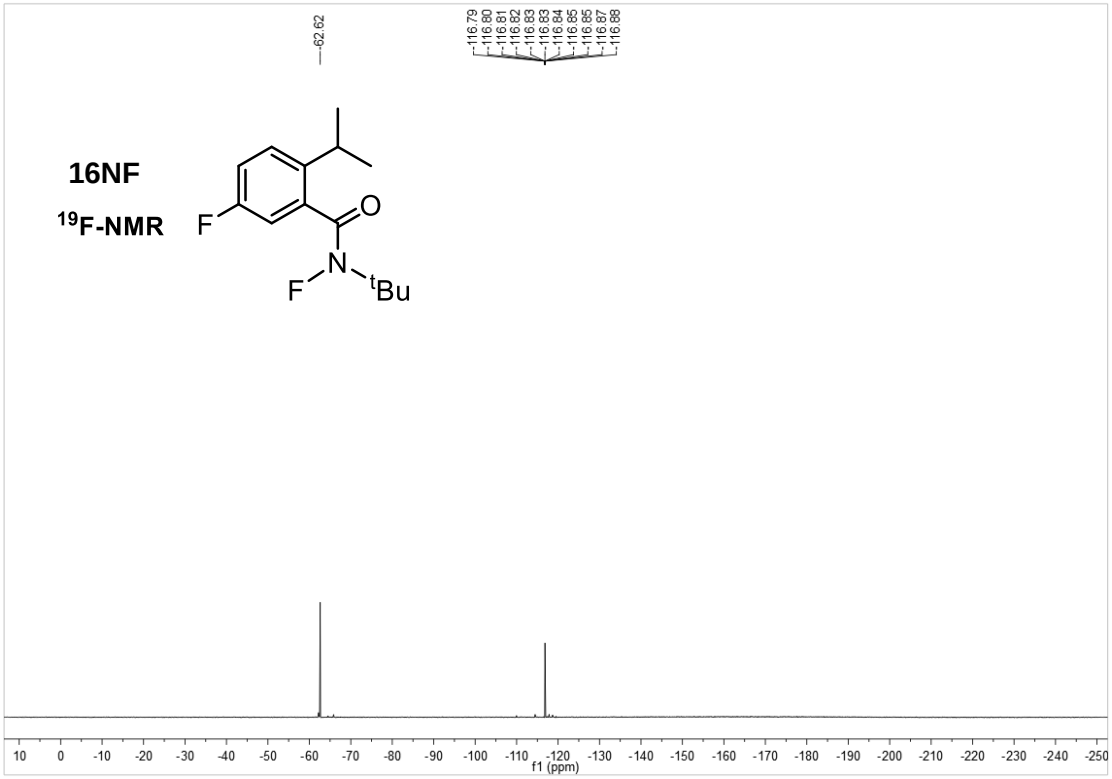
16NF
19F-NMR
F
O
N
F
tBu
-62.62
-116.79
-116.80
-116.81
-116.82
-116.83
-116.83
-116.84
-116.85
-116.85
-116.87
-116.88
f1 (ppm)

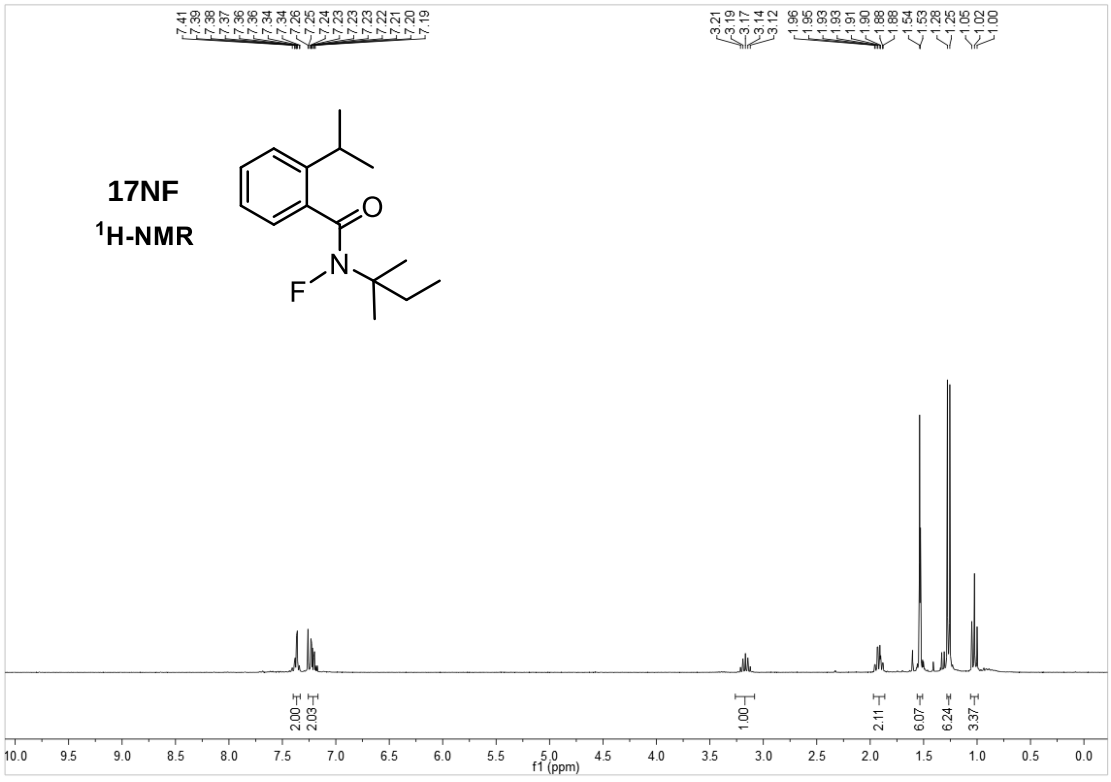
17NF
1H-NMR
O
N
F
7.41
7.39
7.38
7.37
7.36
7.36
7.34
7.34
7.26
7.25
7.24
7.23
7.23
7.23
7.22
7.21
7.20
7.19
3.21
3.19
3.17
3.14
3.12
1.96
1.95
1.93
1.93
1.91
1.90
1.88
1.88
1.54
1.53
1.28
1.25
1.05
1.02
1.00
2.00
2.03
1.00
2.11
6.07
6.24
3.37
f1 (ppm)

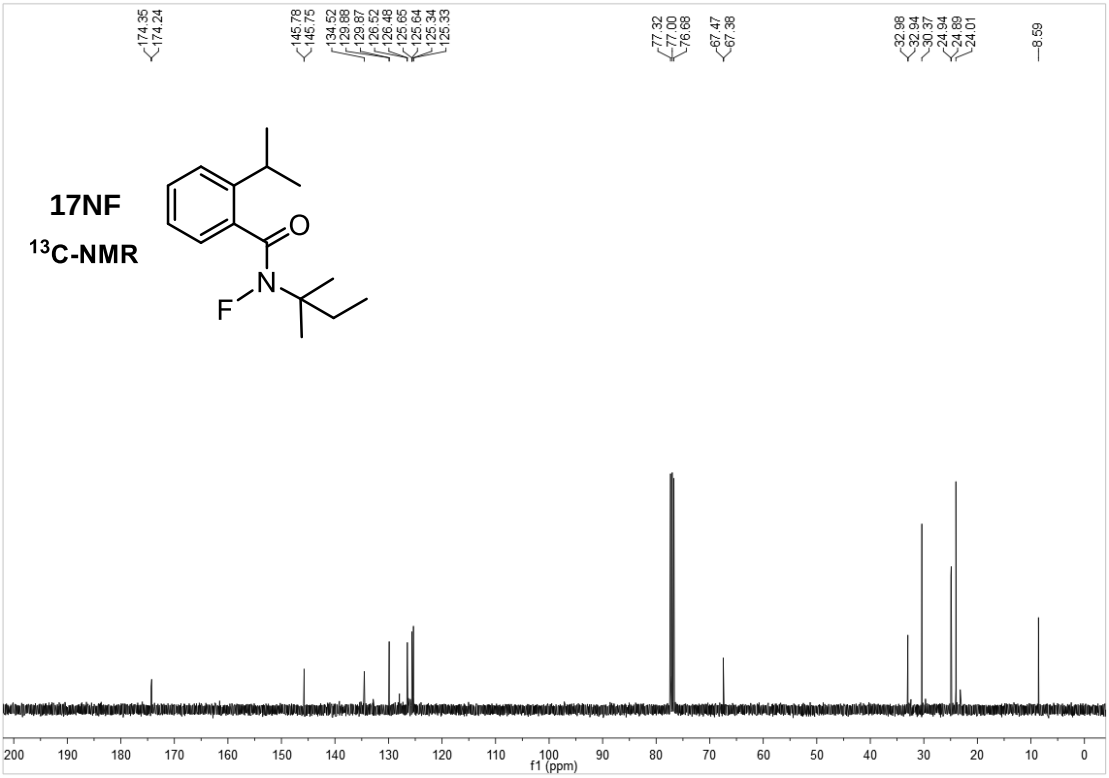
174.35
174.24
145.78
145.75
134.52
129.88
129.87
126.52
126.48
125.65
125.64
125.34
125.33
77.32
77.00
76.68
67.47
67.38
32.98
32.94
30.37
24.94
24.89
24.01
8.59
17NF
13C-NMR
O
N
F
200 190 180 170 160 150 140 130 120 110 100 90 80 70 60 50 40 30 20 10 0
f1 (ppm)

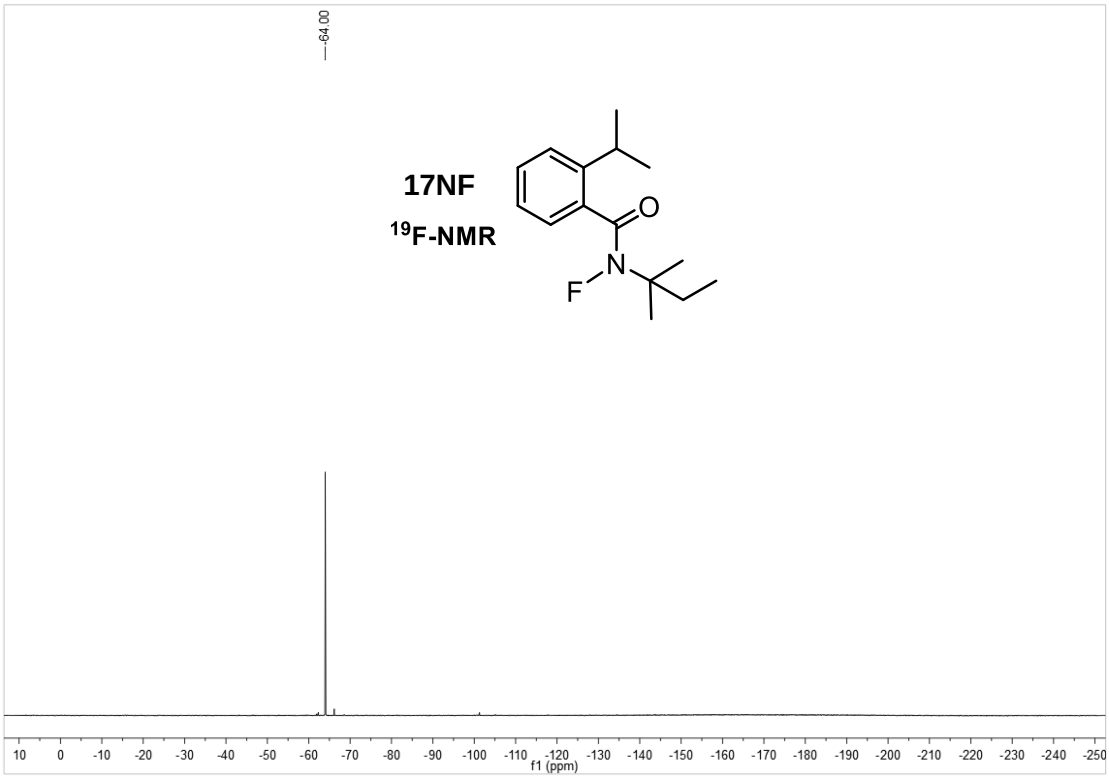
64.00
17NF
19F-NMR
O
N
F
10 0 -10 -20 -30 -40 -50 -60 -70 -80 -90 -100 -110 -120 -130 -140 -150 -160 -170 -180 -190 -200 -210 -220 -230 -240 -250
f1 (ppm)

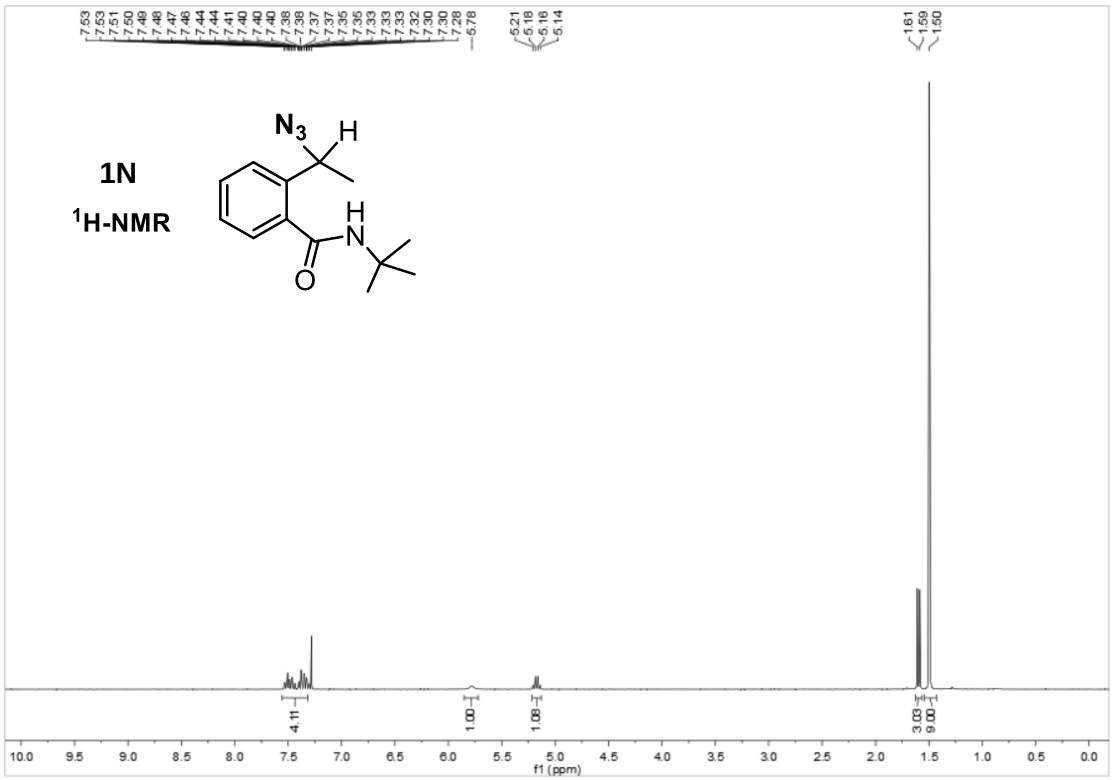
1N
1H-NMR
N3
H
H
N
O
f1 (ppm)

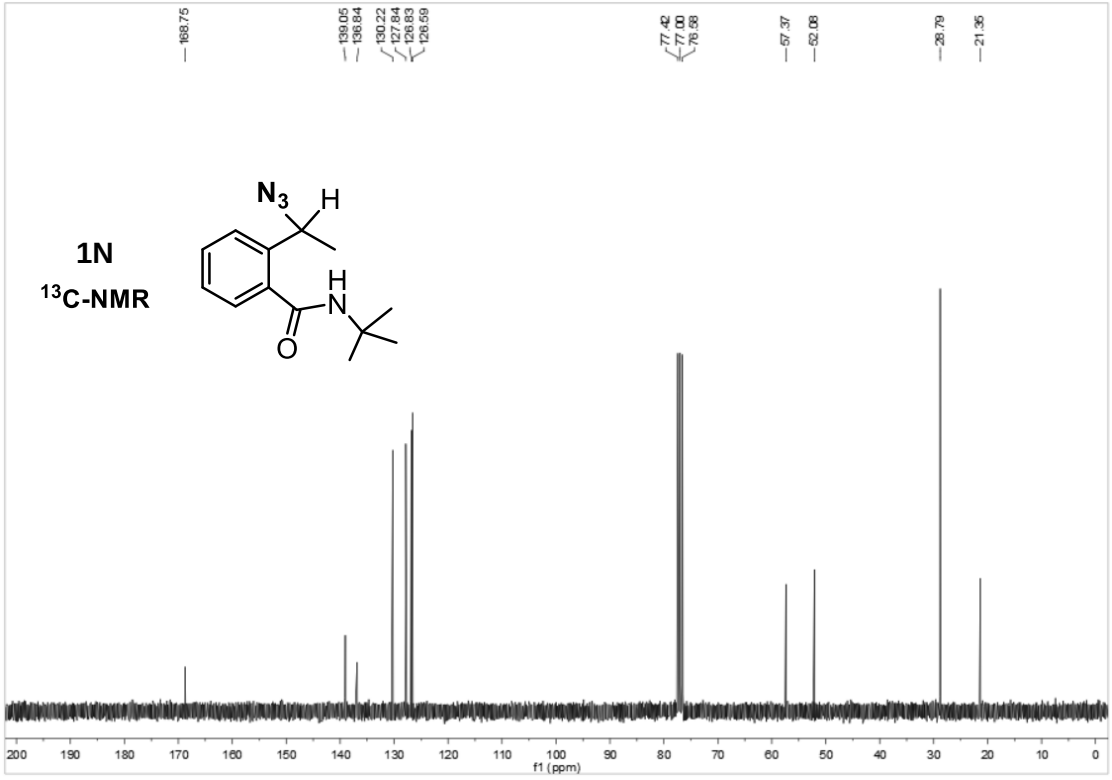
1N
13C-NMR
N3
H
H
N
O
f1 (ppm)

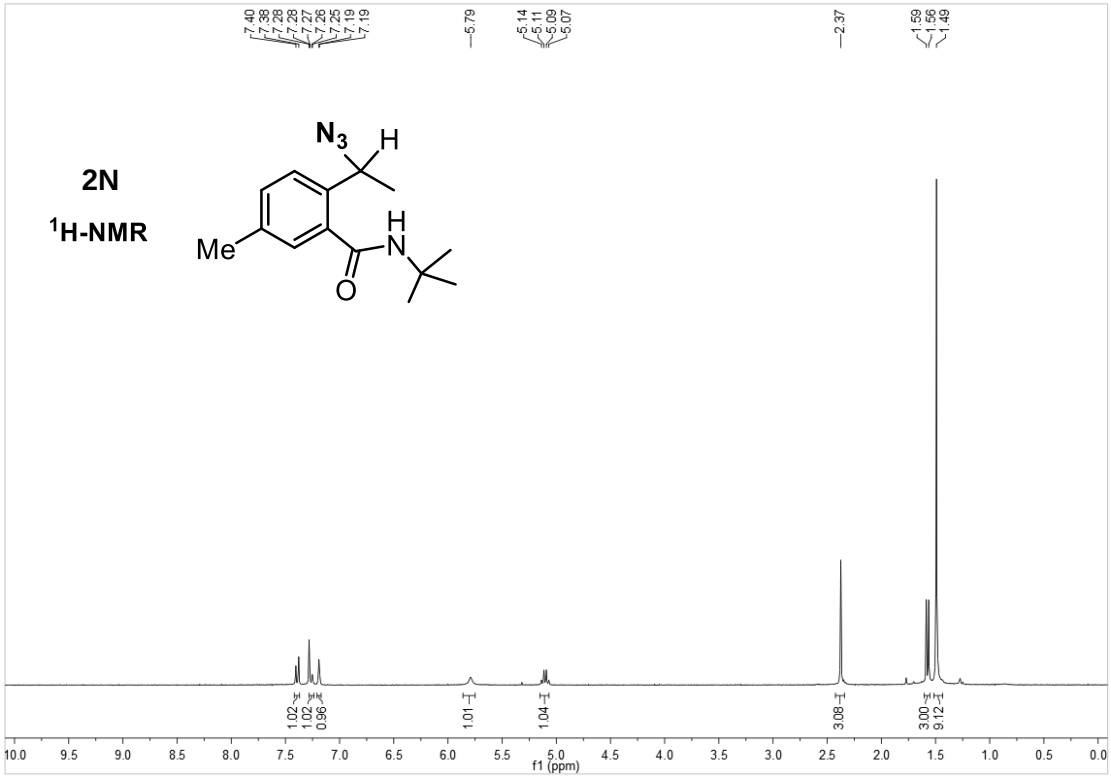
7.40
7.38
7.28
7.28
7.27
7.26
7.25
7.19
7.19
5.79
5.14
5.11
5.09
5.07
2.37
1.59
1.56
1.49
2N
1H-NMR
N3
H
Me
H
N
O
1.02
1.02
0.96
1.01
1.04
3.08
3.00
9.12
f1 (ppm)

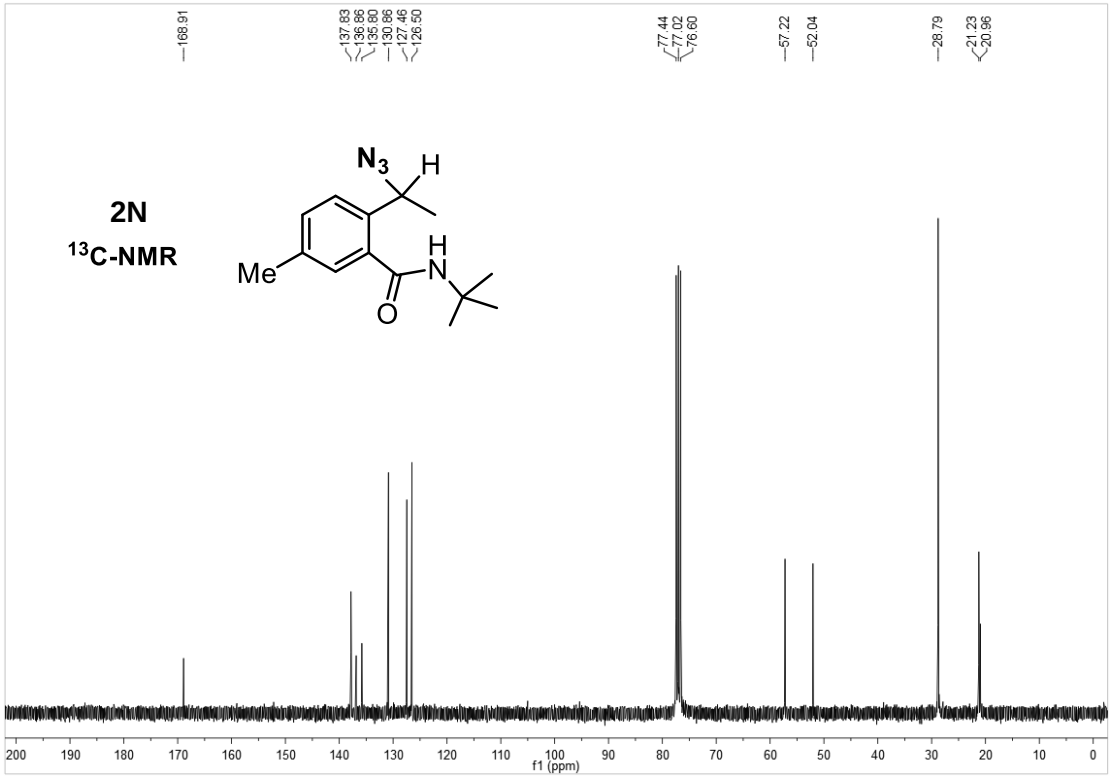
168.91
137.83
136.86
135.80
130.86
127.46
126.50
77.44
77.02
76.60
57.22
52.04
28.79
21.23
20.96
2N
13C-NMR
N3
H
Me
H
N
O
f1 (ppm)

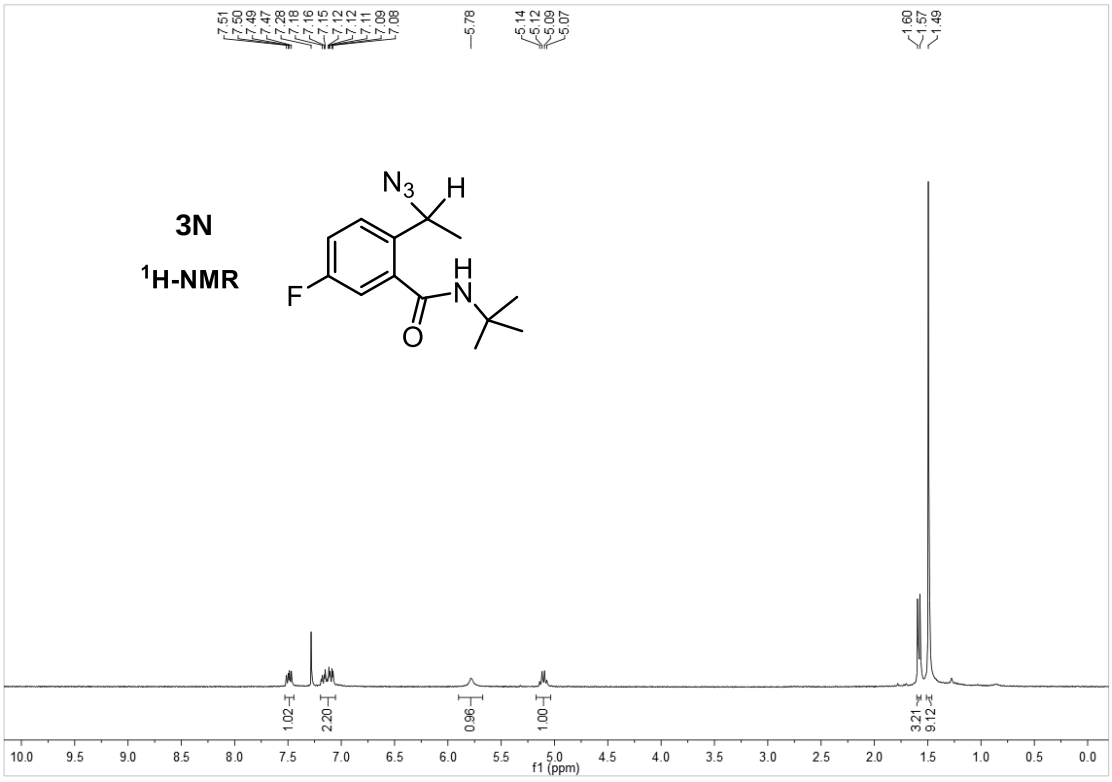
7.51
7.50
7.49
7.47
7.28
7.18
7.16
7.15
7.12
7.12
7.11
7.09
7.08
5.78
5.14
5.12
5.09
5.07
1.60
1.57
1.49
3N
1H-NMR
N3
H
F
H
N
O
1.02
2.20
0.96
1.00
3.21
9.12
f1 (ppm)

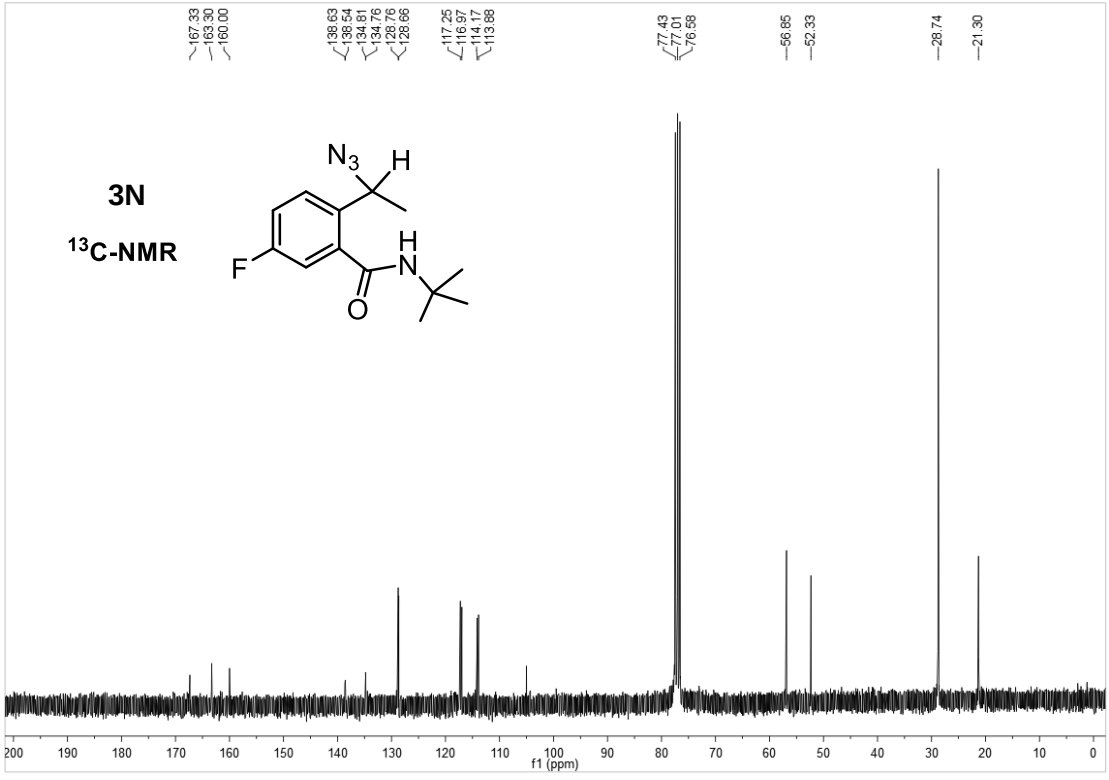
167.33
163.30
160.00
138.63
138.54
134.81
134.76
128.76
128.66
117.25
116.97
114.17
113.88
77.43
77.01
76.58
56.85
52.33
28.74
21.30
3N
13C-NMR
N3
H
F
H
N
O
f1 (ppm)

3N

^{19}F-NMR

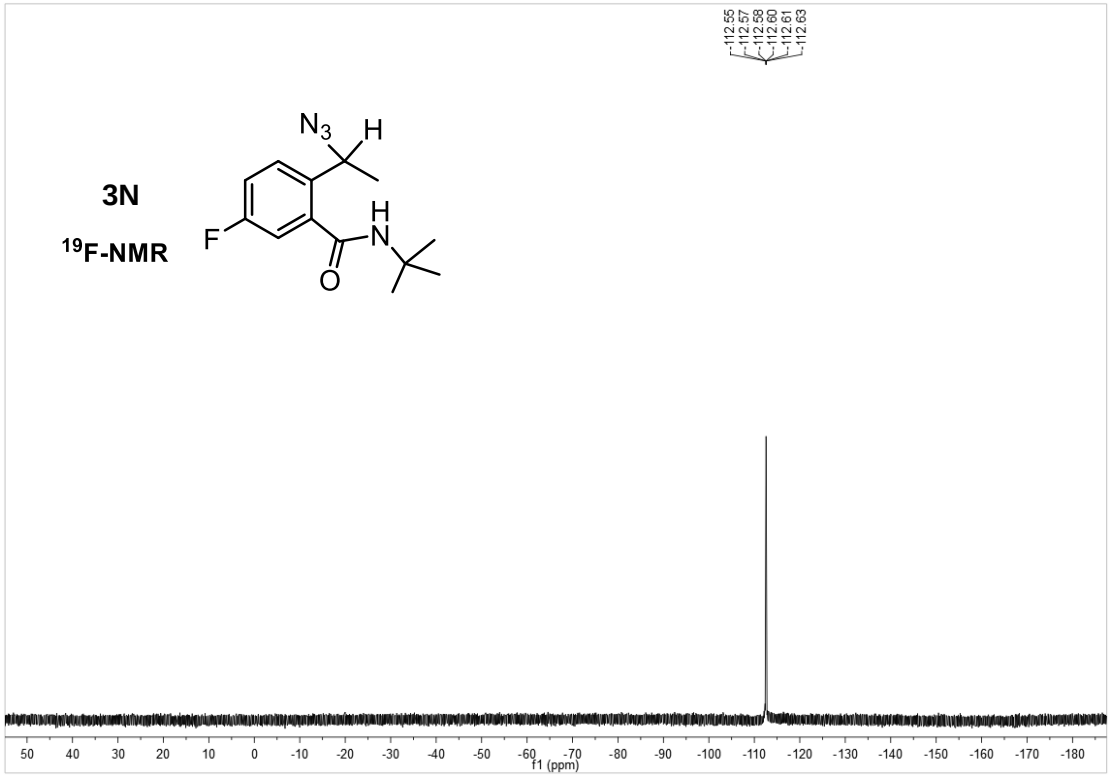

4N

^{1}H-NMR

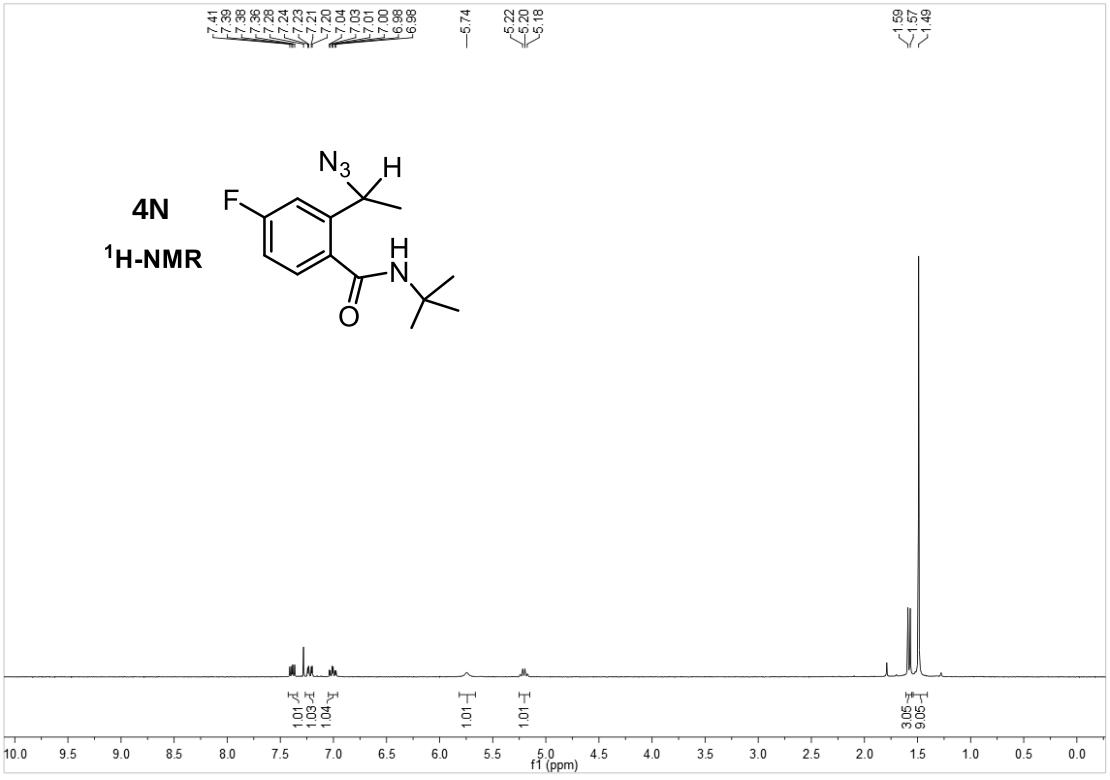

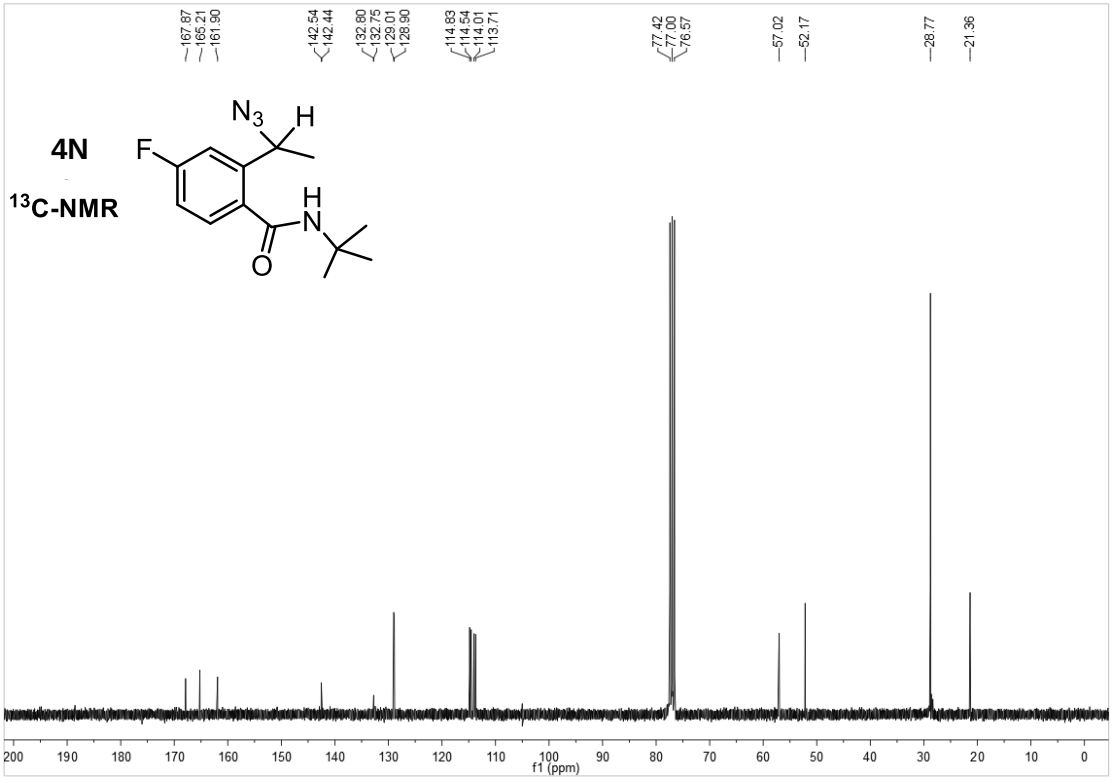
167.87
165.21
161.90
142.54
142.44
132.80
132.75
129.01
128.90
114.83
114.54
114.01
113.71
77.42
77.00
76.57
57.02
52.17
28.77
21.36
4N
13C-NMR
N3
H
F
H
N
O
200 190 180 170 160 150 140 130 120 110 100 90 80 70 60 50 40 30 20 10 0
f1 (ppm)

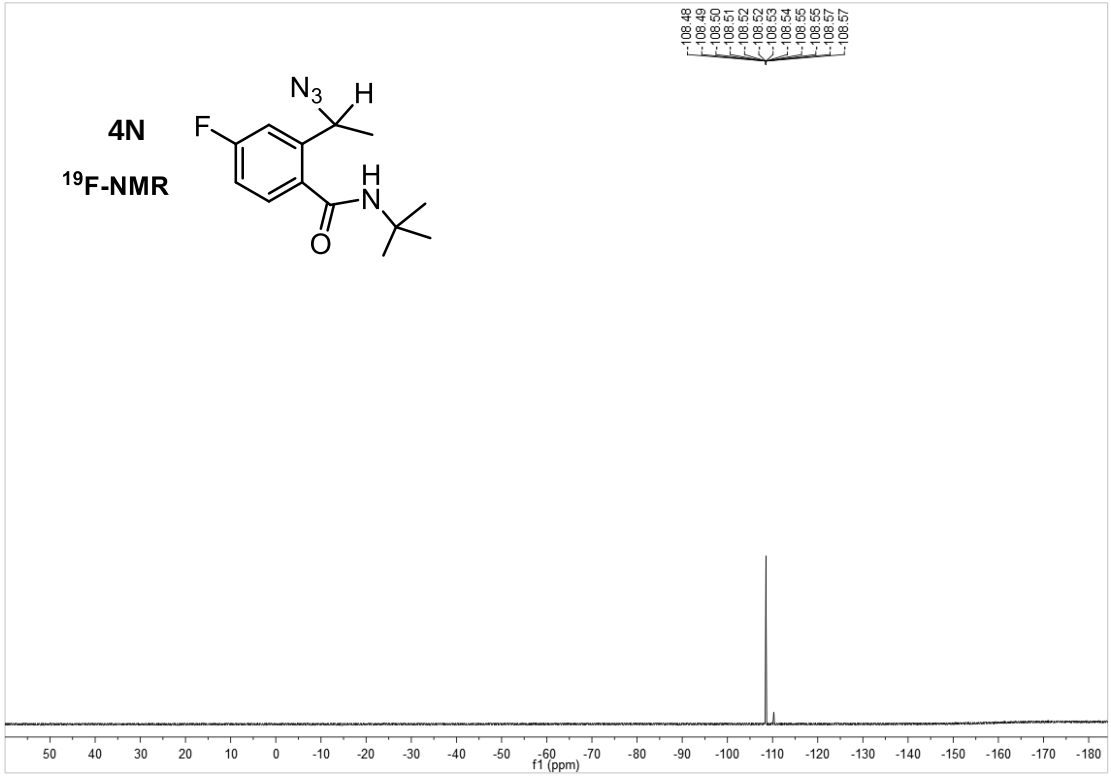
108.48
108.49
108.50
108.51
108.52
108.52
108.53
108.54
108.55
108.55
108.57
108.57
4N
19F-NMR
N3
H
F
H
N
O
50 40 30 20 10 0 -10 -20 -30 -40 -50 -60 -70 -80 -90 -100 -110 -120 -130 -140 -150 -160 -170 -180
f1 (ppm)

5N

^{1}H-NMR

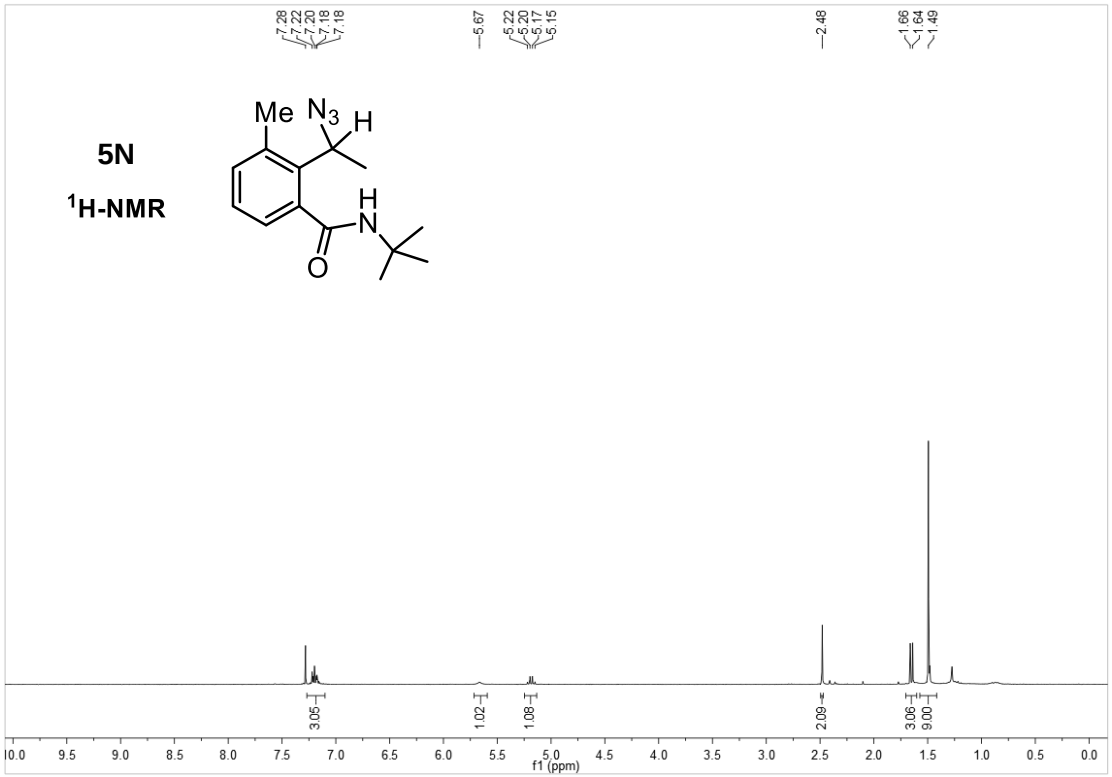

5N

^{13}C-NMR

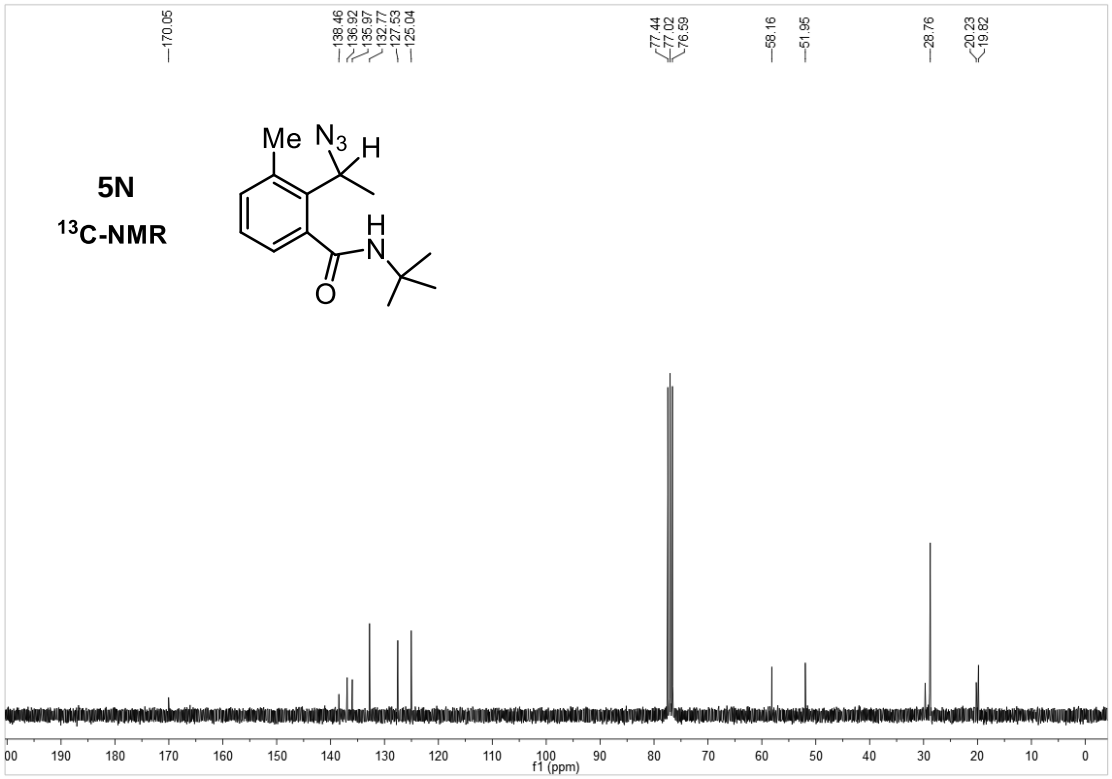

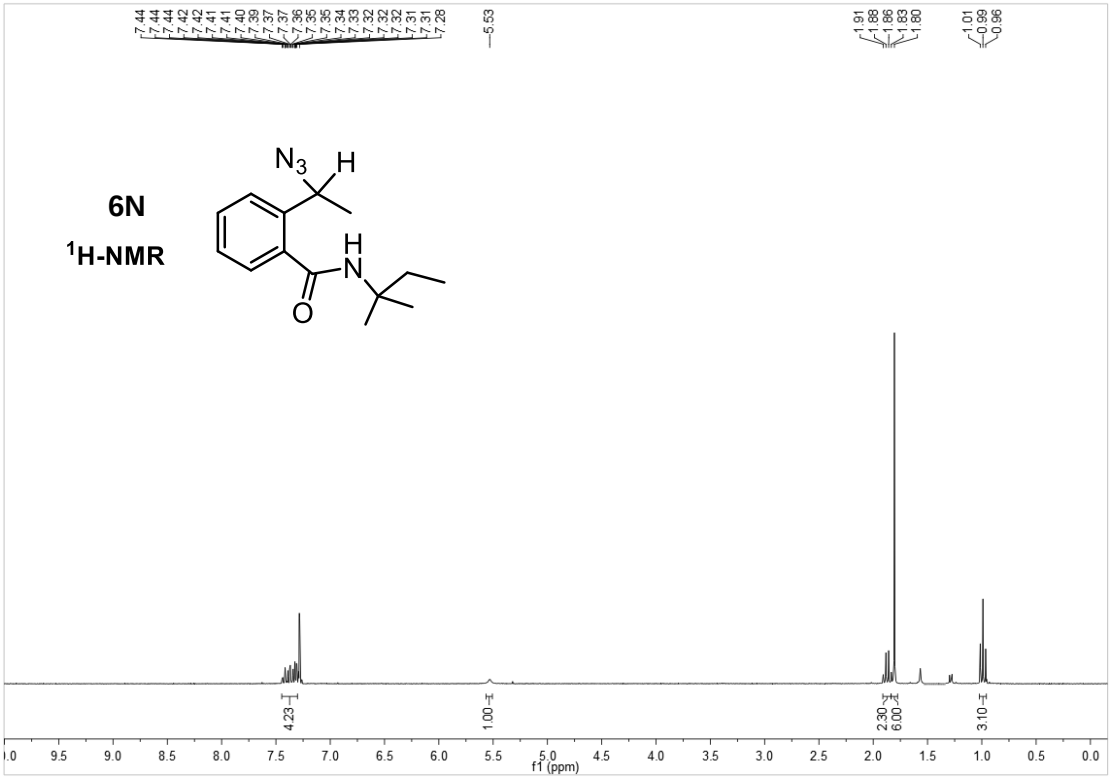
7.44
7.44
7.44
7.42
7.42
7.41
7.41
7.40
7.39
7.37
7.37
7.36
7.35
7.35
7.34
7.33
7.32
7.32
7.32
7.31
7.31
7.28
5.53
1.91
1.88
1.86
1.83
1.80
1.01
0.99
0.96
6N
1H-NMR
N3
H
H
N
O
4.23
1.00
2.30
6.00
3.10
f1 (ppm)

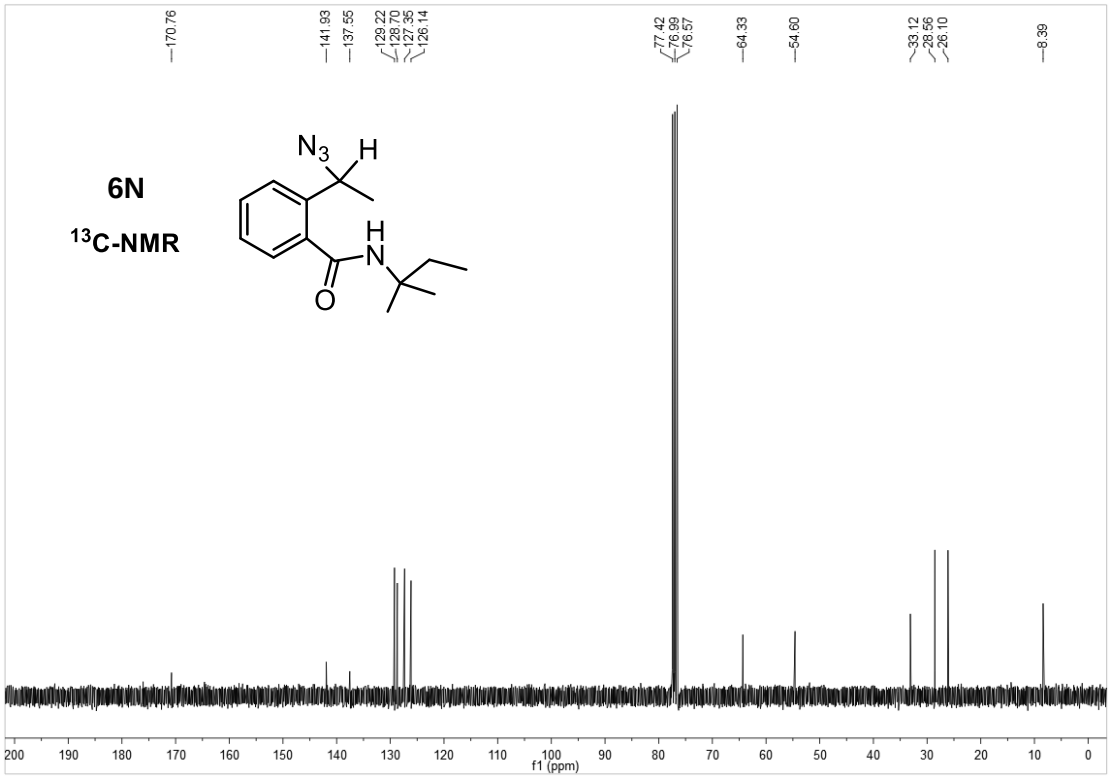
170.76
141.93
137.55
129.22
128.70
127.35
126.14
77.42
76.99
76.57
64.33
54.60
33.12
28.56
26.10
8.39
6N
13C-NMR
N3
H
H
N
O
f1 (ppm)

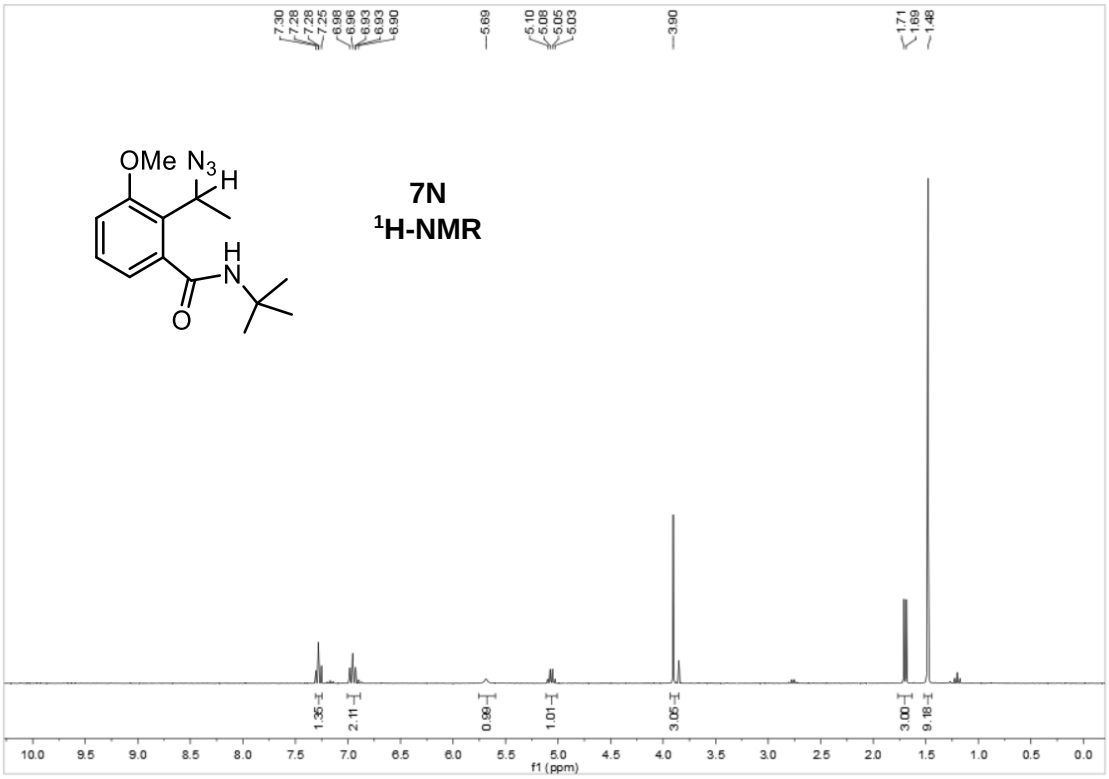
OMe
N3
H
H
N
O
7N
1H-NMR
7.30
7.28
7.28
7.25
6.98
6.96
6.93
6.93
6.90
5.69
5.10
5.08
5.05
5.03
3.90
1.71
1.69
1.48
1.35
2.11
0.99
1.01
3.05
3.00
9.18
f1 (ppm)

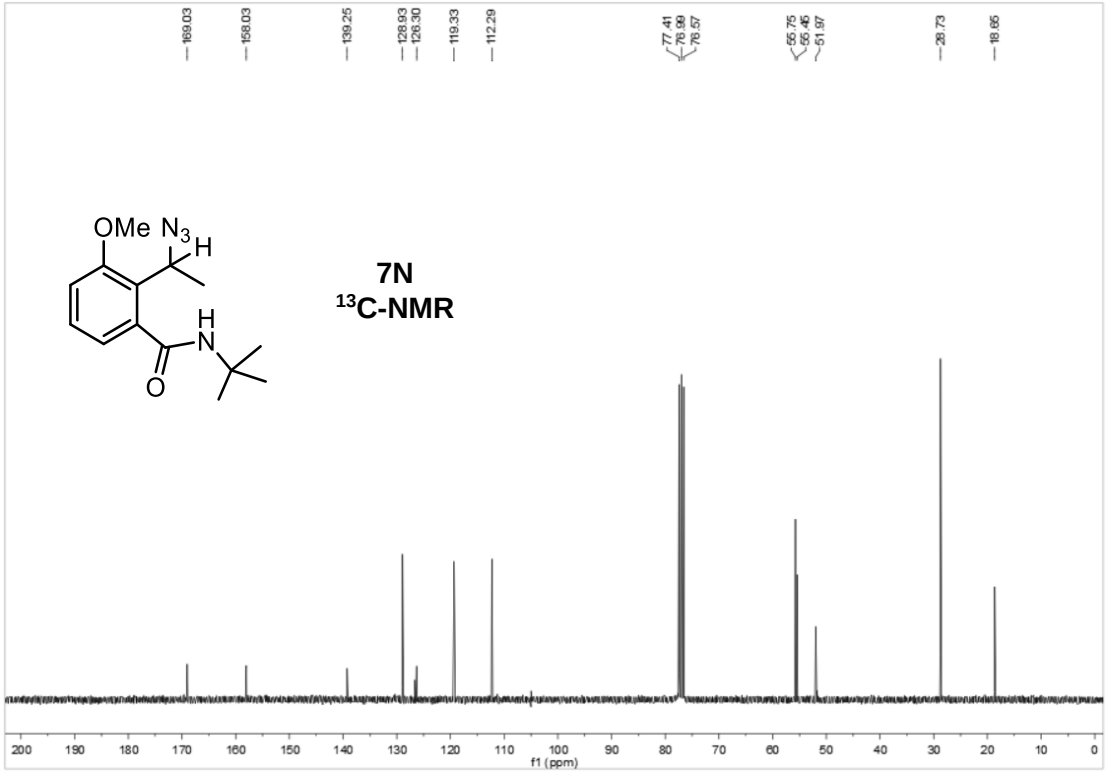
OMe
N3
H
H
N
O
7N
13C-NMR
169.03
158.03
139.25
128.93
126.30
119.33
112.29
77.41
76.99
76.57
55.75
55.46
51.97
28.73
18.65
f1 (ppm)

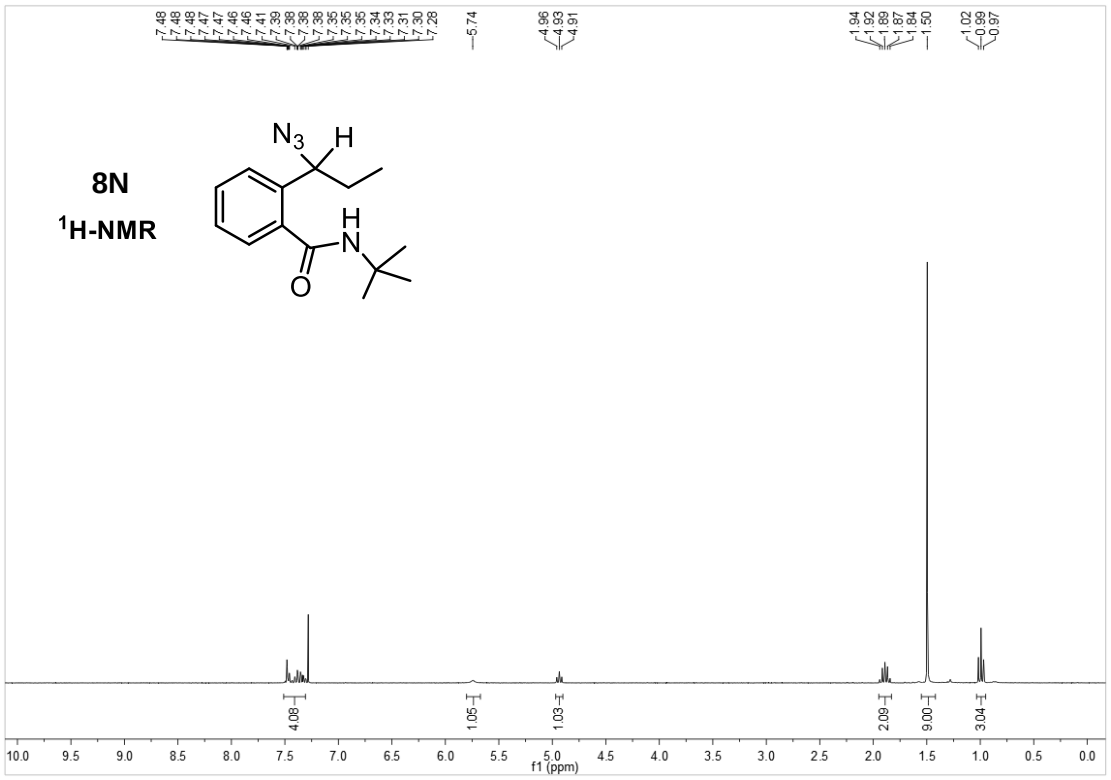
7.48
7.48
7.48
7.47
7.47
7.46
7.46
7.41
7.39
7.38
7.38
7.35
7.35
7.34
7.33
7.31
7.30
7.28
5.74
4.96
4.93
4.91
1.94
1.92
1.89
1.87
1.84
1.50
1.02
0.99
0.97
8N
1H-NMR
N3
H
H
N
O
4.08
1.05
1.03
2.09
9.00
3.04
10.0
9.5
9.0
8.5
8.0
7.5
7.0
6.5
6.0
5.5
5.0
4.5
4.0
3.5
3.0
2.5
2.0
1.5
1.0
0.5
0.0
f1 (ppm)

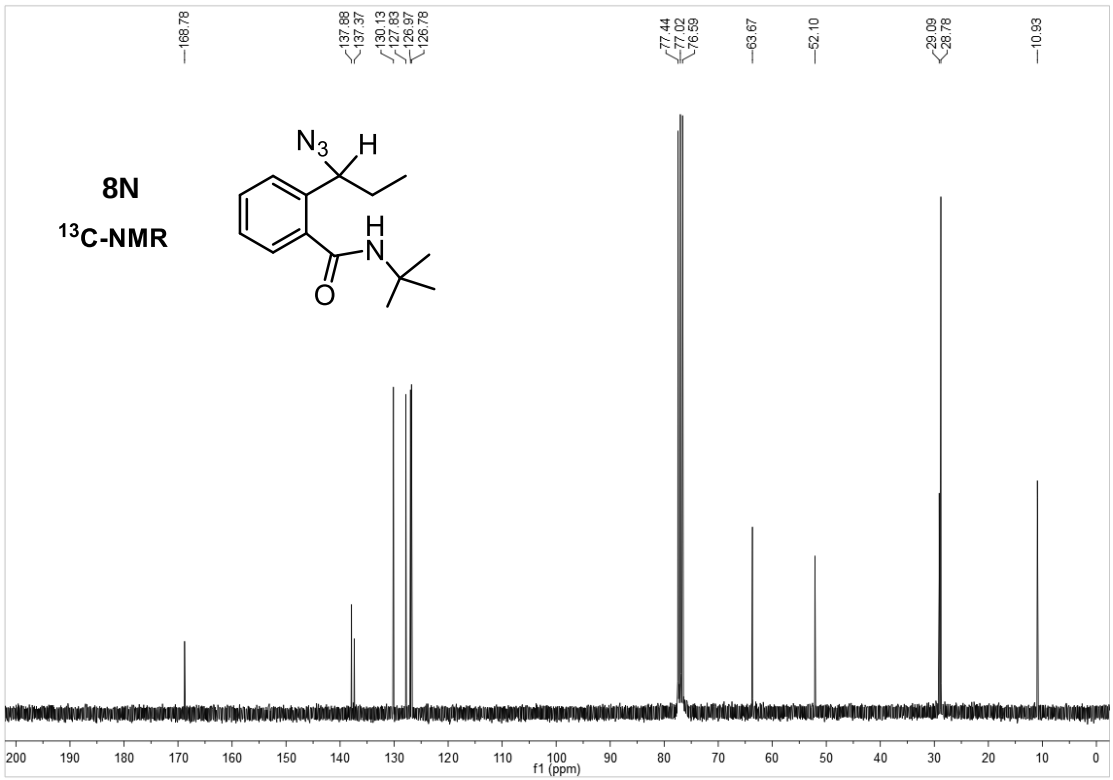
168.78
137.88
137.37
130.13
127.83
126.97
126.78
77.44
77.02
76.59
63.67
52.10
29.09
28.78
10.93
8N
13C-NMR
N3
H
H
N
O
200
190
180
170
160
150
140
130
120
110
100
90
80
70
60
50
40
30
20
10
0
f1 (ppm)

7.48
7.48
7.46
7.46
7.46
7.38
7.38
7.35
7.35
7.33
5.76
5.03
5.01
5.00
4.98
1.87
1.85
1.85
1.84
1.84
1.83
1.82
1.82
1.81
1.81
1.80
1.79
1.51
1.49
0.96
0.95
0.93
9N
1H-NMR
N3
H
H
N
O
4.06
0.81
1.00
1.91
9.41
1.93
3.08
10.0
9.5
9.0
8.5
8.0
7.5
7.0
6.5
6.0
5.5
5.0
4.5
4.0
3.5
3.0
2.5
2.0
1.5
1.0
0.5
0.0
f1 (ppm)

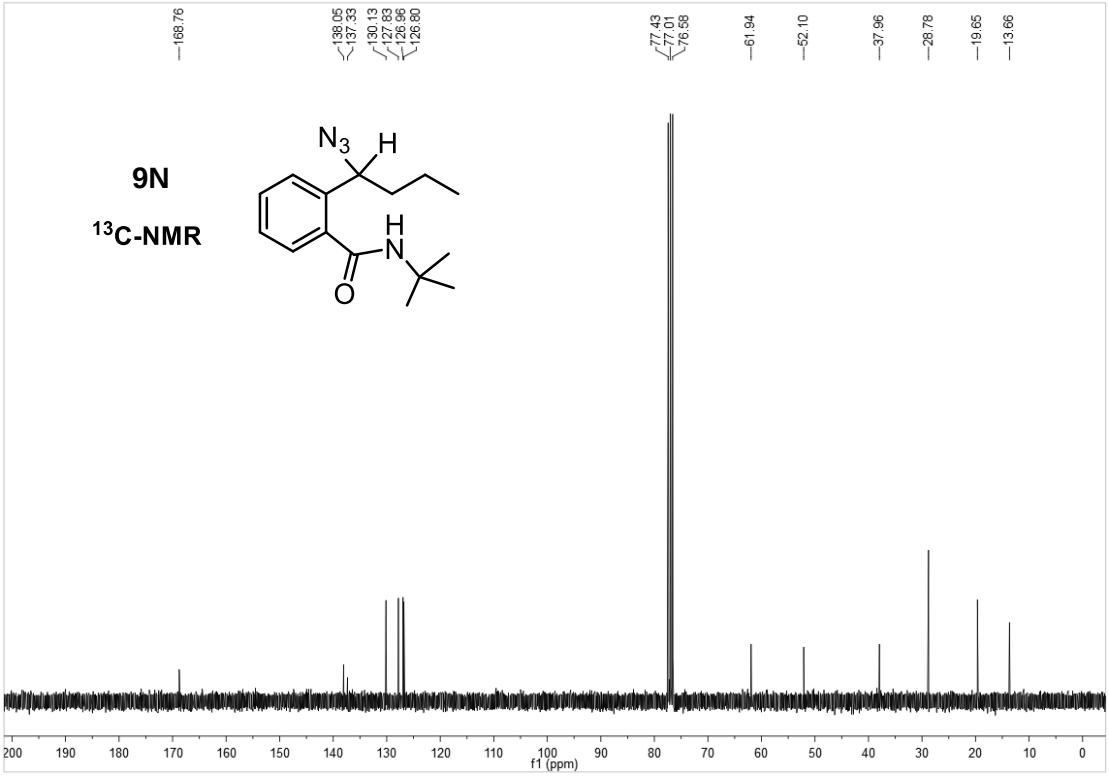
168.76
138.05
137.33
130.13
127.83
126.96
126.80
77.43
77.01
76.58
61.94
52.10
37.96
28.78
19.65
13.66
9N
13C-NMR
N3
H
H
N
O
200
190
180
170
160
150
140
130
120
110
100
90
80
70
60
50
40
30
20
10
0
f1 (ppm)

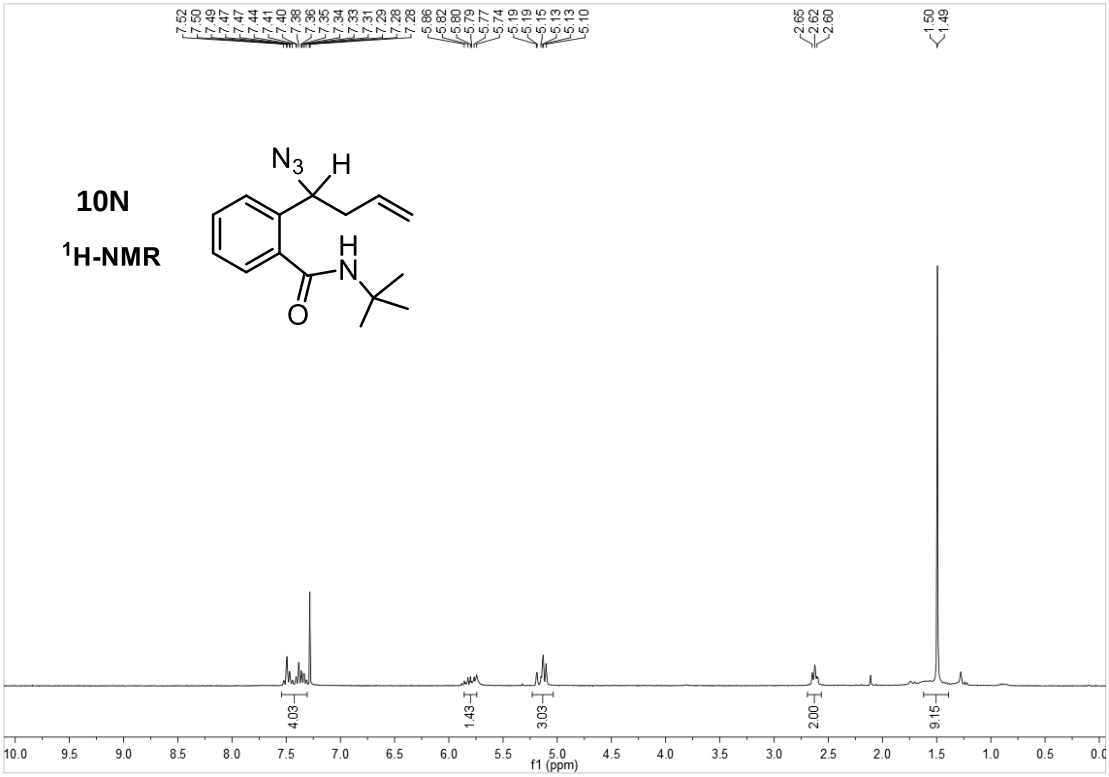
7.52
7.50
7.49
7.47
7.47
7.44
7.41
7.40
7.38
7.36
7.35
7.34
7.33
7.31
7.29
7.28
7.28
5.86
5.82
5.80
5.79
5.77
5.74
5.19
5.19
5.15
5.13
5.13
5.10
2.65
2.62
2.60
1.50
1.49
10N
1H-NMR
N3
H
H
N
O
4.03
1.43
3.03
2.00
9.15
f1 (ppm)

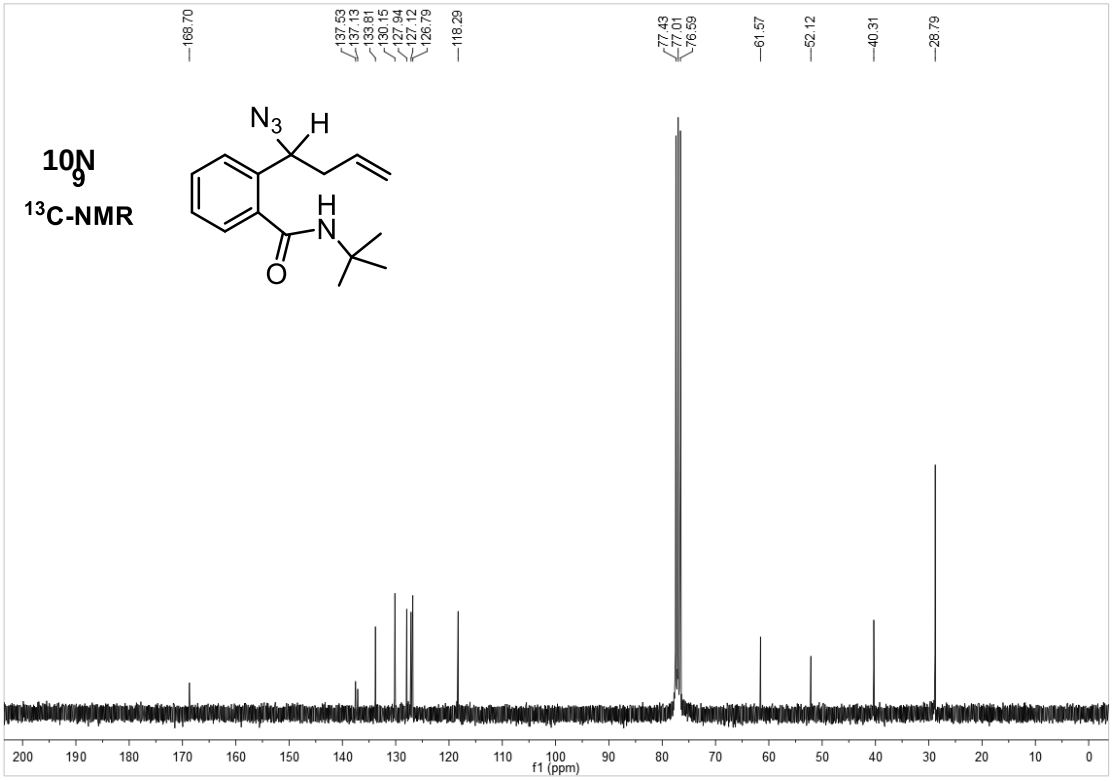
168.70
137.53
137.13
133.81
130.15
127.94
127.12
126.79
118.29
77.43
77.01
76.59
61.57
52.12
40.31
28.79
10N
9
13C-NMR
N3
H
H
N
O
f1 (ppm)

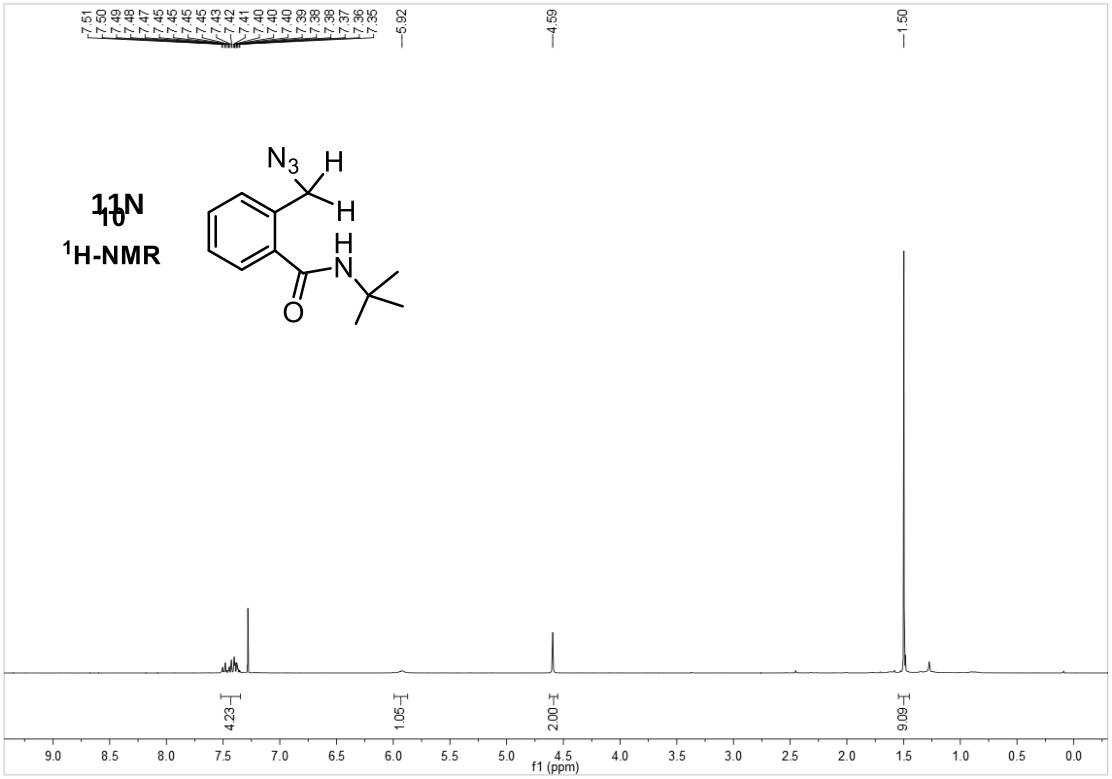
7.51
7.50
7.49
7.48
7.47
7.45
7.45
7.45
7.45
7.43
7.42
7.41
7.40
7.40
7.40
7.39
7.38
7.38
7.37
7.36
7.35
5.92
4.59
1.50
11N
10
1H-NMR
N3
H
H
H
N
O
4.23
1.05
2.00
9.09
9.0
8.5
8.0
7.5
7.0
6.5
6.0
5.5
5.0
4.5
4.0
3.5
3.0
2.5
2.0
1.5
1.0
0.5
0.0
f1 (ppm)

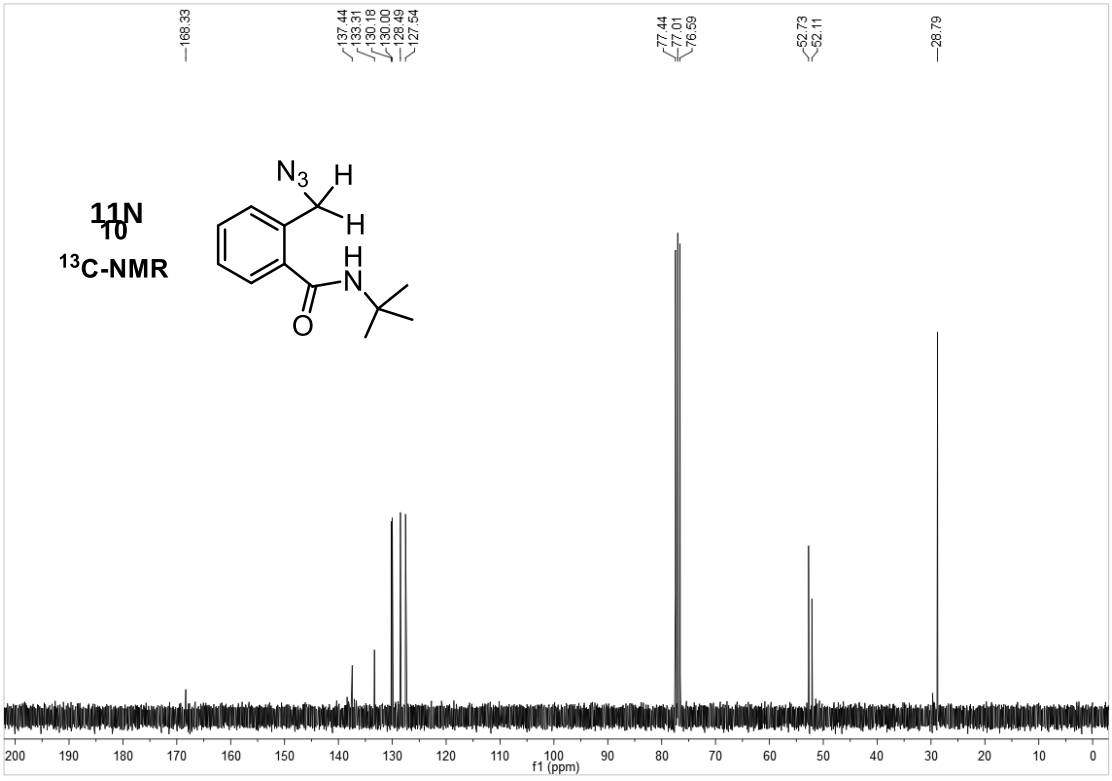
168.33
137.44
133.31
130.18
130.00
128.49
127.54
77.44
77.01
76.59
52.73
52.11
28.79
11N
10
13C-NMR
N3
H
H
H
N
O
200
190
180
170
160
150
140
130
120
110
100
90
80
70
60
50
40
30
20
10
0
f1 (ppm)

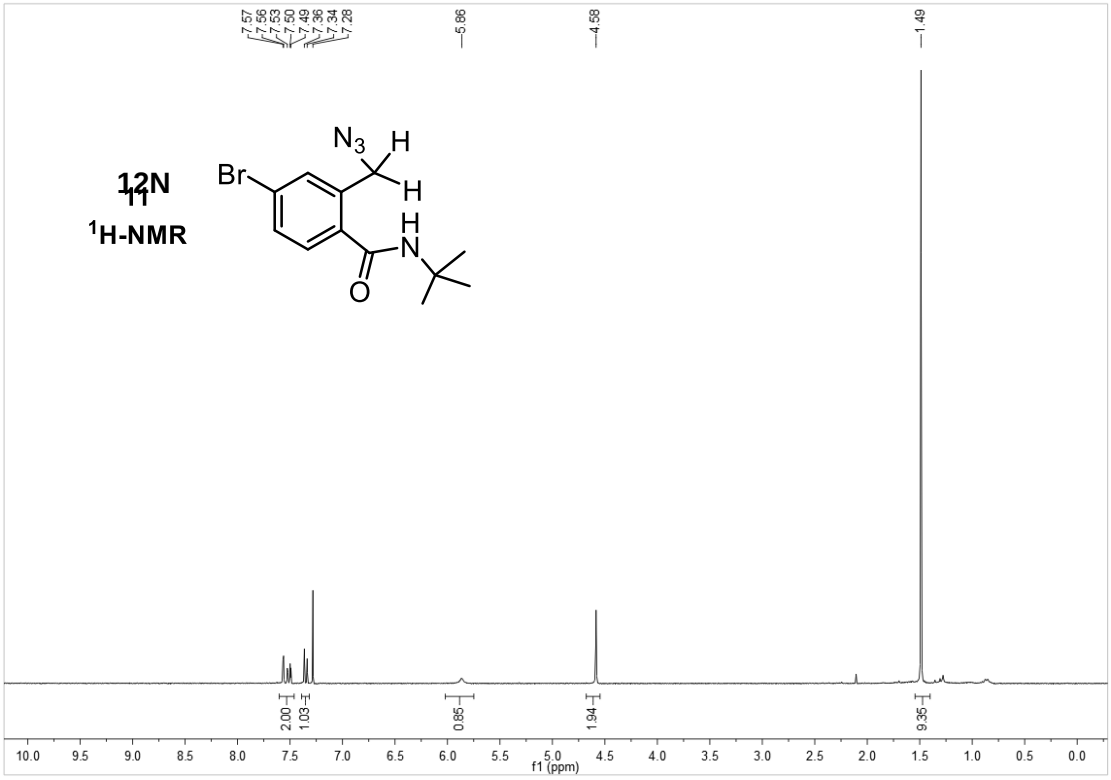
7.57
7.56
7.53
7.50
7.49
7.36
7.34
7.28
5.86
4.58
1.49
12N
11
1H-NMR
N3
H
Br
H
H
N
O
2.00
1.03
0.85
1.94
9.35
f1 (ppm)

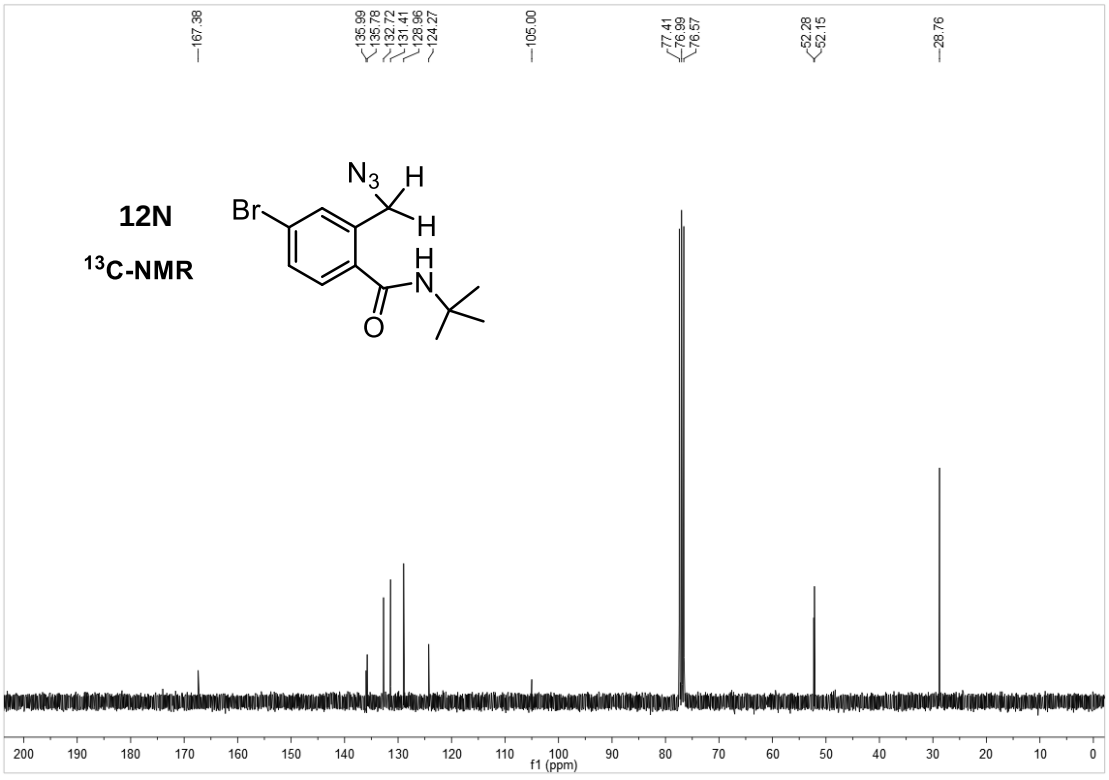
167.38
135.99
135.78
132.72
131.41
128.96
124.27
105.00
77.41
76.99
76.57
52.28
52.15
28.76
12N
13C-NMR
N3
H
Br
H
H
N
O
f1 (ppm)

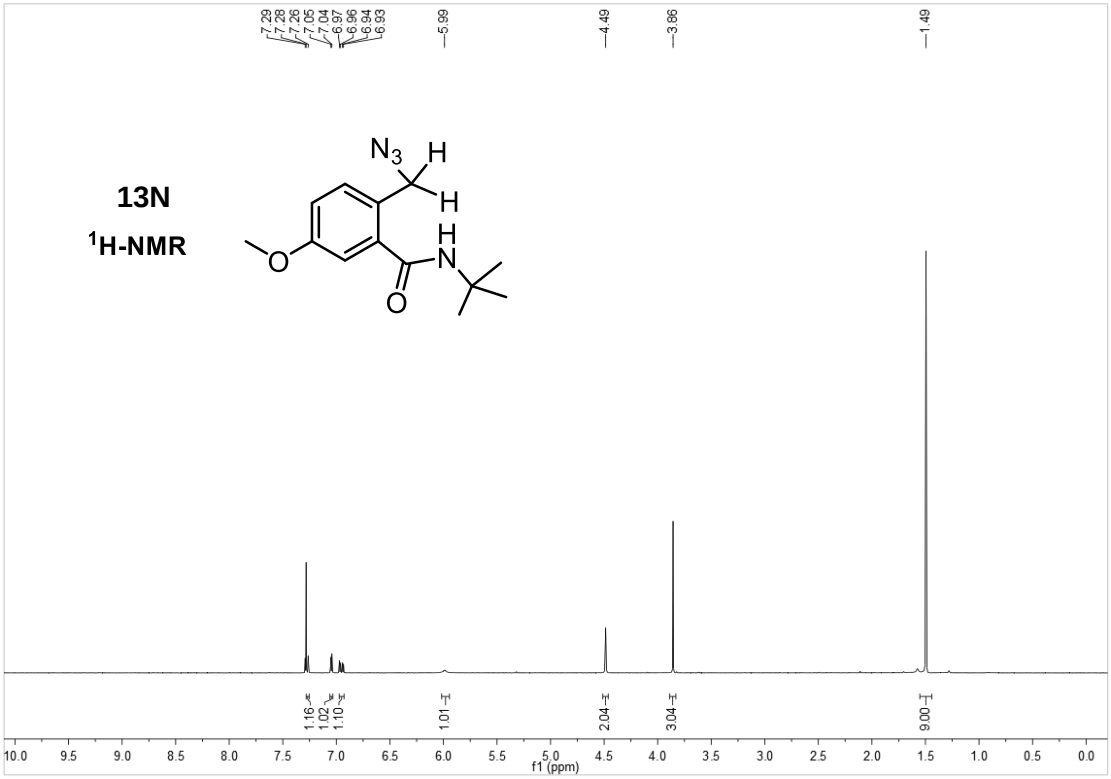
7.29
7.28
7.26
7.05
7.04
6.97
6.96
6.94
6.93
5.99
4.49
3.86
1.49
13N
1H-NMR
N3
H
H
H
N
O
O
1.16
1.02
1.10
1.01
2.04
3.04
9.00
f1 (ppm)

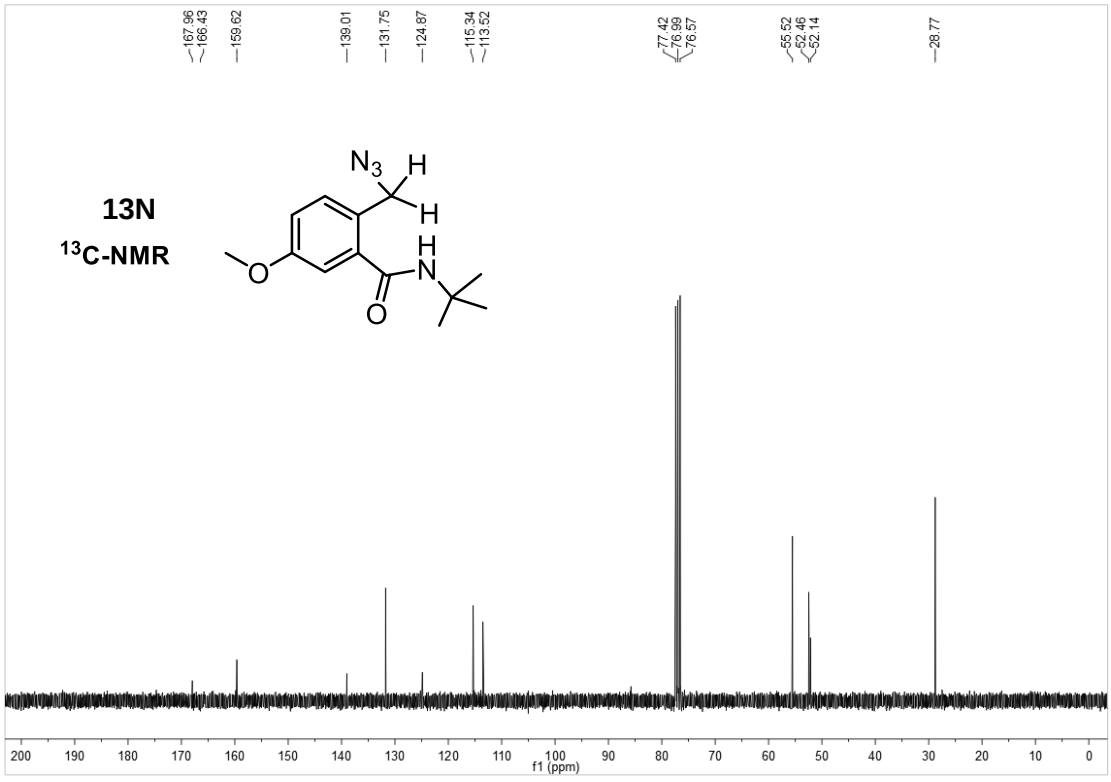
167.96
166.43
159.62
139.01
131.75
124.87
115.34
113.52
77.42
76.99
76.57
55.52
52.46
52.14
28.77
13N
13C-NMR
N3
H
H
H
N
O
O
f1 (ppm)

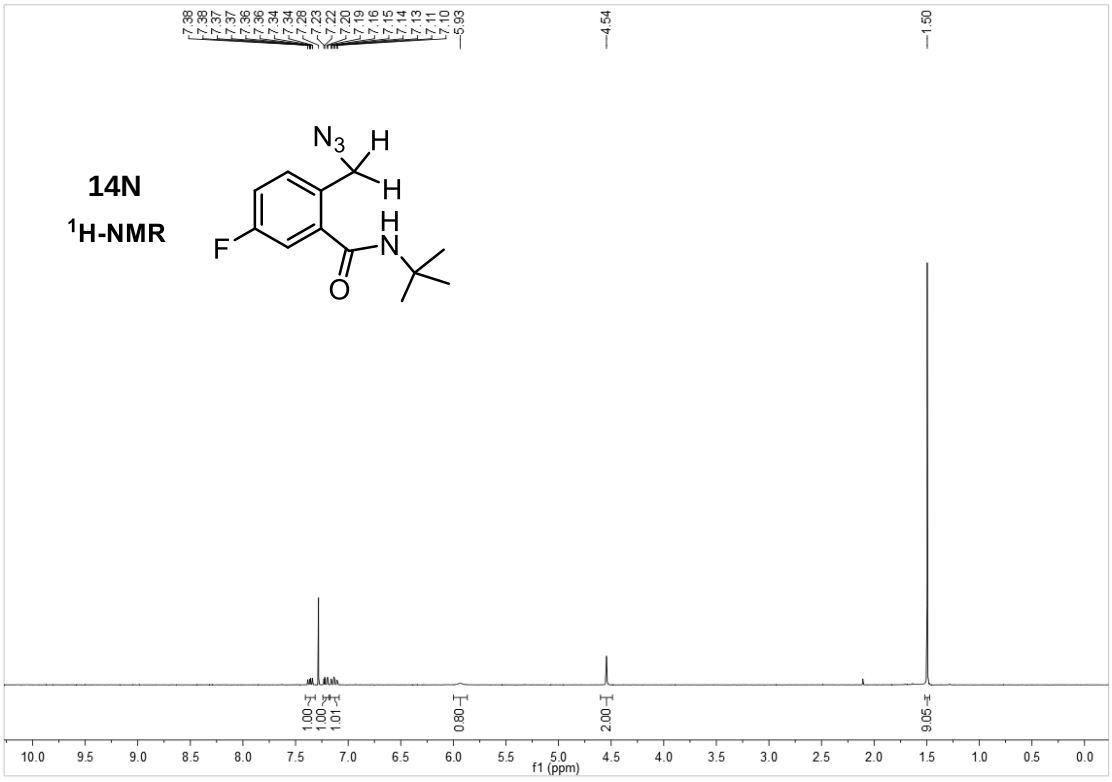
7.38
7.38
7.37
7.37
7.36
7.36
7.34
7.34
7.28
7.23
7.22
7.20
7.19
7.16
7.15
7.14
7.13
7.11
7.10
5.93
4.54
1.50
14N
1H-NMR
N3
H
H
H
N
F
O
1.00
1.00
1.01
0.80
2.00
9.05
f1 (ppm)

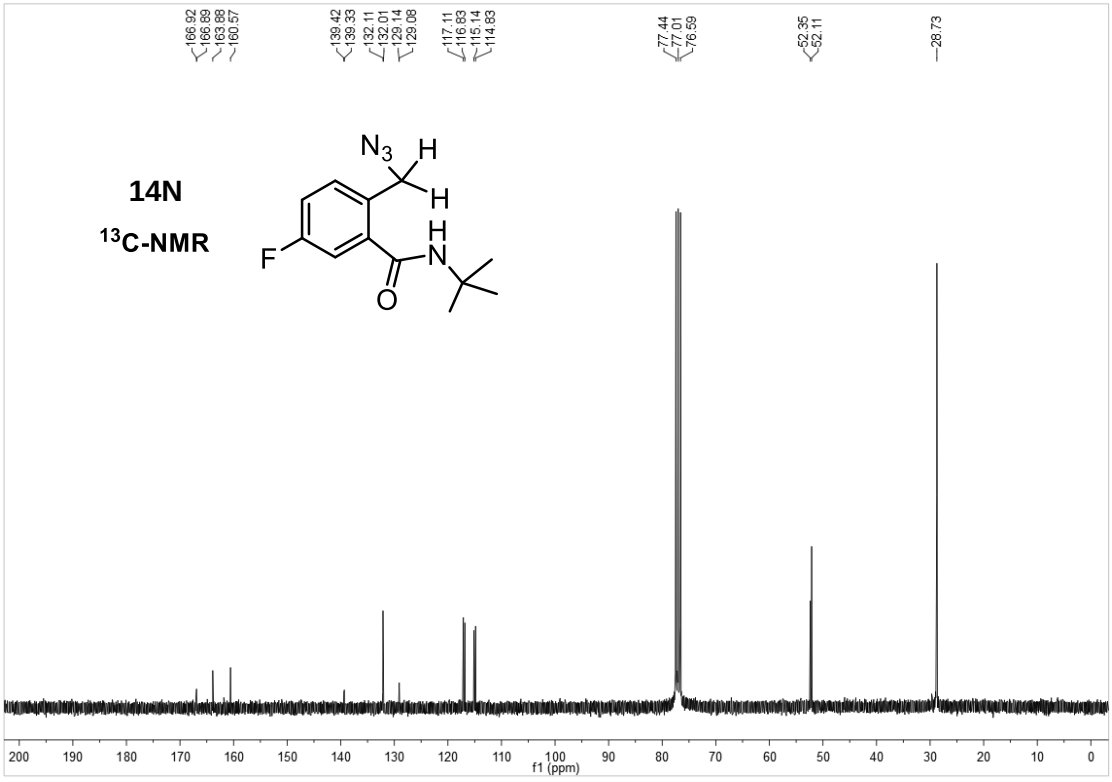
166.92
166.89
163.88
160.57
139.42
139.33
132.11
132.01
129.14
129.08
117.11
116.83
115.14
114.83
77.44
77.01
76.59
52.35
52.11
28.73
14N
13C-NMR
N3
H
H
H
N
F
O
f1 (ppm)

14N

^{19}F-NMR

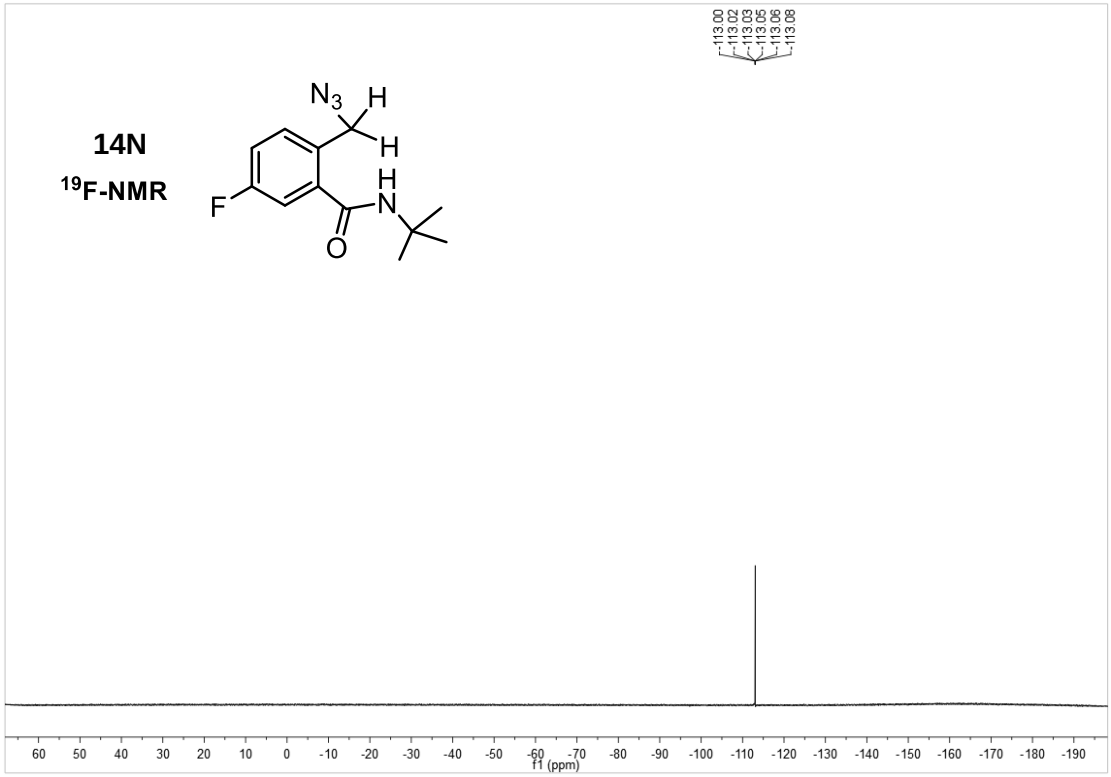

15N

^{1}H-NMR

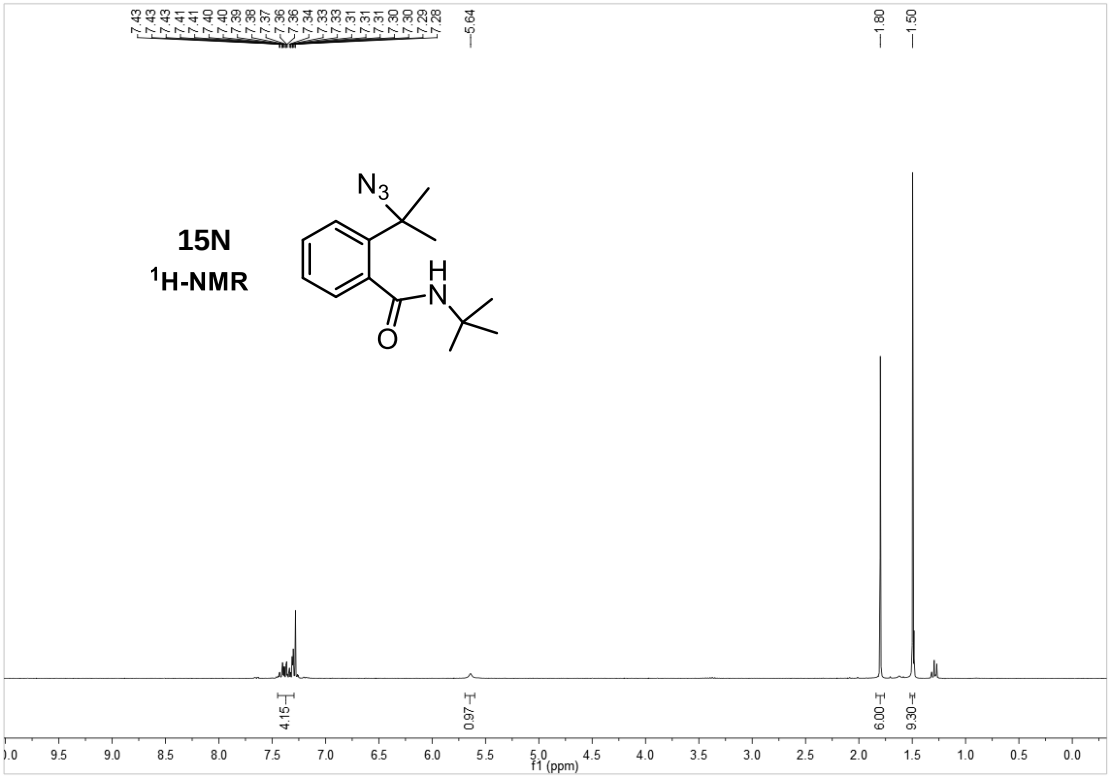

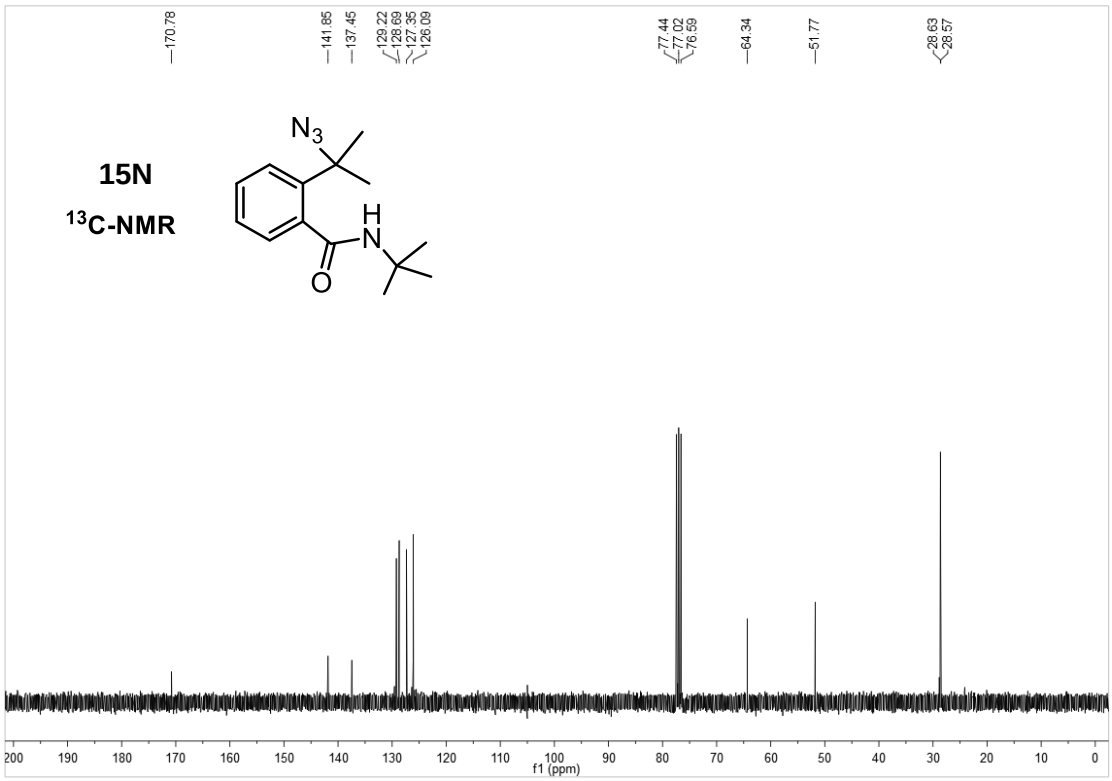
170.78
141.85
137.45
129.22
128.69
127.35
126.09
77.44
77.02
76.59
64.34
51.77
28.63
28.57
15N
13C-NMR
N3
H
N
O
f1 (ppm)

7.41
7.41
7.40
7.39
7.39
7.38
7.37
7.37
7.28
7.08
7.07
7.05
7.05
7.04
7.04
7.03
7.02
7.02
7.01
5.63
1.78
1.49
16N
1H-NMR
N3
F
H
N
O
1.02
2.08
0.71
6.00
9.41
f1 (ppm)

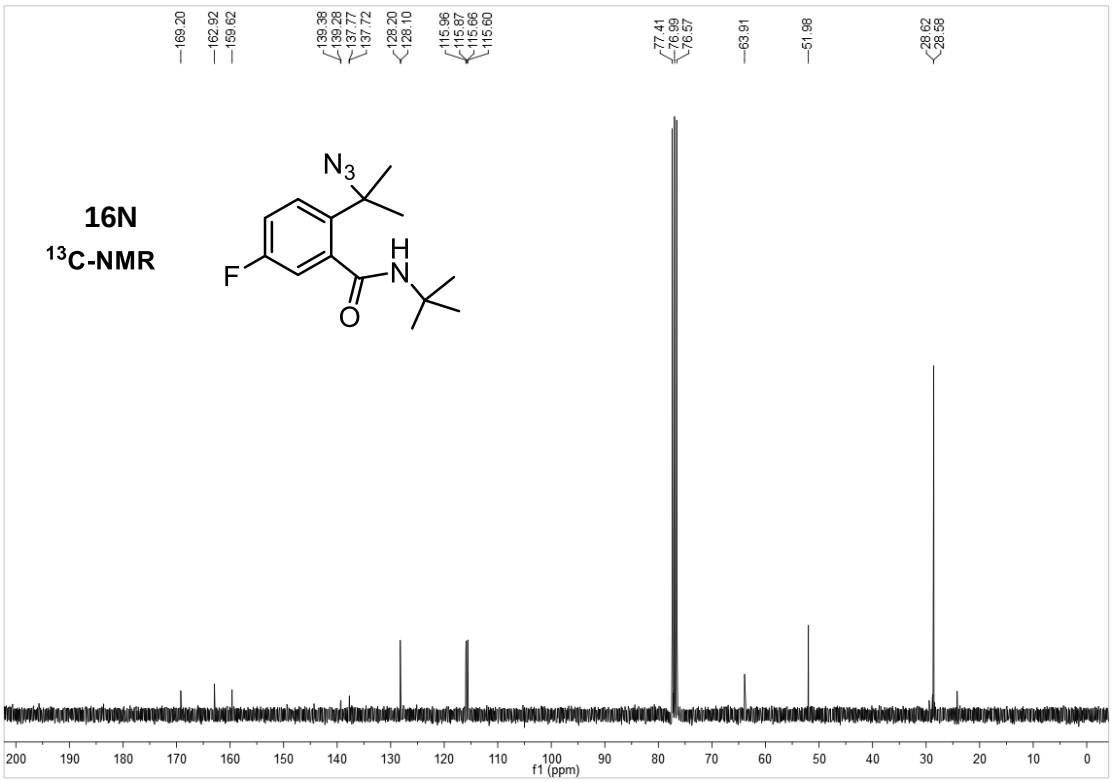
169.20
162.92
159.62
139.38
139.28
137.77
137.72
128.20
128.10
115.96
115.87
115.66
115.60
77.41
76.99
76.57
63.91
51.98
28.62
28.58
16N
13C-NMR
N3
F
H
N
O
200 190 180 170 160 150 140 130 120 110 100 90 80 70 60 50 40 30 20 10 0
f1 (ppm)

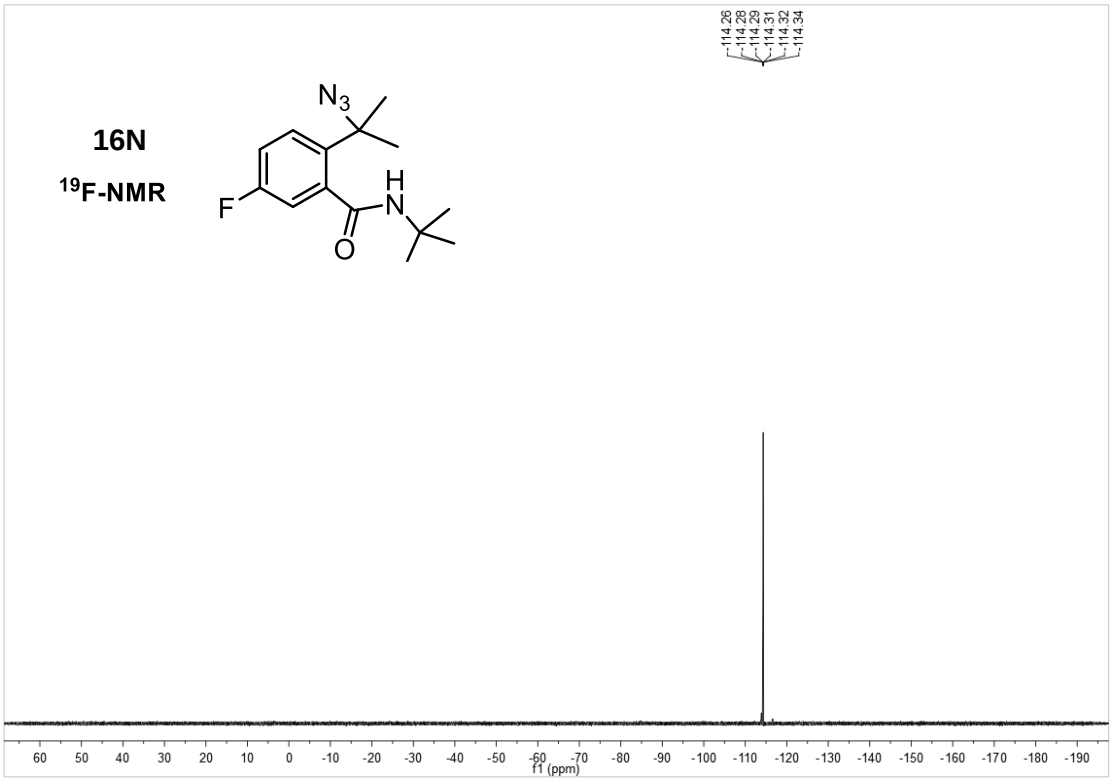
114.26
114.28
114.29
114.31
114.32
114.34
16N
19F-NMR
N3
F
H
N
O
60 50 40 30 20 10 0 -10 -20 -30 -40 -50 -60 -70 -80 -90 -100 -110 -120 -130 -140 -150 -160 -170 -180 -190
f1 (ppm)

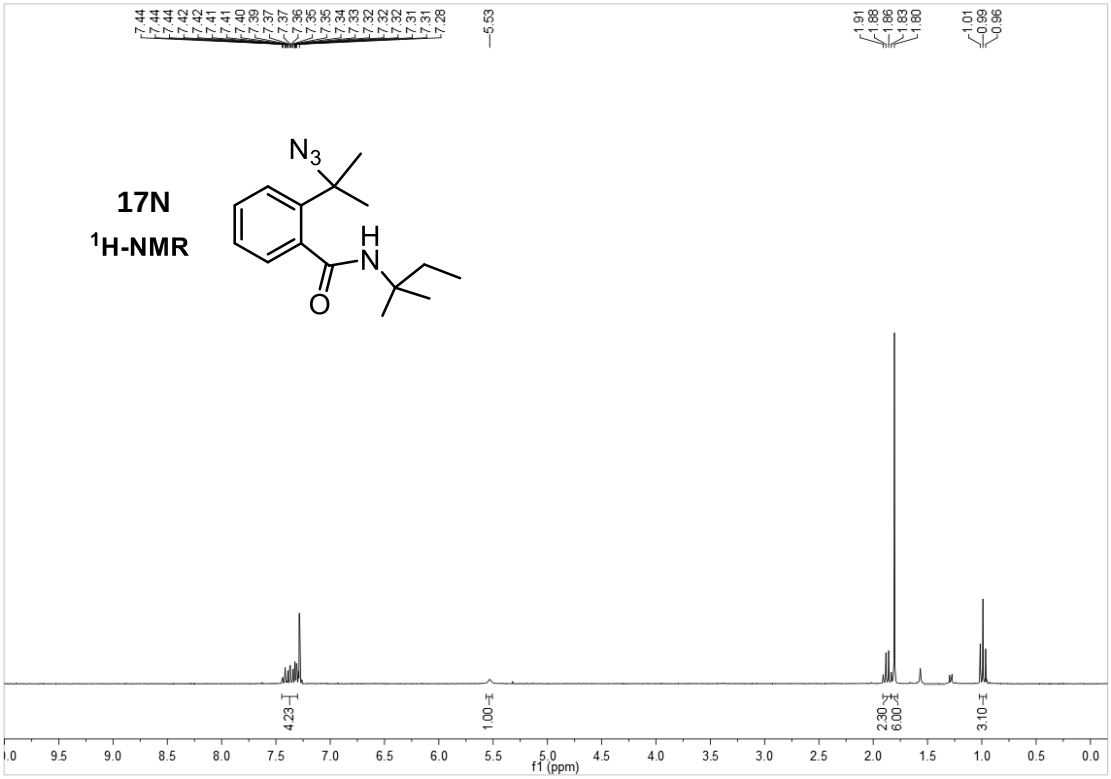
7.44
7.44
7.44
7.42
7.42
7.41
7.41
7.40
7.39
7.37
7.37
7.36
7.35
7.34
7.33
7.32
7.32
7.32
7.31
7.31
7.28
5.53
1.91
1.88
1.86
1.83
1.80
1.01
0.99
0.96
17N
1H-NMR
N3
H
N
O
4.23
1.00
2.30
6.00
3.10
f1 (ppm)

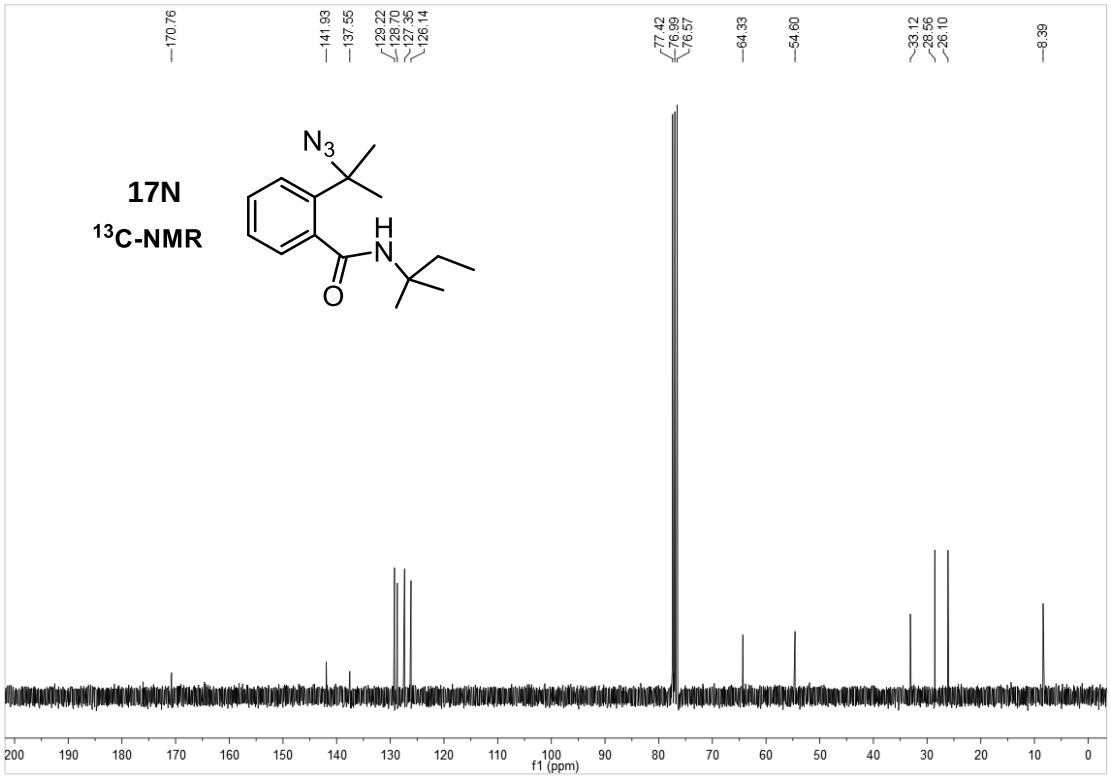
170.76
141.93
137.55
129.22
128.70
127.35
126.14
77.42
76.99
76.57
64.33
54.60
33.12
28.56
26.10
8.39
17N
13C-NMR
N3
H
N
O
f1 (ppm)

19

^{1}H-NMR

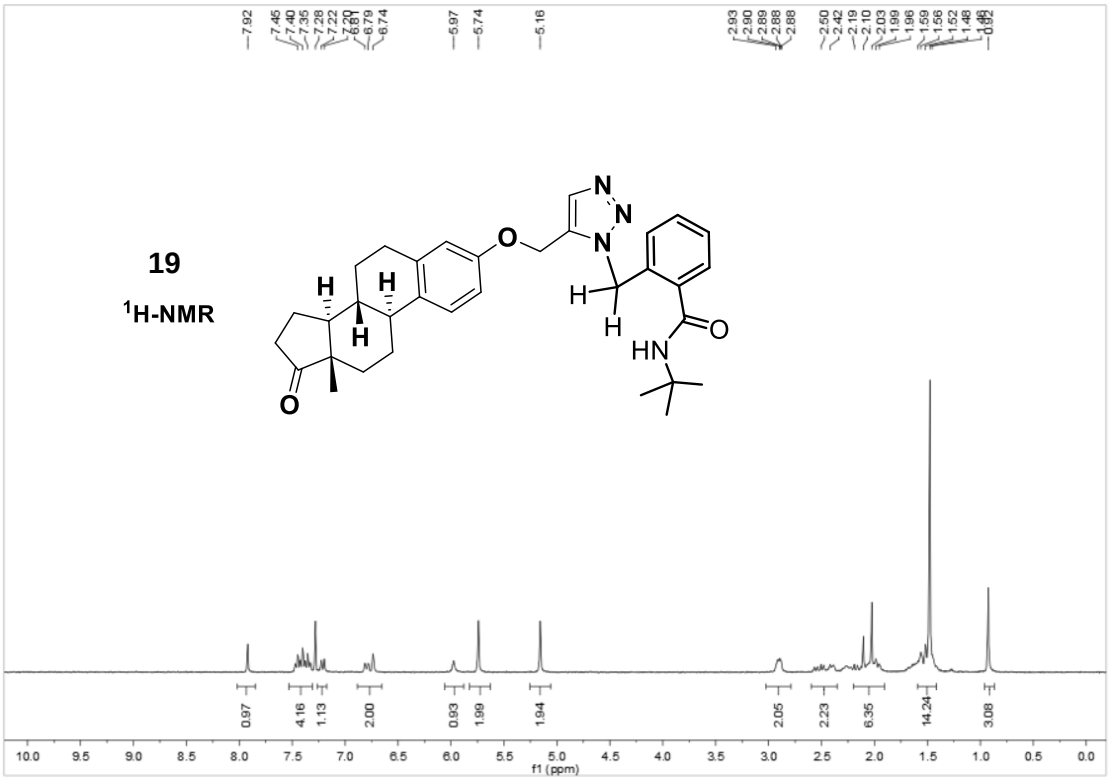

19

^{13}C-NMR

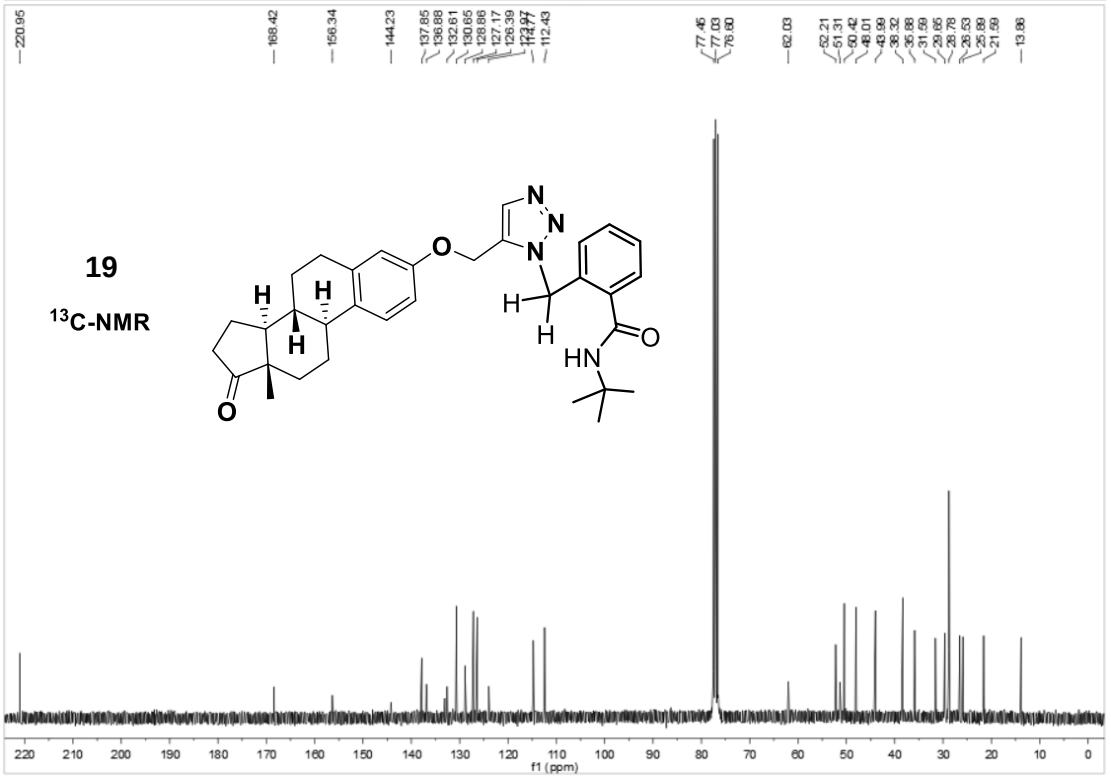

References and notes

1. F. H. Arnold, Directed Evolution: Bringing New Chemistry to Life. *Angew. Chem. Int. Ed.* **57**, 4143–4148 (2018). doi:10.1002/anie.201708408 Medline

2. U. T. Bornscheuer, The fourth wave of biocatalysis is approaching. *Philos. Trans. R. Soc. A* **376**, 20170063 (2018). doi:10.1098/rsta.2017.0063 Medline

3. K. Chen, F. H. Arnold, Engineering new catalytic activities in enzymes. *Nat. Catal.* **3**, 203–213 (2020). doi:10.1038/s41929-019-0385-5

4. O. F. Brandenberg, R. Fasan, F. H. Arnold, Exploiting and engineering hemoproteins for abiological carbene and nitrene transfer reactions. *Curr. Opin. Biotechnol.* **47**, 102–111 (2017). doi:10.1016/j.copbio.2017.06.005 Medline

5. K. F. Biegasiewicz, S. J. Cooper, X. Gao, D. G. Oblinsky, J. H. Kim, S. E. Garfinkle, L. A. Joyce, B. A. Sandoval, G. D. Scholes, T. K. Hyster, Photoexcitation of flavoenzymes enables a stereoselective radical cyclization. *Science* **364**, 1166–1169 (2019). doi:10.1126/science.aaw1143 Medline

6. X. Huang, B. Wang, Y. Wang, G. Jiang, J. Feng, H. Zhao, Photoenzymatic enantioselective intermolecular radical hydroalkylation. *Nature* **584**, 69–74 (2020). doi:10.1038/s41586-020-2406-6 Medline

7. P. Ji, J. Park, Y. Gu, D. S. Clark, J. F. Hartwig, Abiotic reduction of ketones with silanes catalysed by carbonic anhydrase through an enzymatic zinc hydride. *Nat. Chem.* **13**, 312–318 (2021). doi:10.1038/s41557-020-00633-7 Medline

8. L. M. Stateman, K. M. Nakafuku, D. A. Nagib, Remote C-H Functionalization via Selective Hydrogen Atom Transfer. *Synthesis* **50**, 1569–1586 (2018). doi:10.1055/s-0036-1591930 Medline

9. C. Zhang, Z.-L. Li, Q.-S. Gu, X.-Y. Liu, Catalytic enantioselective C(sp^3)-H functionalization involving radical intermediates. *Nat. Commun.* **12**, 475 (2021). doi:10.1038/s41467-020-20770-4 Medline

10. F. Wang, P. Chen, G. Liu, Copper-Catalyzed Radical Relay for Asymmetric Radical Transformations. *Acc. Chem. Res.* **51**, 2036–2046 (2018). doi:10.1021/acs.accounts.8b00265 Medline

11. B. J. Groendyke, D. I. AbuSalim, S. P. Cook, Iron-Catalyzed, Fluoroamide-Directed C-H Fluorination. *J. Am. Chem. Soc.* **138**, 12771–12774 (2016). doi:10.1021/jacs.6b08171 Medline

12. C. Crowe, S. Molyneux, S. V. Sharma, Y. Zhang, D. S. Gkotsi, H. Connaris, R. J. M. Goss, Halogenases: A palette of emerging opportunities for synthetic biology-synthetic chemistry and C-H functionalisation. *Chem. Soc. Rev.* **50**, 9443–9481 (2021). doi:10.1039/D0CS01551B Medline

13. M. L. Matthews, W. C. Chang, A. P. Layne, L. A. Miles, C. Krebs, J. M. Bollinger Jr., Direct nitration and azidation of aliphatic carbons by an iron-dependent halogenase. *Nat. Chem. Biol.* **10**, 209–215 (2014). doi:10.1038/nchembio.1438 Medline

14. M. E. Neugebauer, K. H. Sumida, J. G. Pelton, J. L. McMurry, J. A. Marchand, M. C. Y. Chang, A family of radical halogenases for the engineering of amino-acid-based products. *Nat. Chem. Biol.* **15**, 1009–1016 (2019). doi:10.1038/s41589-019-0355-x Medline

15. C. Y. Kim, A. J. Mitchell, C. M. Glinkerman, F.-S. Li, T. Pluskal, J.-K. Weng, The chloroalkaloid (-)-acutumine is biosynthesized via a Fe(II)- and 2-oxoglutarate-dependent halogenase in Menispermaceae plants. *Nat. Commun.* **11**, 1867 (2020). doi:10.1038/s41467-020-15777-w Medline

16. X. Huang, J. T. Groves, Beyond ferryl-mediated hydroxylation: 40 years of the rebound mechanism and C-H activation. *J. Biol. Inorg.* **22**, 185–207 (2017). doi:10.1007/s00775-016-1414-3 Medline

17. P. Sivaguru, Y. Ning, X. Bi, New Strategies for the Synthesis of Aliphatic Azides. *Chem. Rev.* **121**, 4253–4307 (2021). doi:10.1021/acs.chemrev.0c01124 Medline

18. M. Meldal, C. W. Tornøe, Cu-catalyzed azide-alkyne cycloaddition. *Chem. Rev.* **108**, 2952–3015 (2008). doi:10.1021/cr0783479 Medline

19. A. M. Orville, V. J. Chen, A. Kriauciunas, M. R. Harpel, B. G. Fox, E. Münck, J. D. Lipscomb, Thiolate ligation of the active site Fe2+ of isopenicillin N synthase derives from substrate rather than endogenous cysteine: Spectroscopic studies of site-specific Cys----Ser mutated enzymes. *Biochemistry* **31**, 4602–4612 (1992). doi:10.1021/bi00134a010 Medline

20. C. Bull, J. A. Fee, Steady-state kinetic studies of superoxide dismutases: Properties of the iron containing protein from Escherichia coli. *J. Am. Chem. Soc.* **107**, 3295–3304 (1985). doi:10.1021/ja00297a040

21. K. Meyer, E. Bill, B. Mienert, T. Weyhermüller, K. Wieghardt, Photolysis of *cis* - and *trans* - [Fe ^{III} (cyclam)(N $_3$) $_2$] $^+$ Complexes: Spectroscopic Characterization of a Nitridoiron(V) Species. *J. Am. Chem. Soc.* **121**, 4859–4876 (1999). doi:10.1021/ja983454t

22. C. A. Grapperhaus, B. Mienert, E. Bill, T. Weyhermüller, K. Wieghardt, Mononuclear (nitrido)iron(V) and (oxo)iron(IV) complexes via photolysis of [(cyclam-acetato)$Fe^{III}(N_3)]^+$ and ozonolysis of [(cyclam-acetato)$Fe^{III}(O_3SCF_3)]^+$ in water/acetone mixtures. *Inorg. Chem.* **39**, 5306–5317 (2000). doi:10.1021/ic0005238 Medline

23. J. M. Brownlee, K. Johnson-Winters, D. H. T. Harrison, G. R. Moran, Structure of the ferrous form of (4-hydroxyphenyl)pyruvate dioxygenase from *Streptomyces avermitilis* in complex with the therapeutic herbicide, NTBC. *Biochemistry* **43**, 6370–6377 (2004). doi:10.1021/bi049317s Medline

24. E. N. Pinter, J. E. Bingham, D. I. AbuSalim, S. P. Cook, N-Directed fluorination of unactivated Csp ^{3} –H bonds. *Chem. Sci.* **11**, 1102–1106 (2020). doi:10.1039/C9SC04055B

25. M. L. Matthews, C. S. Neumann, L. A. Miles, T. L. Grove, S. J. Booker, C. Krebs, C. T. Walsh, J. M. Bollinger Jr., Substrate positioning controls the partition between halogenation and hydroxylation in the aliphatic halogenase, SyrB2. *Proc. Natl. Acad. Sci. U.S.A.* **106**, 17723–17728 (2009). doi:10.1073/pnas.0909649106 Medline

26. L. C. Blasiak, C. L. Drennan, Structural perspective on enzymatic halogenation. *Acc. Chem. Res.* **42**, 147–155 (2009). doi:10.1021/ar800088r Medline

27. D. G. Gibson, L. Young, R.-Y. Chuang, J. C. Venter, C. A. Hutchison III, H. O. Smith, Enzymatic assembly of DNA molecules up to several hundred kilobases. *Nat. Methods* **6**, 343–345 (2009). doi:10.1038/nmeth.1318 Medline

28. M. Sawa, T.-L. Hsu, T. Itoh, M. Sugiyama, S. R. Hanson, P. K. Vogt, C.-H. Wong, Glycoproteomic probes for fluorescent imaging of fucosylated glycans *in vivo*. *Proc. Natl. Acad. Sci. U.S.A.* **103**, 12371–12376 (2006). doi:10.1073/pnas.0605418103 Medline

29. T. Fujita, T. Nishioka, *Prog. Phys. Org. Chem.* **12**, 49–89 (1976).

30. X. Bao, Q. Wang, J. Zhu, Copper-catalyzed remote C(sp^3)-H azidation and oxidative trifluoromethylation of benzohydrazides. *Nat. Commun.* **10**, 769 (2019). doi:10.1038/s41467-019-08741-w Medline

31. R. O. Torres-Ochoa, A. Leclair, Q. Wang, J. Zhu, C. Iron-Catalysed Remote, (sp^3) -H Azidation of O-Acyl Oximes and N-Acyloxy Imidates Enabled by 1,5-Hydrogen Atom Transfer of Iminyl and Imidate Radicals: Synthesis of γ-Azido Ketones and β-Azido Alcohols. *Chemistry* **25**, 9477–9484 (2019). doi:10.1002/chem.201901079 Medline

32. K.-J. Bian, C.-Y. Wang, Y.-L. Huang, Y.-H. Xu, X.-S. Wang, Remote azidation of C(sp^3)-H bonds to synthesize δ-azido sulfonamides via iron-catalyzed radical relay. *Org. Biomol. Chem.* **18**, 5354–5358 (2020). doi:10.1039/D0OB00964D Medline

33. Q.-Q. Min, J.-W. Yang, M.-J. Pang, G.-Z. Ao, F. Liu, Copper-catalyzed, N-directed remote C(sp^3) –H azidation and thiocyanation. *Org. Chem. Front.* **8**, 249–253 (2021). doi:10.1039/D0QO01012J

34. Z.-H. Zhang, X.-Y. Dong, X.-Y. Du, Q.-S. Gu, Z.-L. Li, X.-Y. Liu, Copper-catalyzed enantioselective Sonogashira-type oxidative cross-coupling of unactivated C(sp^3)-H bonds with alkynes. *Nat. Commun.* **10**, 5689 (2019). doi:10.1038/s41467-019-13705-1 Medline

35. D. T. Petasis, M. P. Hendrich, Quantitative Interpretation of Multifrequency Multimode EPR Spectra of Metal Containing Proteins, Enzymes, and Biomimetic Complexes. *Methods Enzymol.* **563**, 171–208 (2015). doi:10.1016/bs.mie.2015.06.025 Medline

36. G. W. T. M. J. Frisch, H. B. Schlegel, G. E. Scuseria, M. A. Robb, J. R. Cheeseman, G. Scalmani, V. Barone, G. A. Petersson, H. Nakatsuji, X. Li, M. Caricato, A. Marenich, J. Bloino, B. G. Janesko, R. Gomperts, B. Mennucci, H. P. Hratchian, J. V. Ortiz, A. F. Izmaylov, J. L. Sonnenberg, D. Williams-Young, F. Ding, F. Lipparini, F. Egidi, J. Goings, B. Peng, A. Petrone, T. Henderson, D. Ranasinghe, V. G. Zakrzewski, J. Gao, N. Rega, G. Zheng, W. Liang, M. Hada, M. Ehara, K. Toyota, R. Fukuda, J. Hasegawa, M. Ishida, T. Nakajima, Y. Honda, O. Kitao, H. Nakai, T. Vreven, K. Throssell, J. A. Montgomery Jr., J. E. Peralta, F. Ogliaro, M. Bearpark, J. J. Heyd, E. Brothers, K. N. Kudin, V. N. Staroverov, T. Keith, R. Kobayashi, J. Normand, K. Raghavachari, A. Rendell, J. C. Burant, S. S. Iyengar, J. Tomasi, M. Cossi, J. M. Millam, M. Klene, C. Adamo, R. Cammi, J. W. Ochterski, R. L. Martin, K. Morokuma, O. Farkas, J. B. Foresman, D. J. Fox, Gaussian 09, Revision A.02. (Gaussian Inc., 2009); https://gaussian.com/g09citation/

37. C. Lee, W. Yang, R. G. Parr, Development of the Colle-Salvetti correlation-energy formula into a functional of the electron density. *Phys. Rev. B Condens. Matter* **37**, 785–789 (1988). doi:10.1103/PhysRevB.37.785 Medline

38. A. D. Becke, Density-functional thermochemistry. III. The role of exact exchange. *J. Chem. Phys.* **98**, 5648–5652 (1993). doi:10.1063/1.464913

39. A. D. Becke, Density-functional exchange-energy approximation with correct asymptotic behavior. *Phys. Rev. A* **38**, 3098–3100 (1988). doi:10.1103/PhysRevA.38.3098 Medline

40. M. Cossi, N. Rega, G. Scalmani, V. Barone, Energies, structures, and electronic properties of molecules in solution with the C-PCM solvation model. *J. Comput. Chem.* **24**, 669–681 (2003). doi:10.1002/jcc.10189 Medline

41. V. Barone, M. Cossi, Quantum Calculation of Molecular Energies and Energy Gradients in Solution by a Conductor Solvent Model. *J. Phys. Chem. A* **102**, 1995–2001 (1998). doi:10.1021/jp9716997

42. C. N. Schutz, A. Warshel, What are the dielectric "constants" of proteins and how to validate electrostatic models? *Proteins* **44**, 400–417 (2001). doi:10.1002/prot.1106 Medline

43. R. F. Ribeiro, A. V. Marenich, C. J. Cramer, D. G. Truhlar, Use of solution-phase vibrational frequencies in continuum models for the free energy of solvation. *J. Phys. Chem. B* **115**, 14556–14562 (2011). doi:10.1021/jp205508z Medline

44. Y. Zhao, D. G. Truhlar, Computational characterization and modeling of buckyball tweezers: Density functional study of concave-convex π...π interactions. *Phys. Chem. Chem. Phys.* **10**, 2813–2818 (2008). doi:10.1039/b717744e Medline

45. I. Funes-Ardoiz, R. S. Paton, Goodvibes, version 2.0.3, Zenodo (2018); http://doi.org/10.5281/zenodo.1435820.

46. C. Legault, Cylview, 1.0 B (2009); http://www.cylview.org.

47. L. L. C. Schrödinger, The Pymol Molecular Graphics System, Version 1.8. (2015); https://pymol.org/2/

48. D. A. Case, R. C. Walker, T. E. Cheatham III, C. Simmerling, A. Roitberg, K. M. Merz, R. Luo, T. Darden, J. Wang, R. E. Duke, D. R. Roe, S. LeGrand, J. Swails, D. Cerutti, G. Monard, C. Sagui, J. Kaus, R. Betz, B. Madej, C. Lin, D. Mermelstein, P. Li, A. Onufriev, S. Izadi, R. M. Wolf, X. Wu, A. W. Götz, H. Gohlke, N. Homeyer, W. M. Botello-Smith, L. Xiao, T. Luchko, T. Giese, T. Lee, H. T. Nguyen, H. Nguyen, P. Janowski, I. Omelyan, A. Kovalenko, P. A. Kollman, *Amber 2016 Reference Manual*, (2016).

49. J. Wang, R. M. Wolf, J. W. Caldwell, P. A. Kollman, D. A. Case, Development and testing of a general amber force field. *J. Comput. Chem.* **25**, 1157–1174 (2004). doi:10.1002/jcc.20035 Medline

50. C. I. Bayly, P. Cieplak, W. Cornell, P. A. Kollman, A well-behaved electrostatic potential based method using charge restraints for deriving atomic charges: The RESP model. *J. Phys. Chem.* **97**, 10269–10280 (1993). doi:10.1021/j100142a004

51. U. C. Singh, P. A. Kollman, An approach to computing electrostatic charges for molecules. *J. Comput. Chem.* **5**, 129–145 (1984). doi:10.1002/jcc.540050204

52. B. H. Besler, K. M. Merz, P. A. Kollman, Atomic charges derived from semiempirical methods. *J. Comput. Chem.* **11**, 431–439 (1990). doi:10.1002/jcc.540110404

53. P. Li, K. M. Merz Jr., MCPB.py: A Python Based Metal Center Parameter Builder. *J. Chem. Inf. Model.* **56**, 599–604 (2016). doi:10.1021/acs.jcim.5b00674 Medline

54. W. L. Jorgensen, J. Chandrasekhar, J. D. Madura, R. W. Impey, M. L. Klein, Comparison of simple potential functions for simulating liquid water. *J. Chem. Phys.* **79**, 926–935 (1983). doi:10.1063/1.445869

55. J. A. Maier, C. Martinez, K. Kasavajhala, L. Wickstrom, K. E. Hauser, C. Simmerling, ff14SB: Improving the Accuracy of Protein Side Chain and Backbone Parameters from ff99SB. *J. Chem. Theory Comput.* **11**, 3696–3713 (2015). doi:10.1021/acs.jctc.5b00255 Medline

56. T. Darden, D. York, L. Pedersen, Particle mesh Ewald: An *N* ·log (*N*) method for Ewald sums in large systems. *J. Chem. Phys.* **98**, 10089–10092 (1993). doi:10.1063/1.464397

57. D. R. Roe, T. E. Cheatham III, PTRAJ and CPPTRAJ: Software for Processing and Analysis of Molecular Dynamics Trajectory Data. *J. Chem. Theory Comput.* **9**, 3084–3095 (2013). doi:10.1021/ct400341p Medline

58. O. Trott, A. J. Olson, AutoDock Vina: Improving the speed and accuracy of docking with a new scoring function, efficient optimization, and multithreading. *J. Comput. Chem.* **31**, 455–461 (2010). Medline

59. M. Srnec, E. I. Solomon, Frontier Molecular Orbital Contributions to Chlorination versus Hydroxylation Selectivity in the Non-Heme Iron Halogenase SyrB2. *J. Am. Chem. Soc.* **139**, 2396–2407 (2017). doi:10.1021/jacs.6b11995 Medline

60. X. Huang, T. M. Bergsten, J. T. Groves, Manganese-catalyzed late-stage aliphatic C-H azidation. *J. Am. Chem. Soc.* **137**, 5300–5303 (2015). doi:10.1021/jacs.5b01983 Medline

61. G. M. Sheldrick, Crystal structure refinement with SHELXL. *Acta Crystallogr. C Struct. Chem.* **71**, 3–8 (2015). doi:10.1107/S2053229614024218 Medline